UNIVERSITY
of
GLASGOW

SOME LABORATORY STUDIES OF ANISOTROPY OF PERMEABILITY OF KAOLIN

AbuBakar Hamidon
B.Sc(Eng), MSCE

A thesis submitted for the degree of
Doctor of Philosophy at the University of Glasgow

Department of Civil Engineering - June 1994

Dedikasi & terima kasih kepada

Isteriku

Maznah

dan anak-anak

Muhammad Firdaus

M. Faruq

Faizah

&

M. Faris

ACKNOWLEDGEMENTS

Alhamdulil-lah, I thank God for making the completion of this thesis a reality.

I should like to acknowledge with deep gratitude the advice and invaluable guidance given to me by my supervisor, Prof. D Muir Wood who has always been very understanding and appreciative towards the many challenges that I have been facing in the research work and laboratory testing in the Soil Mechanics laboratory. His patience and expectation in my work greatly helped me finish this academic work in an orderly fashion.

I should also like to extend my thanks to Dr. G Herbertson, Head of the Civil Engineering Department for providing the use of the Soil Mechanics laboratory and the departmental computer facilities.

I should also like to thank Dr. Peter Smart for allowing me to use the filter press apparatus and for some of his advice, and Dr William Stewart and Dr, Trevor G Davies for the occasional advice and encouragement given in the early and later part of my study.

My special thanks are due to Mssrs. W Henderson (Chief Technician), Tim Montgomery and Ian Dickson (Technicians), and John Tran for all the helps given in the laboratory particularly machining some parts of the cylindrical moulds and computer set up of the testing apparatus.

To my colleagues in the Department, especially V J Kumar, Ashraf Osman and Suhol Bu, I am indebted for their consideration and heartfelt friendship. To my friends in Glasgow, thanks for help in one way or the other.

The work presented in this thesis has only been made possible by the financial support from the Government of Malaysia (JPA & MSD) and the University of Malaya which provided me the essential study leave. Support and assistance from these authorities are gratefully acknowledged. Some support from the Registrar's Office, University of Glasgow is also gratefully acknowledged.

I am grateful to our children for being easy going and least troublesome while mum & dad grappled with their work in the laboratories.

I should like to express my gratitude to my wife for being understanding during our trying period in Glasgow. I must say that for her devotion and sacrifices - together and separately, are indeed our unforgettable moments. To my family, I am grateful for their prayers. Special thanks to my father-in-law for helping to spare some time in Glasgow for the children. My prayers and memories will always be to my late mother-in-law who had involved much of her time helping me - *Al-Faatihah.*

With regards to this thesis, I hereby certify that except where specific reference has been made to the work of others, its contents are my original composition, that it is a record of work conducted by myself, and that it has not previously been submitted for a higher degree at this or any other university.

TABLE OF CONTENTS

LIST OF TABLES

LIST OF FIGURES

NOTATION

In this study only a few equations are involved and therefore it is felt that a list of symbols is not necessary. Some symbols have more than one meaning and some might have the same meaning. To avoid confusion the symbols are defined when they first appear in the text.

SUMMARY

This thesis is concerned with an investigation into some aspects of the permeability measurement and permeability characteristics of reconstituted saturated supreme kaolin clay. Development of permeability anisotropy is investigated when the sample has experienced: (1) anisotropic consolidation, and (2) undrained shear.

Conventional step-loaded consolidation tests, constant flow rate and some constant head permeability tests were conducted on the kaolin slurry and block samples. For every conduct of testing, a pair of identical samples were tested: one underwent vertical drainage and the other radial drainage conditions. Both, however, were subjected to one dimensional deformation in the vertical direction.

Permeability of the clay was evaluated both directly and indirectly, from results of the permeability tests and consolidation tests, respectively. Data from the constant flow rate and constant head permeability tests yield the same values of permeability for both cases of vertical or radial flow (k_v not necessarily equal to k_h). Theoretical considerations of the transient phase of the experimental record of the constant flow rate permeability test are found to be applicable to form the basis of evaluation of permeability, coefficient of consolidation, and coefficient of volume compressibility of the clay sample.

Experimental results showed that during the progress of anisotropic consolidation of the kaolin slurry, the clay's vertical and horizontal permeability exhibited unique relationships with the void ratio which are linear on the logarithmic-linear scale [linear (lg k vs e) plot]. These relationships were found to be independent of the overconsolidation ratio. A lack of permeability anisotropy was observed in the early part of compression or at the initial void ratio, e = 3.1, but as the compression proceeds, development of permeability anisotropy was observed to reach a value of up to 2.1 which correspond to a void ratio of 1.30, where the corresponding vertical effective stress was 530kPa.

Experimental results for the block samples that had experienced undrained shear also showed the unique relationships of the clay's vertical and horizontal permeability with void ratio. Development of permeability anisotropy, however, was somewhat in opposition with that of the slurry sample observed during anisotropic consolidation. For samples sheared to vertical strains of 7.9 to 11.5%, an initial permeability anisotropy of 1.3 at a void ratio of 1.66 was observed to decrease with compression and developed into isotropic condition at a void ratio of 1.50, where the corresponding vertical effective stress was 120kPa. For samples sheared to vertical strains of 2.0 to 5.0%, an initial permeability anisotropy of 2.5 at a void ratio of 1.30 was observed to decrease very little with compression and the degree of anisotropy remained to a value

of 2.3 at a void ratio 1.05, where the corresponding vertical effective stress was 480kPa.

Solutions from both the Terzaghi's and Biot's consolidation theories were used to evaluate the experimental data of the axisymmetric problem of consolidation with radial drainage to inner and outer fixed boundaries. Compared with measured values, permeabilities of the samples calculated from both the Terzaghi's and the Biot's solutions and using the Taylor's square root of time method, are underestimated by a factor of 10 to 100 (ie. k_{cal}/k_m = 1/10 to 1/100). Furthermore, the calculated permeabilities are less orderly in the lg.k vs e plot while the variation is more ordered and linear for the measured values.

CHAPTER 1

1. INTRODUCTION

Permeability of clays represents an important basic property virtually required in steady state and transient flow problems in geotechnical engineering. Traditionally and until the present day it has an important bearing on problems of seepage, consolidation and stability which form a major part of soil and rock engineering analysis and design. However, compared to the other major properties of clay ie. shear strength and compressibility, earlier investigations on permeability of clay are somewhat less extensive and are more directed at the analysis of the property based on Darcy's Law rather than measurement on the value itself (Hansbo,1960; Olsen,1966; Swartzendruber,1968).

Interest in accurate measurement of permeability of clays has increased significantly in the past ten years (Tavenas et al.1983 I&II; Edil & Erickson, 1985; Al-Tabbaa & Wood,1987; Aiban & Znidarcic,1989; Leroueil et al.1990). There are two main reasons for this growing interest. Firstly, there is an increasing need to use actual permeability data as primary input parameter in consolidation problems using numerical procedures. This is especially useful for cases involving two and three dimensional effects which will somehow involve anisotropic behaviour in permeability (Davis & Poulos,1972; Christian et al,1972; Murray, 1978). As for the one dimensional consolidation, more accurate model is realised by considering the actual permeability and void ratio relationship of the clay (Mesri & Choi,1985). Secondly, for clays associated with the containment and disposal of hazardous wastes, permeability of the material represents one of the most crucial parameters required in evaluating the contaminant transport. Accurate permeability as input values are essential for reliable prediction of pollution migration through the clay barrier. Permeability measurements of clays for this purpose had been dealt with by Zimmie et al.,1981; Olson & Daniel,1981; Fernandez & Quigley,1985; and in the ASTM STP, publication No. 874 edited by Johnson, Frobel, Cavalli and Pettersson,1985. Such factors as the types of permeability testing, sample types, preparation and testing procedures, and permeants not only limited to water, had been considered.

Apart from the above main reasons testing is required to investigate the influence of stress history on permeability characteristics of clay when the stress is made up of consolidation and some amount of shearing. The influence of stress history on strength parameters is quite well studied, however, it is not the case when permeability characteristics are concerned. The particular influence of stress history

on permeability of clays is most commonly seen in studies on compacted clays and one dimensionally consolidated clays (Mitchell et al.,1965; Seed & Chan,1959; Mesri & Olson,1971). The main object of this study is therefore to concentrate on laboratory testing of clays with the main attention devoted to permeability behaviour. 1-D consolidation and consolidated undrained shear would be the two types of stress histories considered. Permeability measurements will be conducted in two directions (vertical and horizontal), so as to enable an investigation into the development permeability anisotropy be made.

1.1 Aims and scope of the research

The general aims of the research are as follows:

1.1.1 To establish reliable methods of laboratory permeability testing of saturated clays over a wide range of consistency limits and in two orthogonal directions;

1.1.2 To investigate the development of permeability anisotropy of clay which has experienced one-dimensional compression but through two different histories of drainage directions;

1.1.3 To investigate the influence of undrained shear of clay on its permeability and particularly on development of its permeability anisotropy.

This research is concerned with measurements of permeability of clay samples to investigate the development of permeability anisotropy in clay subject to: (1) One dimensional compression, and (2) Undrained shear.

A single clay type (supreme kaolin) with water as permeant is considered. The various stages of the experimental procedure adopted in setting up the clay sample starting from slurry form up to permeability testing are shown schematically in *Fig.*-1.1. The setting up and testing process pass through three passages and the one dimensionally compressed samples all end up in the vertical and radial flow oedometers for measurements of their vertical and horizontal permeabilities respectively. The study is divided into 2 parts:

Part 1: Consists of permeability measurements on samples which have passed through *Passage 1* and *Passage 2* in *Fig.*-1.1. These tests meet the aim stated in Section 1.1.2 above;

Part 2: Consists of permeability measurements on samples which have passed through *Passage 3* in *Fig.*-1.1. These tests meet the aim stated in Section 1.1.3 above.

In both parts, wherever possible permeability measurements of the larger mass of clay (in consolidation tank and triaxial cylinder) were carried out with the object of accumulating more permeability data for comparison with results from oedometer tests.

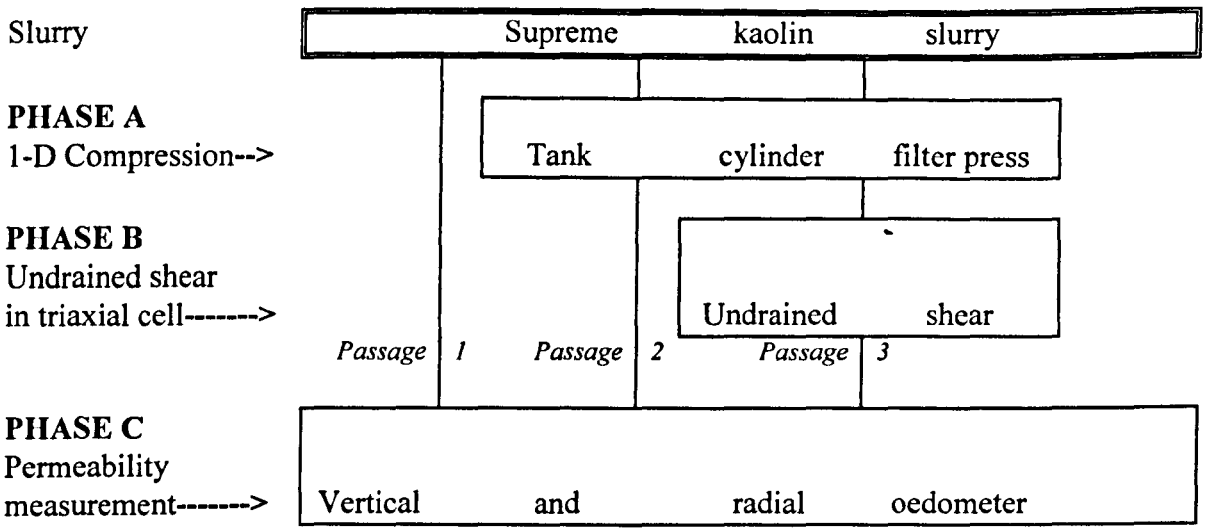

Fig.-1.1 Schematic stages of experimental procedure in setting up and testing of clay samples

1.2 Outline of the thesis

In Chapter 2, a review of literature on permeability of clays, its measurements and the influence of stress history on clay behaviour are presented. Anisotropic behaviour of the clay during the formation stage from slurry up to the stage where the sample is to be tested is briefly reviewed. The eventual discussion is on the possible development of anisotropy in permeability of the clay as observed in the ground and the development as a result of imposed stress history during testing.

Chapter 3 presents the programme of experimental work and describe the various pieces of apparatus required to carry out the laboratory testing. Details of the experimental procedure, sample preparation, methods of testing and calculation procedure are also presented. The consolidation test consists of the standard incremental step-loaded type while the main permeability testing consists of the constant flow rate method.

Chapter 4 presents the theoretical considerations relevant to obtain the necessary equations for vertical and radial permeability of the clays. Irrespective of whether drainage is purely vertical or purely radial, Darcy's law is explicitly implied to arrive at the appropriate expressions for vertical and radial permeabilities, k_v and k_h respectively. This is the case for which the flow has reached steady state condition and forms the most common basis in the direct measurement of permeability of clays. As with most soils testing involving the generation or dissipation of pore pressures, the steady state condition is always preceded by the transient phase and with the correct physical model of the process associated with the relevant mathematical formulations, solutions of the governing equation would appropriately yield the results giving the properties of the clay medium, particularly the permeability in this study.

The results of tests and their analyses are presented in Chapter 5. The main properties of interest are the vertical and horizontal permeabilities, and the variables are the void ratio, and the consolidation parameters. The empirical law of variation of permeability with void ratio is proposed after considering all the available test data. Chapter 6 provides the summary, conclusions and recommendations for further study.

1.3 Background

Permeability of clays is a basic property that deserves investigation both in the laboratory and in the field. Accurate knowledge of this property to be assigned to the clay material in question is essential for solving geotechnical problems successfully and economically with a reliable margin of safety.

At least three categories of geotechnical problems where permeability data are essential may be recognised: (1) Dams and water retaining earth structures; (2) settlements of earth structures on deposits of soft clays all over the world; and (3) environmental problems of toxic and hazardous waste disposal.

An important practical example is stressed by Louis *et al.*(1977) on the implication created by a dam. A dam by its very nature artificially creates a large hydraulic gradient. In the dramatic example of the Malpasset Dam, Louis *et al.*(1977) quoted Bernaix (1967) who showed that under the load of the dam, permeabilities in the foundation were reduced in a ratio of approximately 10^2. As a result an

'underground hydraulic barrier' was created, where the concentrated action of seepage forces contributed to the failure by sliding of the dam foundation along a fault located under the structure.

The natural foundations of large structures and natural or man-made rock slopes are often subject to subsurface water flows which are related to natural hydrogeological conditions or rains. This conditions, like river floods are essentially hazardous and their cosequences can be dangerous because they are hard to forecast. Hydraulic gradients, in these cases, are certainly small in comparison to those induced by dams, but the important point is that these gradients generate forces of the same order of magnitude as those acting on the masses due to the gravity alone.

While the hydraulic barrier beneath dams require proper analyses and counter measures, the same barrier introduced underneath a waste impoundment scheme would certainly retard the migration of pollutants and help protect ground water sources.

Recent years have seen more of permeability testing of clays using artificial and natural liquid wastes as permeants in addition to the traditional methods of using water. Use of different permeants on clays subjected to a multitude of stress histories to duplicate as close as possible field conditions or the final intended use of the material, has created opportunity of research on, as well as routine permeability testing of clays all over the world. Permeability data greater than or lower than $1x10^{-7}$m/s must be established reliably to support decision of whether the clay should not or should be considered safe impervious lining medium. In permeability testing, careful considerations are sometimes overlooked or sacrificed especially in the samples' thicknesses and application of pressure gradients so as to obtain quick results because of the time and financial constraints.

Development of consolidation testing has led to the need for permeability values of the clay sample. Therefore permeability testing and/or its most representative interpretation must form part of the programme of consolidation tests. Often testing time present a crucial part of geotechnical project. Therefore again, the time constraint and the need to produce reliable results prevail over other considerations. Perhaps a test system would consist of the standard step-loaded consolidation test adopting the NGI procedure of loading - this will reduce consolidation testing times from 24h to say 6h per consolidation stage. As for the permeability test, the constant flow rate test (CFR) could be adopted as this method of testing is claimed to require shorter testing times compared to the more conventional constant head or falling head tests.

Development of *in-situ* permeability testing has also led to the need for knowledge of permeability ratio of the tested clay deposits. Permeability equations for either the infiltration tests for shallow deposit or the self-boring permeameter testing method for

deeper and thicker clay deposits require the knowledge of the horizontal permeability of the clay. The flow in infiltration test is dominantly vertical while that in self-boring permeameter is mainly horizontal. For successful application of these permeability equations for field testing, one has to guess or perform laboratory permeability tests on undisturbed specimens to determine (k_h/k_v).

All of the above considerations require the need to conduct permeability testing to investigate effects of changing stress history on permeability of clays. *Fig.*-1.2 shows the varied situations where permeability data is required; particularly for analyses of embankment over clay deposits (a); and (b) feeding of data in field permeability testing using the self-boring permeameter and single-ring infiltrometer.

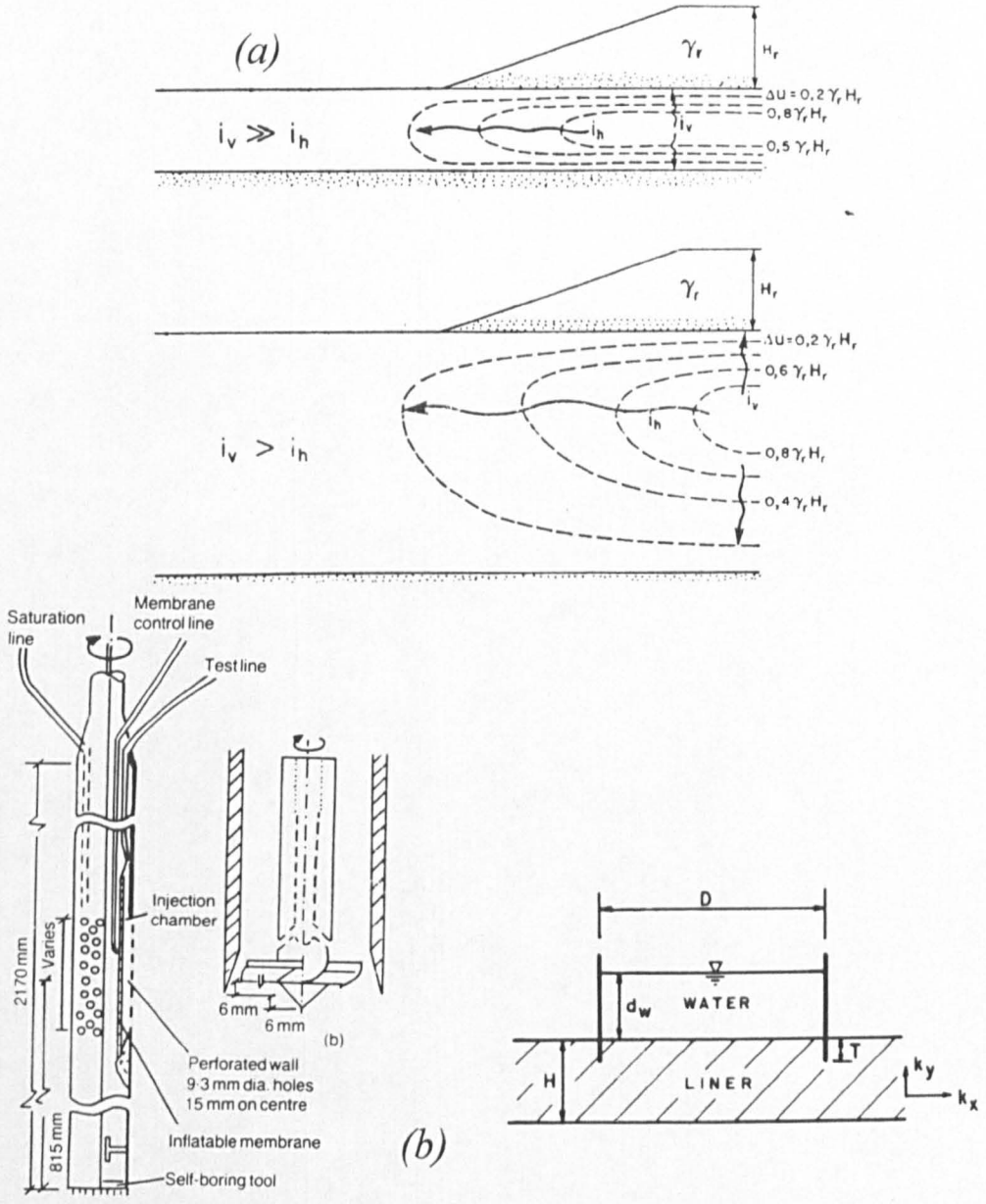

Fig.-1.2 Relevance of permeability data of clay in geotechnical engineering problems
(a) Analyses of embankment on soft clay ,Leroueil *et al.*(1990); (b) In situ permeability tests for permeability data, Chandler *et al.*(1990); Day & Daniel (1985)

CHAPTER 2

2. REVIEW OF LITERATURE

2.1 Permeability of clays

The classical work of Darcy in 1856 on the experimental studies of the flow of water through columns of sand led to the conclusion that the flow is proportional to the hydraulic gradient as given by:

$$q/A = - k i \qquad (2.1)$$

where q is the flow rate, A is the cross-section normal to direction of flow, i is the hydraulic gradient, and k is the hydraulic conductivity or simply permeabilty. This formulation of the flow law which is referred to as Darcy's law has become the basis of most theoretical and experimental work of flow through porous media. Numerous studies of Darcy's law have concentrated on the general form of Eq. (2.1) and also on the factors controlling the property of the medium, k. The main concern of this Section will be on the property k of clays in general and reconstituted supreme kaolin in particular.

A large number of factors are known to influence permeability of clays. For a given type of clay and at a given void ratio, the permeability values could vary by orders of magnitude depending on whether the clay sample whose permeability is measured is compacted, or reconstituted from slurry or trimmed from an undisturbed block. In this instance specimen type and also the method of sample preparation could be the cause of the great difference in permeability values.

The factors affecting permeability might be conveniently grouped into mechanical and compositional variables. In the broadest sense, mechanical variables consist of the testing methods and procedures, initial stress conditions, hydraulic gradient, and the degree of saturation. Compositional variables include the permeant characteristics, clay mineralogy and content of the various clay minerals. These variables are often inter-related and their compounded effects on permeability are sometimes represented by the way they influence the clay structure and fabric. *Table*-2.1 presents the various variables most frequently studied in the subject of permeability of clays. Other controlling factors which can significantly affect permeability of clays are temperature variation and ageing effects of clay samples called thixotropy.

Table-2.1 Most frequently studied variables in permeability of clays

Sample types	Permeant characteristics	Material parameters
1. Reconstituted from slurry	1. Unit weight	1. Particle size
2. Compacted	2. Viscosity	2. Void ratio
3. Undisturbed	3. Polarity	3. Composition
	4. Dielectric constant	4. Fabric
	5. Solubility	5. Degree of saturation
		6. OCR
		7. Vertical strain
		8. Consolidation pressure

Theoretical expressions for permeability of porous media are developed by considering the fundamental principles governing viscous flow of fluids through small conduits. Starting from the Hagen-Poiseuille equation of flow through capillary tubes,

$$V_{ave} = \rho_p R^2 i / (8\mu) \tag{2.2}$$

where V_{ave} = average flow velocity and R = internal radius of the capillary, ρ_p = density of pore fluid and μ = viscosity of pore fluid, Kozeny (1927) and Carman (1956) considered the flow in a skeleton consisting of flow channels of varying shapes and sizes within the limits of laminar flow, and in combination with Darcy's law (Eq.-2.1), arrived at the expression for permeability as,

$$k = \frac{T}{C S^2} \frac{\gamma_p}{\mu} \frac{e^3}{(1 + e)} \tag{2.3}$$

where γ_p and μ are the specific weight and viscosity of the permeant, C = pore shape factor, S = specific surface per unit volume of particles, e = void ratio, and T = tortuosity factor is defined as,

$$T = \left(\frac{L}{L_e}\right)^2 \tag{2.3a}$$

where L is the apparent flow length and L_e is the effective flow length.

Principally the effects of permeant characteristics are accounted for when the absolute permeability, K, is taken as,

$$K = k \mu / \gamma_p \tag{2.4}$$

Eq.-(2.3) is the well known Kozeny-Carman equation which is one of the most thoroughly tested correlations between permeability and the physical properties of porous media. The principal assumptions underlying Eq.-(2.3) are that (1) Darcy's law is valid, (2) viscous flow obeys Poiseuille's law, (3) the tortuosity of the flow channels is a constant and approximately equal to $\sqrt{2}$, and (4) the flow channels or pores are equal in size. Furthermore, Eq.-(2.3) together with Darcy's law gives excellent prediction for flow rates through liquid-saturated porous media provided that the

media particles are approximately equidimensional, uniform, larger than 1μ but small enough to ensure laminar flow conditions (Loudon, 1952; Carman, 1956). The above mentioned 4 principal assumptions together with the 3 latter conditions could be reasonably fulfilled in sands and therefore it is logical to observe the successful application of Eq.-(2.1) and Eq.-(2.3) when predicting hydraulic flow rates through sands. Theoretical evidence to support this validity has been well documented in early treatise(Scheidegger,1954; 1974; Bear,1972). In contrast to sand, attempts to predict the flow rates based on the two equations, Eqs.-(2.1) and (2.3) *per se* have been shown to break down when applied to clays. This inadequacy for saturated clays has long been recognised. Terzaghi (1925) emphasized the importance of the non uniformity of the voids on clay permeability and the substantial dependence of the permeability on the void ratio. He considered that the physical properties of the pore water changed in the immediate vicinity of the clay surfaces such as to affect the viscous flow model. Early studies by Lambe (1954) on compacted clay indicated the influence of moulding water content, soil composition, permeant characteristics and void ratio on permeability. He concluded that: (1) the Kozeny-Carman equation does not account for compositional changes, (2) the term (μ / γ_p) is not adequate to represent permeant characteristics, and (3) the void ratio is not an independent parameter. It is then concluded that clay structure plays an important role in controlling the permeability. Explanations of the discrepancies of observed behaviour compared to what is to be predicted from the Kozeny-Carman equation lead to the conclusion that the deviations mainly result from the existence of unequal pore sizes in the clay fabric (Taylor, 1948; Michaels & Lin, 1954; Leonards, 1962; Mitchell et al., 1965; Olsen 1965, 1966). Consequences of having unequal pore sizes have been examined by a cluster model developed by Olsen (1962). From results of consolidation-permeability tests for several clay systems, Olsen obtained the ratio of the measured flow rate to the flow rate predicted by the Kozeny-Carman equation plotted against porosity as shown in *Fig.*-2.1. The figure shows that: (1) The measured permeability can be greater or less than the predicted value, (2) for compression at porosities greater than about 40%, the measured permeability decreases more rapidly with decreasing porosity than predicted, (3) for compression at porosities less than about 40%, the measured permeability decreases less rapidly than predicted, and (4) for rebound, the permeability increases less rapidly than predicted.

Considering that the flow is mainly through the intercluster pores (the large pore mode developed between clusters of clay particles) rather than the intracluster pores (the small pore mode in the cluster), the ratio of the estimated flow rate for the cluster model, q_{cm}, to flow rate predicted by the Kozeny-Carman equation, q_{kc}, is derived by Olsen (1962) as,

$$\frac{q_{cm}}{q_{kc}} = N^{2/3} \frac{(1 - e_c / e_t)^3}{(1 - e_c)^{3/4}} \qquad (2.5)$$

where $e_t = e_c + e_p$

and e_t = total void ratio, e_c = intracluster void ratio, e_p = intercluster void ratio, and N = the number of particles per cluster.

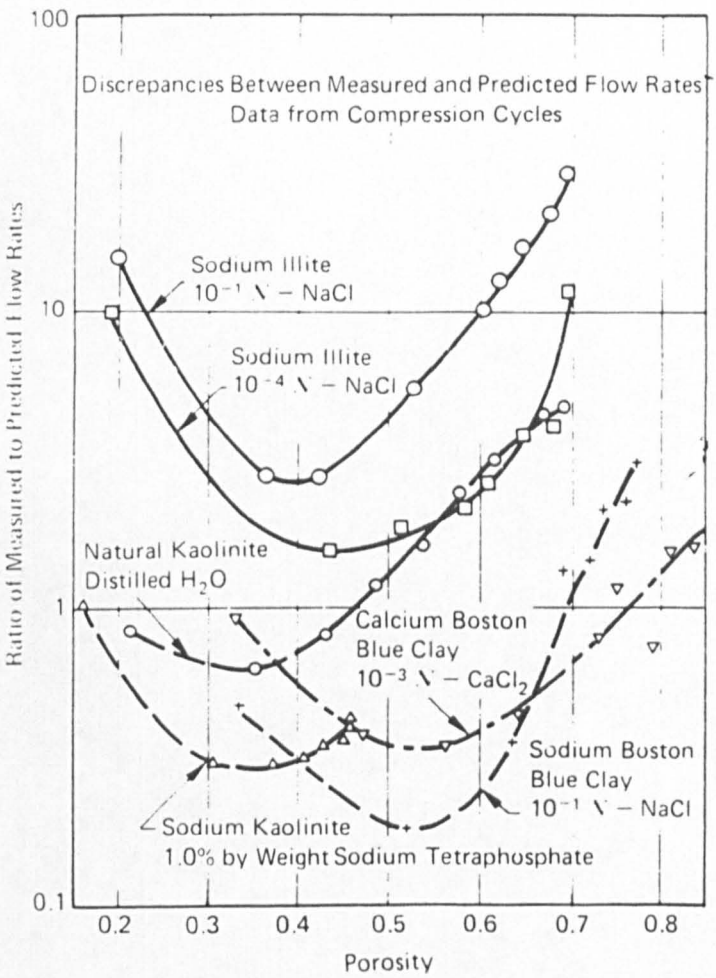

Fig.-2.1 Ratio of measured flow rate to theoretical flow rate versus porosity (Olsen, 1962)

Predictions using Eq.-(2.5) using the relationship between e_t and ($e_c + e_p$) are shown in *Fig.*-2.2 for three values of N. As shown in *Figs.*-2.1 and 2.2, Olsen obtained quantitatively and qualitatively good agreement between the discrepancy of the cluster model (q_{cm}/q_{kc}) and predicted values, and the discrepancy between measured flow rates (q_m/q_{kc}) and predicted values, where q_m = measured flow rates. Unequal pore sizes were later observed by optical and electron microscope (Morgenstern & Tchalenko, 1967; Collins & McGown, 1974). Thus the factors incorporated in the Kozeny-Carman equation are significant for sands, but in the case of clays, are not sufficient to predict permeability.

While Darcy's law has provided the basis for describing the macro scale flow law in sands or clays, theoretical equations for the permeability of the medium are largely based on the Kozeny-Carman equation. Despite its inability to describe adequately the permeability of clays, it has provided the foundation for further development of empirical laws of the variation of permeability of clay with void ratio. Thus keeping the other factors constant the equation indicates the linearity of plots of k versus $e^3 / (1 + e)$. Other relations of k as functions of void ratio e, have suggested the relationship given by k versus $e^2 / (1 + e)$ or k vs e^2 (Lambe & Whitman,1969 p.316). Thus, in accord with the theoretical model of the porous medium, these functional variations of permeability with void ratio indicate the direct dependence of permeability on the second power of the diameter of the flow channel or the flow rate on the fourth power of the latter. Based on this dependency, many predictive permeability equations have been developed which relate k to some power of porosity or void ratio.

Having noted the limitations of Eq.-(2.3) when applied to clays, Taylor (1948) suggested an empirical linear relationship between the logarithm of permeability and the void ratio,

$$\Delta \lg k = (1/C_k)\, \Delta e \qquad (2.6)$$

or

$$\lg k = \lg k_o - (e_o - e) / C_k \qquad (2.7)$$

where C_k is a permeability change index and k_o, e_o are *in-situ* or reference values. This type of relationship has become the most common way of expressing the variation of the permeability of clays with void ratio and is generally valid for the range of void ratio changes encountered in engineering practice. *Fig.*-2.3 presents permeability data of some clays on the (lg.k vs e) plot. Considering the different origins of the clays and variations in methods of tests the small range of C_k values

obtained (0.9~1.34) is quite remarkable. However, for any given value of void ratio, the difference in values of k is quite large amounting to 2 orders of magnitude. Thus the index C_k is relatively insensitive to the types of clay and their stress histories but the initial values of k are not. Mesri & Choi (1985) noted that for a wide variety of clays and shales $C_k \approx 0.02$ to 5 and for majority of soft clays $C_k \approx 0.5$ to 2.

For a very wide range of void ratio, Eq.-(2.7) may not be consistently valid and a linear relationship between lg k and lg e is often used, (Mesri & Olson, 1971):

$$\lg k = A \lg e + B \tag{2.8}$$

Samarasinghe et al., (1982) suggested a slightly modified version of the Kozeny-Carman equation in the form of,

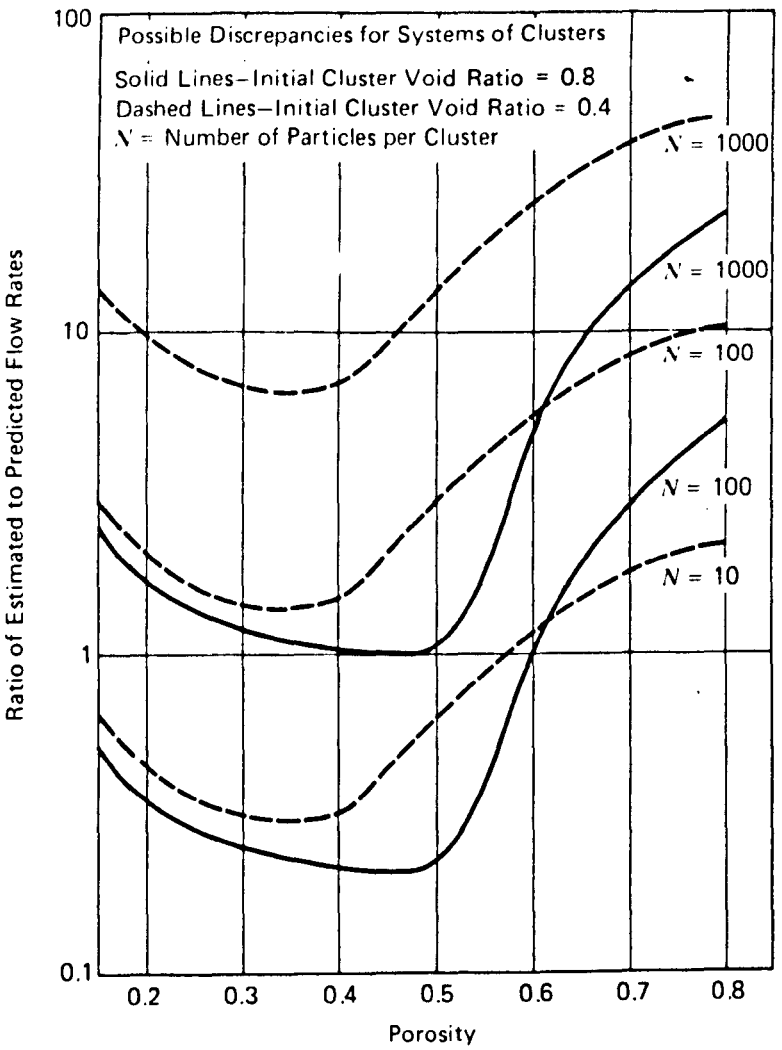

Fig.-2.2 Ratio of cluster model flow rate to theoretical flow rate versus porosity (Olsen, 1962)

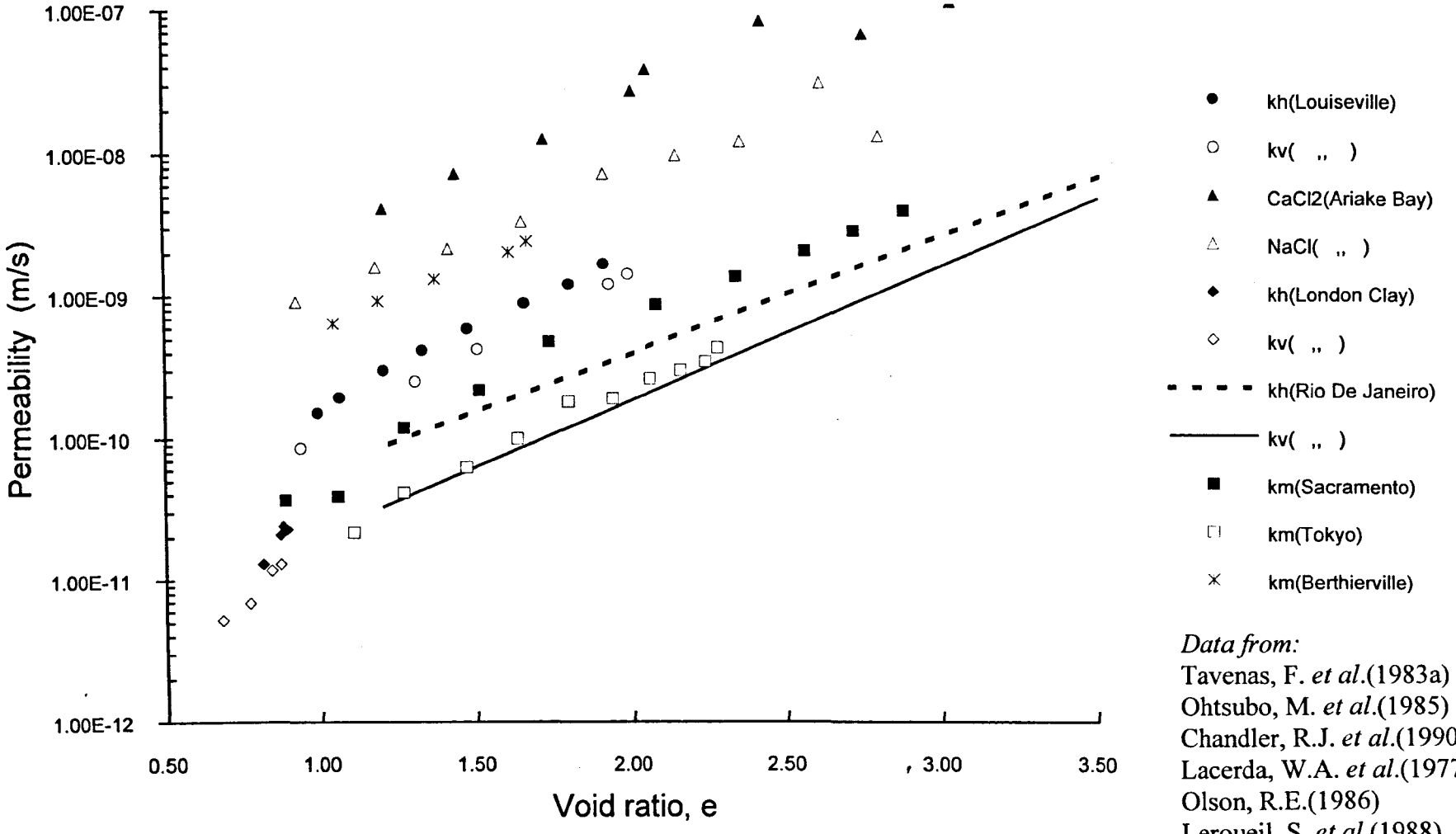

Data from:
Tavenas, F. *et al.*(1983a)
Ohtsubo, M. *et al.*(1985)
Chandler, R.J. *et al.*(1990)
Lacerda, W.A. *et al.*(1977)
Olson, R.E.(1986)
Leroueil, S. *et al.*(1988)

Fig.-2.3 Permeability of some clays obeying the linear variation of logarithmic of permeability with void ratio

$$k = C\, e^n / (1 + e) \qquad (2.9)$$

for normally consolidated clays, with the power n typically in the order of 4 to 5, and C a reference permeability indicating the soil characteristics.

The above equations were generally developed from tests on artificial or remolded clays. From the experimental laboratory study on the permeability of some intact soft clays from Canada, the USA, and Sweden, Tavenas et al. (1983-II) concluded that none of the above Eqs.-(2.7), (2.8), and (2.9) is unique in describing the variation of permeability with void ratio. It appears that different clays may fit differently into one or other of the above permeability-void ratio relationships and the choice is conditional on the type of clay, the initial void ratio, and the range of void ratio change. It is also possible that different equations may fit perfectly into portions of the experimental permeability data at various applicable range of void ratio to account for different modes of structural changes that occur as the void ratio decreases. Despite the difficulty of expressing a unique (e-k) relationship, another permeability equation claimed to be of general validity has been proposed by Juarez-Badillo (1984, 1986, 1991). Such an equation reads

$$k = k_1 \left(\frac{1+e}{1+e_1} \right)^{\kappa} \qquad (2.10)$$

where (e_1, k_1) is a known point and κ is a constant parameter called the coefficient of permeachange.

When applied to a series of experimental data for natural soft clays of various geological origins, (Mesri & Tavenas,1983), Tavenas *et al.*, (1984) found that the Eq.-(2.10) fitted well only 2 out of 10 clays tested. The other eight experimental data could be well fitted either at the beginning or at the later range of void ratio. This led to the conclusion that Eq.-(2.10) is no more general than any of the above equations stated earlier.

Experimental results of the variation of permeability with void ratio obtained by various researchers fitted to any one of the above equations are shown in *Fig.*-2.4.

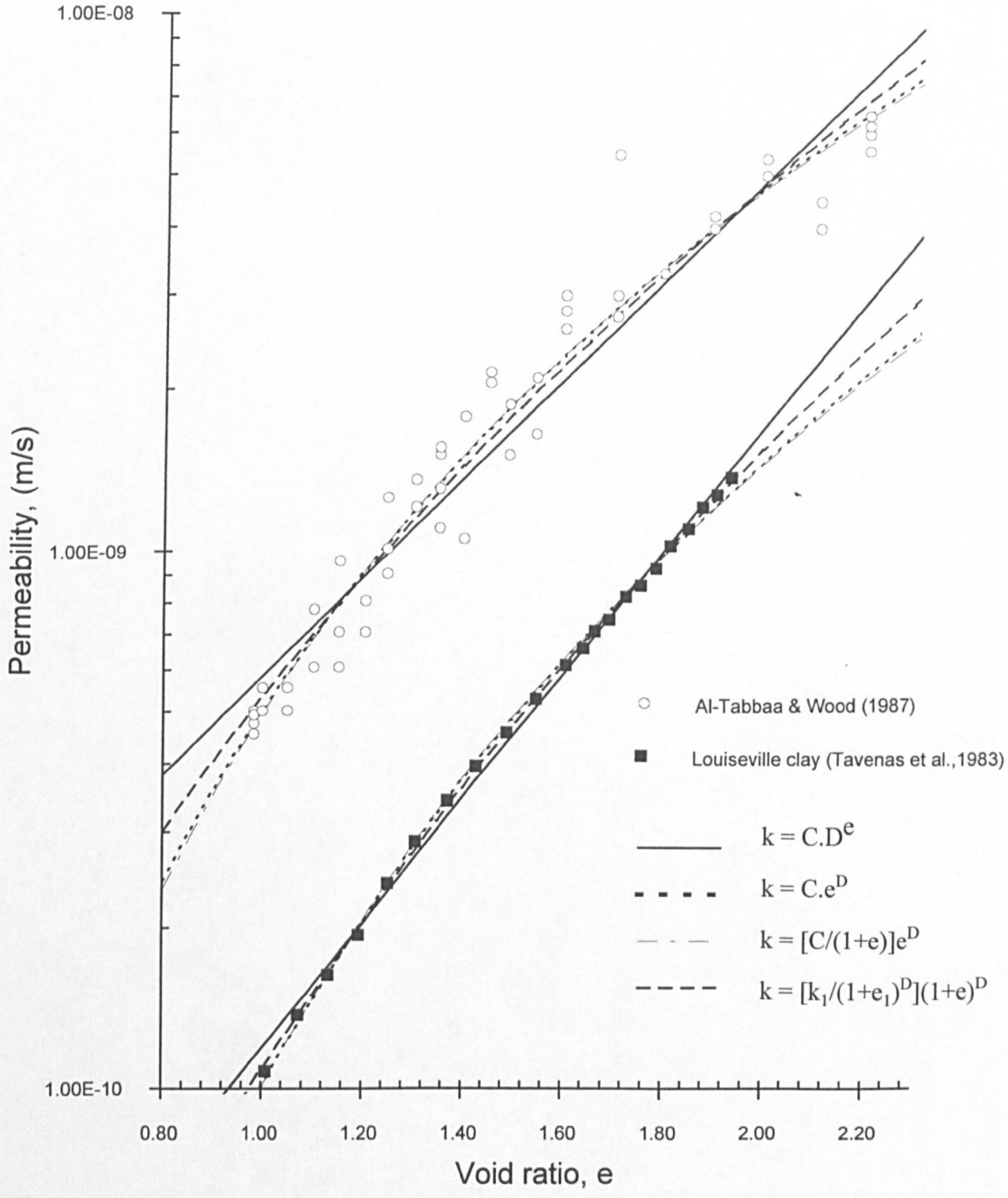

Fig.-2.4 Experimental permeability data with void ratio fitted by various forms of semi-empirical permeability equations

2.2 Permeability measurements of clays

A detailed state of the art review for permeability testing of clay has been presented by Olson & Daniel (1979). A review of current practice of permeability determination in the laboratory indicates the importance to control the following factors more thoroughly than usual: (1) The influence of initial consolidation stress on the samples and the subsequent stress history up to the time when permeability tests are conducted; (2) hydraulic gradient; (3) saturation condition; (4) sample consolidation during testing, and (5) time effects.

Careful controls over details of test apparatus and procedure have given much problem and various experimental techniques and approaches have been utilised to minimise these errors. The common sources of errors are listed in *Table*-2.2 in which they are categorised into three possible groups in relation to equipment, specimen and testing procedure. A review by Dunn and Mitchell (1984) on the state of practice in laboratory measurement of permeability of saturated soils indicated that few standard test methods are available and the extensive degree of variation in the test procedures used in practice can result in measurements of saturated permeability varying over two or three orders of magnitude for a given soil. Consequently an experimental set up and testing procedure must account for all these procedural variations so that errors associated with them are eliminated and factors describing the actual behaviour of the clay could be reasonably distinguished.

Accurate measurement of permeability has proved to be a difficult task with regard to the low permeability of the clay. The constant head and the falling head tests are widely employed both for routine and research purposes. The methods of observing very small flow in capillary tube or recording head drops in small vertical tube have become a classic part of the tests. For both cases long periods of time are required to observe the flow rate or to obtain appreciable head drops in these conventional constant head or falling head tests respectively.

Selection of the proper gradients to use in testing has seldom been based on duplicating gradients in the field but more from consideration of the time required for testing and the need to keep gradients as low as possible. Typical magnitudes of gradient encountered in the field and in the laboratory test are shown in *Table*-2.3. Testing at low gradients will require a few days or even weeks while at high gradients the testing time is reduced to a few hours. The effects of high gradient, however, will give rise to plugging or unplugging of voids within the sample (Mitchell & Younger, 1967) and a large variation of effective stresses across the drainage boundaries is created causing local swelling and consolidation (Hardcastle & Mitchell, 1974; Edil & Erickson, 1985). Either effect may cause the sample to become less homogeneous

resulting in measurable changes in permeability, usually in a decreasing trend with time (Aiban & Znidarcic, 1989).

Application of low hydraulic gradients on the sample will less adversely affect the physical state of the clay but the long time required to register measurable flow rates or head drops is undesirable for various reasons: growth of bacteria or microorganisms is encouraged in the sample and this tends to decrease the permeability (Allison & Quirk, 1960). The control of low pressure difference and measurement of small flow rates over time are difficult to achieve accurately resulting in unacceptable experimental errors.

Table-2.2 Common sources of error in laboratory permeability testing of clays

Sources of errors	
Equipment	1. Resolution of volume or pressure measurement 2. Leakage 3. Contamination in capillary tubes 4. Evaporation 5. Temperature variation 6. Diffusion of air in permeant or sample
Specimen	1. Sample volume changes 2. Duplication of sample 3. Thixotropic effects 4. Unstable structure or fabric 5. Changes in pore fluid chemistry 6. Growth of micro-organism
Methods of test	1. Application of gradients

Table-2.3 Hydraulic gradients in the field and laboratory

Classification (arbitrary)	Hydraulic gradient	Where applicable
very low	< 1	1. Naturally occuring groundwater systems 2. Laboratory
low	1 - 20	1. Seepage blankets 2. Compacted soil liners 3. Laboratory
high	20 - 200	1. Laboratory

Pane *et al.* (1983) present evidence that small gradients (i_{av}<5) are required to obtain valid permeability measurements when the samples consist of soft clays. For higher average gradients (10<i_{av}<80), results of the standard falling head method suffer from apparent deviations from Darcy's law. These difficulties associated with the conventional techniques of permeability testing leave one with a paradox. The constant flow rate permeability test introduced by Olsen(1966) has been suggested to overcome the difficulty since it has shown to be capable of reducing testing time considerably while still maintaining the gradient very low. In this test the low pressure difference is much easier to measure accurately while the small flow rate is being easily controlled by the flow pump. In the constant head test, however, the double difficulty arise in which it is rather difficult to measure the low flow rate for a given controlled low pressure difference and also the constant low pressure difference itself is difficult to control.

In the constant head test, an ideal method of applying gradient to initiate flow is to let the swelling and consolidation near the two drainage boundaries have compensating effects on each other resulting in negligible net sample volume change. This could be achieved by limiting the pressure difference to an arbitrary small fraction of the existing consolidation pressure (say $\Delta u < 10\%$ of σ'_v) (Olsen, 1962; Mitchell, 1969). The effect of gradient is shown in *Fig.*-2.5 for a vertical flow sample. It is desired to perform permeability test when the state of the sample is at A on the

(e - lg σ'_v) curve. To balance up the swelling and consolidation taking place, the ratio (σ'_{vt} - σ'_v) / (σ'_v - σ'_{vb}) must be less than 1 so that the average void ratio of the sample still remains at e_A, ie (e_B + e_T) / 2 = e_A. It follows that the ratio of pore pressures at the top and bottom of the sample must be less than unity ie. Δu_t / Δu_b = (u - u_t) / (u_b - u) < 1. This is the key requirement of applying the pressure difference whereby the effects of differential and seepage induced consolidation and swelling could be minimised. Since this requires the knowledge of the slopes of the virgin and rebound curve of the sample, (ie. compression and rebound index, C_c and C_r), most investigators adopted the condition Δu_t / Δu_b = 1 and maintaining Δu = (u_b - u_t) as small as practicable, normally less than 10% of σ'_v. Assuming $\Delta u = 0.1\sigma'_v$ the gradient is then simply:

$$i = \frac{0.1\,\sigma'_v}{\gamma_w\, H} \qquad (2.10)$$

where σ'_v is the current consolidation pressure in the sample, γ_W is the unit weight of water, and H = current height of sample.

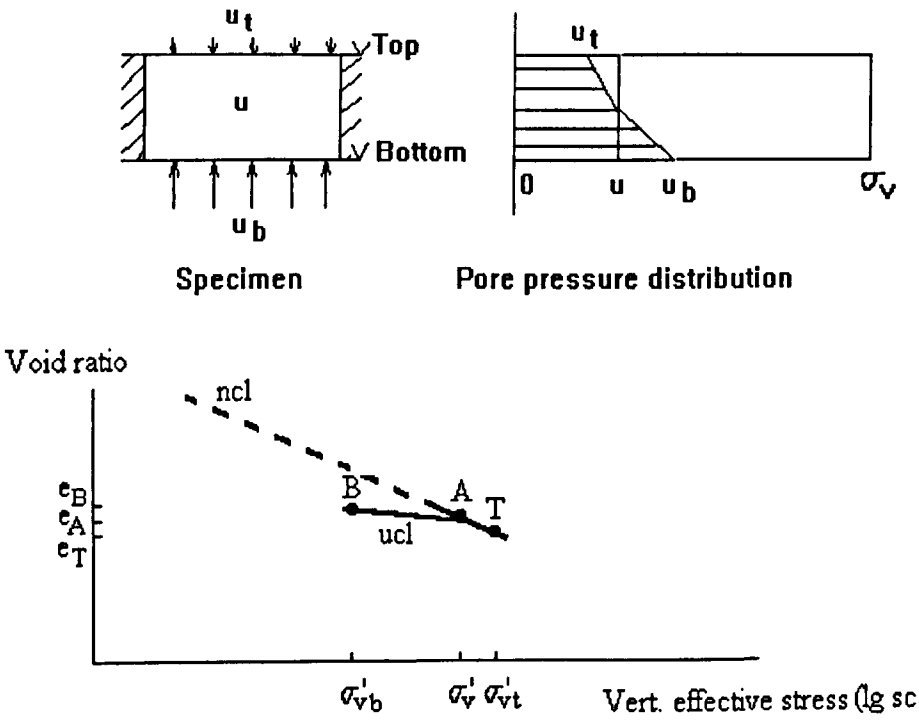

Fig.-2.5 Effect of pressure gradient on consolidation and swelling for a vertical flow sample

2.3 Anisotropy in behaviour of clays

The causes of anisotropy in clay are fundamentally related to its mode of deposition and the prevalent state of stresses in the clay, while the effects of anisotropy are related to the properties and behaviour of the material.

A departure from a state of isotropy in a clay mass would result in anisotropic behaviour in clays. The most common departure from an isotropic state in a clay mass is found in the orientation or preferred alignment of the clay particles in the horizontal direction and this can be associated with the absence of isotropy in the present and past states of stresses. Where clays have been formed by sedimentation followed by one- dimensional consolidation over long periods of time, then the one-dimensional deformation results in an anisotropic structure. Anisotropic histories of formation of clays may be regarded as the rule whether induced by natural causes, such as is found in natural alluvial and sedimentary deposits, or by human causes as in the construction of clay fills where clay materials are dumped in horizontal lifts. The making of a clay sample from slurry which has been consolidated one-dimensionally in a smooth rigid tube has a similar effect. For these conditions, marked differences in many aspects of the behaviour of the clays may be noted in the vertical and horizontal directions; however, the behaviour is frequently found to be identical in any horizontal direction. This form of anisotropy is termed transverse anisotropy or cross anisotropy. Thus there is some plane (in this case, horizontal) in which all stress-strain relations are isotropic; so, for example, it makes no difference how the axes are chosen within the plane, the elastic constants will be the same. The elastic constants for stresses and strains in other planes will be different. Cross anisotropy results from the anisotropic past history of one dimensional consolidation of the clay which is mainly responsible for leaving a preferred particle alignment perpendicular to the vertical axis of symmetry. Also, it is found that if a clay is subjected to an anisotropic state of stresses at an earlier (high void ratio) stage of its existence, then it is more likely to develop and retain anisotropic material properties and behaviour than if that state of stress is applied at much later stages where the void ratio is lower and the clay is rather stiff and has already fully developed its structure.

Particles of clay minerals seem to develop preferred orientations at very early stages of compression at overburden pressures less than around 100kPa. The process is greatly enhanced when the initial water content is high. In the case of kaolinite sedimented in flocculating and deflocculating pore fluids, Morgenstern & Tchalenko (1967) found that stresses as low as 10kPa were sufficient to produce orientation. Normally consolidated (nc) clay deposits showed lower degrees of orientation than

over-consolidated (oc) clays and the tendency is found to depend also on the type and concentration of electrolytes in the pore water, soil mineralogy and the initial fabric.

Anisotropy in clays can be described in various forms, the most common being firstly, the geometrical aspects of the arrangement of the clay particles: this is more often referred to as the clay fabric; and secondly the existing states of stresses which can be either isotropic or anisotropic. Most effects of anisotropy that have been studied have been related to deformation and strength while anisotropy with respect to permeability has been given more of a macroscale description.

An early definition of anisotropy in clays is due to Casagrande & Carillo (1944). They distinguished between two forms of anisotropy in soils which they called *inherent* and *induced* anisotropy. Inherent anisotropy was defined as "physical characteristics inherent in the material, and entirely independent of the applied strains", whereas induced anisotropy was defined as "due exclusively to the strain associated with the applied stresses". These are fundamental definitions developed to describe strength anisotropy. Since then many other definitions have been developed to provide various explanations of observed strength behaviour of clays. Ladd *et al.* (1977) distinguished between three forms of anisotropy: inherent, stress-system induced, and combined. Inherent anisotropy reflects the depositional characteristics of the soil while the stress-system induced component arises whenever the stress state to which the soil is subjected is not isotropic - for example, when the coefficient of earth pressure at rest (K_o) is not equal to unity. Since a certain state of stress always exists within the material, the resultant form of anisotropy is likely to be due to the nett effects of the inherent and stress-system induced anisotropies which is termed the combined anisotropy by Ladd *et al.*

Menzies & Simons (1978) considered soil strength anisotropy to arise from two interacting anisotropies of geometry anisotropy and of stress anisotropy. Geometrical anisotropy arises at deposition when the sedimented particles tend to orientate with their long axes horizontal seeking positions of minimum potential energy. The horizontal layering or bedding which results is further established by subsequent deposition which increases the overburden pressure. Stress anisotropy arises because of a combination of stress history and the geometrical anisotropies of both the particles themselves and of the packed structure they form. The nett effect is a clear strength and stress-strain anisotropy.

Parry & Wroth (1981) considered anisotropic behaviour in clay to arise from two sources: (1) *structural anisotropy* such that the linear strain in any direction produced by a principal effective stress increment in that direction will differ with the direction in the soil, and (2) *stress anisotropy*, such that the linear strain produced in any

direction by an increase in principal compressive effective stress in that direction will be different in magnitude from the linear strain produced by a corresponding decrease in principal effective stress in that direction.

Thus in the development of anisotropy of any property in a clay, the initial fabric and the subsequent structure of the material play important roles during formative stages right up to the point where sampling or testing is carried out to determine the property. At the early stage of the soil formation process the clay fabric will be very loose (that is, the void ratio will be very large) and the soil structure will obviously be very weak and unstable (Monte and Krizek, 1978). Structure is defined here as the geometrical arrangements of particles together with the various forces that interact among them, whereas fabric is understood to be only the geometrical arrangement of particles (orientation and spacing) (Mitchell, 1976, p135).

The above considerations point to the fact that anisotropy in clays can describe both the property of the material and the behavioural response of the material when placed under test. Despite the complexity and confusion that may arise from the expansion of the number of definitions of anisotropy and special terms, Tavenas(1981) is of the opinion that the distinctions that have been drawn between inherent and stress induced anisotropy in clays are often irrelevant. Most clays, especially in their natural state, exhibit anisotropic properties and response, and what is required is a form of testing capable of identifying the effects of anisotropy and of measuring the properties themselves - free from boundary defects.

One of the simplest methods of investigating variation of strength with orientation of the failure plane is to trim specimens at different inclinations relative to the direction of deposition in the field and perform consolidated undrained triaxial tests. As a standard well-established practice, the *in-situ* vertical axis is normally assumed to represent the axis of deposition in the field. By this approach a vertical triaxial sample is one in which its axis of deposition is parallel to the direction of the applied compressive stress, and a horizontal sample has its axis of deposition perpendicular to the applied major principal compressive stress. These are the customary definitions of so-called vertical and horizontal specimens.

Many investigators were aware early that shear strength can vary with the direction of the failure plane and with the direction of the applied stress. For example Rendulic (1938), reported that the shear strength with respect to the effective stresses in a soil is higher (7 to 9 %) in axial extension than in axial compression tests. Casagrande & Carillo (1944) investigated analytically the shear strength of anisotropic materials. They showed that anisotropy may have a marked influence on the expected angle of inclination of failure planes.

Experimental results on the strength anisotropy and deformation parameters of clays have been published by many investigators. Deformation parameters are normally represented by the Young's moduli for samples in vertical and horizontal directions, E_v and E_h, while the strength parameters usually refer to undrained shear strengths in compression loading in the vertical and horizontal directions, S_v and S_h, respectively. Ward et al. (1965) have shown that the ratio of the elastic moduli E_v and E_h for London clay determined by triaxial tests varies between 0.41 and 0.83. Lo (1965) has shown that the ratio of the undrained shear strengths S_h/S_v varies from 0.80 to 0.64 for block samples of lightly overconsolidated clay. Sangrey and Townsend (1969) have found that Labrador clay is anisotropic with regard to cementation failure and weaker when compression is in the horizontal direction. Aas (1967) and DiBiagio & Aas (1967) have determined the anisotropy of some Norwegian sensitive clays by a special series of tests using vanes with different shapes, or by *in situ* direct shear test. The anisotropy ratio S_h/S_v is found to vary between 1.5 and 2.0 for normally consolidated clays, and is about 1.0 for the slightly overconsolidated quick clay.

2.4 Development of permeability anisotropy

Anisotropic consolidation, shearing, transportation by wind, water, ice or man during or after deposition, and methods of sample preparation for remoulded or compacted clays in the laboratory may result in anisotropic fabrics. Fabric anisotropy on a macroscale usually results in anisotropy of mechanical properties and values of properties measured in different directions may be significantly different. So far as laboratory studies are concerned, the amount of shear or compression required for development of anisotropic fabric in clays varies and depends on such factors as clay mineralogy, composition of pore fluid and initial fabric. Development of fabric anisotropy is not limited only to plate-shaped clay particles but can also be seen in assemblages of sand particles or spherical particles.

The effects of one-dimensional compression on development of permeability anisotropy have been studied quite extensively, whereas the effects of shearing are less well understood. Studies on shear deformation and failure patterns of clays have in the past been conducted using unconfined compression tests, compression tests in the triaxial cell, and shear box tests. Samples which have received different histories have then been prepared for observation and measurement of changes in their structures and fabric using methods of electron and polarizing optical microscopy.

The degree of anisotropy of a clay sample can be quantified in many ways, ranging from visual, subjective, assessment of fabric to more objective quantitative

determination of indices which describe the orientations and arrangements of particles. When subjected to examination using optical or electron microscopes, the degree of anisotropy can be defined as the ratio of the minimum and maximum intensities of transmitted polarized light through an image obtained by optical or transmission or scanning electron micrographs. The degree of anisotropy can be described by the measure of the degree of particle orientation, β, which is the ratio of the transmitted polarized light intensities.

$$\beta = I_{min} / I_{max} \tag{2.11}$$

β approaches zero for 'perfect' orientation, and unity for 'random' arrangements. This definition is given by Foster & De(1971). Smart (1966a) defined an Anisotropy Index, A_I, as:

$$A_I = \frac{I_{max} - I_{min}}{I_{max} + I_{min}} \tag{2.12}$$

where I is the intensity of the light transmitted. The value of the anisotropy index A_I ranges from 0, which indicates a random arrangement of particles, to 1, which indicates an ideal arrangement of particles, with all particles having the same orientation.

Published reports of effects of shear deformation on permeability of clays have been mostly of a qualitative nature and no published evidence has been found concerning the relationships between shear deformation and anisotropy of permeability. Information concerning the development of anisotropy of soil fabric with shear deformation has been collected for several decades. From various hypotheses concerning the development of arrangements of clay plates and domains during pre-peak shear deformation, Smart (1985) suggested that deformation increases the fabric anisotropy of initially isotropic clays and decreases the anisotropy of initially strongly anisotropic clays: so that there may be a critical anisotropic state just as there is a critical void ratio for many types of soils (the value of critical void ratio is dependent on stress level). This observation is summarized in *Fig.*-2.6, from Smart(1993), which shows the change in anisotropy during shear deformation as a function of the initial anisotropy, from measurements made using polarising microphotometry.

Recent studies have made use of digital image analysis combined with polarising microscopy to study the deformation of normally consolidated kaolin subjected to undrained shearing (Bai & Smart, 1994). The methods of optical microscopic analysis employed were the PMPA (Polarising Micro-Photo-metric Analysis), and POLMAP (Polarising Micro-Photometric Mapping). The results of analysis show the anisotropy

index vs axial strain as measured by PMPA and POLMAP in *Fig.*-2.7. The data show a lot of scatter and it may be difficult to discern clear patterns.

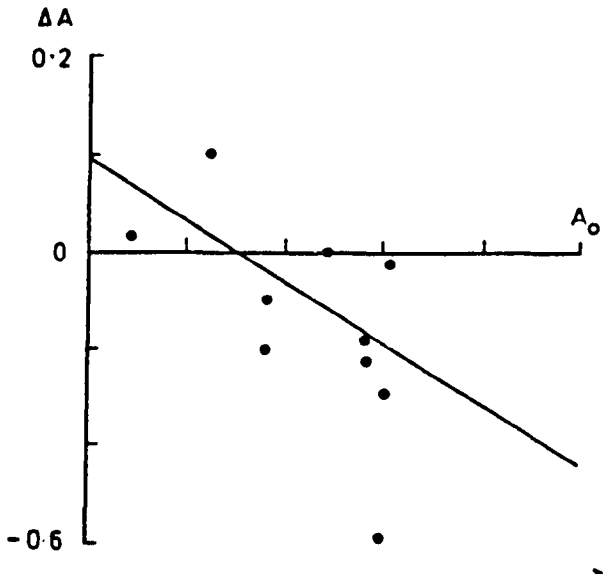

Fig.-2.6 Change of Anisotropy vs Initial Anisotropy during shear deformation of clay (Smart, 1993)

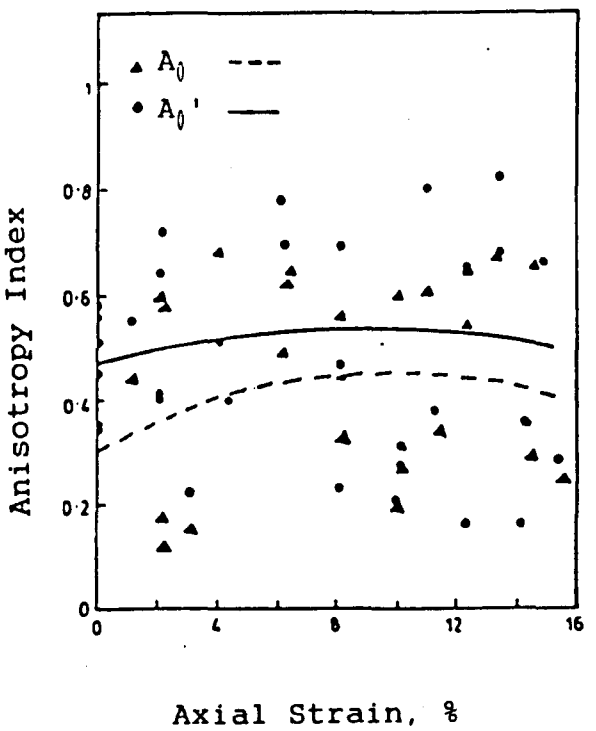

Fig.-2.7 Anisotropy index vs axial strain (Bai & Smart, 1994)

However, it has been proposed that the anisotropy index starts at a moderate value and ends at a moderate value. At the early stages of the test, the anisotropy index seems to increase; and at the later stages of test, it seems to decrease.

Permeability of clay is very much influenced by fabric. Fabric anisotropy therefore could cause substantial permeability anisotropy, although the relationship is rather indirect and it is unlikely that there would be a direct equivalence between the two measures of anisotropy. Indeed, as observed by Lapierre *et al.*(1990), quantified, intense fabric anisotropy as observed using the SEM may only indicate moderate permeability anisotropy, for the case of intact Louiseville clay and Champlain Sea clays of Canada. Otherwise, the most obvious effects of fabric anisotropy on permeability anisotropy are due to the laminations and continuous permeable lenses often featured in varved and lacustrine clays (Rowe,1972); recent studies on permeability of Bothkennar clay and soil fabric indicate permeability anisotropy of as high as 8 due to the presence of silt and fine sand laminations (Little *et al.*, 1992). Data regarding permeability anisotropy r_k (= k_h / k_v) for sands and clays have been scarce and scattered. It is not uncommon to see values of r_k calculated from values of vertical and horizontal permeability that were each obtained from different types of permeability tests, direct or indirect, or even *in-situ* and in the laboratory. This is evident when one refers to r_k values and the types of soils that go with them as tabulated in various sources (see for example Robertson & Campanella, 1983; Leroueil,1988; Chapuis *et al.*,1989). Many of the data available fall into two broad groups: (1) those related to stratified, varved and layered soils and clays such as are encountered in embankments and dams and (2) those related to uniform homogenous clays where material anisotropy can be described on a microscale.

Remoulding an undisturbed clay has been found to reduce the permeability of several clays by a factor of from 1 to 4, with an average of about 2 (Mitchell, 1956). Not much is known of the effect of remoulding on permeability anisotropy. Some indications of permeability anisotropy, r_k, reported by various investigators are shown in *Table*-2.4 for natural and laboratory prepared clays. Values of permeability anisotropy are probably less certain by comparison with values for other types of anisotropy (for example, anisotropy of strength or stiffness or deformation response). Where the need to use permeability anisotropy arises, considerable engineering judgement is of upmost importance in order to arrive at the most appropriate quantity. This difficulty in obtaining data on permeability anisotropy may be attributed to the problems of sampling and setting up of samples for permeability testing, which inevitably lead to some disturbance and destruction of the soil fabric, and also to the very wide range of permeability values that may be measured. The restoration of *in-situ* effective stresses for permeability testing after samples are retrieved from the

ground often involves stress paths that will produce significant changes to the fabric and hence to the actual permeability of the sample.

Table-2.4 Some values of permeability anisotropy of clays

Soil types and brief description		Values of r_k	Reference
Uniform, homogeneous	Fissured, layered or varved		
Undisturbed samples of several different clays		less than 1 to more than 7	Mitchell,1956
	Laminated plastic clay from Govan, Glasgow	1 to 4	McKinlay. 1961
1-D consolidated kaolinite 4 to 256 atm		1.3 to 1.7	
Illite and Boston blue clay over 200 atm		0.9 to 4.0	Olsen, 1962
Kaolinite over range of e for σ_v' up to 4atm		2	Morgenstern & Tchalenko,1967a
	Varved clay from New Liskeard	3 - 5	Chan & Kenney, 1973
Massive marine clays		1.1	Larsson, 1981; Tavenas *et al.* 1983a
Rio de Janeiro soft clay. No sand or silt lenses were found. Predominantly kaolinitic in nc range		1.5 - 2.1	Lacerda *et al.*, 1977
Marine clays		1 - 1.5	
	Varved clays	1.5 - 40	Olson & Daniel. 1981
1-D lab. consolidated kaolin		3/e e=void ratio	Al-Tabbaa & Wood, 1987
1-D lab.consolidated kaolin. Hydrostatic when measuring k.			Aiban & Znidarcic, 1989

Field values of r_k for soft clays:		
No macrofabric, or slightly developed macrofabric, essentially homogeneous deposits.	1 - 1.5	
From fairly well to well-developed macrofabric, eg. sedimentary clays with discontinuous lenses and layers of more permeable material.	2 - 4	
Varved clays and other deposits containing embedded and more or less continuous permeable layers.	3 - 15	Jamiolkowski *et al.*, 1985 (cited in Leroueil, 1988)
Natural clay with no evidence of layering.	1.2±0.2	
Slight layering eg. sedimentary clays with occasional silt dustings to random lenses.	2 to 5	Baligh & Levadoux, 1980
Varved clays in Northeastern U. S.	10±5	(in Robertson &Campanella, 1983)
nc and loc London clay	2	Chandler *et al.*, 1990

CHAPTER 3

3. APPARATUS AND EXPERIMENTAL PROCEDURE

3.1 Introduction

Within the scope of the present research, a programme of experimental work is planned to meet the aims stated in Section 1.1 earlier. In brief, permeability measurements are carried out on samples of supreme kaolin after they have experienced a number of different sample preparation and setting up as shown in *Fig.*-3.1 and as described in *Part 1* and *Part 2* also in Section 1.1. The various stages of the experimental work are as described in Section 3.2 below.

Consideration of the various factors that contribute to the sources of error in permeability measurement, as reviewed in Section 2.2, indicates the need for proper assembly of equipment and materials together with correct testing procedures.

Many of the so-called constant head test lack the ability to provide a truly constant pressure head through the sample when the water interface for the inflow and outflow are monitored in the vertical direction. Significant errors resulted when testing is performed at low gradients. Also, the use of deaired water as the permeant would become meaningless when back pressure is allowed at the pressurised air/water interface without any form of impermeable membrane. The effect of neglecting this aspect of equipment details would result in a high air content in the previously deaired permeant resulting in dissolved air bubbling out of the specimen during the dismantling stage at the end of permeability test. Dissolved air in the water must be cut to a minimum so that no appreciable differences in the air content exist at the inflow and outflow boundaries of the sample because internal swelling and consolidation within these boundaries could possibly lead to error in volumetric or induced pressure measurement. Olsen(1966) indicated the suitability of the constant flow rate test set up for achieving this requirement and more recently similar principle was introduced for volatile permeants (Fernandez & Quigley,1985; 1991).

Consequently, a completely closed circuit pressure system is assembled in which the movement of permeant for the volume and pressure measurement is held in the horizontal direction. The apparatus set-up is suitable for either the constant flow rate or the constant head permeability testing by implementing minor changes in testing procedure. The apparatus and sample set-up is explained in Section 3.3 which follows.

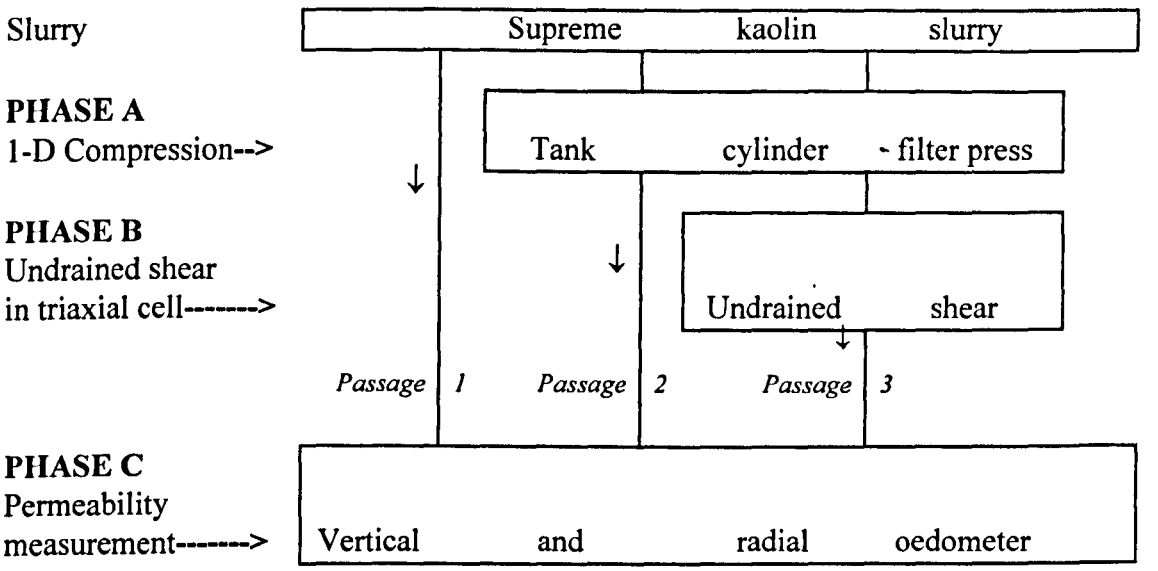

Fig.-3.1 Phases of testing in Phase A: Slurry consolidation, Phase B: Sampling, set up and shear, and Phase C: Sampling, set up and permeability

3.2 Programme of experimental work

3.2.1 Phases of testing

Three phases of testing are involved namely, Phase A: Consolidation of slurry in tank and cylinder, Phase B: Sampling, setting up and undrained shear in triaxial cell, and Phase C: Sampling, setting up and permeability testing in oedometers.

All tests are conducted on samples of kaolin which originate from the same batch of slurry. The actual relationship between the various phases of testing is also shown in *Fig.*-3.1. Thus for one value of consolidation pressure three pairs of permeability data (vertical and horizontal) could be obtained from tests in Phase C which is sufficient to enable the investigation into the influence of stress history on permeability anisotropy of the clay to be made.

The essential steps in each phases of testing are outlined in *Table* 3.1.

3.2.2 Testing programme

An overall schedule of the testing programme is shown in *Fig.*-3.2. This schedule shows the three phases of testing to be carried out on the clay and the approximate duration of testing for each phase in relation to each other.

Phase A consists of one dimensional consolidation of the kaolin slurry in 300mm dia. circular steel tank and 100mm dia. aluminium cylinder. The object of this phase of test is to produce high quality uniform clay samples. Consolidation of the clay slurry takes place in conditions of full saturation with double drainage in vertical directions. Details of the loading history are shown in *Table*-3.2. Initial vertical pressure was 10kPa (ie. at consolidation stage S1 in *Table*-3.2). The next increment was 10kPa (ie. S2) and thereafter the pressure increment was 20kPa. The next pressure increment was introduced after completion of the primary consolidation stage under the previous stress observed from the usual interpretation of settlement versus $\sqrt{t}$ or settlement versus log t curve.

Normally, this phase of the testing programme was temporarily halted to make way for cutting for the block sample and waxing.

In relation to field conditions, natural clays as they occur in situ have been deposited by sedimentation in lakes or seas, and they have been consolidated under one dimensional strain condition. Consequently, the stress history adopted in Phase A of the experimental programme should represent a reasonable duplication of the stress history experienced by natural clays.

Table-3.1 Essential experiment checklist in the testing programme

Phases of testing	Description of test
Phase A	Consolidation of slurry in tank, cylinder or filter press 1. loading 2. permeability tests
Phase B	Undrained shear of samples from tank, cylinder or filter press 1. unload from tank, cylinder or filter press 2. set up 3. back pressuring and reconsolidate 4. load to near failure 5. unload, sample out and trim 6. set up in oedometer for permeability test
Phase C	Tests in oedometer 1. unload from tank, cylinder or filter press 2. sample out and trim 3. set up 4. vacuum and back pressuring 5. reconsolidate 6. permeability tests 7. unload 8. sample out and final measurement (ht., water content)

	Year 1				Year 2				Year 3			
	1	2	3	4	1	2	3	4	1	2	3	4
Phase A												
Consolidation of slurry in tank and cylinder	***	***	***	***	***	***	***	***				
Permeability tests		**	**	**	**	**	**	**	**			
Phase B												
Sampling, setting up and undrained shear tests in triaxial cell			**	**	**	**	**	**	**	**	**	**
Phase C												
Sampling, setting up and permeability tests in oedometers	***		***		***		***		***		***	
	***	***	***	***	***	***	***	***	***	***	***	***

Notes: * ≡ 4 weeks

Fig.-3.2 Schedule of testing programme

Table-3.2 Load history for slurry in tank and cylinder

σ_v' kPa	L	UL,S	RL	UL.S	RL	UL,S	RL	UL,S	RL	UL,S	RL	UL,S	RL	UL,S	RL	UL,S	RL	UL,S
0	S0	US0	.	US10	.	US20	.	US30	.	US40	.	US50	.	US60	.	US70	.	US80
10	S1	.	.	.	.	.	.	.	.	.	.	.	.	.	.	.	.	.
20	S2	US2	RS2	US12	RS12	US22	RS22	US32	RS32	US42	RS42	US52	RS52	US62	RS62	US72	RS72	US82
40	S3	.	.	.	.	.	.	.	.	.	.	.	.	.	.	.	.	.
60	S4	→↑	RS4	US4	RS14	US14	RS24	US24	RS34	US34	RS44	US44	RS54	US54	RS64	US64	RS74	US74
80	S5	←	↵	.	.	.	.	.	.	.	.	.	.	.	.	.	.	.
100	S6			.	.	.	.	.	.	.	.	.	.	.	.	.	.	.
120	S7	.	→	↑	RS7	US7	RS17	US17	RS27	US27	RS37	US37	RS47	US47	RS57	US57	RS67	US67
140	S8	.	←	.	↵	.	.	.	.	.	.	.	.	.	.	.	.	.
160	S9					.	.	.	.	.	.	.	.	.	.	.	.	.
180	S10	.	.	→	.	↑	RS10	US10	RS110	US110	RS210	US210	RS310	US310	RS410	US410	RS510	US510
200	S11	.	.	←	.	.	↵	.	.	.	.	.	.	.	.	.	.	.
220	S12							.	.	.	.	.	.	.	.	.	.	.
240	S13	.	.	.	→	.	.	↑	RS13	US13	RS113	US113	RS213	US213	RS313	US313	RS413	US413
260	S14	.	.	.	←	.	.	.	↵	.		.	.	.	.	.	.	.
280	S15									.		.	.	.	.	.	.	.
300	S16	.	.	.	.	→	.	.	.	↑	RS16	US16	RS116	US116	RS216	US216	RS316	US316
320	S17	.	.	.	.	←	.	.	.	.	↵	.	.	.	.	.	.	.
340	S18											.	.	.	.	.	.	.
360	S19	.	.	.	.	.	→	.	.	.	.	↑	RS19	US19	RS119	US119	RS219	US219
380	S20	.	.	.	.	.	←	.	.	.	.	.	↵	.	.	.	.	.
400	S21													.	.	.	.	.
420	S22	.	.	.	.	.	.	→	.	.	.	.	.	↑	RS22	US22	RS122	US122
440	S23	.	.	.	.	.	.	←	.	.	.	.	.	.	↵	.	.	.
460	S24															.	.	.
480	S25	.	.	.	.	.	.	.	→	.	.	.	.	.	.	↑	RS25	US25
500	S26	.	.	.	.	.	.	.	←	.	.	.	.	.	.	.	↵	.
520	S27																	.
540	S28																	.
560	S29	.	.	.	.	.	.	.	.	→	.	.	.	.	.	.	.	↑

Notes: L - load; UL,S - unload followed by sampling out and set-up; RL - reload; Back pressure = 0 kPa; Arrow shows direction of unloading or reloading.

Phase B consists of anisotropic unloading, sampling, setting up, reconsolidation and performing consolidated isotropically undrained triaxial compression test (CIU) on the block samples taken from Phase A test. This phase is meant to obtain the test specimens after the kaolin slurry has been consolidated anisotropically in the tank and cylinder. Maximum vertical consolidation pressures chosen were 100kPa and 600kPa before the removal operation for the block samples were performed. Samples obtained after the CIU tests therefore fall into 2 groups:

Group I - σ'_{vmax} = 100kPa

σ'_3 = 100kPa

σ_3 = 300kPa (since u_b = 200kPa)

Group II - σ'_{vmax} = 600kPa

σ'_3 = 300kPa

σ_3 = 500kPa (also since u_b = 200kPa)

These 2 groups of samples were then set up into oedometers for permeability measurements.

Phase C part of the experimental programme consists of permeability tests on samples obtained from Phase A and Phase B.

3.3 The apparatus and sample set-up

The equipment used to perform the consolidation and permeability tests consists of the hydraulic oedometers, hydraulic actuators (also called digital pressure controllers and hereinafter would be simply called GDS, after the manufacturer - GDS Instruments Ltd.), and the conventional air/bladder/water pressure cell for the provision of regulated fluid (water) pressure controls. A scheme of the equipment set-up is shown in *Fig.*-3.3. Two sets of such a set-up were assembled: one for the radial flow oedometer and the other for the vertical flow oedometer.

Pressurised deaired water is used to exert the necessary vertical stress to the top of the sample at the rubber jack chamber of the oedometer. This water comes from the air/bladder/water cell (see *Fig.*-3.3). Drainage through the clay specimen is controlled at the inflow and outflow boundaries by the pair of GDS devices, GDS 2 and GDS 1. Pressure and drainage lines are of the small bore nylon tubings (4mm O.D., 1.6mm I.D.) with push-pull quick fittings for the connections. Valves are of the 'on-off', no-volume displacement type. All tubings, couplings and valves are supplied by Legris.

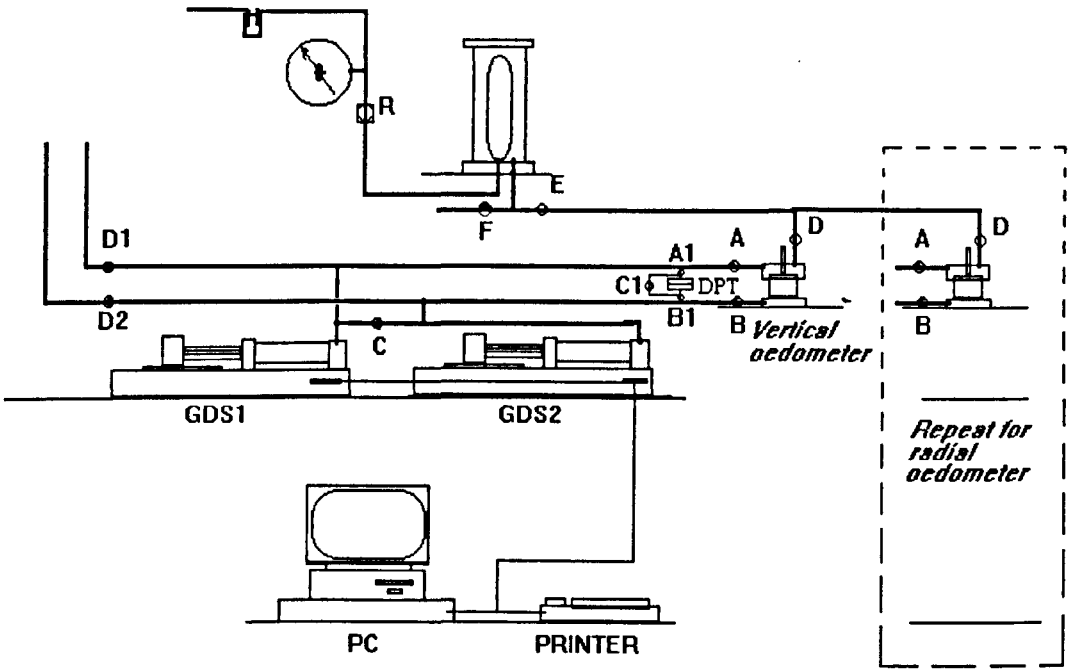

A, A1, B, B1, C, C1, D, D1, D2,

E & F - Valves

R - Pressure regulator

DPT-Differential pressure transducer

Fig.-3.3 Schematic of equipment set up for the consolidation permeability test

In a typical consolidation stage, the two GDS are programmed to maintain a constant backpessure in the sample (ie. at u_b = 50kPa) while volume changes occuring at the two sample boundaries are monitored to the nearest 0.5mm^3 with time.

For the triaxial testing standard triaxial equipment (Wykeham-Farrance Eng. Ltd.) is used consisting of a constant rate of deformation machine (mechanical jack operated by motorized gearbox), and triaxial cell for 100mm nominal diameter sample with specially made enlarged smooth platens.

3.3.1 Hydraulic oedometer for permeability testing

Hydraulic oedometers, (Rowe cells) were used to perform consolidation and permeability tests. A section of the vertical and radial flow Rowe cells are shown in *Figs.*-3.4(a) and 3.4(b) respectively. For the mesurement of vertical permeability the oedometer was used in the standard way: ie. pressure difference is introduced between the bottom and top drainage boundaries of the specimen and the resulting volume of inflow and outflow is monitored with time (constant head test). Likewise, in the constant flow rate test, a constant flow rate is introduced at the bottom(inflow) and withdrawn at the top(outflow) boundaries of the specimen, and the resulting pressures developed at the boundaries are monitored with time.

For the measurements of the horizontal permeability, the oedometer base was slightly modified to enable a porous central drain to move downward as the sample consolidates during consolidation stage. This technique, developed by Al-Tabbaa & Wood (1987), avoided the use of sand drain (Shields & Rowe, 1965) or geotextile material (Leroueil *et al.*,1990) which may easily interfere with vertical compression of the specimen as well as making the specimen lose some lateral confinement at the vicinity of the central drain. A similar technique but with the central drain fixed in position while the top platen slide through it had been used by Lefebvre *et al.*(1984) in measuring horizontal permeability of peat in a radial flow, one dimensional oedometer. Moser (1977) also used a perforated metal tube which could glide in a casing in the bottom of the container so as not to hinder the settlement of the clay. During a constant flow rate permeability test, a constant flow rate is introduced at the central drain (inflow) and withdrawn at the peripheral drain (outflow), and the resulting pressures developed at these boundaries are monitored with time.

The drainage ports of each oedometer were connected to the two GDS (GDS 1 and GDS 2) which provide the facility for pressure and volume controls. A microcomputer linked to the two GDS performs two main tasks: (1) Data acquisition and logging, and (2) providing the necessary control during consolidation or permeability tests.

(a)

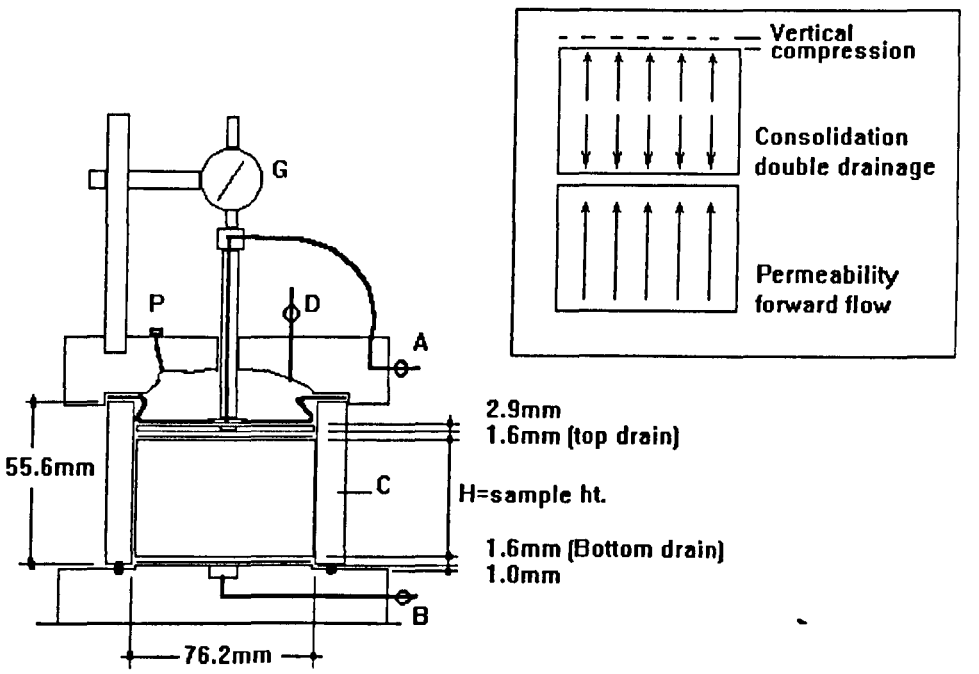

(b)

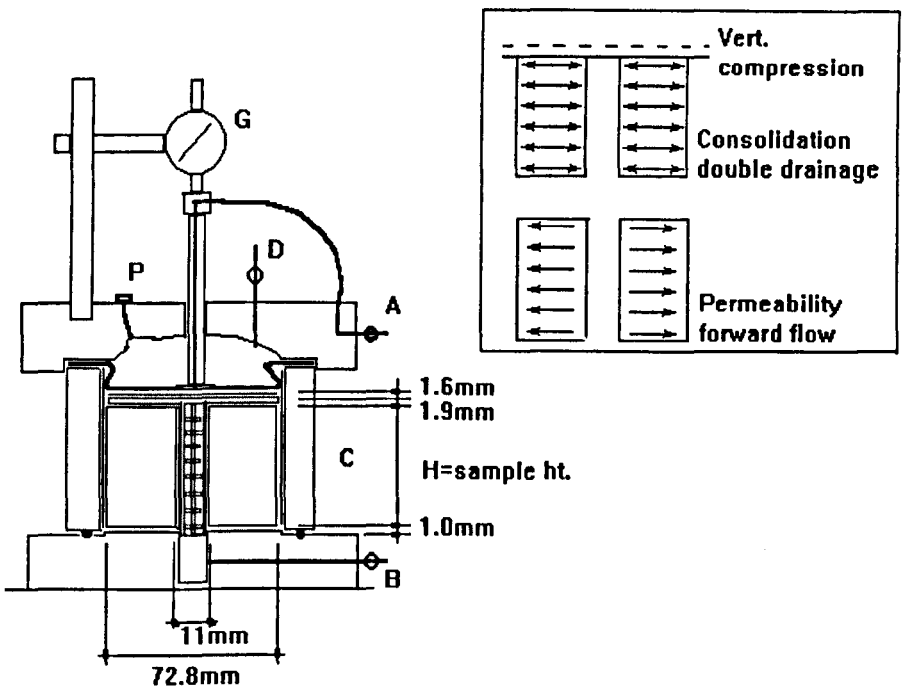

Fig.-3.4 Vertical section of the hydraulic oedometer (a) Vertical flow; (b) Radial flow

3.3.2 Triaxial cell for shearing test

The triaxial cell used is shown in *Fig.*-3.5(b), consists of cell base (A), cell body integrated with top cover (B), loading piston or plunger (C), and the two loading caps (base pedestal and top cap). The plumbing arrangement connected to the triaxial cell is shown schematically in *Fig.*-3.5(a) to allow for application of cell pressure and back pressure to the specimen, and measurement of sample volume changes and pore water pressure in the specimen as appropriate. The built-in valves connected to the cell base are denoted in the *Fig.*-3.5(b) as: A(pore pressure line), B(back pressure line), C(cell pressure line), and D(optional back pressure line). In all stages of the test, pore water pressure is measured at the base of the specimen using an electrical pressure transducer (furnished by Bell & Howell Ltd., Type 4-327-L226, serial No. L82913, Range 0-150psi. operated with a Sensonics Ltd. Signal conditioning system). The output of the transducer was monitored with a digital voltmeter (ie. Multimeter Precision Gold M125). The back pressure is applied to the specimen at both top and bottom ends through valves B and D. Any volume changes occurring in the sample during saturation and consolidation stage are monitored by movement of the red-dye paraffin/water interface in vertical burette (resolution, 0.01cc., 25cc.capacity) connected to the back pressure line [*Fig.*-3.5(a)].

The axial deformation of the sample was measured by means of Mercer dial gauge (G1) sensitive to 0.001" (0.0254mm) movement and has a travelling range of 2.0" (50.8mm). The gauge was fitted to rigid attachments at the bottom of the proving ring and rested on adjustable arm clamped to pillars screwed on the top cover of the triaxial cell. The high tensile steel proving ring (Y), (Type No.800, Serial No.1070) attached between the top of the triaxial plunger and the crossbar of the load frame was used to measure the axial load. It has a compression capacity of 10kN and a stiffness constant of 1.6N/div. of the load dial gauge (G2) also of Mercer type.

Compression testing of triaxial samples sitting on standard pedestals often results in non-uniformity of stresses and strains within the sample because of the frictional restraint acting between the platens and the sample ends. The indications of non-uniformity have been observed by measurements of moisture contents (Olson,1960), pore pressures, (Blight,1963), and the axial and radial strain distributions (Roscoe *et al.*,1963; Januskevicius & Vey,1965). Many triaxial testings have since used frictionless pedestals introduced by Rowe & Barden (1964) to reduce this friction effect and obtained a more uniform distribution of stresses and strain in the sample (Bishop & Green,1965). The consequent uniformity is also reflected in a more uniform distribution of pore water pressures in undrained tests.

The end caps used in this study take the form of smooth perspex surface with enlarged diameter of 118mm to allow for any radial strain exceeding 10%. Drainage surfaces (12mm dia.) are provided at the centre of the caps and connected to drainage ports through 1-mm diameter drilled holes. Negligible friction is obtained between the

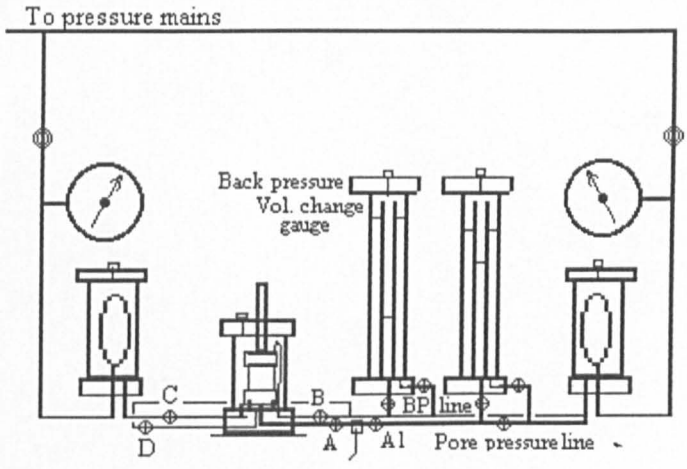

(a)

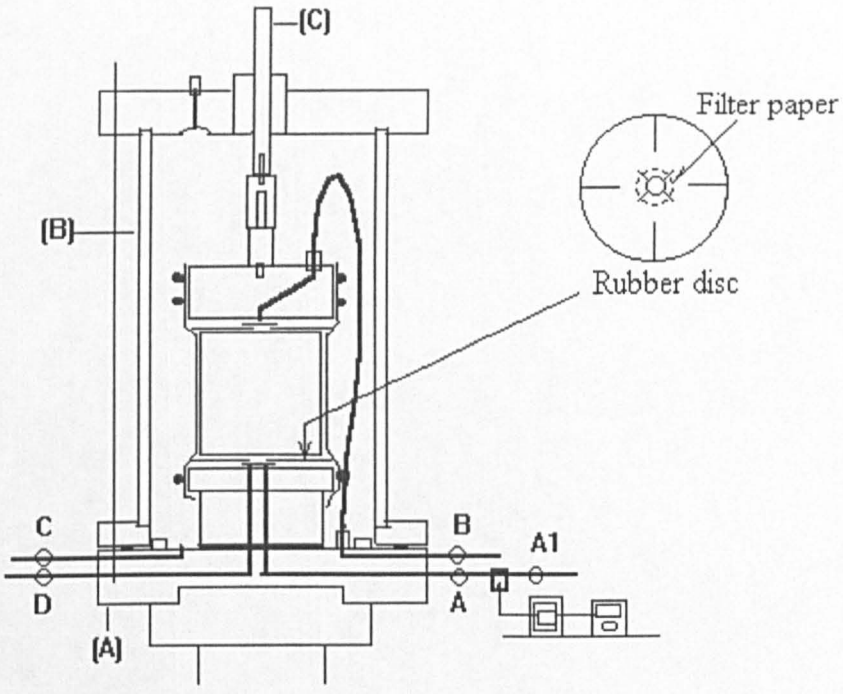

(b)

Fig.-3.5 Triaxial cell for 100mm diameter sample: (a) General layout;

(b) Details of cell and sample set up

specimen ends and the loading caps by lubricating the latter and placing a layer of rubber membranes (dia.=102mm, thk.=0.2mm). To allow for drainage and pore pressure measurement, a central hole 10mm dia. is made on the membranes to coincide with drainage areas at the top and base pedestals. Also, four radial cuts, 17mm long are made at right angles on the menbranes to minimise circumferential stress arising as a result of radial expansion at the ends of the specimen during compression test. A screw connection at the top cap ensure that specimen surface remains horizontal and tilting is avoided.

3.4 Experimental procedure

3.4.1 Consolidation test

After the sample had been set up in the oedometer and the apparatus assembled as in *Fig.*-3.3, the volumes displayed by the two GDS and the dial gauge reading, indicating the current position of the sample, were recorded. C and D1 were opened. The jack pressure was raised from 0 to 5kPa basically to provide an initial seating pressure and close up any gaps that might occur at the sample boundaries. A pressure of 5kPa was arbitrarily chosen to overcome the initial friction that might develop between the rigid top plate and side of the oedometer ring. This pressure was also small enough to avoid any squeezing out of the slurry. For block sample the initial jack pressure of 10kPa was used. When the dial gauge reading ceased to move indicating completion of consolidation, the jack pressure was further raised to 10kPa for the case of slurry sample. After consolidation was complete valves C and D1 were closed.

The sample was then ready for back pressuring stage and followed by consolidation stage which formed part of the main test. The proposed application of vertical effective stress to the specimen in the consolidation test is shown in *Table* 3.3.

Typically, consolidation under a given load increment was allowed to occur over a period of 24h followed by permeability measurement over the next couple of hours.The test cycle was then repeated for the next load increment. The resulting actual loading history for a typical test series is shown in *Fig.*-3.6.

In the consolidation test, the equal strain loading to maintain a uniform sample thickness was applied with double drainage occuring for both the vertical and radial flow oedometers. To start the test the initial conditions of the apparatus and specimen have normally reached the following conditions:

Valves: A, A1, B, B1, D, E - open;

C, C1, D1, D2, F - closed;

GDS 1 and GDS 2: Target pressure set to 50kPa and data logging was switched on;

Cell pressure regulator, R: Pressure set to 60kPa;

Dial gauge, G: Readings monitored regularly until completion of consolidation was evident.

This initial stage had been previously set and left for about 24h to let the specimen stabilise with a pore pressure of 50kPa and vertical effective stress of 10kPa. The dial gauge reading was noted and the data logging was switched on at 1-min interval.

Consolidation test commenced by quickly adjusting the cell pressure regulator R to raise the jack pressure to 70kPa and immediately start recording the dial gauge readings at elapsed times of 15, 30s, 1, 2, 4, 8, 15, 30min, 1, 2, 4, 8, and 24h. It was advisable (to avoid excessive data too closely spaced) that after the first 15min, to log the GDS at 15-min interval.

Data recorded were given serial name H2 and V2 (typical) for the radial and vertical drainage cases respectively. The data consisted of pressure and volume quantities corresponding to elapsed time. In the serial names above, H represents radial flow and V the vertical flow case. The numeral 2 represents the consolidation stage taking place ie. at the vertical consolidation stress of 20kPa. This system of serial names is similarly applied to permeability data.

The above is a typical consolidation test run on the sample which is followed by permeability tests and the consolidation test repeated for the next vertical consolidation stress of 40kPa ie. R increased to 90kPa. It was noted that when performing consolidation tests, closing and opening of valves was avoided as much as possible to minimise the effects of vibration and disturbance on the sample.

3.4.2 Permeability test

Two methods of permeability tests namely the constant head and constant flow rate were performed on the specimens to provide comparative results and investigate the merits of each method. In all tests, the pressure head required to initiate flow or that induced was limited up to 30% of the current consolidation pressure to minimise the problem of seepage induced consolidation. Flow was from bottom to top for the vertical flow oedometer and radially from the central to the peripheral drains for the radial flow oedometer. These flow directions are denoted as forward flow [see

Table-3.3 Load history for slurry or block samples during consolidation/permeability tests

σ_V'	σ_V			*Vertical flow oedometer*				*Radial flow oedometer*			
kPa	kPa			L	UL	RL	UL	L	UL	RL	UL
0	50		S0			.	UV0		.	.	UH0
10	60		S1	V1	UV1	.	UUV1	H1	UH1	.	UUH1
20	70		S2	V2	.	.	.	H2	.	.	.
40	90		S3	V3	UV3	RV3	UUV3	H3	UH3	RH3	UUH3
60	110		S4	V4	.	.	.	H4	.	.	.
80	130		S5	V5	UV5	RV5	.	H5	UH5	RH5	.
100	150		S6	V6	.	.	.	H6	.	.	.
120	170		S7	V7	UV7	RV7	UUV7	H7	UH7	RH7	UUH7
140	190		S8	V8	.	.	.	H8	.	.	.
160	210		S9	V9	UV9	RV9	.	H9	UH9	RH9	.
180	230	→	S10	V10	↑	RV10	.	H10	↑	RH10	.
200	250	←	S11	V11	←	↵	UV11	H11	←	↵	UH11
220	270		S12	V12			.	H12			.
240	290		S13	V13			.	H13			.
260	310		S14	V14			.	H14			.
280	330		S15	V15			UV15	H15			UH15
300	350		S16	V16			.	H16			.
320	370		S17	V17			.	H17			.
340	390		S18	V18			.	H18			.
360	410		S19	V19			UV19	H19			UH19
380	430		S20	V20			.	H20			.
400	450		S21	V21			.	H21			.
420	470		S22	V22			.	H22			.
440	490		S23	V23			UV23	H23			UH23
460	510		S24	V24			.	H24			.
480	530		S25	V25			.	H25			.
500	550		S26	V26			.	H26			.
520	570		S27	V27			UV27	H27			UH27
540	590		S28	V28				H28			
560	610	→	S29	V29	→	→	↑	H29	→	→	↑

Notes: L - load; UL - unload; RL - reload; Back pressure = 0 kPa; Arrow shows direction of unloading or reloading.
Back pressure in sample, u=50kPa;
Jack pressure $= \sigma_V$;
Consolidation pressure $= \sigma_V'$

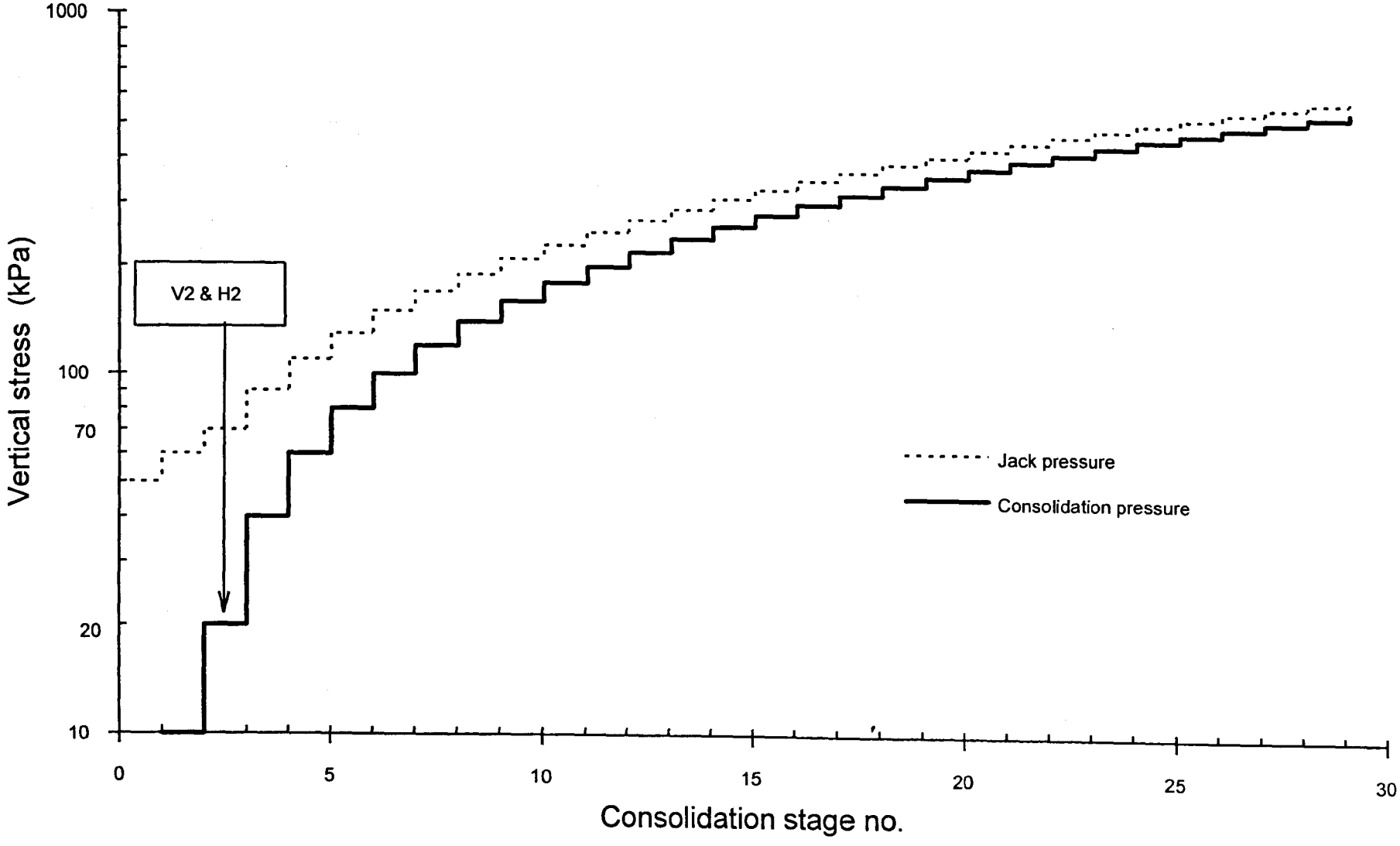

Fig.-3.6 Loading history for the consolidation / permeability test

inset of *Figs.*-3.4(a) & 3.4(b)]. Also by this convention, reverse flow is denoted by flow from the top to bottom drains for the vertical flow oedometer and radially from the peripheral drain to the central drain for the radial flow oedometer, respectively.

Application of pressures or flow rate from the GDS to the specimen boundaries were completely controlled from the computer. Similar to starting the consolidation test, closing and opening of valves were avoided. Starting or stopping of flow in permeability tests was accomplished from the computer keyboard.

Permeability tests using various gradients (or flow rates) during forward flow and reversed flow were also performed to check the general validity of Darcy's law. Side flow along the impervious boundaries, if it ever exists might give rise to an important source of error in permeability values. This needs to be checked especially at low consolidation pressure and if the pressure difference applied was excessive in relation to the stress at the boundaries. From permeability test of specimen in triaxial cell, the effective lateral stress required to avoid side flow was found to be in the order of 25kPa. (Tavenas *et al.*,1983:I). Testing at various gradients (or flow rates) would therefore help identify whether side flow occurs or not.

Procedures to carry out permeability tests are described below.

3.4.2.1 Constant head test

This test was normally performed first after the end of every consolidation stage. However, the constant flow rate test was sometimes performed first in order to observe the time taken by the transient phase to reach steady state condition of the flow process.

In the constant head test, a constant pressure difference was imposed across the specimen and the resulting flow was monitored with time. The initial conditions of the apparatus and specimen were checked and should be similar as for the consolidation test with the exception that R (the cell pressure regulator) being set to a particular total consolidation pressure. Dial gauge reading was also noted before permeation started to verify that volume change in the specimen had diminished. As an example, a test run following completion of consolidation stage H2 is described.

It was required to create a constant pressure difference across the inner and outer drainage boundaries and this was achieved by setting pressures in GDS1 and GDS2 to 49.5kPa and 50.5kPa respectively giving a pressure difference of 1kPa. A constant head gradient was thus imposed [average gradient = $\Delta p / (\gamma_w \Delta R) = 1$ kPa / (9.81 kN/m^3 x 0.0307 m) = 3.2] between the central and peripheral drain, when the GDS were logged, hence starting the permeability test.

The GDS were initially logged at 1-min interval for the first 15 min and later on switched to 15-min interval. Monitoring of the observed inflow and outflow volumes was followed from the recorded data and when their difference became constant or reached negligible values, the next method of permeability test could proceed. Data from constant head test were given serial names 3H2 and 3V2 for radial and vertical flow respectively. (note - Serial names were given at the start of logging on the computer when data files were created and stored in the computer hard disc).

3.4.2.2 Constant flow rate test

Constant flowrate permeability test was performed either after the constant head test to take advantage of the steady state flow condition which had then developed or immediately following the consolidation stage. In this test a constant flow rate (in at one boundary and out at the other), was introduced through the specimen and the corresponding induced pressure difference developed was then monitored with time.

The test was started by setting GDS1 and GDS2 into withdrawal and infusion modes respectively. This was done by setting +ve. and -ve. ramps of volume change with time on GDS 1 and GDS 2, respectively, and logging the data at 1-min interval. Once the pressure difference monitored became constant with time, the test was concluded. If the test was performed immediately following the consolidation stage, the development of the pressure difference from zero to a steady value indicated the transient phase of the test.

Pressures in the GDS were again set back to the initial backpressure (ie. 50 kPa) which was maintained throughout the consolidation stage.

Data logged from the constant flow rate test were given serial names 4H2 and 4V2 for radial and vertical flow respectively. Here volumes recorded were the controlled quantities whereas the pressures were the measured quantities to be monitored. A ramp, R of 1s represents a constant flow rate of 0.5 mm^3/s or 5×10^{-4} cm^3/s. Similarly R = 10s produces a constant flow rate of 5×10^{-5} cm^3/s.

Consequently a suitable flow rate must be imposed such as to develop an induced pressure difference of not greater than 30% of the current consolidation pressure. Inspection of the earlier constant head test would provide a convenient magnitude of the flow rate required and hence the ramp value of the GDS controller. For example if the measured flow rate was observed to be 14.5 mm^3/min for stage H2 (σ'_v=20kPa), the ramp required would be $R = (5 \times 10^{-4}) / (14.5 \times 10^{-3} / 60) = 2.069s$ say 2.5s

and this would ensure a pressure difference induced not to exceed 1 kPa and less than 30% of σ'_v.

3.4.3 Triaxial shear test

In the triaxial shear test, the sample undergoes three main testing stages before the final compression is applied. The sample was subjected to: (1) saturation, (2) consolidation, and (3) compression stages. In all stages of the test, pore water pressure was measured at the base of the sample using an electrical pressure transducer (a Bell & Howell Ltd. type 4-327-L226, serial no. L82913, Range 0-150psi. - see Section 3.3.2). With this system, pore water pressure could be monitored over arbitrary ranges from a maximum range of 34.5kPa to a minimum range of 0.1kPa with a resolution of about 0.1kPa

The sample was saturated by back pressure applied in 3 increments. The back pressure was applied to the specimen following every undrained increment of cell pressure. The first two cell pressure increments were 50kPa and the third was 100kPa. A differential of 10kPa (ie. cell pressure - backpressure = 10kPa) is maintained after each backpressure increment. The final backpressure is 200kPa ie. when the cell pressure is 210kPa.

The consolidation stage follows immediately after the saturation stage. Consolidation of the specimen is isotropic although drainage condition is approximately one way (ie. toward the backpressure line at the top pedestal). The object of the consolidation stage is to bring the specimen to the state of effective stress required for carrying out the compression test. The effective stress in the specimen is increased to the desired value by raising the cell pressure and dissipating the resulting excess pore pressure to an appropriate backpressure. The specimen is consolidated in one single stress increment (ie. by completely opening valve B to start dissipation of the excess pore pressure). The end of primary consolidation was defined at 98% excess pore water pressure dissipation at the base of the sample.

The final stage in the triaxial shearing test series is the conducting of the undrained compression shear test. The test is designated as CIU test with pore pressure measurement. It is an isotropically consolidated undrained test. In the test during the compression stage the cell pressure is maintained constant while the specimen is sheared at a constant rate of axial deformation (ie. strain-controlled deformation) until a certain axial strain is reached. No drainage is permitted and therefore the moisture content remains constant during compression. The resulting changes in pore pressure are measured at the base of the specimen, and the rate of axial deformation is applied

slowly enough to ensure adequate equalization of excess pore pressures. Compression was carried out until vertical strain reached about 5%, 10% and 20% (proposed values) for each of the samples tested followed by sampling out and setting up in the hydraulic oedometers for permeability tests.

CHAPTER 4

4. THEORETICAL CONSIDERATIONS

4.1 Introduction

This Chapter presents the equations which are used in Chapter 5 to evaluate the vertical and horizontal permeabilities of supreme kaolin. Permeability equations from the constant head, constant flow rate (occasionally abbreviated as CFR), and falling head tests are all widely known and these are briefly stated in Section 4.2. Analysis of the initial transient phase of the CFR test is also considered to enable a development of the necessary governing equations and their solutions be made in order to evaluate the permeability and consolidation characteristics using data from permeability tests. Analysis for vertical flow is first considered followed by the radial flow case.

Solutions to the theories of one-dimensional consolidation applicable for vertical flow and radial flow are presented in Section 4.3. The extent of two- and three-dimensional consolidation has normally been examined using the simple diffusion theory of consolidation (Terzaghi,1943) or by means of the complete theory of consolidation formulated by Biot(1941). Terzaghi's theory considers only the flow of pore water through the clay mass, whereas the Biot theory considers consolidation as a process in which the pore water movement is coupled to the soil's deformation.

Developments of equations in Section 4.2 and Section 4.3 are mainly drawn from the analogous treatment of conduction of heat in solids (Carslaw & Jaeger,1959) and the theoretical model of well hydraulics (Domenico,1972 p.315).

4.2 Permeability tests

4.2.1 Constant head permeability test

For a constant head permeability test in which flow through the sample is purely vertical, see *Fig.*-3.4(a), the vertical permeability can be determined by a direct application of Darcy's law. The formula for vertical permeability k_V is given by:

$$k_V = (Q / t)(\gamma_W H / \Delta p)(1/A) \qquad (4.1)$$

where Q = volume of outflow or inflow;

t = elapsed time;

Δp = pressure difference between the inflow and outflow drainage boundaries;

H = height of sample;

γw = unit weight of water; and

A = cross sectional area of sample normal to direction of flow.

For the same permeability test but in which the flow is purely radial across the sample annulus, see *Fig.*-3.4(b), the horizontal permeability k_h, can also be determined by a direct application of Darcy's law to give,

$$k_h = [1 / (2\pi)](Q / t)(1 / H)(\gamma_W / \Delta p)\ln (D/d) \qquad (4.2)$$

where D = diameter of sample;

d = diameter of central drain well; and

Q, t, Δp, H and γ_W are as defined earlier.

In Eqs.-(4.1) and (4.2), in addition to Darcy's law, the following are assumed:

(1) steady state condition, and (2) the permeability of the clay sample is uniform and remains constant with time.

4.2.2 Constant flow rate permeability test

Calculations of permeability are determined from the same formulae as those for the constant head test. The term (Q/t), however, represents a controlled constant flow rate imposed on the sample which depends on the ramp R of the GDS and the pressure difference induced Δp, should be the steady state value. The digital pressure controller, GDS, used in this testing, produces a constant flow rate of $0.5mm^3/s$ when the ramp R is designated as 1s. Thus the relationship between (Q/t) and R is given by:

$$(Q/t) = 0.5/R \ mm^3/s \qquad (4.2a)$$

where R is in s.

4.2.3 Falling head permeability test

This test is used to measure vertical permeability k_V of the sample in the cylinder as shown in *Fig.*-4.1.

$$k_V = \frac{aL}{A(t_2 - t_1)} \ln\left(\frac{H_1}{H_2}\right) \tag{4.3}$$

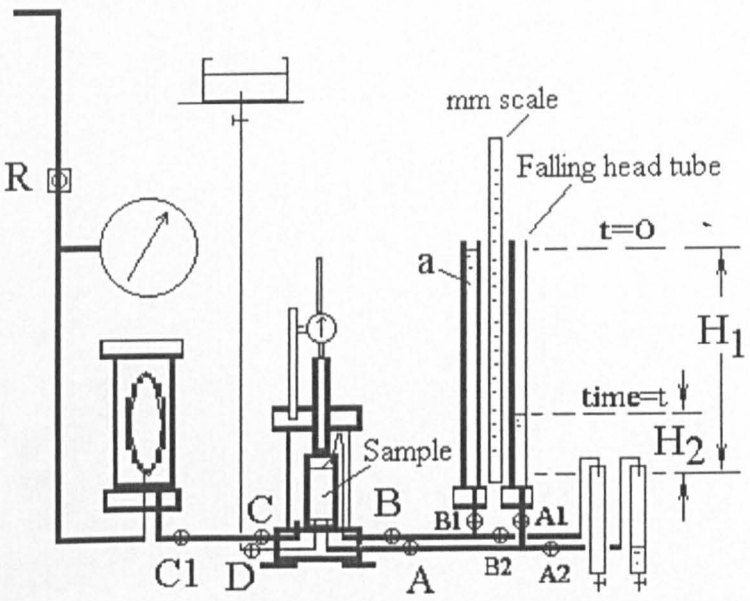

$$k = \frac{aL}{A(t_2 - t_1)} \ln\left(\frac{H_1}{H_2}\right)$$

$$\Delta t = \frac{a\,L}{k\,A} \ln H_1 - \frac{a\,L}{k\,A} \ln H_2$$

$$k = -\frac{a\,L}{A\,S}$$

where S = slope of (Δt vs ln H_2) plot, $\Delta t = (t_2 - t_1)$, L= length of sample.

Fig.-4.1 Permeability of sample by the falling head permeability test

where L = height of sample;

H_1 = height of water level in falling head tube above datum at time t_1;

H_2 = height of water level in falling head tube above datum at time t_2;

and a = cross sectional area of the falling head tube.

4.2.4 Transient phase of the constant flow rate permeability test

4.2.4.1 Vertical flow

In the constant flow rate (CFR) permeability test, a constant flow rate of water is introduced at a drainage boundary of the sample and the same magnitude of flow rate is withdrawn at the other boundary. The induced differential hydraulic head across the two boundaries is measured. The record of the induced differential head with time observed consists of the initial transient phase which eventually stabilises to a steady state value across the sample. A corresponding value of permeability is determined from this steady state value using Darcy's law. This technique of permeability testing has been developed by Olsen(1962,1966,1969) and has since been adopted by others in permeability testing of soils [e.g.Fernandez & Quigley 1985,1991; Aiban & Znidarcic,1989]. The original procedure of applying the constant flow rate by Olsen [Olsen(1962); Olsen *et al.*, 1985] slightly differed from the above description whereby the flow rate was introduced at one boundary while a constant head was maintained at the other. The CFR test has the advantage of eliminating some of the errors and limitations associated with the constant head or falling head permeability tests (Olsen *et al.*,1985; Aiban & Znidarcic,1989).

The transient phase of the CFR permeability test has been examined theoretically by Morin & Olsen (1987), who showed that, analogous to the problem of heat flow, the formulation is based on the same governing equation involving diffusion of excess pore pressures in the description of one-dimensional consolidation of clay. The boundary conditions, however, are of slightly different nature. Thus the differential head ratio termed as $\overline{H}$ [ie. as defined by Eq.-(4.7b)] in the CFR test is analogous to the average degree of consolidation $\overline{U}$ in the Terzaghi's theory of one-dimensional consolidation.

In the CFR permeability test (vertical flow), Morin & Olsen (1987) showed that the differential hydraulic head, h, can be described by (*Fig.*-4.2),

$$\frac{\partial h}{\partial t} = \frac{\kappa}{S_s} \frac{\partial^2 h}{\partial z^2} \qquad (4.4)$$

where for the sample, z = height, κ = hydraulic conductivity and S_S = specific storage or storativity.

Initial condition: $h(z,0) = 0$ at $0 \le z \le L$ (4.4a)

Boundary condition: $h(0,t) = 0$ $t \ge 0$ (4.4b)

$$\frac{Q}{\kappa A} - \frac{\partial h(L,T)}{\partial z} = 0 \qquad t > 0 \tag{4.4c}$$

Morin & Olsen (1987) based the solution of this problem on that presented by Carslaw & Jaeger (1959) for an analogous conductive heat transfer application, given by:

$$h = \frac{Q z}{\kappa A} - \frac{8 Q L}{\kappa A \pi^2} \sum_{n=0}^{\infty} \frac{(-1)^n \exp[-\alpha (2n+1)^2 \pi^2 t / (4L^2)]}{(2n+1)^2} \cdot \frac{\sin(2n+1)\pi z}{2L} \tag{4.5}$$

Where the term $\alpha = \kappa / S_S$ is the hydraulic diffusivity which is also the coefficient of consolidation, c_V. h is measured across the entire length of the sample. In the testing, h is measured at $z = L$ and $z = 0$, therefore putting $z = L$ reduces Eq.-(4.5) to the following expression:

$$h = \frac{Q L}{\kappa A} \left[1 - \frac{8}{\pi^2} \sum_{n=0}^{\infty} \frac{\exp[-\alpha (2n+1)^2 \pi^2 t / (4L^2)]}{(2n+1)^2} \right] \tag{4.6}$$

The time imposed condition of the experimental method is satisfied since $h = 0$ at $t = 0$ and also at large times, Eq.-(4.6) simplifies to the steady state solution defined by Darcy's law. Eq.-(4.6) provides a basis for graphical method of obtaining values permeability, κ and storativity, S_S of the sample from data of the CFR test. In terms of $\overline{H}$ and T_V, the analytical solution gives the familiar Terzaghi's solution for $\overline{U}$, the average degree of consolidation :

$$\overline{H} = 1 - \sum_{n=0}^{\infty} \frac{2}{M^2} \exp(-M^2 T_V) \tag{4.7}$$

where $$M = \frac{1}{2}\pi\ (2n + 1) \tag{4.7a}$$

$$\overline{H} = \frac{h\,\kappa\,A}{Q\,L} \tag{4.7b}$$

$$T_V = \frac{\alpha\ t}{L^2} = \frac{c_v\ t}{L^2} \tag{4.7c}$$

Eq.-(4.7) plotted on logarithmic scales produces a unique type-curve solution for the flow model of *Fig.*-4.2. The type-curve is shown in *Fig.*-4.3. By matching

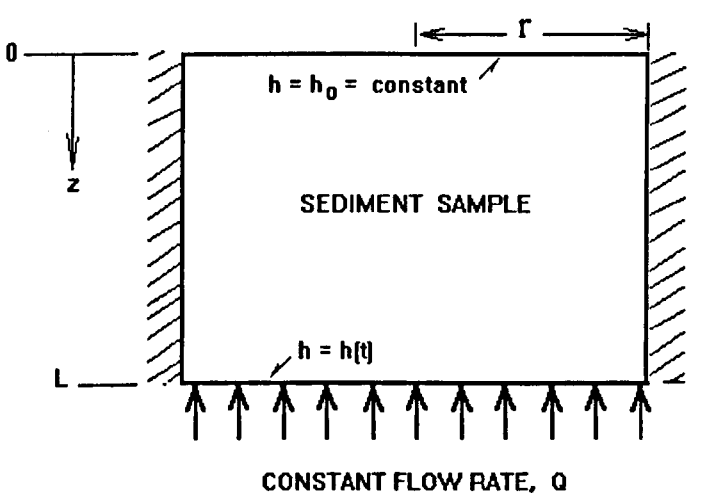

Fig.-4.2 Constant flow rate test: Vertical flow - Problem formulation for development of pressure difference (Morin & Olsen, 1987)

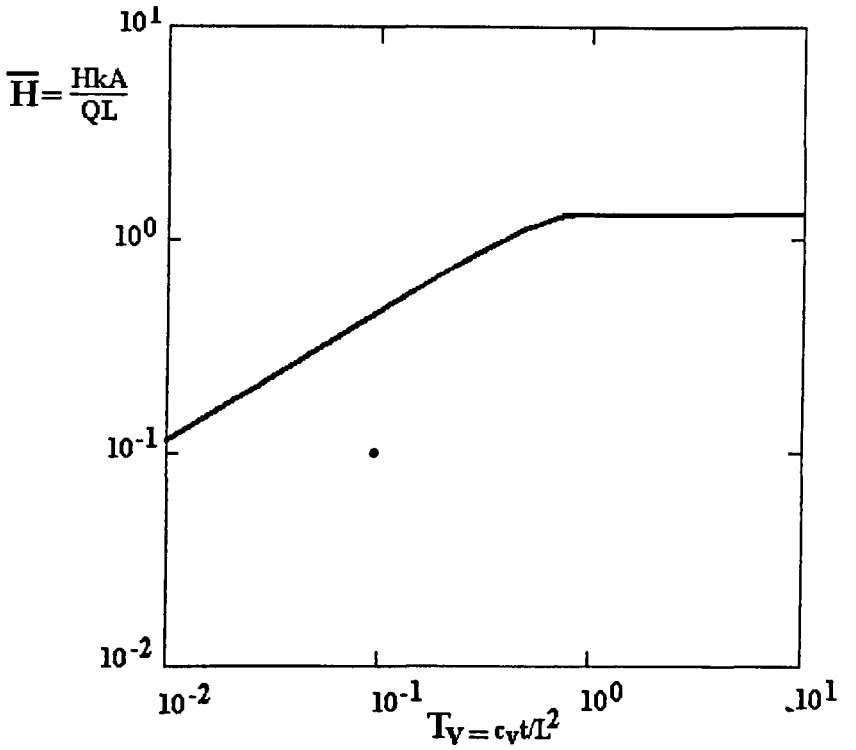

(a)

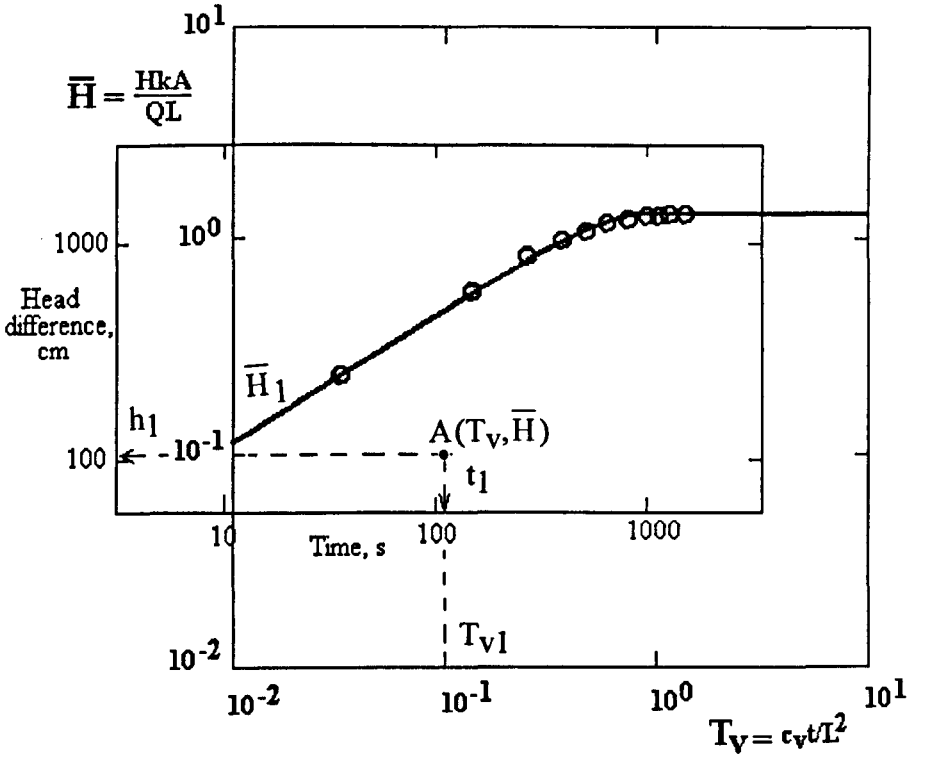

(b)

Fig.-4.3 (a) Type curve of Eq.-(4.7); (b) Curve matching of constant flow rate permeability data to analytical type-curve (Morin *et al.*,1989)

experimental curves (also on logarithmic axes of same dimensions as the type-curve axes) from CFR permeability tests on to the type-curve of *Fig.*-4.3(a), values of actual time t_1 and differential head h_1 on the abscissa and ordinate axes of the experimental curve can be obtained corresponding to any chosen values of $A(T_V, \overline{H})$, say equal to T_{v1} and $\overline{H}_1$. Hence from Eq.-(4.7c), $c_v = \frac{L^2 T_{v1}}{t_1}$ and from Eq.-(4.7b), $\kappa = \frac{Q L \overline{H_1}}{h_1 A}$. The technique illustrated schematically in *Fig.*-4.3(b) is basically a visual trial-and-error method of solving a set of nonlinear simultaneous equations. An important requirement of this procedure is that the abscissa and ordinate axes of the experimental curve and type-curve must be parallel to each other. This solution procedure of matching experimental curve with analytical type-curve called Theis method (De Wiest,1965; Todd,1980) was originally developed for analysing aquifer properties from pumping tests in which the flow is horizontal. Using experimental data of constant flow rate test, Morin *et al.*(1989) showed that the method is equally applicable to the interpretation of specific storage, S_S ($S_S = k/c_V$), and permeability of the sample for flow in vertical direction.

4.2.4.2 Radial flow

The constant flow rate permeability test for radial flow in a clay sample is shown in *Fig.*-4.4(a) whereby the inner drain is subject to a withdrawal of constant flow rate of water while the peripheral drain is maintained to a constant head, h_0. By approximating this flow process to that of a heat flow to a vertical line sink or that of a well pumping in homogeneous aquifer, [*Fig.*-4.4(b)], it can be shown that the governing equation is the polar-coordinate form of the diffusion equation given by,

$$\frac{\partial^2 h}{\partial r^2} + \frac{1}{r}\frac{\partial h}{\partial r} = \frac{1}{c_v H_S}\frac{\partial h}{\partial t} \tag{4.8}$$

Initial condition: $h(r, 0) = h_0 \qquad 0 \le r \le r_2$ (4.8a)

Boundary conditions: $h(\infty, t) = h_0 \qquad t \ge 0$ (4.8b)

$$\lim_{r \to 0}\left(r \frac{\partial h}{\partial r}\right) = \frac{Q}{2\pi c_v S_s^2} \qquad t > 0 \tag{4.8c}$$

Eq.-(4.8) is essentially a consolidation equation in polar coordinates with h representing the drawdown, s with time at a distance r from the well in the well flow problem [*Fig.*-4.4(b)]. In the radial flow sample, *Fig.*-4.4(a), h represents the induced

head difference, $\Delta p/\gamma_w$ at the central drain that develops with time. Hence the trace of h with time can be typically referred from the pressure response curve of the CFR test.

Theis published in 1935 (Todd,1980) a paper concerning the solution of Eq.-(4.8) based on the analogy between groundwater flow and heat conduction. With the above initial and boundary conditions, Theis solution for the drawdown s, is given by,

$$s = \frac{Q}{4\pi T} \int_u^\infty \frac{e^{-u}\, du}{u} \tag{4.9}$$

$$u = \frac{r^2 S}{4 T t} \tag{4.9a}$$

Eq.-(4.9) is known as the nonequilibrium, or Theis equation. The integral is a function of the lower limit u and is known as an exponential integral.

The nonequilibrium equation permits determination of the formation constants S and T of the aquifer by means of pumping tests of wells. The assumptions inherent in Eqs.-(4.8) and (4.9) are:

(1) The aquifer is homogeneous, isotropic, of uniform thickness, and of infinite areal extent; (2) Before pumping, the piezometric surface is horizontal; (3) The well is pumped at a constant discharge rate; (4) The pumped well penetrates the entire aquifer, and flow is everywhere horizontal within the aquifer to the well; (5) The well diameter is infinitesimal so that storage within the well can be neglected, and (6) Water removed from storage is discharged instantaneously with decline of head.

Because of the direct similarity of analogy between radial flow in the Rowe cell and radial flow to a pumping well, the Theis method of solution to the former problem could be adopted to estimate the equivalent formation constant S and T of the sample in the Rowe cell leading to finally the coefficient of consolidation and permeability of the sample. Eq.-(4.9) may be simplified to:

$$s = \left(\frac{Q}{4\pi T}\right) W(u) \tag{4.10}$$

where W(u), termed the well function of u, is a convenient symbolic form of the exponential integral. Rewriting Eq.-(4.9a) as:

$$\frac{r^2}{t} = \left(\frac{4T}{S}\right) u \tag{4.11}$$

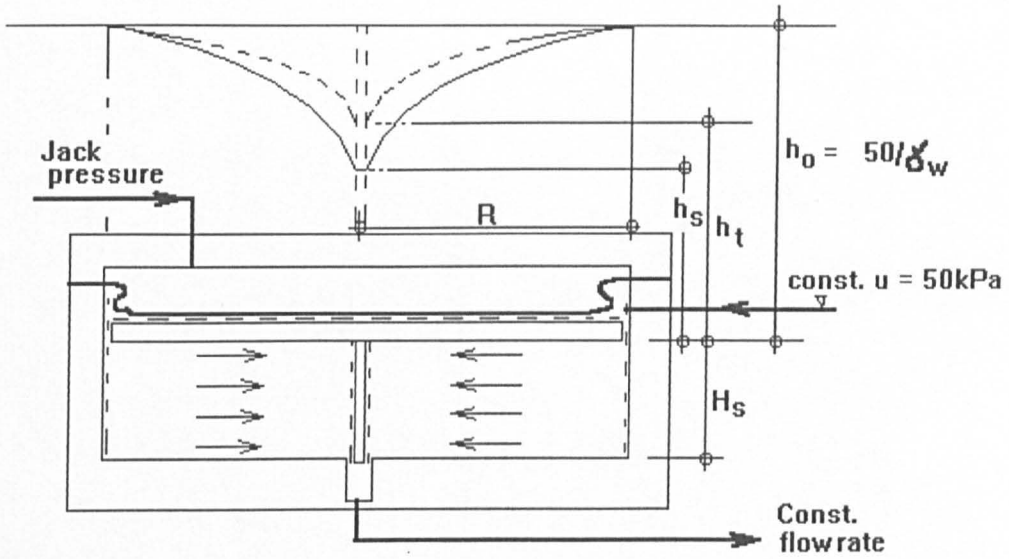

(a)

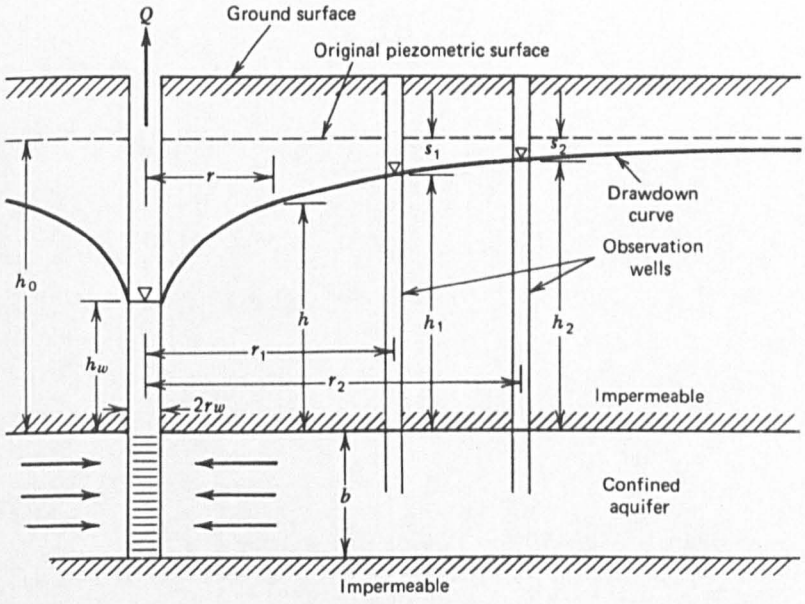

(b)

Fig.-4.4 (a) Constant flow rate permeability test: Radial flow

(b) Radial flow to a well penetrating an extensive confined aquifer (Todd, 1980)

it can be recognised that the relation between W(u) and u must be similar to that between s and r^2/t because the terms in parentheses in the two equations are constants. Given this similarity Theis suggested an approximate solution for S and T based on a graphic method of superposition.

A plot of logW(u) versus log u known as a type-curve is prepared. Another plot of log s versus $\log(r^2/t)$ on the same scale as the type-curve (this plot called experimental curve) is made. The experimental plot can now be superimposed on the type curve keeping the coordinate axes of the two curves parallel, and adjusted until a position is found by trial whereby most of the plotted points of the observed data fall on a segment of the type curve. Any convenient point is then selected, and the coordinates of this match point are recorded. With values of W(u), u, s and r^2/t thus determined, S and T can be obtained from Eqs.-(4.10) and (4.11).

Another method of solution to the Theis' equation is due to Cooper and Jacob (Todd,1980). The Theis equation can be expanded as a convergent series so that Eq.-(4.9) becomes:

$$s = \frac{Q}{4\pi T}\left[-0.5772 - \ln u + u - \frac{u^2}{2\cdot 2!} + \frac{u^3}{3\cdot 3!} - \frac{u^4}{4\cdot 4!} + \cdots\right] \qquad (4.12)$$

Three important modifications of the non-equilibrium equation were made by Cooper and Jacob (1946), namely that the sum of the series of Eq.-(4.12) beyond ln u becomes negligible when u becomes small. This occurs for large values of time or small value of distance r. The modified non-equilibrium equation then becomes

$$s = \frac{Q}{4\pi T}\left(-0.5772 - \ln\frac{r^2 S}{4 T t}\right) \qquad (4.13)$$

This equation may be applied to: (1) Drawdown/time observations made in a single well, as in the original nonequilibrium method; (2) Recovery-time observations made in a single observation well after a pumping well is shut down (recovery method), and (3) Drawdown observations made in different wells at the same time (distance-drawdown method). Direct application from the well analyses is applied to results of the CFR test in accordance to the problem of type (1) above.

In terms of decimal logarithms, Eq.-(4.13) becomes,

$$s = \frac{2.30Q}{4\pi T} \lg \frac{2.25\,T\,t}{r^2\,S} \qquad (4.14)$$

From Eq.-(4.14) a plot of s versus lgt produces a straight line whose slope is $2.30Q/(4\pi T)$. Hence $T = 2.30Q/[(4\pi) \times (\text{slope})]$ and it follows that $S = 2.25Tt_0/r^2$ where t_0 is the time obtained from the lgt intercept.

4.3 Consolidation test

In the conventional oedometer testing of clays, the incremental load type of testing in the fixed ring has been established for quite a long time and widely used as a standard laboratory practice both for routine and research purposes. Because of its established position and the large amount of data accumulated from this type of testing, it is considered the standard type of test whose results are often being referred to when compared to other types of newer tests (eg. CRS, CGT, CL, and RF tests).

For one-dimensional vertical compression of a saturated clay sample in the conventional consolidation test, the closed-form solution of Terzaghi's one-dimensional consolidation theory is utilised with the following assumptions: (1) strains are small and one dimensional; (2) the clay is saturated; (3) the clay minerals and the pore fluid are incompressible; (4) the clay is homogeneous; (5) the clay's compressibility and permeability are constant during the consolidation process; (6) flow is one-dimensional and follows Darcy's law; (7) there is a linear relationship between effective stresses and strains; (8) the clay presents no creep or secondary deformations.

Terzaghi's equation developed after considering the above assumptions is given by:

$$\frac{\partial u}{\partial t} = C_v \frac{\partial^2 u}{\partial z^2} \tag{4.15}$$

in which C_v is the coefficient of consolidation, assumed constant and equal to:

$$C_v = \frac{k}{m_v \gamma_w} \tag{4.16}$$

$$= \frac{k(1+e)}{a_v \gamma_w} \tag{4.17}$$

where k = permeability, m_v = coefficient of volume compressibility, and a_v = coefficient of compressibility.

Terzaghi's equation, [Eq.-(4.15)], relates the diffusion of excess pore pressure, u with time t at any given layer of clay z. The excess pore pressure develops as a result of applying an increment of effective vertical stress at one boundary face of the clay.

Numerous methods have been proposed to evaluate the coefficient of consolidation from laboratory tests. The well known techniques are the so-called fitting methods which are based on the similarity between observed compression-time curves and the

theoretical U_S versus T_V curves obtained from the Terzaghi theory. Curve matching is essentially accomplished between the experimental and theoretical curves following their accurate parabolic fit for values of U_S less than 0.6.

An improved comparison is possible when the time is plotted to a square root or a logarithmic scale which has become to be known as Taylor's square-root-of-time method or the Casagrande logarithm-of-time fitting methods described in most textbooks on soil mechanics.

A review on consolidation and settlement by Balasubramaniam and Brenner (1981) refers to Ladd(1973) that with experience, C_V values obtained from the square-root-of-time fitting method for normally consolidated clays are typically 2±0.5 times larger than those obtained by the log-time fitting method. Ladd *et al.*(1977) concluded that, for incremental oedometer tests, the log-time fitting method are better suited than the square-root-of-time fitting method. In the *State of the Art*: Consolidation Testing, Olson(1986) concluded that the $\sqrt{t}$ fitting method gives both the zero and 100% primary points in an unambiguous fashion without the need for trial-and-error matching for parabolic fit as in the log-time fitting method.

Various fitting methods are also available for determining the coefficient of consolidation for radial flow.

The square-root-of-time ie. the Taylor's $\sqrt{t}$ fitting method will be adopted in this study to obtained C_V values from experimental data. The method is shown in *Fig.*-4.5(a) for the vertical flow sample. To obtain the t_{90} a line is drawn from the corrected initial settlement (on the compression axis) at a slope of 1/1.15 times the slope of the experimental line. The abscissa of the point where this line cuts the experimental curve represents the square root of t_{90}. The coefficient of consolidation is calculated from the expression,

$$C_V = T_{90} H^2 / t_{90} \qquad (4.18)$$

where $T_{90} = 0.848$ for the vertical flow sample.

In the Taylor's method of curve fitting construction, the slope factor α [see *Fig.*-4.5(b) for the more general radial flow case] is made equal to 1.15 so that the curve fitting line AC in *Fig.*-4.5(a) cuts the theoretical average degree of consolidation curve at $T_{90} = 0.848$ and $\overline{U_V} = 0.9$ which represents the basis for calculation of c_V once the value of $\sqrt{t}_{90}$ is obtained.

For the case of radial flow sample with drainage to both the peripheral and inner boundaries, the coefficient of consolidation c_r is defined by the time factor T_r such that,

$$T_r = c_r t / [(R - r_0) / 2]^2 \qquad (4.19)$$

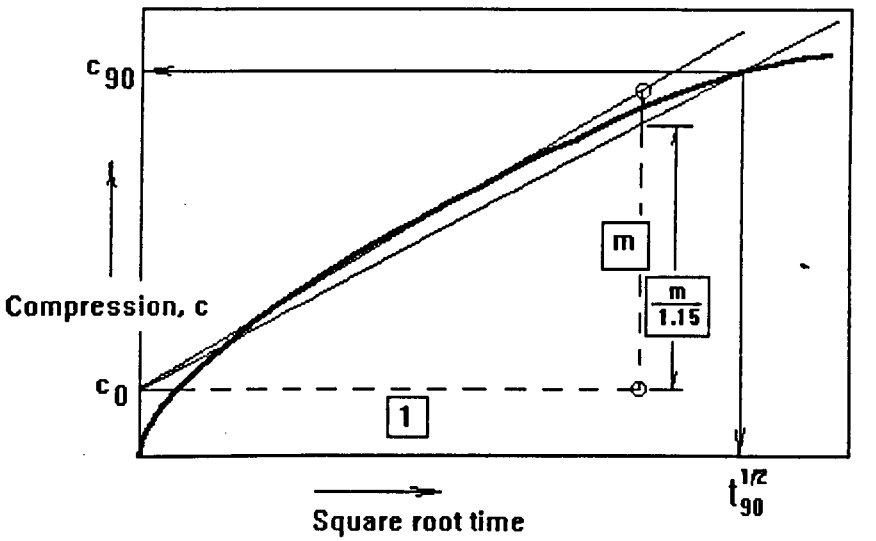

(a)

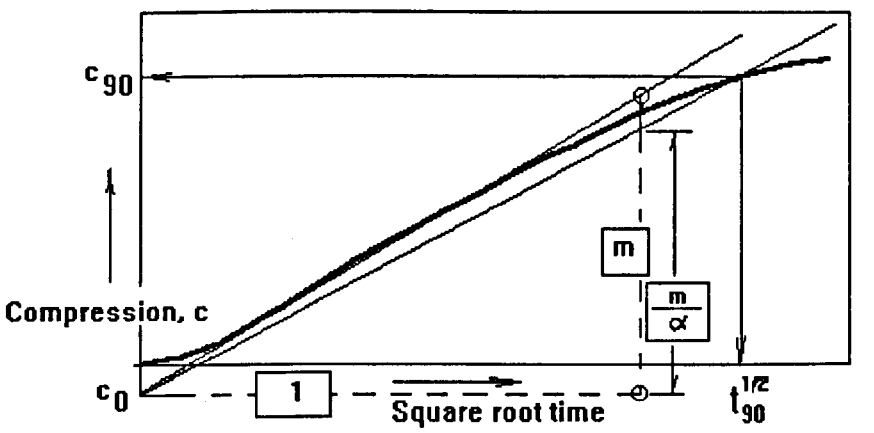

(b)

Fig.-4.5 Determination of c_v by Taylor's square-root-of-time method:
(a) Vertical flow; (b) Radial flow

or $$c_r = T_r (R - r_0)^2 / (4t_r) \quad (4.20)$$

The slope factor α [*Fig.*-4.5(b)] is not fixed as for the vertical flow case but varies according to the proportion of inner and outer drain radii or radius ratio, $\chi = r_0/R$.

Analysis of the problem by Al-Tabbaa(1987) provides the necessary value of time factor for 90% consolidation based on the closed form solution of Terzaghi's theory of consolidation or the Biot's fully coupled theory of consolidation. Results of Al-Tabbaa's analysis indicated the dependence of time factor, T_r and slope factor, α upon the radius ratio, $\chi = r_0/R$, and variations of T_r and α are presented for various values of the radius ratio. Also, for specified values of $\overline{U_r}$ and χ, the time factor is different depending on whether Terzaghi's theory or Biot's theory is used. Typical factors compiled by Olson(1986) for $\chi = 0.2$ and extracted from Al-Tabbaa's results for $\chi = 0.205$ and 0.154 are shown in *Table*-4.3.

Thus in this study where $\chi = 0.151$, c_r is calculated from Eq.-(4.20) using the slope factor α of 1.21 for t_{90} and $T_{90} = 0.81$ based on the Terzaghi's solution. For the same value of the radius ratio χ, the factors based on Biot's solution are $\alpha = 1.1725$ for t_{90} and $T_{90} = 0.892$.

Table-4.3 Factors for use with radial flow consolidation tests in root time curve fitting method

	Outflow		Inflow		Outflow and inflow	Outflow and inflow
	Radius ratio, χ = 0.2				χ = 0.205	χ = 0.154
	Equal strain	Free strain	Equal strain	Free strain	Equal strain	Equal strain
Root power (n)	0.83	0.47	0.83	0.67	0.5	0.5
Slope factor (α)	1.61	1.22	1.61	1.31	1.21 (Terz) 1.17 (Biot)	1.21 (Terz) 1.1725 (Biot)
Time factor, T_r at $\overline{U}_r$ = r%	T_{45} = 0.075	T_{45} = 0.049	T_{45} = 0.280	T_{45} = 0.264	T_{90} = 0.8(Terz) T_{90} = 0.886(Biot)	T_{90} = 0.81(Terz) T_{90} = 0.892(Biot)

4.3.1 Compression parameters, a_v, m_v, and C_c

The compression of clays in the one dimensional consolidation test can be described by (1) coefficient of compressibility a_v; (2) coefficient of volume compressibility, m_v; and (3) compression index, C_c. These parameters are all essentially interchangeable, and the choice may be made for reasons of mathematical convenience rather than necessary for the accuracy with which they can represent experimental data.

The coefficient of compressibility is given by,

$$a_v = \frac{e_2 - e_1}{\delta\sigma'_v} = -\frac{\delta e}{\delta\sigma'_v} \tag{4.21}$$

and is introduced during the Terzaghi analysis of one-dimensional consolidation. Data of one-dimensional compression are usually plotted in terms of void ratio (or specific volume) and vertical effective stress, and the coefficient of compressibility merely expresses the local slope of the relationship.

The coefficient of volume compressibility is given by,

$$m_v = \frac{a_v}{1 + e_1} = \frac{1}{1 + e_1}\left(-\frac{\delta e}{\delta \sigma'_v}\right) \tag{4.22}$$

and is a one-dimensional compliance (strain increment divided by stress increment). Eq.-(4.22) defines m_v as the change in volume, per unit volume, per unit change of effective stress, and it is also called the coefficient of volume change or coefficient of volume decrease, ie.

$$m_v = -\frac{1}{V}\frac{dV}{d\sigma'_v} \tag{4.23}$$

For 1-D compression of the sample of thickness H,

$$m_v = -\frac{1}{H}\frac{dH}{d\sigma'_v} \tag{4.24}$$

It is recognised that from their definitions, m_v, (Eq.-4.23) and permeability, (Eq.-2.1), are fundamental in character depending on basic variables like volume and differential head, respectively. Therefore, it is not unreasonable to consider these parameters as fundamental properties (when compared to coefficient of consolidation c_v which is a composite parameter dependent on both compressibility and permeabilty) of the deforming clay undergoing consolidation. Consolidation is a process of squeezing out of a volume of pore water due to a change of effective stress, and this phenomenon is controlled by two important properties of the clay: (1) The permeability of the clay controls the rate at which pore water can escape through the

voids of the clay, resulting in a time dependency of the observed boundary deformation under load; (2) The reduction in the volume of voids in the clay that is necessary to allow the clay to respond to the imposed changes in stress, and which controls the amount of pore water that needs to escape, is described by the constrained modulus of deformation, D, which is the inverse of the coefficient of volume compressibility m_v. Whereas traditionally values of coefficient of consolidation c_v have been deduced from observations of transient deformations in oedometer tests, a preferred alternative method of describing the time-dependent consolidation response of soils would be to return to the fundamental parameters: the variations of permeability and coefficient of volume compressibility with void ratio, which should be experimentally established to be used for calculations of 'correct' values of coefficient of consolidation c_v. This approach has been proposed by Ducasse *et al.*(1986), Leroueil *et al.*(1990) and Sandbaekken *et al.*(1986). An extension of this approach is essential if finite element analyses of transient response of geotechnical prototypes are to be performed since these will rarely involve one-dimensional situations, and proper description of the permeability characteristics of the soils and of their generalised stiffness properties will be required.

The coefficient of volume compressibility m_v seeks a constant compliance (or stiffness) for the soil. It is frequently observed that the stiffness tends to increase in proportion to the effective stress level. The compression index C_c is introduced to reflect this variation. When the clay is normally consolidated, the (e-logσ'_v) line can be expressed in the form

$$e = e_0 - C_c \lg\left(\frac{\sigma'_v}{\sigma'_{vo}}\right) \tag{4.25}$$

where e_0 is the void ratio at a vertical effective stress of σ'_{vo} and the compression index,

$$C_c = \frac{\delta e}{\delta(\lg \sigma'_v)} \tag{4.26}$$

None of these parameters is able to describe the contrasting stiffnesses that are observed on virgin loading and on unloading of soils. A parameter similar to C_c can be used: swelling index C_s. In any analysis it is important to use an appropriate description of the volumetric response. As noted by Butterfield (1979) it may sometimes be preferable to seek a linear relation between logarithm of vertical effective stress and logarithm of specific volume, and this may apply over a wider range of values of effective stress than Eq.-(4.25).

4.4 Reduction of experimental data and calculations

4.4.1 Calculation of void ratio, e

The current void ratio of the sample at any stage of a test can be computed in a number of ways based on the height of sample measured before or after each test. The relationship between sample height H and gauge reading G is shown schematically in *Fig.*-4.6. From the figure it is immediately recognised that there are four expressions for the void ratio, e in terms of the sample height (initial or final) and the initial or final void ratio.

From *Fig.*-4.6 the current sample height based on initial readings is given by,

$$h_{s(i)} = h_i - (G_i - G_s) \tag{4.27}$$

If based on final readings, the current sample height is given by,

$$h_{s(f)} = h_f - (G_s - G_f) \tag{4.28}$$

The void ratio can then be computed from Eqs.-(4.27) and (4.28) based from *Fig.*-4.6 as given below:

Based on initial sample height and initial void ratio:

$$e = (1 + e_i)\frac{h_{s(i)}}{h_i} - 1 \tag{4.29a}$$

Based on initial sample height and final void ratio:

$$e = (1 + e_f)\frac{h_{s(i)}}{h_f} - 1 \tag{4.29b}$$

Based on final sample height and initial void ratio:

$$e = (1 + e_i)\frac{h_{s(f)}}{h_i} - 1 \tag{4.30a}$$

Based on final sample height and final void ratio:

$$e = (1 + e_f)\frac{h_{s(f)}}{h_f} - 1 \tag{4.30b}$$

In the most careful of measurements, the void ratios calculated from Eqs.-(4.29) and (4.30) seldom equal each other because the actual h_i and h_f could easily differ from the measured h_i and h_f after and before the sample was in the oedometer, respectively. Calculated initial and final void ratios, e_i and e_f, from mass measurements could also suffer from experimental errors which make them unrepresentative of the actual e_i and e_f of the sample immediately before and after testing.

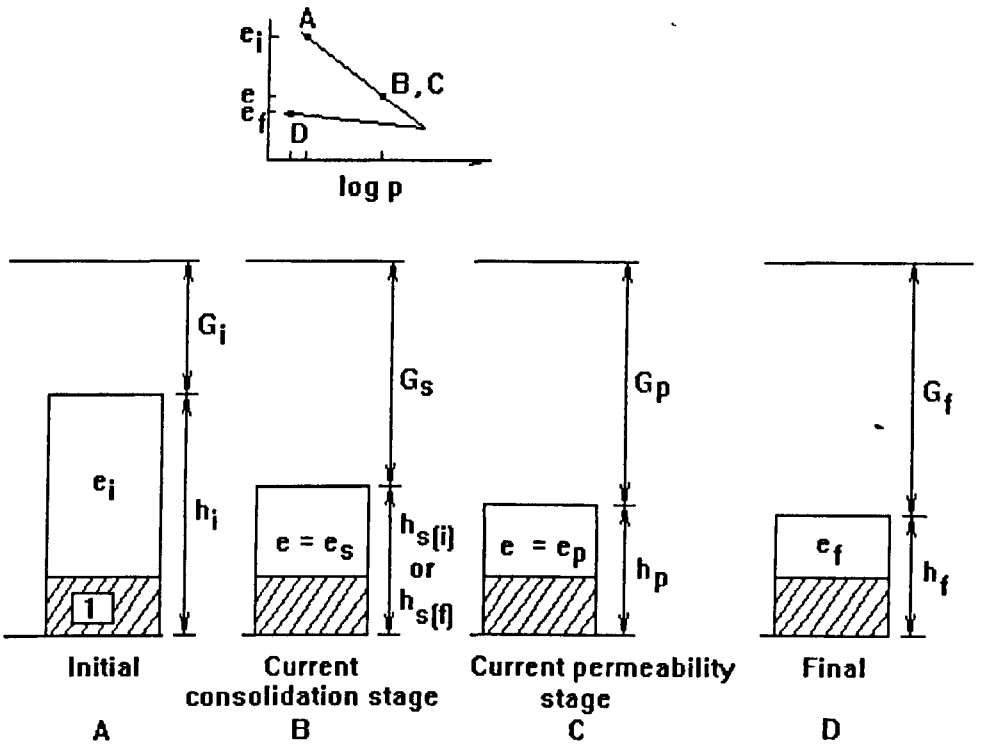

Initial readings: w_i = initial water content of sample

h_i = initial sample height

G_i = initial dial gauge reading

e_i = initial void ratio;

Current readings: h_s, h_p = height of sample at the end of consolidation and permeability stage

G_s, G_p = dial gauge readings at the end of consolidation and permeability stage

e_s, e_p = void ratio at consolidation and permeability stage;

Final readings: h_f = final height of sample

G_f = final dial gauge reading

w_f = final water content

e_f = final void ratio

Fig.-4.6 Sample height and void ratio at various stages of the test

4.4.2 Height of sample in permeability calculation

If the current sample heights based on Eqs.-(4.27) and (4.28) do not differ much (ie. within ±0.5%), the average of the two is taken for the sample height at the end of consolidation stage given by,

$$h_S = \frac{1}{2}\left(h_{S(i)} + h_{S(f)}\right) \tag{4.31}$$

The void ratio for the end of consolidation stage is also taken from the average of the two closest values calculated from Eqs.-(4.29) and (4.30) denoted as e_S.

Given the dial gauge reading at the end of permeability stage as G_p, the corresponding sample height h_p is then given by,

$$h_p = h_S - \frac{1}{2}\left(G_S - G_p\right) \tag{4.32}$$

and the void ratio $e_p = (1 + e_S)\frac{h_p}{h_s} - 1$ (4.33)

4.4.3 Permeability calculation from direct test

Calculations of permeability follow directly from the relationships given in Sections 4.2.1 and 4.3 for permeability and consolidation tests data respectively. Using the dimensions of the apparatus used in the testing, the vertical permeability from constant head test follows from Eq.-(4.1) and *Fig.*-3.4(a).

$$k_v = (Q/t)(\gamma_w H/\Delta p)(1/A) \tag{4.1}$$

$$= (10^{-6}/465)(Q/t)(H/\Delta p) \quad m/s \tag{4.34}$$

where $A = (\pi/4)(76.2)^2$ mm^2

$\gamma_w = 9.81$ kN/m^3

(Q/t) in units of mm^3 / s, H in mm and Δp in kPa.

Similarly, the horizontal permeability from constant head test follows from Eq.-(4.2) and *Fig.*-3.4(b),

$$k_h = [1/(2\pi)](Q/t)(1/H)(\gamma_w/\Delta p)\ln(D/d) \qquad (4.2)$$

$$= [1/(2\pi)]\,(9.81 \times 10^{-6})\ln(72.8/11.4)\,(Q/t)(1/H)\,(1/\Delta p) \quad m/s$$

$$= 2.894 \times 10^{-6}\,(Q/t)(1/H)\,(1/\Delta p) \quad m/s \qquad (4.35)$$

where (D/d) = (72.8 / 11.4), and the terms (Q / t), H, Δp, and γ_w are in similar units as those in Eq.-(4.34).

Calculations for permeability from the constant flow rate permeability test data use the same equations above (Eqs.-4.34 and 4.35) with the term (Q / t) replaced by 0.5/R where R is the ramp in unit of second. Therefore the vertical and horizontal permeabilities from constant flow rate permeability tests are given by:

$$k_v = (10^{-6}/930)(1/R)(H/\Delta p) \quad m/s \qquad (4.36)$$

$$k_h = 1.447 \times 10^{-6}\,(1/R)(1/H)\,(1/\Delta p) \quad m/s \qquad (4.37)$$

4.4.4 Permeability calculation from indirect test

From consolidation test data, permeability is calculated indirectly from Eq.-(4.16) in Section 4.3 in which the experimental values of the coefficients of consolidation and volume compressibility are the two consolidation test parameters being used. The vertical permeability follows from Eq.-(4.16),

$$k_v = c_v\, m_v\, \gamma_w \qquad (4.38)$$

In terms of the experimental readings from the consolidation test, using Eq.-(4.18),

$$c_v = 0.848\,\frac{h^2}{t_{90}} \qquad (4.39)$$

Adopting the following units, c_v[m^2/yr], h[mm], t_{90}[min] and for double drainage [see *Fig.*-3.4(a)],

$$c_v = 0.112\,\frac{H^2}{t_{90}} \quad m^2/yr \qquad (4.40)$$

$$= \frac{0.112}{t_{90}} \left[(H_{i-1} - H_i)/2\right]^2 \quad m^2/yr \tag{4.41}$$

where H_{i-1} and H_i are sample heights at the beginning and end of the ith. consolidation stage respectively, and t_{90} is read off from the experimental curve following *Fig.*-4.5.

The coefficient of volume compressibility, m_v as defined in Eq.-(4.24) can be written in terms of the experimental readings giving,

$$m_v = \frac{\Delta H_2 - \Delta H_1}{H_0 - \Delta H_1} \times \frac{1000}{P_2' - P_1'} \quad m^2/MN \tag{4.42}$$

where ΔH_1 = cumulative change in height of the specimen up to the end of the previous consolidation stage, in mm;

ΔH_2 = cumulative change in height of the specimen up to the end of the consolidation stage being considered, in mm;

H_0 = the initial height of the specimen, in mm;

P_1' = effective pressure applied to the specimen for the previous consolidation stage, in kPa;

P_2' = effective pressure applied to the specimen for the consolidation stage considered, in kPa.

In the case of radial flow, the horizontal permeability k_h, follows the same form as in Eq.-(4.38) with the coefficient of consolidation c_r referring to the radial flow case. The formula for the coefficient of volume compressibility m_v remains the same as in Eq.-(4.42). Thus,

$$k_h = c_r m_v \gamma_w \tag{4.43}$$

where $c_r = T_r (R - r_0)^2 / (4t_r)$ from Eq.-(4.20). For the case of 90% average degree of consolidation, and referring to *Fig.*-3.4(b) for the values of R and r_0, (in mm) the two expressions for the coefficients of consolidation based on Terzaghi's and Biot's solutions are given by, respectively,

$$c_r(Terz) = \frac{0.81}{4t_{90}}(R - r_0)^2 \tag{4.44}$$

$$= \frac{0.81}{4t_{90}}\left(\frac{36.4 - 5.7}{1000}\right)^2 \quad m^2/min \tag{4.45}$$

$$= 100.382 / t_{90} \quad m^2/yr \tag{4.46}$$

$$c_r(\text{Biot}) = \frac{0.892}{4t_{90}}(R - r_0)^2 \tag{4.47}$$

$$= 110.544 / t_{90} \quad m^2/yr \tag{4.48}$$

where t_{90} in min are read off from the experimental curves using the appropriate slope factors, α.

4.5 Observations on some aspects of experimental data

4.5.1 The trend of pressure response with time

The extent of local consolidation and swelling near the two boundaries of the sample is examined by considering the actual variation of top and bottom pore pressures, u_t and u_b, in the sample during the permeability tests.

Some results of the CFR permeability test from data in the test series 2T240V at σ'_v=100kPa are considered for the discussion. *Figs.*-4.7 presents the actual development of the top and bottom pore pressures in the sample after starting the test. The initial back pressure of u = 50kPa is indicated by the horizontal line. Typical results of the CFR test consist of u_b rising above and u_t declining below the 50kPa level, to some constant pressures when steady state condition is achieved: - for the forward flow case. In the case of R=1s, u_b=65.5kPa and u_t=37.5kPa giving the difference $\Delta p = (u_b - u_t)$ =28kPa which represents the induced pressure difference used to calculate the permeability [see also *Fig.*-5.6(a)]. It is noted that although Δp seems to be reaching a constant value with time, the indication of steady state condition based on constant Δp will not be sufficient without monitoring the development of u_b and u_t, and checking the significance of the consolidation/swelling effects on void ratio.

The effect of this pressure difference in permeabilty testing on stress changes in the sample is traced by referring to the (e-lgσ_v') diagram in *Fig.*-4.8. Thus the initial state of stress is represented by point A at σ_v' = 100kPa in the figure, and with time during the testing, stresses in the top and bottom of the sample would move from A to T, σ_{vt}' = 112.5kPa and from A to B, σ_{vb}' = 84.5kPa, respectively, with the corresponding changes in void ratio of 0.27%. Both B and T lie on the rcl rather than the ncl in this case.

4.5.2 Calculations of permeability

The present method of calculating the permeability from the CFR test data consists of obtaining the average slope of the pressure-flow rate plot where some 2 to 5 different flow rates are involved to achieve sufficient data for the calculation. Both forward and reverse flows are involved to ensure first, the validation of Darcy law before embarking on using it. Consideration of *Figs.*-4.9 give way to at least 3 methods of working out the permeability. Assuming Procedure A in *Fig.*-4.9 as the standard practice, the results on some typical data are shown in *Figs.*-4.10 where for each point the ordinate represents calculated k_v following either Procedures B or C compared with calculated k_v following Procedure A on the abscissa. Thus Procedure A gives a k_v value of 1.41×10^{-9} m/s for Series 2T120V (at σ_v'=100kPa, e=1.55) shown as point A in *Fig.*-4.10(a). Calculations by Procedures B and C give some

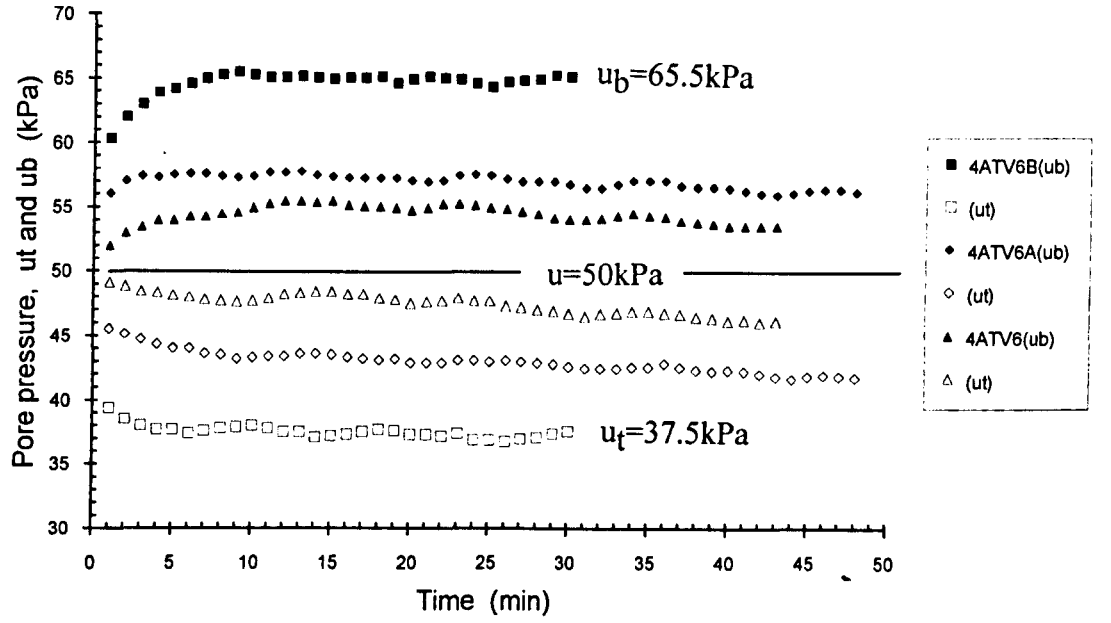

(a)

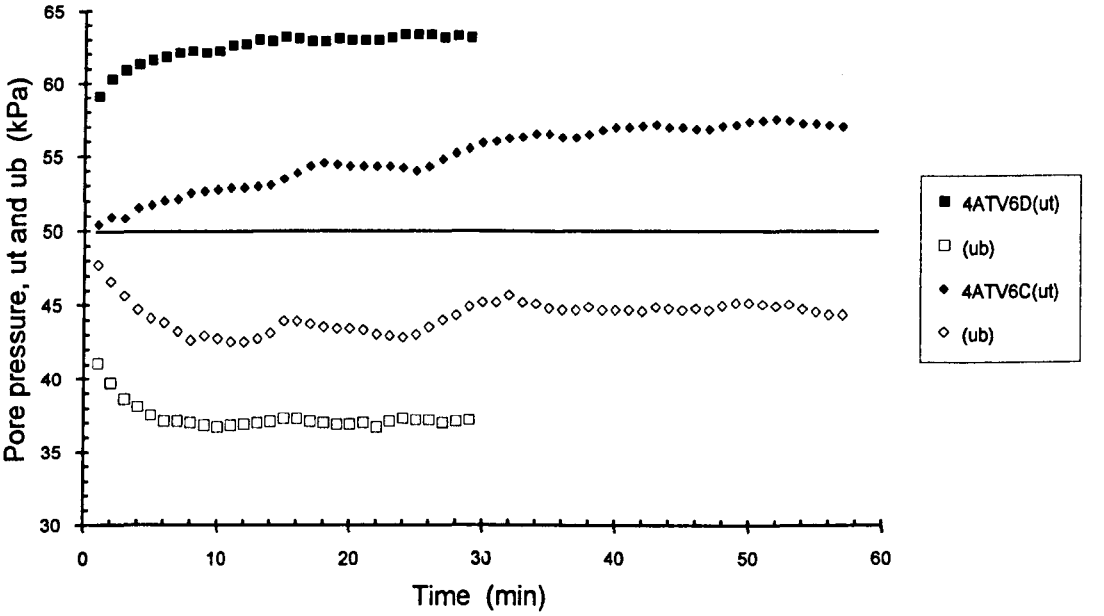

(b)

Fig.-4.7 Records of the constant flow rate permeability test: Top and bottom pore pressures vs time for test series 2T240V at σ_v'=100kPa - (a) Forward flow; (b) Reverse flow

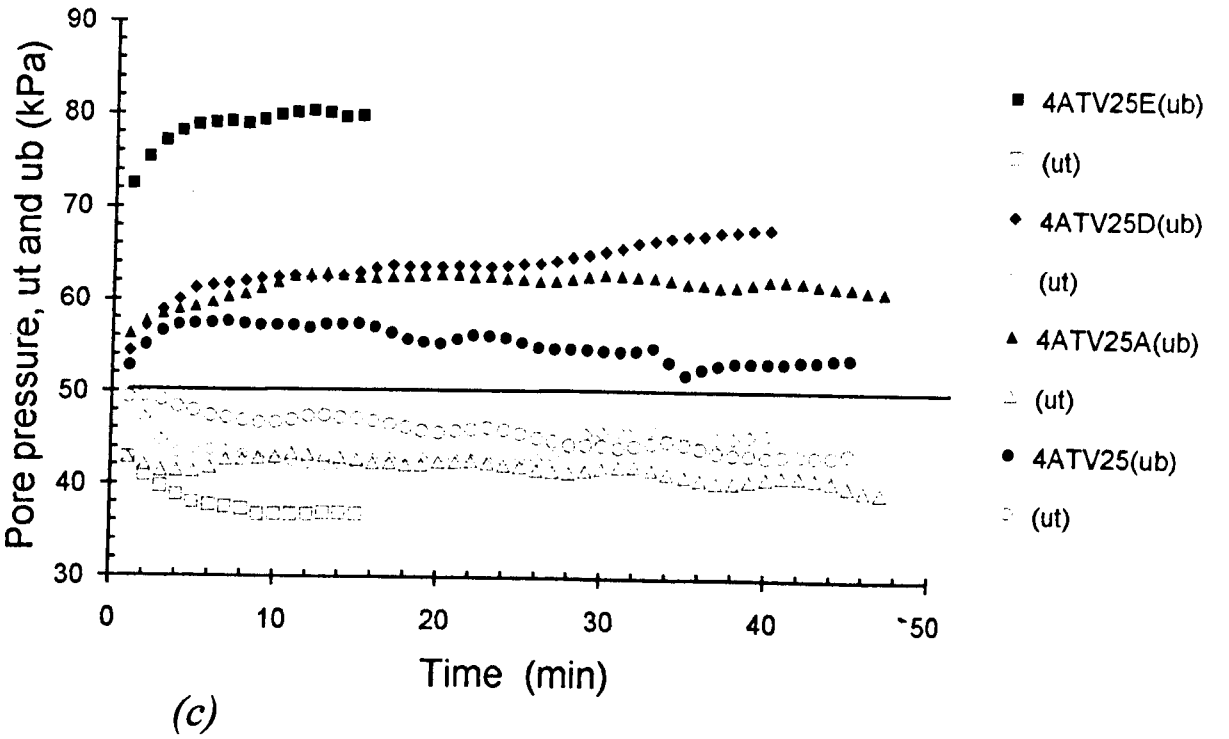

(c)

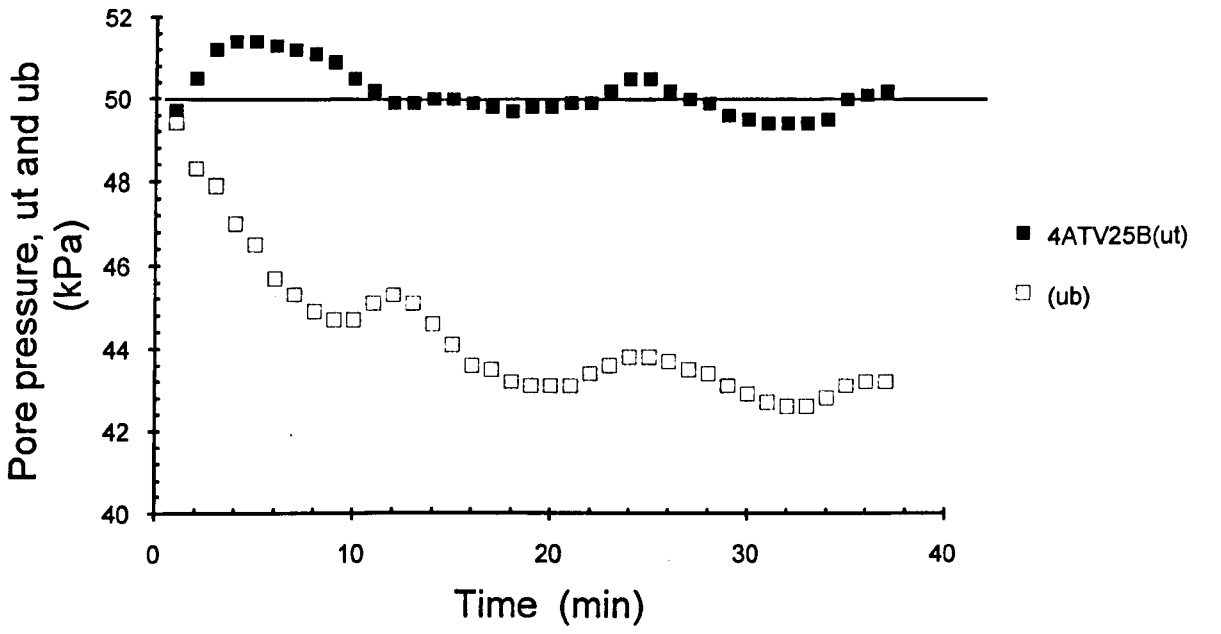

(d)

Fig.-4.7 *contd.* Records of the constant flow rate permeability test: Top and bottom pore pressures vs time for test series 2T240V at σ_V'=480kPa - (c) Forward flow (d) Reverse flow

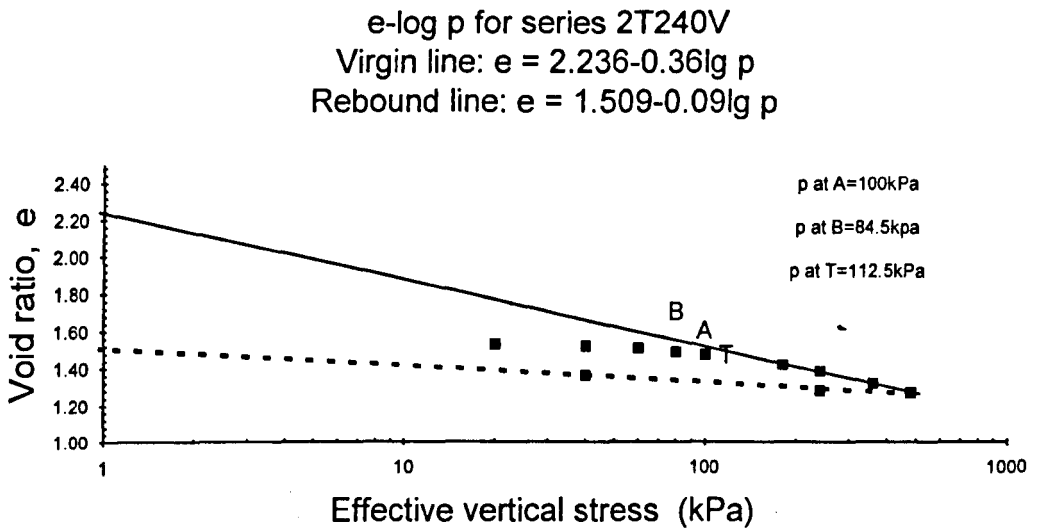

2T240V at σ_v' = 100kPa; u_b-u = 15.5; u-u_t = 12.5; $\Delta u = u_b - u_t$ = 28kPa;
Points B, A and T above lie on rcl and not ncl.

$\Delta u/\sigma_v' = (28/100)x100\% = 28\%$

$\Delta e_b = 0.09lg15.5 = 0.107$

$\Delta e_t = 0.09lg12.5 = 0.099$

$\therefore \Delta e = 0.206$

$e_p = 1.475$

$e_p = (1/2)[(1.475+0.107)+(1.475-0.099)]$

change in void ratio = (1.479-1.475)/1.475

= 0.27%

Fig.-4.8 1-D compression for test Series 2T240V

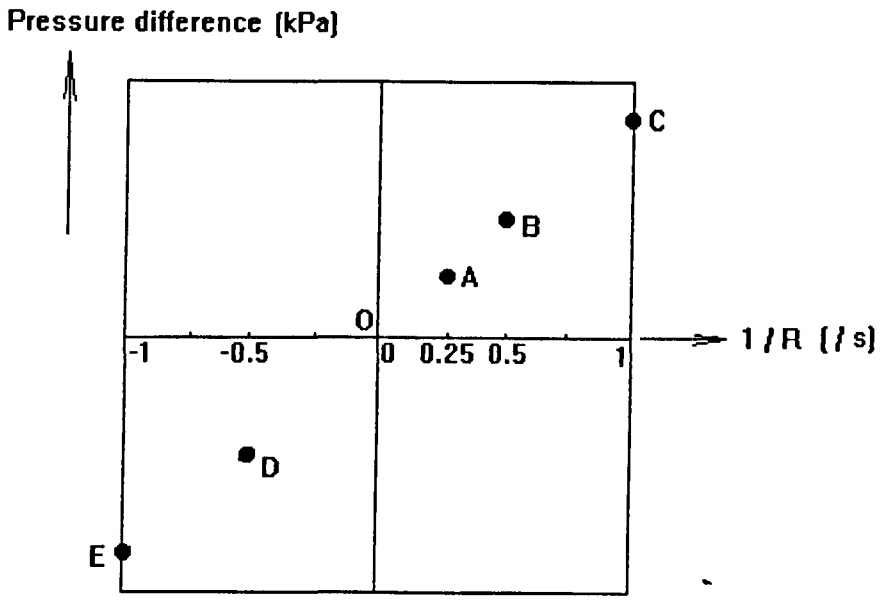

Procedure A

$k_V = (10^{-6} \times h_p) / (930 \times S)$ m/s; $k_h = 1.447 \times 10^{-6}/(h_p S)$ m/s

where S = slope of regressed line through all points (ie.E,D,A,B&C)

= mean slope

h_p = current height of sample (mm)

Procedure B

$k_V = (10^{-6} \times h_p) / (930 \times S_1)$ m/s; $k_h = 1.447 \times 10^{-6}/(h_p S_1)$ m/s

where S_1 = slope of regressed line through all points in forward flow or reverse flow only (ie. A,B&C or E&D)

Procedure C

$k_V = (10^{-6} \times h_p) / (930 \times S_2)$ m/s; $k_h = 1.447 \times 10^{-6}/(h_p S_2)$ m/s

where S_2 = slope of line through origin and individual points only (ie. lines OA, OB & OC - in forward flow; DO & EO - in reverse flow)

Fig.-4.9 Calculations of permeability by Darcy's law using various slopes of data in the (Δp vs 1/R) plot

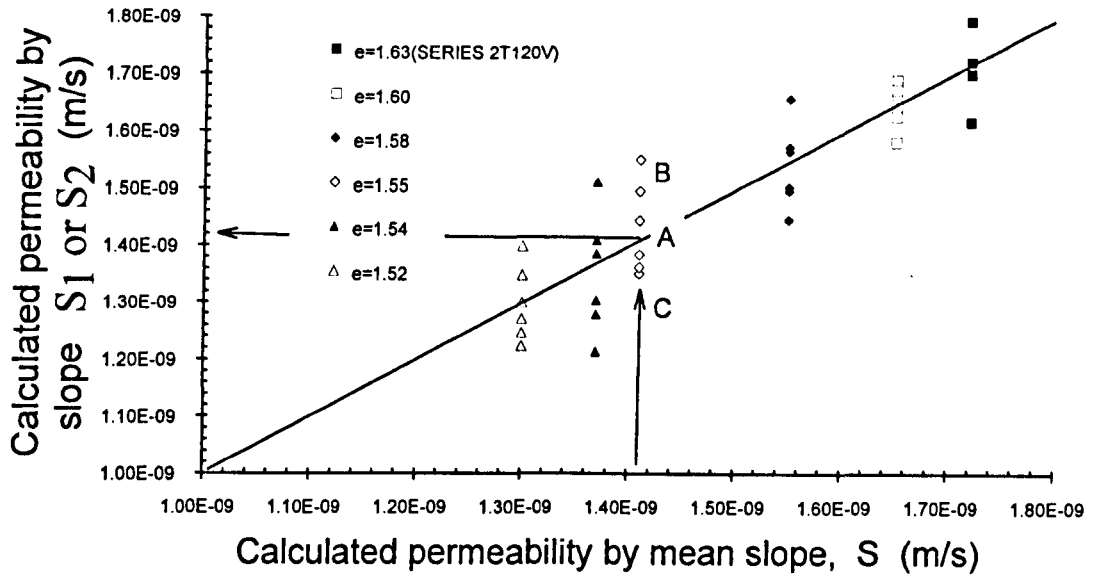

(a)

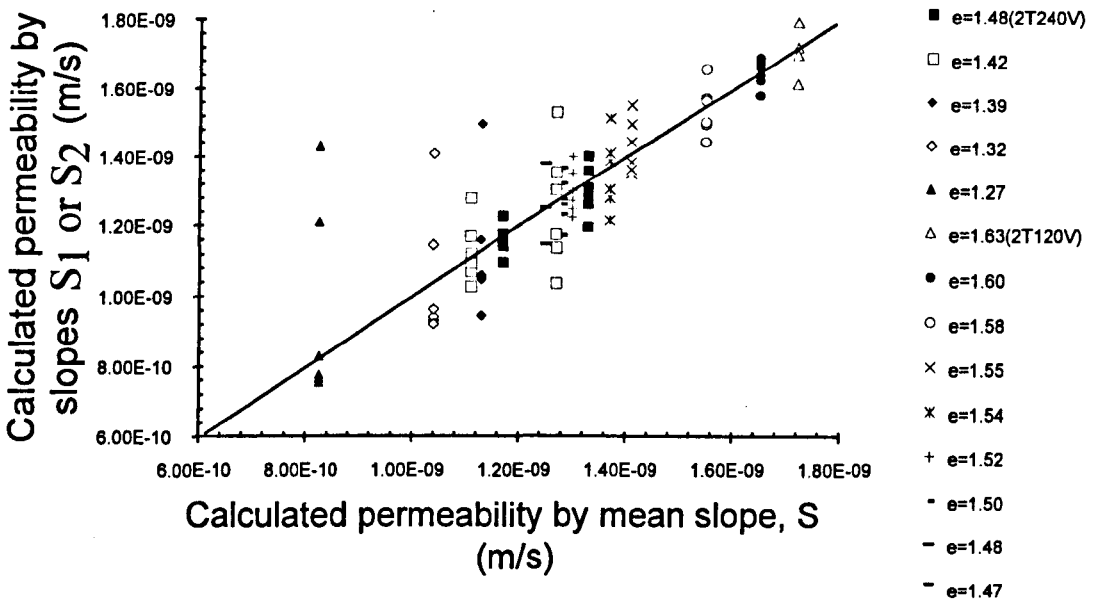

(b)

Fig.-4.10 Calculations of measured permeability by Procedures B or C compared to Procedure A (a) Series 2T120V; (b) Series 2T120V and 2T240V

values of k_v as shown in the figure as $1.55x10^{-9}$ and $1.35x10^{-9}$m/s ie. at points B and C. Calculations by Procedures B and C compared to Procedure A for other void ratios give the results in *Fig.*-4.10(a) showing that Procedure A provide the best calculation procedure for the measured permeability in that it is always consistent with its more or less middle of the range position. More permeability data are presented in *Fig.*-4.10(b) for Series 2T240V compared to Series 2T120V where results using Procedure B or C could over- or under estimate those using Procedure A.

4.5.3 Dial gauge readings and fluid volume measurement

Although the GDS readings afforded the calculations of void ratios by referring to volumetric measurements of fluid(water) expelled out or taken in during consolidation or rebound, the present data are based on changes of vertical heights as observed from the dial gauge readings. However, some volumetric records will be discussed to obtain important characteristics of the present 75-mm Rowe cell.

Fig.-4.11(a) presents the comparison between the volume readings and vertical compression of the sample top during the various consolidation stages for the sample in test series 1H. Corresponding to a compression reading, the volume of water recorded came from both the top and bottom drains. An idealised result is shown as the straight line AB passsing through the origin where a 1-mm vertical movement is equivalent to a volumetric change of $4162mm^3$. (ie.= 1mm x sectional area of sample). This result could have been achieved in a hypothetical zero-error-free device which might take the form of a fully tight barrel-piston type of syringe instead of the rubber jack used in the Rowe cell.

It is noted in *Fig.*-4.11(a) that a certain amount of relatively large volume of fluid was recorded at the beginning of all stages of consolidation, ie. during the first minute of reading, with the value decreasing as the rubber jack pressure gets higher. Thus for the case of consolidation stage 1H-B, (jack pressure=70kPa, σ_v'=20kPa), the volume increases from 0 to $6212.5mm^3$ corresponding to a vertical compression of 0.3315mm which occurs in the first minute [see *Fig.*-4.11(b)]. Thereafter, the volume increases linearly with compression with a slope of $3460mm^3/mm$ giving an equivalent fictitious contact area A_c between rubber jack and platen of $3460mm^2$. Thus it appears that at the start of each stage of the consolidation test, whereby a zero or very small movement of the loading platen occurs, some volume of water is expelled primarily from the dead space between the rubber jack and wall ring. This volume continues to be expelled during the 1-min duration and thereafter, the remaining volume remains trapped with further movement of the top loading platen. With each jack pressure there exist a trapped volume as represented by the volume intercept at h = 0mm. A plot of these volumes vs jack pressures is shown in *Fig.*-4.12. Thus, although the

trapped volume decreases with increasing jack pressure, its influence on the magnitude of fictitious contact area between the rubber jack and platen would be indicated by whether the lines in *Figs.*-4.11 are parallel to each other with a constant slope.

The fictitious contact area A_c as given by (V/h) could record values smaller or greater than the actual sectional area A(=A_h or A_v) of the sample depending on whether there is further lodging or escape of fluid into the dead space, as the jack/platen moves down during a given magnitude of jack pressure. The actual contact area A_a can be less than or equal to but not greater than A. If $A_c > A_h$, the excess area (A_c-A_h) is contributed by the expulsion of fluid from the dead space and similarly, if $A_c < A_h$, the deficit is due to the fluid being dislodged into the dead space rather than flowing out through the top drainage.

In order to examine the possible mechanism that could cause a volumetric discrepancy, a pressure test on the oedometer using perspex dummy sample was conducted. The arrangement is shown in *Fig.*-4.13 involving similar setting up and test procedure as for the consolidation test. Results of the pressure test is shown in *Fig.*-4.14 for both the radial and vertical flow oedometers where the volume of water expelled is plotted against the jack pressure for loading (AB) and unloading (CD) cycles. Although the rubber jacks were quite identical for the two oedometers, there is a marked difference in their volume compliance depending on whether they were inside the radial flow or vertical flow oedometers. This difference could be attributed to the effect of the peripheral drain in the radial flow oedometer which allows for more drainage to take place for a given magnitude of jack pressure.

The trapped volume corresponding to a jack pressure in the loading cycle can be identified as the difference between total volume at that pressure and at the pressure *preceding* it. For the unloading cycle, *preceding* becomes *subsequent to* in the previous sentence. A plot of the trapped volumes taken from the actual consolidation test (*Fig.*-4.12), and the pressure test (*Fig.*-4.14) is presented in *Fig.*-4.15.

The experimental results reported in this Section indicated that the effect of the trapped volume leads to an over-estimate value of the actual compression of the sample while the trapped volumes themselves could also participate in the areal reduction of the rubber jack and loading platen interface. The fictitious contact area A_c as interpreted by the slope of the graphs in *Figs.*-4.11 varies with increasing jack pressure as shown in *Fig.*-4.16. Based from these contact areas, A_c extracted from the slopes of volume-compression plots, the apparent pressure on the sample is given by $\sigma_v'(A_c/A)$ and is compared with the common σ_v' as shown in *Fig.*-4.17 for the test series 1H, 1V, 2C240H and 2C240V. Also based on A_c as obtained from

results of the consolidation tests, the apparent force can be calculated and compared with the nominally calculated value as shown in *Fig.*-4.18 for the test series 1H, 1V, 2C240H and 2C240V. Shields(1976) reported the actual force exerted by the rubber jack-platen on proving ring (without actual sample and for similar type of oedometer - vertical flow only), and compared with the corresponding force calculated on the basis of jack pressure as shown in *Fig.*-4.19. Shields' results indicated a consistently low actual force, between 0.8 to 1 of the calculated force whereas the results in this study indicate that the apparent force could be lower or higher than the assumed values depending on the consistency of the sample and rubber jack system. Although the actual force from Shields' results correctly does not exceed the calculated force, the apparent force in this study exceeded calculated values due to the hypothetical nature of the fictitious contact area $A_c > A_h$ which violates the fact that the actual contact area should not exceed A_h. Thus it is important to calibrate on representative sample and dummy sample with the oedometer ring and cover in place rather than separately so that among other things it is possible to examine the finite interval of time required to expel the trapped fluid and get the dead volume equilibrated before the actual compression of the sample can take place.

It is evident from the preceding figures that volumetric measurements of water going into or out of the sample enable important calibration to be evaluated while the actual testing is being conducted on the sample. Assessement of the actual jack/platen contact area could be estimated to give an actual corrected pressure and force on the sample.

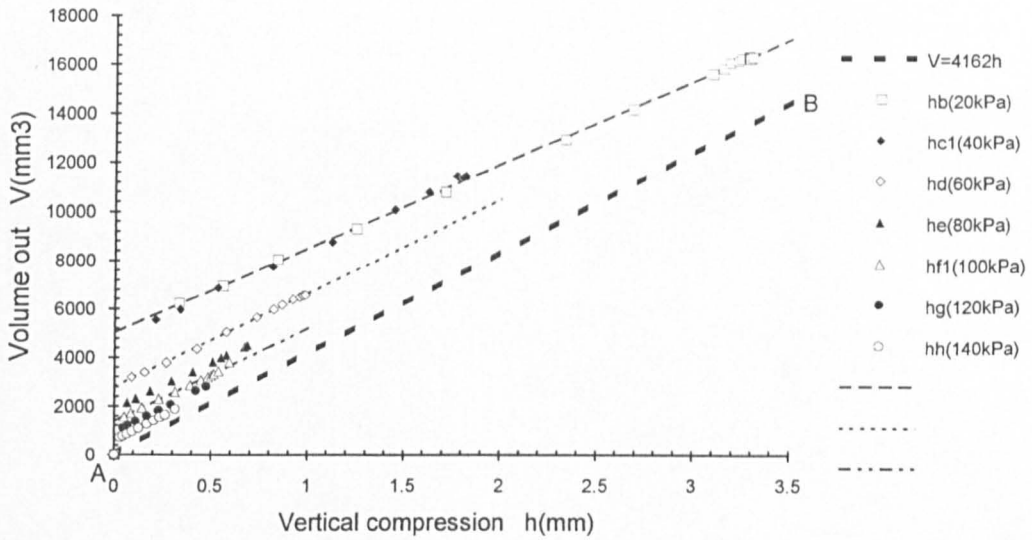

(a)

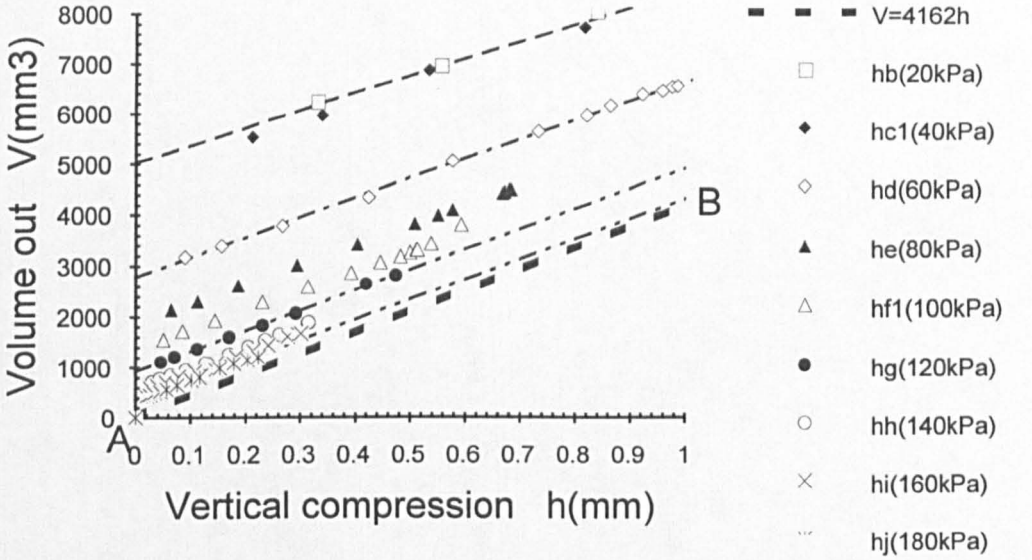

(b)

Fig.-4.11 (a) Volume vs vertical compression of test Series 1H in the radial flow oedometer; (b) Detail of (a) for compression of 0 to 1mm

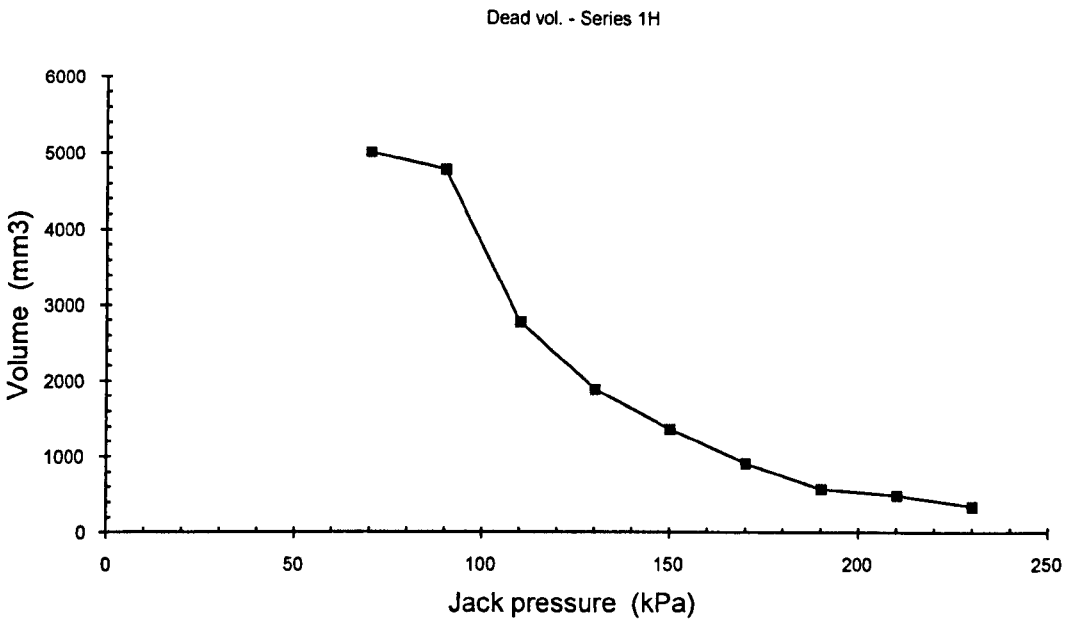

Fig.-4.12 Dead volume vs jack pressure in the consolidation test

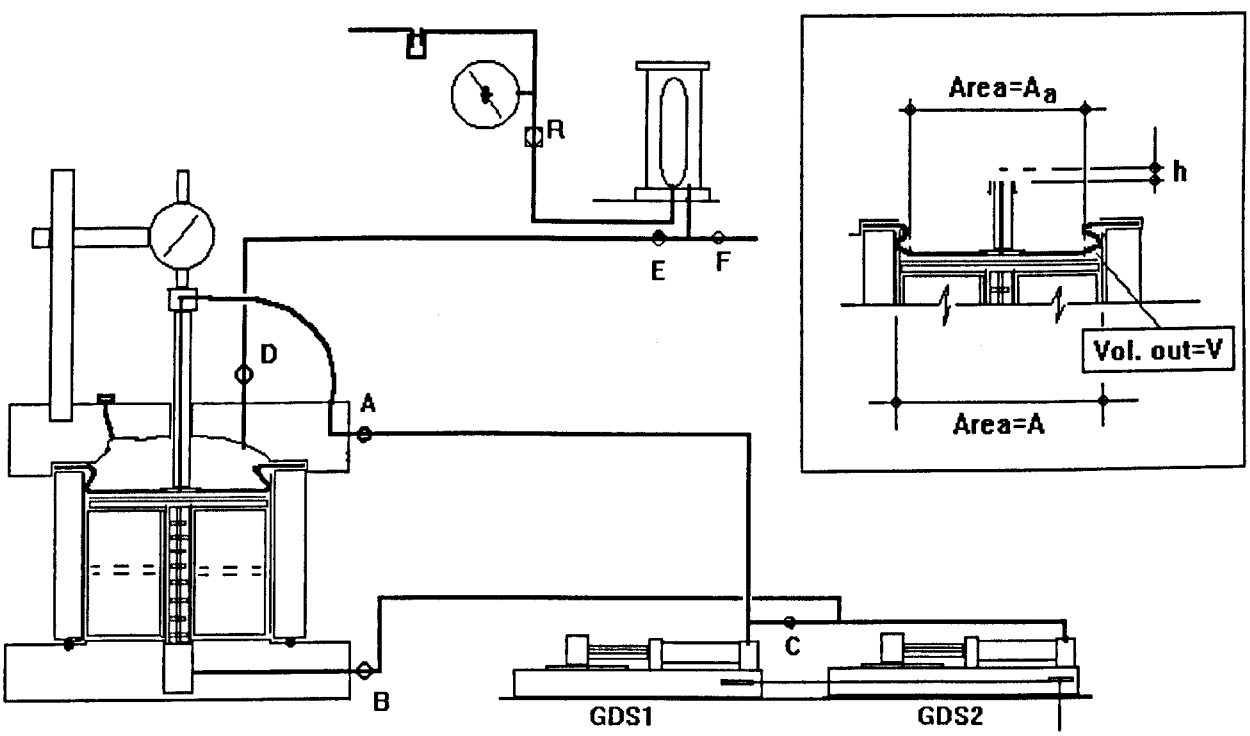

Fig.-4.13 Pressure test arrangement to investigate dead volume in the Rowe cell

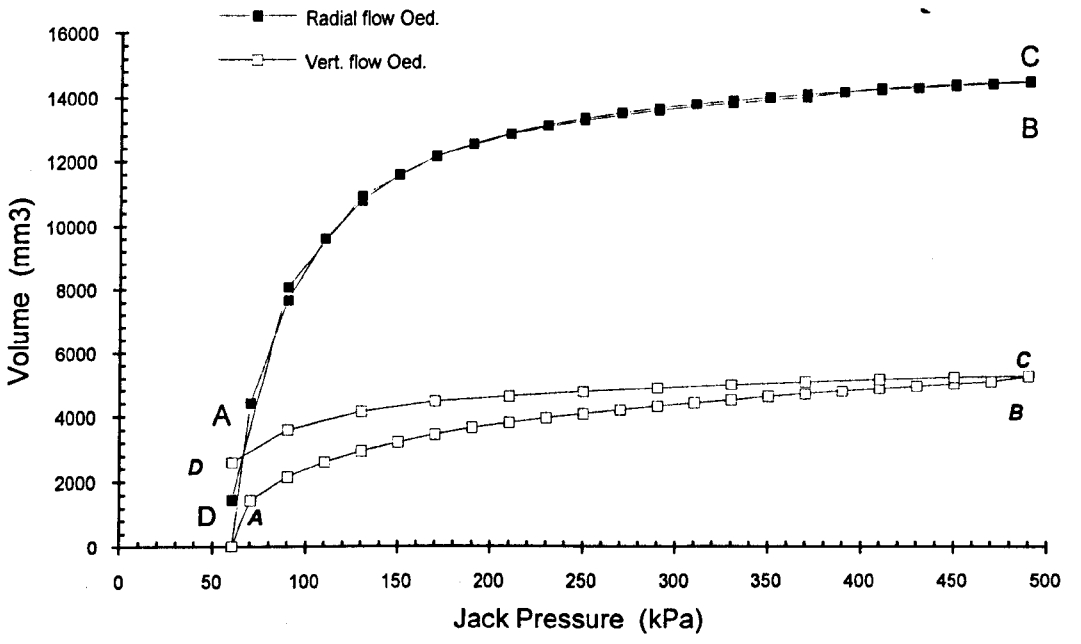

Fig.-4.14 Volume of expelled fluid vs jack pressure for the radial flow and vertical flow oedometers

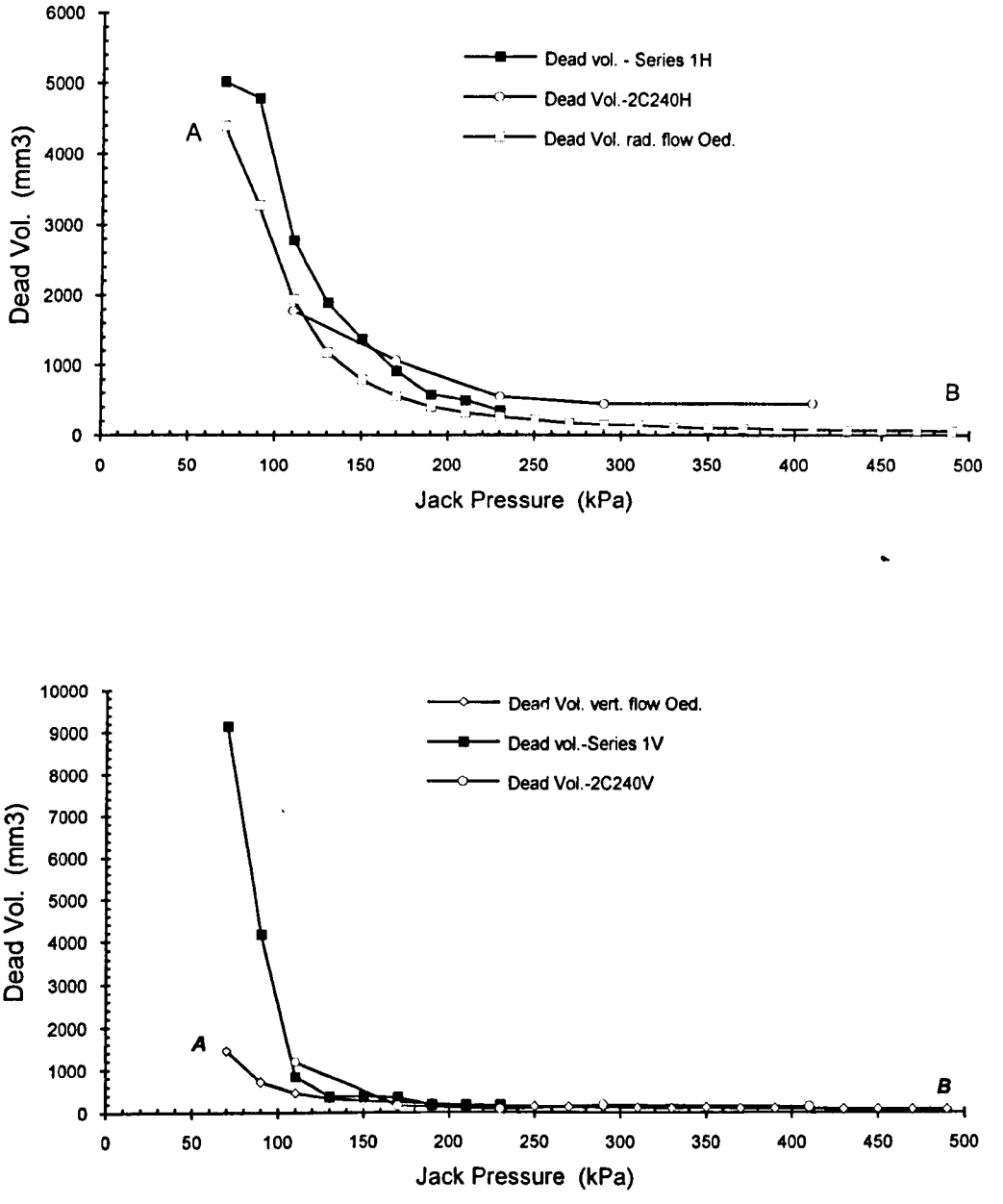

Fig.-4.15 Dead volume as obtained from the consolidation test compared with that from the pressure test

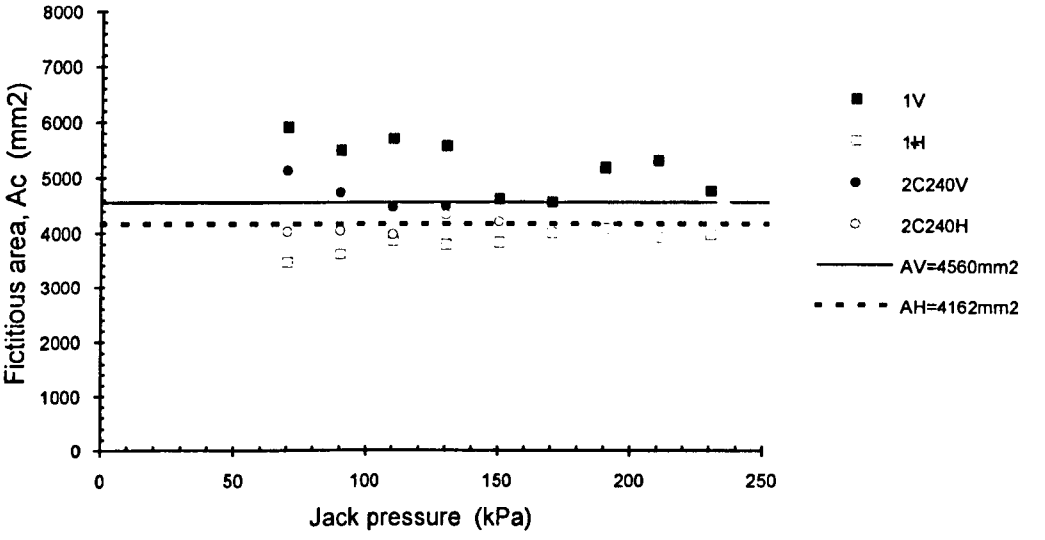

Fig.-4.16 Fictitious contact area, (A_c=V/h) vs jack pressure for the radial flow and vertical flow oedometers

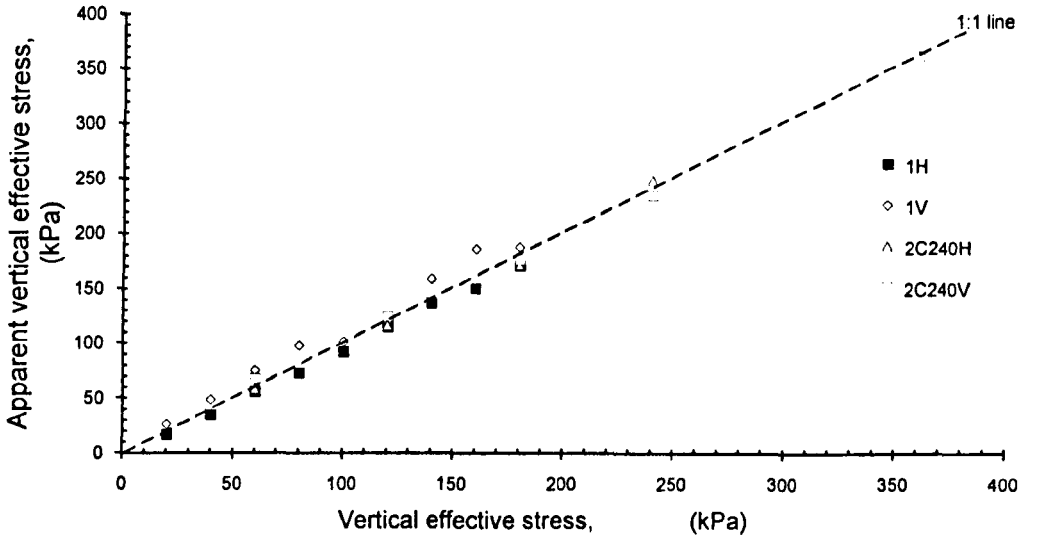

Fig.-4.17 Apparent vertical effective stress compared with the vertical effective stress from readings of jack pressure: Test Series 1H, 1V, 2C240H and 2C240V

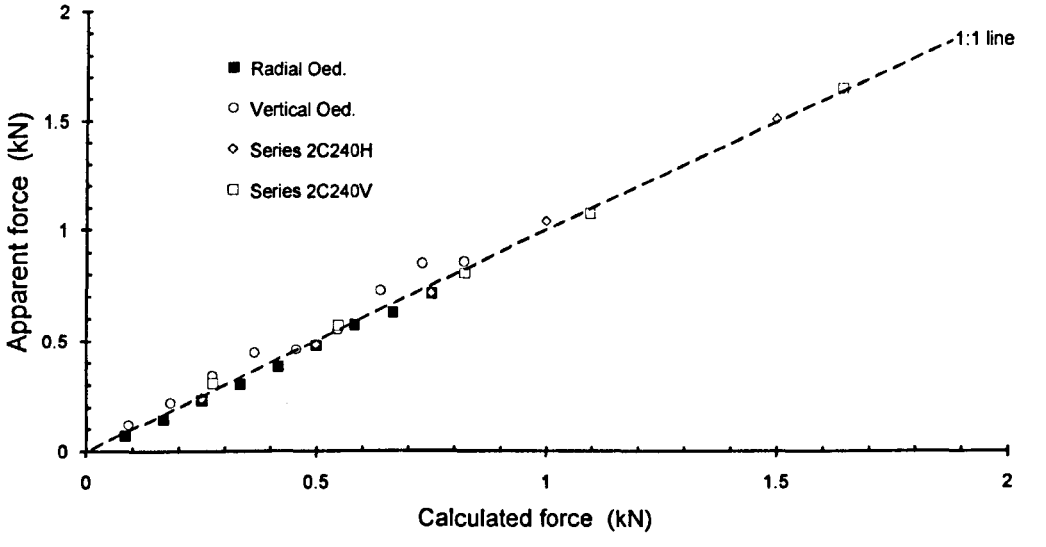

Fig.-4.18 Apparent force vs calculated force on sample: Test Series 1H, 1V, 2C240H and 2C240V

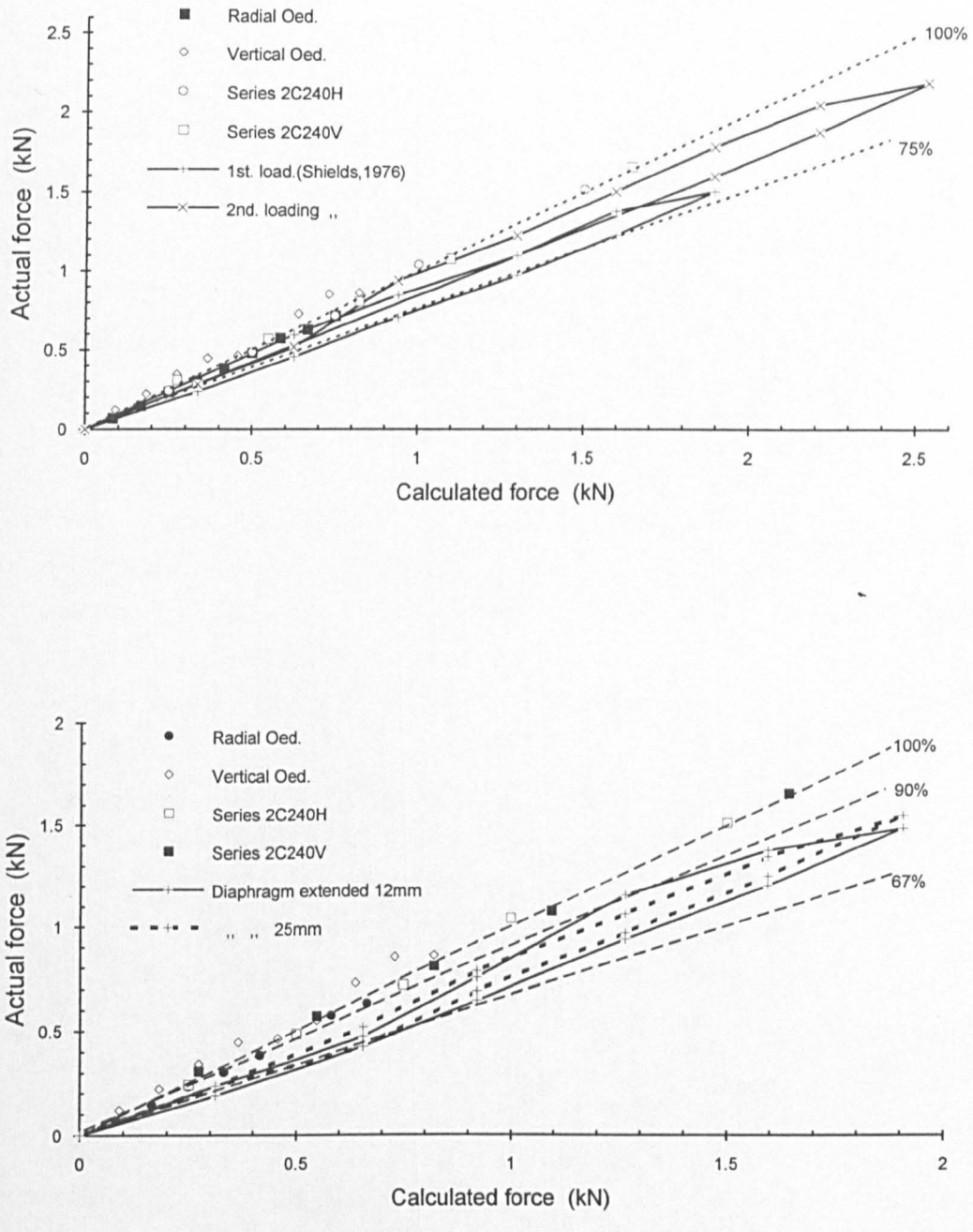

Fig.-4.19 Actual force vs assumed force on proving ring: Results of Shields(1976) compared with the apparent force obtained from this study

CHAPTER 5

5. RESULTS AND DISCUSSION

5.1 Introduction

In this chapter the results of the experimental investigation carried out on the permeability characteristics of supreme kaolin are presented and discussed. The permeability characteristics considered are: the variation of permeability with void ratio, development of permeability anisotropy resulting from varying stress history, and the interpretation of permeability data as deduced from consolidation tests.

Initially, the 1-D consolidation history of the clay samples is presented from results of the consolidation tests. These data will provide the basic void ratio vs $\lg.\sigma_v'$ relationships for all test series. Typical results from the constant flow rate permeability tests are next shown which provide the basic form of data for the calculation of permeabilities of all the samples tested.

Permeability values of the kaolin are obtained from both direct and indirect tests. The direct tests consist of constant head and constant flow rate permeability tests. Direct application of Darcy's law is applied to data from these tests. The indirect test consists of the conventional step-loaded consolidation test. Permeability is deduced from results of this test since it is one of the main material properties that govern the rate of consolidation. Obviously permeability values calculated from the direct tests may differ with those from the indirect tests since in the former, water is led to pass through the clay medium in which deformation has completed (permeability test), while in the latter, water is squeezed out of the clay undergoing time dependent deformation (consolidation test). Darcy's law is directly applied in permeability test whereas the law is coupled with the consolidation and compressibility characteristics of the clay in consolidation test.

Consolidation characteristics of the clays from the constant flow rate permeability tests are also evaluated and compared with data from the conventional step-loaded consolidation tests.

A summary of the test series whose results are discussed is as shown in *Table*-5.1. Designation of test series follows in accordance to the passage of sample routes as conceptualised in *Fig.*-3.1 of Section 3.2.1 - 'Phases of testing'. Thus there were 3 test series denoted as Series 1, Series 2 and Series 3. Series 1H and 1V indicate the slurry samples that passed through Passage 1 and were tested in Phase C. Letters H and V denote tests in radial flow and vertical flow oedometers, respectively.

Table-5.1 Summary of samples tested

No.	Test series	Sample taken from:	Max. pressure in virgin loading	Cell pressure	Back pressure	Effective stress in sample before shear	Max. strain in undrained shear	Max. pressure in oedometer	Remarks
			σ'_{vp}(kPa)	(kPa)	(kPa)	σ'_{3iso}(kPa)	ε_v(%)	σ'_{vc}(kPa)	
(1)	(2)	(3)	(4)	(5)	(6)	(7)	(8)	(9)	(10)
	Series 1:								
1	1H & 1V	S	580	-	-	-	-	580	Phase A and phase C test
	Series 2:								
2	2C40H & 2C40V	C	40	-	-	-	-	160	Phase A and phase C test
3	2T120H & 2T120V	T	120	-	-	-	-	240	" "
4	2T240H & 2T240V	T	240	-	-	-	-	480	" "
5	2C240H & 2C240V	C	240	-	-	-	-	360	" "
6	2C360H & 2C360V	C	360	-	-	-	-	580	" "
	Series 3:								
7	3F1,1,1H & 3F1,1,1V	F	100	300	200	100	3.9	480	Phase A, phase B and phase C test
8	3F1,1,2H & 3F1,1,2V	F	100	300	200	100	7.9	120	" " "
9	3F1,1,3H & 3F1,1,3V	F	100	300	300	100	11.5	120	" " "
10	3T1.2,2,1H & 3T1.2,2,1V	T	120	400	200	200	10.3	480	
11	3T2.4,2,1H & 3T2.4,2,1V	T	240	450	250	200	1.0	360	" " "
12	3T6,3,1H & 3T6,3,1V	T	600	500	200	300	11.0	480	" " "
13	3T6,3,2H & 3T6,3,2V	T	600	500	200	300	11.2	480	" " "

Notes: σ'_{vp} = Max. vertical effective stress applied to sample during 1-D consolidation of slurry

σ'_{vc} = Max. vertical effective stress applied to sample during consolidation / permeability test

σ'_{3iso} = Isotropic effective stress existing in sample before undrained shear

Phase A = Consolidation of slurry in tank (T), cylinder (C), filter press (F) or oedometer (S)

Phase B = Undrained shear test of samples from Phase A test

Phase C = Consolidation / permeability test of samples from Phase A or Phase B tests

Series 2C40H and 2C40V indicate block samples that had been previously consolidated in the consolidation cylinder to maximum vertical effective stress σ'_{vp} of 40kPa, through Passage 2, and sampled out into the radial and vertical flow oedometers. Consolidation of the parent sample (also from slurry) in the consolidation cylinder and tank was designated as Series CV and TV, respectively - C for cylinder and T for tank.

Series 3F1,1,1H and 3F1,1,1V indicate block samples that had undergone CIU compression tests. Thus 3F1,1,1H refers in the following order to: 3 for Series 3, or block sample that passed through Passage 3; F for sample taken from filter press; 1 for σ'_{vp}=100kPa; the next 1 for σ'_{3iso}=100kPa; and 1H - horizontal permeability test for strain ε_v no.1.

The Series notation such as 2C40H, 2C40V, 3F1,1,1H, 3F1,1,1V etc will also be used to replace k for permeability whenever it is found convenient to do so in later Sections.

The clay used in all tests was supreme kaolin obtained from English Clays Lovering and Pochin Ltd. The material had been hydraulically mined from weathered granite near St. Austell, Cornwall. The index properties of this clay as determined by standard soil classification tests are given below. The water content of the slurry was found to be 114%.

Index properties, % (BS 1377: 1975)	
Liquid limit [Test 2(A)]	80.49
Plastic limit (Test 3)	34.50
Plasticity index (Test 4)	45.99
Specific gravity (Test 6)	2.62
Finer than 2-μm size, % [Test 7(D)]	95

5.2 Consolidation test data

One dimensional compression of the supreme kaolin slurry in the oedometers, cylinder and tank is presented as (e-lg.σ'_v) curves in *Fig.*-5.1. Compression data in the figure consist of Series 1H and 1V from the radial and vertical oedometers. The tank and cylinder Series TV and CV are for vertical flow only since there was no provision for radial flow facilities in these apparatus as they were meant to produce 1-D compressed samples with drainage path always in vertical direction.

The shapes of the curves are very similar but complete matching of individual data points (void ratio) or individual curves is a rare event for the given range of vertical effective stress of 10kPa to 580kPa. In terms of slopes, the variability of rebound line is less than the normal consolidation line. For the Series 1 tests, the vertical compression curve 1V is observed to be lower than the horizontal series 1H and the difference in void ratio Δe is about 0.25 at the low vertical effective stress of 10kPa and decreases proportionately [in the (e-lg.σ'_v) plot] to negligible value at higher vertical effective stresses of 300kPa and above. For the Series C which consisted of three replicate tests each conducted one after the other in the same cylinder, a comparable range of void ratio difference to that seen in Series 1V and 1H is observed. ie. Δe is largest at low σ'_v and reduced to zero at large σ'_v.

For reasons of both practical purposes and common 'geological' origin of the sample, it is reasonable to approximate the curves in *Fig.*-5.1 into average normal and rebound/recompression lines as characterised by the compression and rebound/recompression index, C_c and C_r. Such consolidation lines as evolved are shown in *Fig.*-5.2 with the upper and lower limit of the scatter shown. The normal compression line is seen to be bilinear on the (e-lg.σ'_v) plot with the kink occurring at σ'_v=180kPa and e=1.60.

Differences in results could be due to several reasons: (1) effects of apparatus sizes, ie. height, diameter; (2) effect of slight differences in placement water content of the slurries; and (3) assumption of equal nominal pressure readings. Differences in void ratio seems to become small as the vertical effective stress increases. Thus at low stresses, say σ'_v=10kPa the value of e ranges from 3.2-2.8 and this range decreases from 1.5 to 1.4 at higher stress level of 500kPa. The order of accuracy expected from the calculation of void ratio amounts to about ±0.05.

The values of compression and rebound index for all three series are generally close to each other with average values of C_c = -1.10, & -0.62 and C_r = -0.12. This observation is consistent with the generally held concept that C_c depends primarily on the type of material being tested.

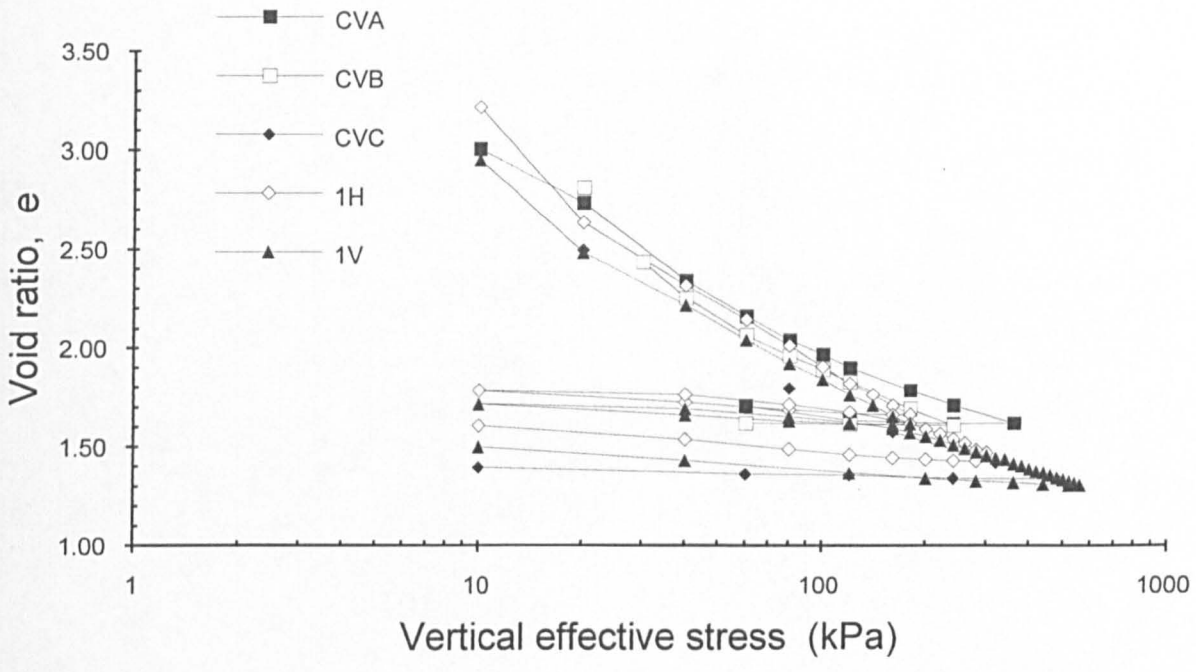

Fig.-5.1 1-D compression of kaolin slurry in oedometers (1V & 1H); and cylinder (CVA, CVB & CVC)

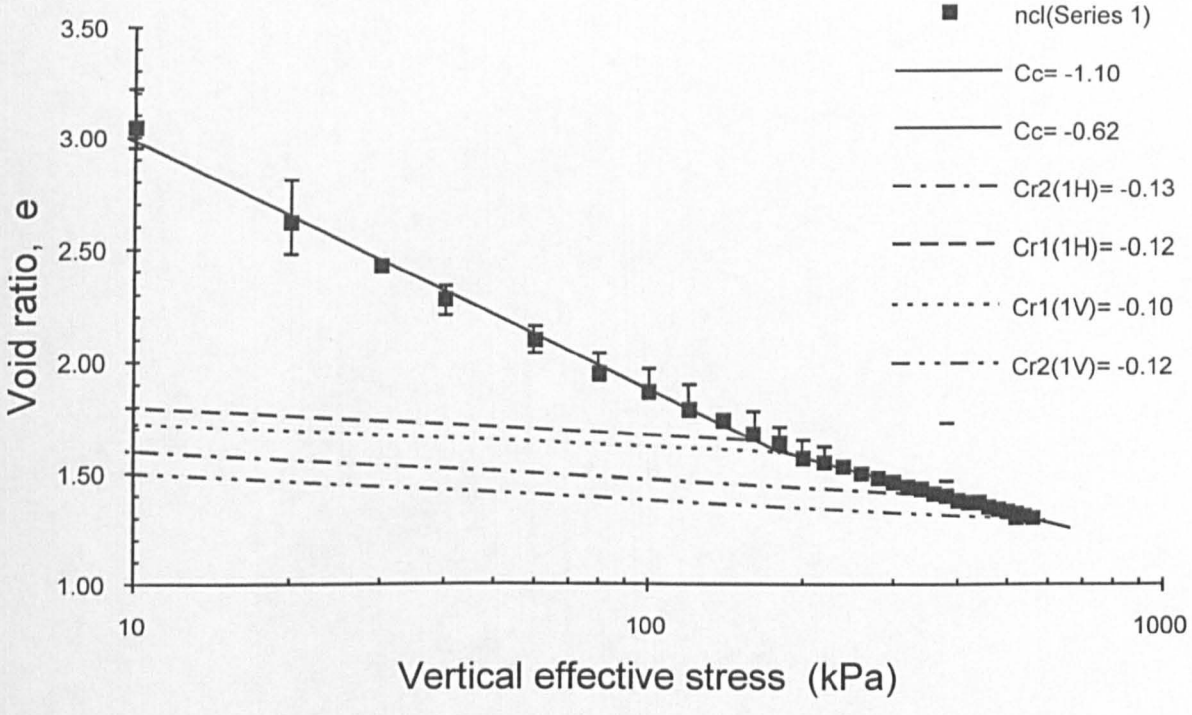

Fig.-5.2 1-D compression of supreme kaolin slurry: Average data from results in *Fig.*-5.1

One dimensional compression of the supreme kaolin block samples trimmed from the previously consolidated slurries (ie. Series CV & TV), and reconsolidated in the radial and vertical flow oedometers, is presented as Series 2 in the (e-lg.σ'_v) curves in *Fig.*-5.3. Compression data in this figure are averages of Series 2C40H & 2C40V denoted as 2C40; 2T120H & 2T120V denoted as 2T120; 2T240H & 2T240V denoted as 2T240, etc. Referring to *Figs.*-5.1 and 5.3, an indication of disturbance resulting from the sampling out, trimming and setting up operation could be seen by comparing the normal compression lines and the differences in void ratios between Series CV or TV and Series 2 at the maximum past consolidation pressures σ'_{vp}. For the case of Series 2C and CV, the relevant data are as shown in *Fig.*-5.4 for the normal compression lines. The differences in void ratio between the 'parent' clay and the 'sample' are $\Delta e = 0.35$, 0.27, and 0.39 at $\sigma'_{vp} = 40$, 240, and 360kPa respectively.

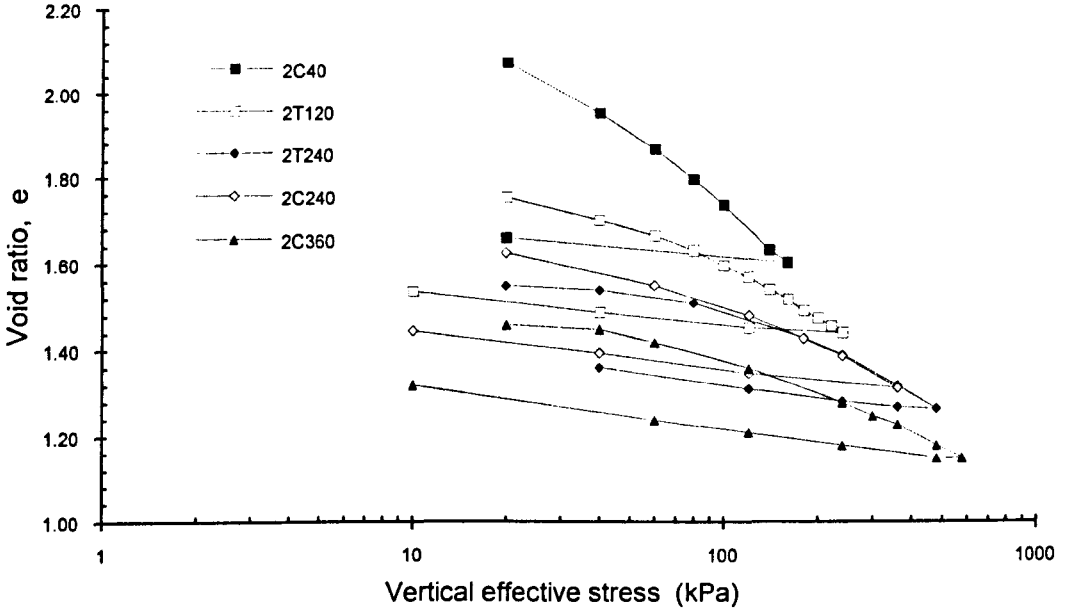

Fig.-5.3 1-D compression of supreme kaolin block samples (Series 2C & 2T)

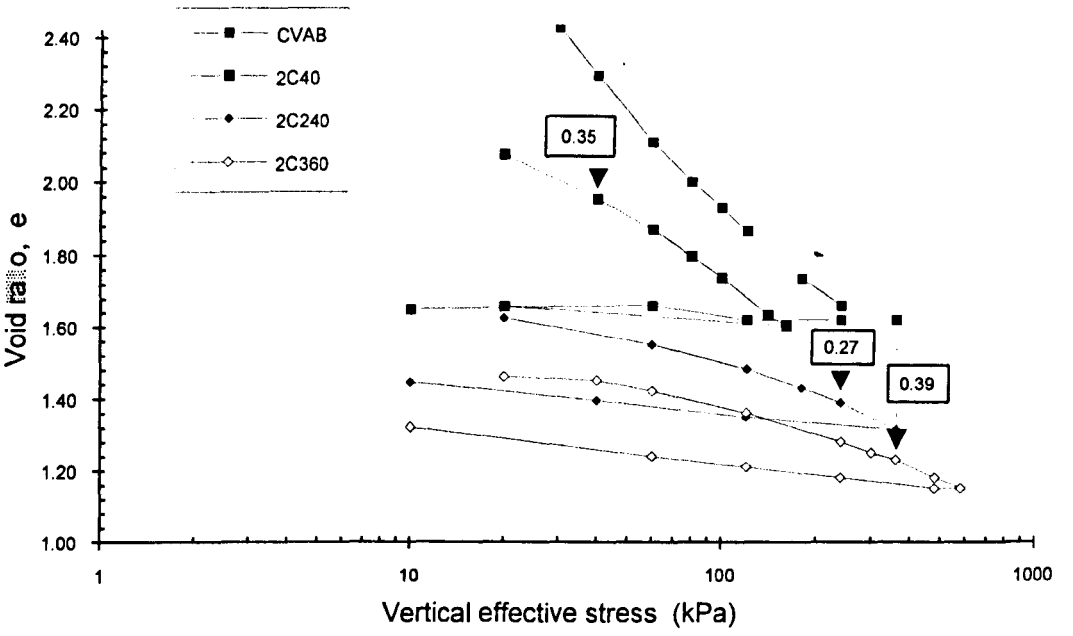

Fig.-5.4 Disturbance effect on void ratio during sample preparation

A summary of data for each of the test series is presented in *Table*-5.2, showing the compression/rebound and permeability parameters (C_c, C_r, C_k) together with the reference void ratios (e_o, $e_{\sigma'_{vp}}$, $e_{\sigma'_{3iso}}$, $e_{\sigma'_{vc}}$).

Table-5.2 Values of compression and rebound index C_c, C_r and permeability change index C_k for 1-D consolidated samples

Test series:				Exponential law model: $\sigma_v' = C \cdot D^e$ $C = 1/\lg D$					
		σ'_{vp}(kPa)	σ'_{vc}(kPa)	Cc	Cr	C_k	e_o	$e_{\sigma'_{vp}}$	$e_{\sigma'_{3iso}}$
Test series 1:									
1.	1H	from	580	-1.02	-0.14,	1.64	3.22		
	1V	slurry			-0.13	1.28	e_{10}=3.02		
1H(Al-Tabbaa)		from							
1V(Al-Tabbaa)		slurry				1.97*	2.20		
Test series 2:									
2.	2C40H	40	160	-0.64	-0.05	1.99	2.20	1.97	
	2C40V			-0.64	-0.06	1.07	2.21	1.94	
3.	2T120H	120	240	-0.4	-0.07	1.51	1.51	1.43	
	2T120V			-0.28	-0.07	0.94	1.51	1.41	
4.	2T240H	240	480	-0.39	-0.08	1.10	1.44	1.39	
	2T240V			-0.36	-0.09	1.03	1.45	1.48	
5.	2C240H	240	360	-0.38	-0.08	1.30	1.72	1.40	
	2C240V			-0.33	-0.09	1.21	1.62	1.38	
6.	2C360H	360	580	-0.29	-0.10	1.08	1.50	1.21	
	2C360V			-0.35	-0.11	0.98	1.60	1.24	

Notes: σ'_{vp} = Max. vertical effective stress applied to the sample during 1-D consolidation (ie. from slurry, in cylinder, tank and filter press)

σ'_{vc} = Max. vertical effective stress applied to sample during the consolidation/permeability test

e = void ratio;

C_k = permeability change index defined by $\Delta e = C_k \Delta \lg.k$

C_k = C_{kv} for vertical flow and $k = k_v$

= C_{kh} for radial flow and $k = k_h$

* = from Al-Tabbaa (1987) assuming e_o=2.2 and $k_{vo} = 7 \times 10^{-9}$m/s

Some of the (e-lg.σ'_v) curves for kaolin clays published in the literature are shown in *Fig.*-5.5 together with the results in this study. There is a wide range of scatter with the author's results forming an upper band in the void ratio at all values of vertical effective stress. This scatter may be related to a number of factors including the mineralogical and the clay content difference of the kaolin, use of different apparatus and sample sizes, and difference in the initial states of the sample.

Samples having lower values of liquid limit LL and plasticity index PI tend to require lower initial equilibrium void ratio at the same low starting vertical effective stress compared to those having high LL. Despite the scattering of positions of compression curves, similar values of the compression index C_c are seen to develop as the vertical effective stress increases. From the figure it is reasonable to quote a single value of C_c at vertical effective stresses of 200kPa or higher.

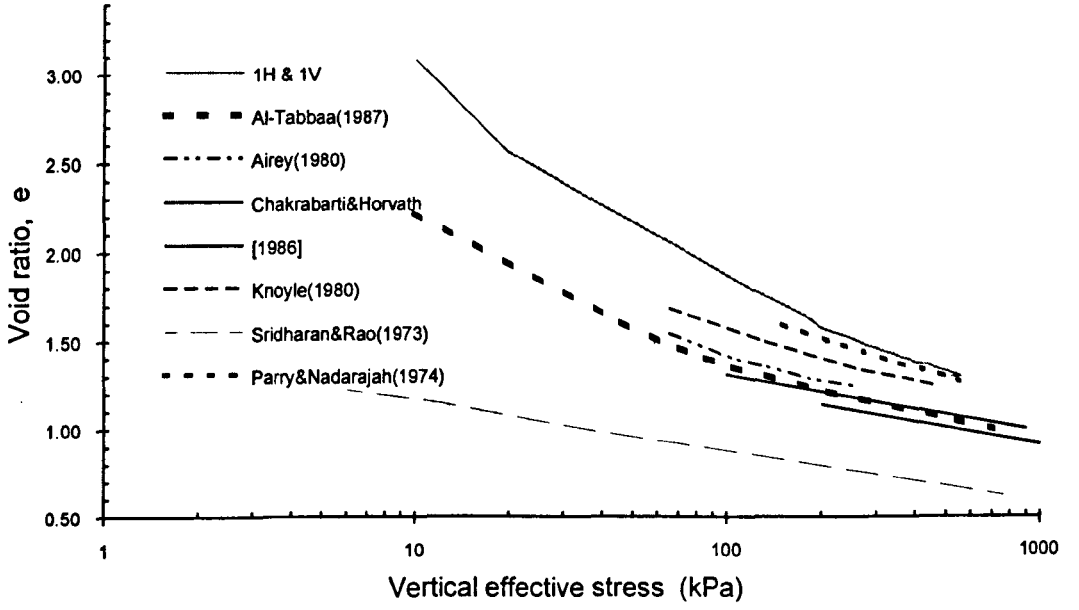

Fig.-5.5 Some 1-D normal compression lines obtained by various research workers

5.3 Permeability test data

The data obtained from permeability tests are discussed below. The main equations used to calculate the permeability and void ratio are as given in Chapter 4.

Results of permeability tests are shown in the form of induced pressure difference with time (called pressure response curve) and pressure difference vs. flow rate relationships.

The characteristics of the data obtained from the constant flow rate tests are illustrated in *Figs.*-5.6(a), 5.6(b) and 5.6(c) for the sample in test series 2T240V (vertical permeability) at consolidation stages of 100, 240 and 480 kPa respectively. *Fig.*-5.6(a) shows the development of induced pressure difference with time for various flow rates imposed on the sample which had stabilised at consolidation pressure of 100 kPa. The positive pressure differences indicate an upward flow through the sample from bottom to top while the the negative values indicate a downward flow from top to bottom. An interval of time, hereinafter called the response time elapses from the moment of imposing the flow rate until the pressure difference reaches steady state value. It is observed that the time responses of the induced pressure difference for various flow rates and for upward and downward flows are approximately the same. Visual inspection of *Fig.*-5.6(a) indicates that steady state pressure conditions are achieved after about 30 min of flow had elapsed.

Fig.-5.7 shows the plot of pressure differences against flow rate for the data of *Figs.*-5.6. The consistency of the data with Darcy's law is evident from linearity of the line. Permeability of the sample for this particular consolidation stage is given by Eqs.-(4.1) and (4.34) in Chapter 4 modified as:

$$k_v = (10^{-6}/930)(h_p/S) \text{ m/s}$$

where S [$=\Delta p/(1/R)$] is the slope of the plot in *Fig.*-5.7 and h_p is the current sample height in mm.

Similar results for the sample in test series 2T240H (radial permeability) are shown in *Figs.*-5.8(a), 5.8(b), 5.8(c) for the pressure response curves at consolidation stages of 180, 240 and 480 kPa respectively, and Fig.-5.9 for the pressure difference flow rate relationships. Permeability of this sample is derived from Eqs.-(4.2) and (4.35) in Chapter 4 as:

$$k_h = 1.447\text{x}10^{-6}(1/R)(1/h_p)(1/\Delta p) \text{ m/s}$$
$$= 1.447\text{x}10^{-6}(1/S)(1/h_p) \text{ m/s}$$

where S is the slope of the plot in *Fig.*-5.9 and h_p is the current sample height in mm.

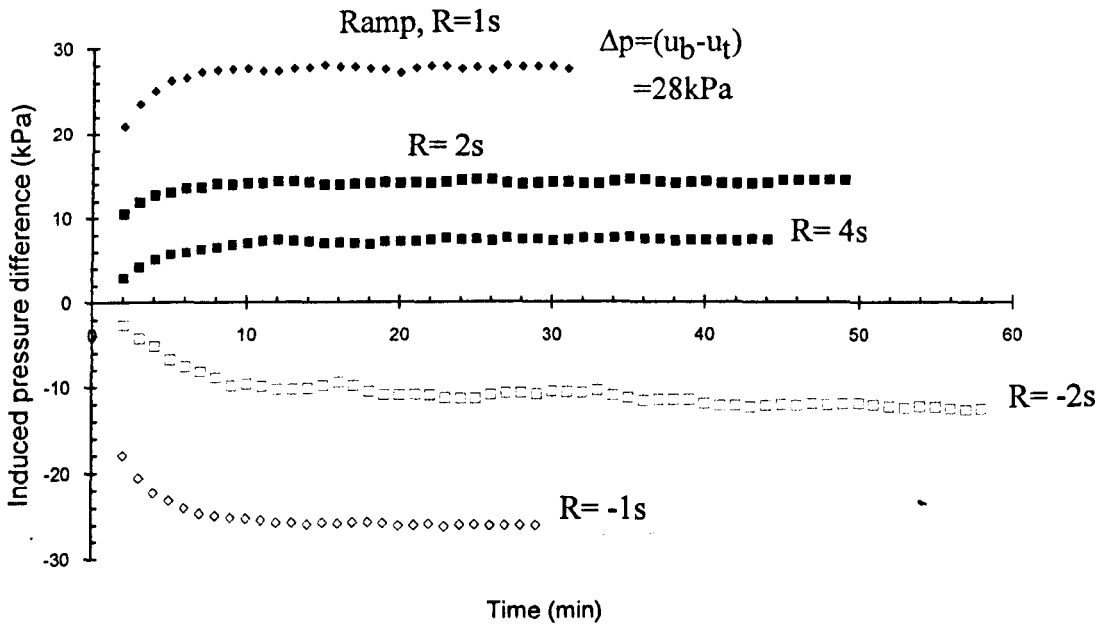

(a)

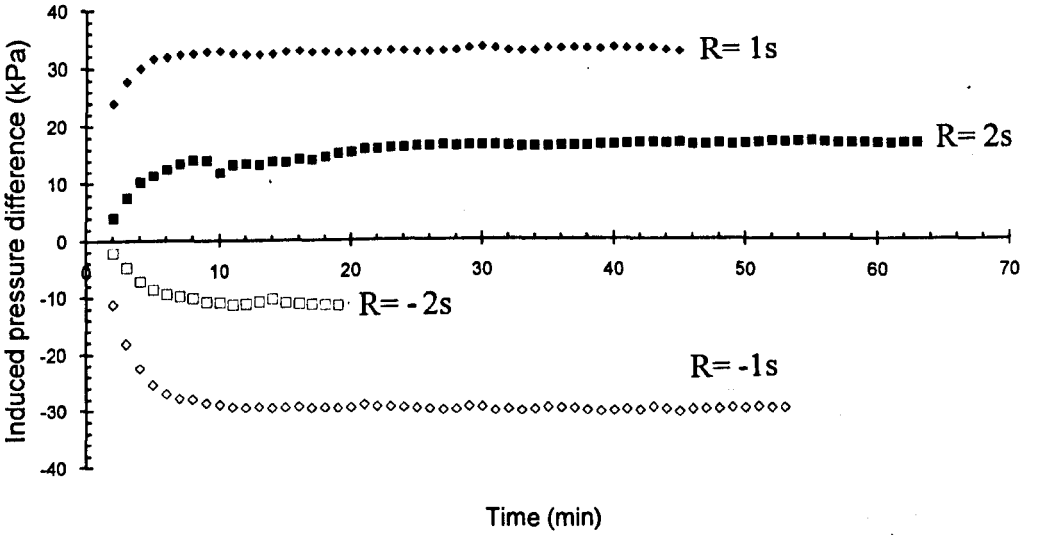

(b)

Fig.-5.6 Results of constant flow rate permeability tests for:
(a) Series 2T240V at σ_v' = 100kPa;
(b) Series 2T240V at σ_v' = 240kPa

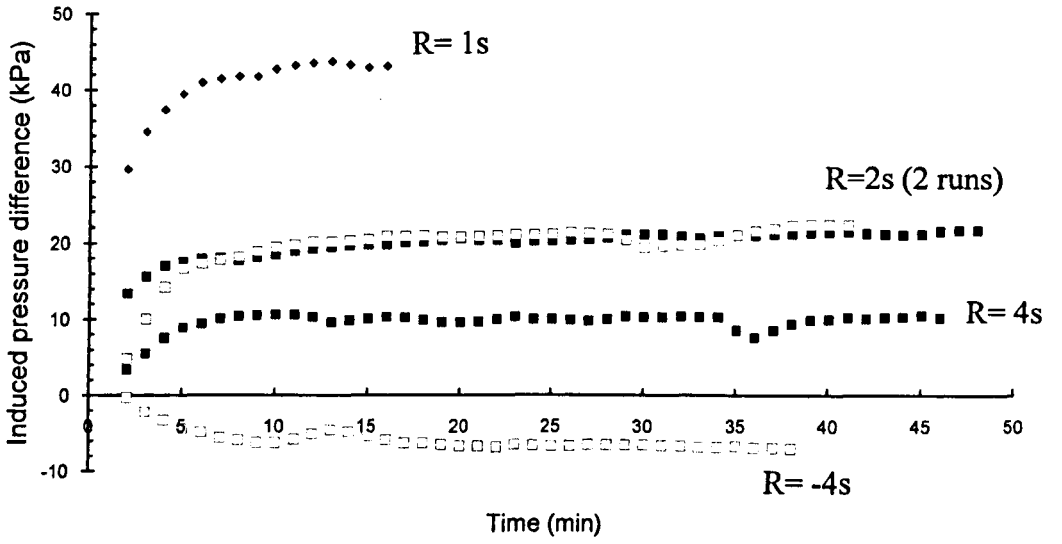

(c)

Fig.-5.6 *cont.* (c) Series 2T240V at σ_v' = 480kPa

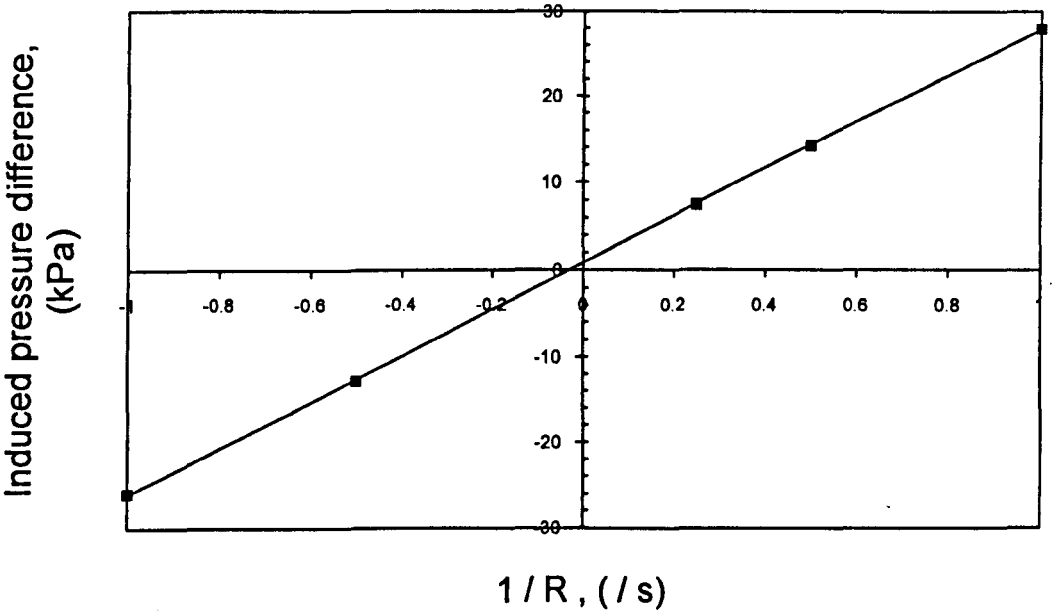

Fig.-5.7 Induced pressure difference vs flow rate for sample in test Series 2T240V at σ_v' = 100kPa

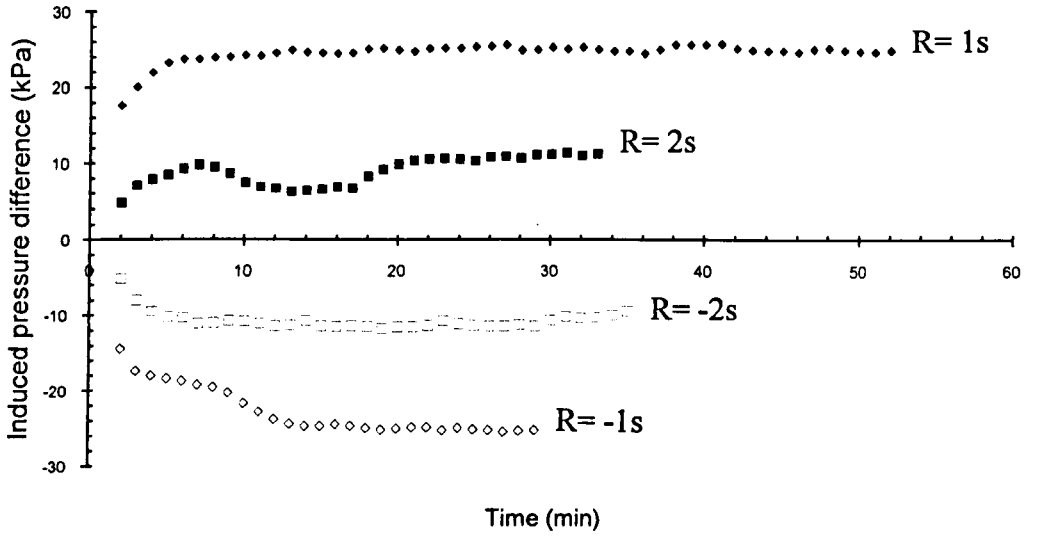

(a)

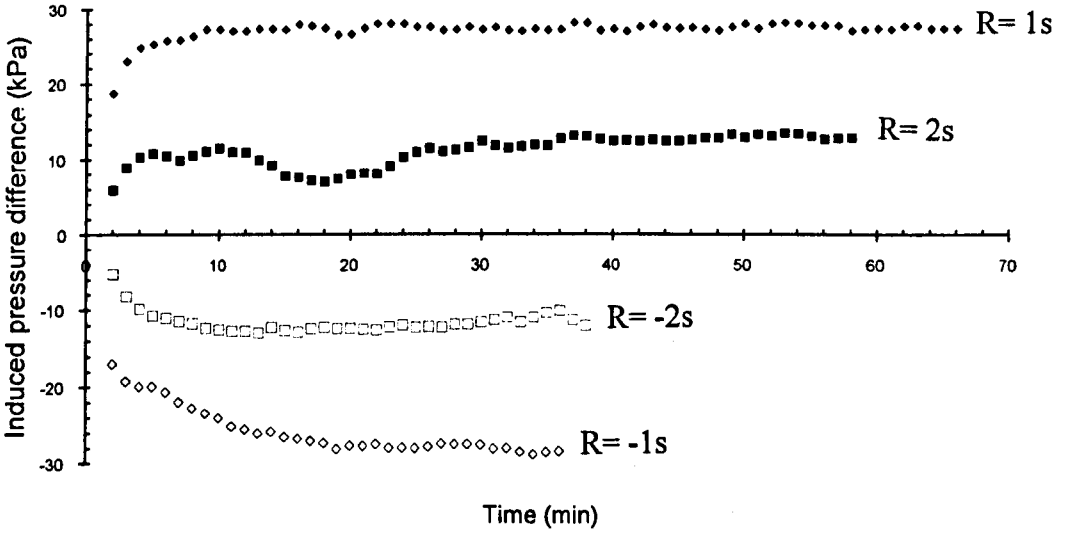

(b)

Fig.-5.8 Results of constant flow rate permeability tests for:
(a) Series 2T240H at σ'_v = 180kPa;
(b) Series 2T240H at σ'_v = 240kPa

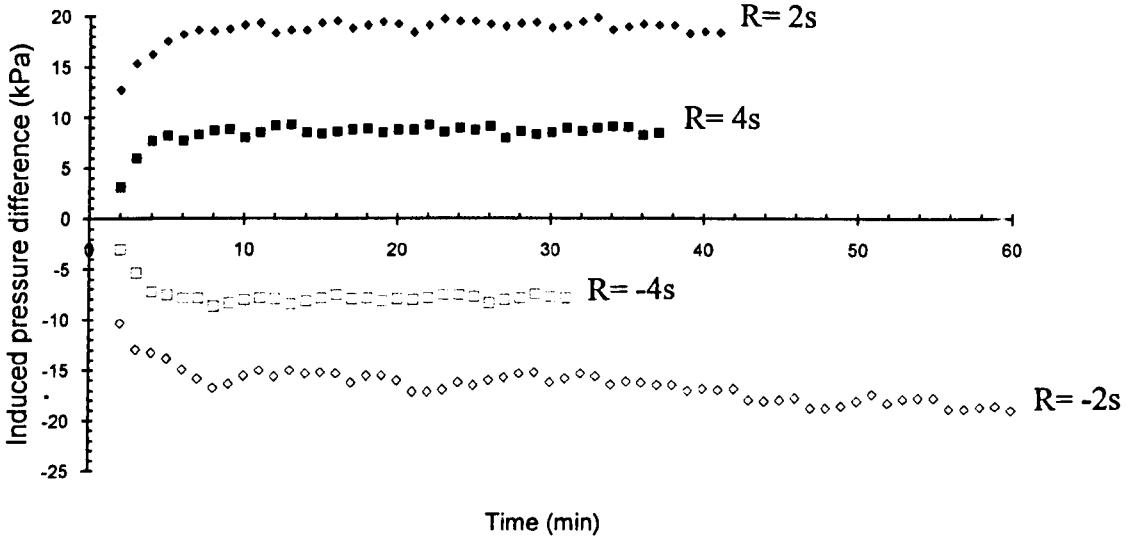

(c)

Fig.-5.8 *contd.* (c) Series 2T240H at σ'_v = 480kPa

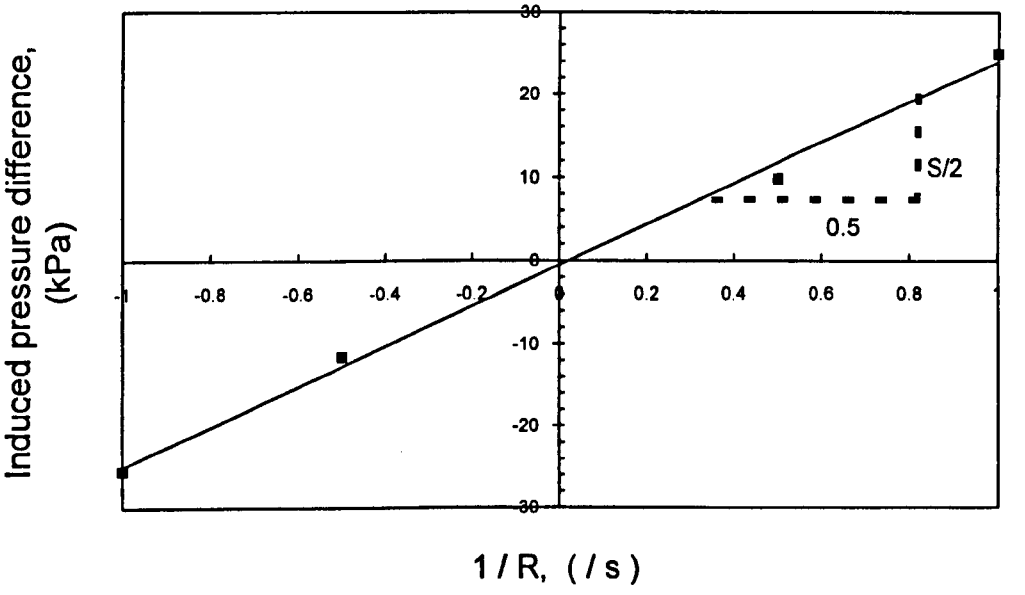

Fig.-5.9 Induced pressure difference vs flow rate for sample in test Series 2T240H atσ'_v = 180kPa

Pressure differences against flow rate relationships at other consolidation stages for the samples in test series 2T240V and 2T240H are shown in *Figs.*-5.10(a) and 5.10(b) respectively. It is noted that each pressure difference in the figures represents the average steady state value from pressure response curve such as that shown in *Fig.*-5.6. The slopes S, of the lines in *Figs.*-5.7, 5.9, and 5.10 used for the calculation of permeability are the best linear fit obtained by linear regression through the appropriate points.

During the course of permeability test, the dial gauge reading is observed to decrease or increase slightly from the stabilised value of the consolidation stage. Typical variation of the gauge reading for the permeability test data of *Fig.*-5.6(a) lies in the range of 0 to 0.031mm. This effect on the height of the sample and hence the calculations of void ratio and permeability is found to be negligible. The ratio of the induced pressure difference to the current consolidation pressure, $\Delta u / \sigma'_v$ in this case is 28kPa / 100kPa = 28%.Under this condition the pressure difference during permeability tests is kept to within 28% of the consolidation pressure which seems to keep volume changes of the sample small in order not to affect the current sample height and void ratio during permeability tests.

The current sample height, h_p used for the calculation of permeability is based on the gauge reading G_p taken at the end of permeability test. The void ratio corresponding to the permeability value is based on this value of the current sample height. Hence from the available experimental data, permeability characteristics of the kaolin are examined from the relationship of permeability with void ratio typically in the logarithmic linear plot. Results from the various test series are presented in the following Sections.

5.4 Permeability and void ratio

5.4.1 Vertical permeability and void ratio

As discussed earlier in Section 2.1, the most commonly adopted relationships between permeability and void ratio for clays are those described by Eqns.-(2.7), (2.8) and (2.9), namely the simple lg k with linear e and lg k with lg e plots, or the combined lg [k(1+e)] with lg e relationship. These equations endeavour to fit closely experimental data and as such they are successful only for the range of experimental void ratio considered, together with some appropriate curve fitting parameters. Tavenas et al.(1983 II) pointed out that none of these equations could offer descriptions of permeability characteristics with void ratio of general validity but the simple (lg.k vs e) relation appears to give a reasonable and practical approximation for the range of volumetric strains encountered in engineering practice involving soft,

nc clays. Another attraction of adopting the (lg.k vs e) relation is its similar form to the compression law [linear(e vs lg.σ'_v)] where the permeability index C_k is analogous to the compression index C_c. Consequently, the variation of permeability with void ratio will be mainly discussed with reference to the simple linear (lg.k vs e) relationships. Permeability data fitted by the power law model, ie. linear (lg.k vs lg.e) are also worked out and tabulated for completeness. This latter model was also found to fit accurately experimental permeability data over much wider range of void ratios especially for clays sedimented from slurry.

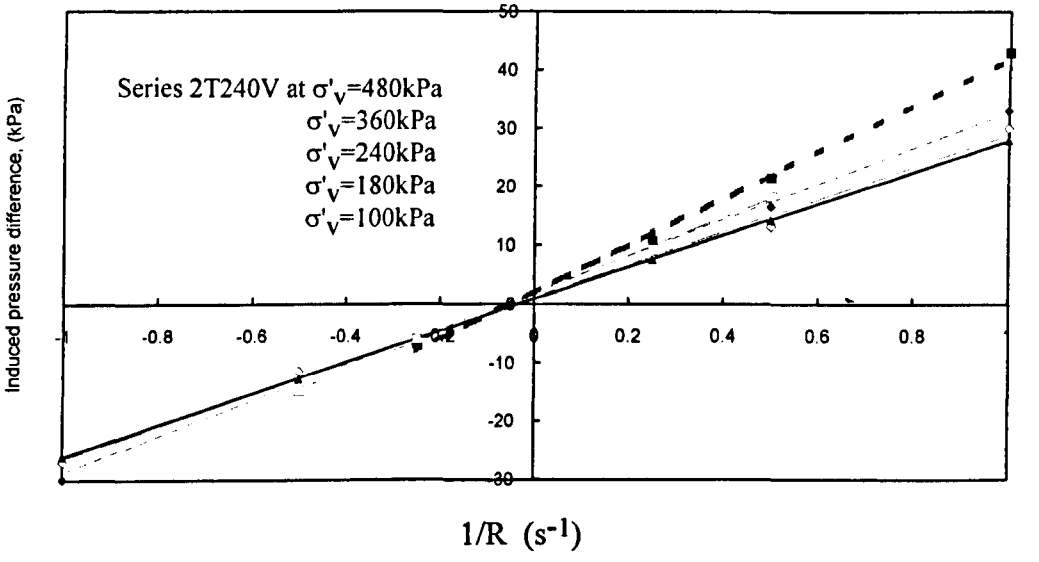

(a)

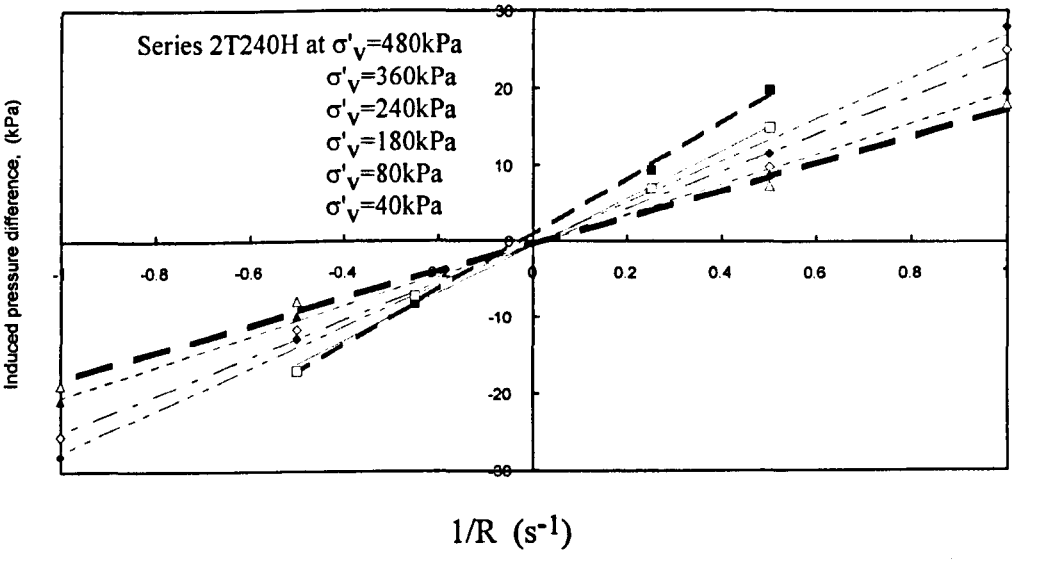

(b)

Fig.-5.10 Induced pressure difference vs flow rate at various consolidation pressures (a) Series 2T240V; and (b) Series 2T240H

The variation of the vertical permeability with void ratio is shown on a ($lg.k_v$ vs e) plot in *Fig.*-5.11 for the slurry sample (Series 1V). It is observed in the figure that the logarithm of vertical permeability decreases with void ratio in a linear fashion. The variation is approximately linear for the void ratio ranging from about 2.40 down to about 1.60 which corresponds roughly to the normally consolidated line (ncl) of the ($e\text{-}lg.\sigma'_v$) plot [see also *Fig.*-5.15(b)]. A least square fit to the data is shown in the figure as solid line for the exponential law model with the following curve fitting expression:

$$k_v = 1.38 \times 6.08^{\,e} \times 10^{-10} \text{ m/s} \qquad (5.1)$$

$$C_{kv} = 1.28 \qquad (5.1a)$$

where C_{kv} is a permeability change index associated with Eq.-(5.1).

Vertical permeability of other kaolin clays reported in the literature are shown in *Fig.*-5.12 together with the data obtained in this study for comparison.

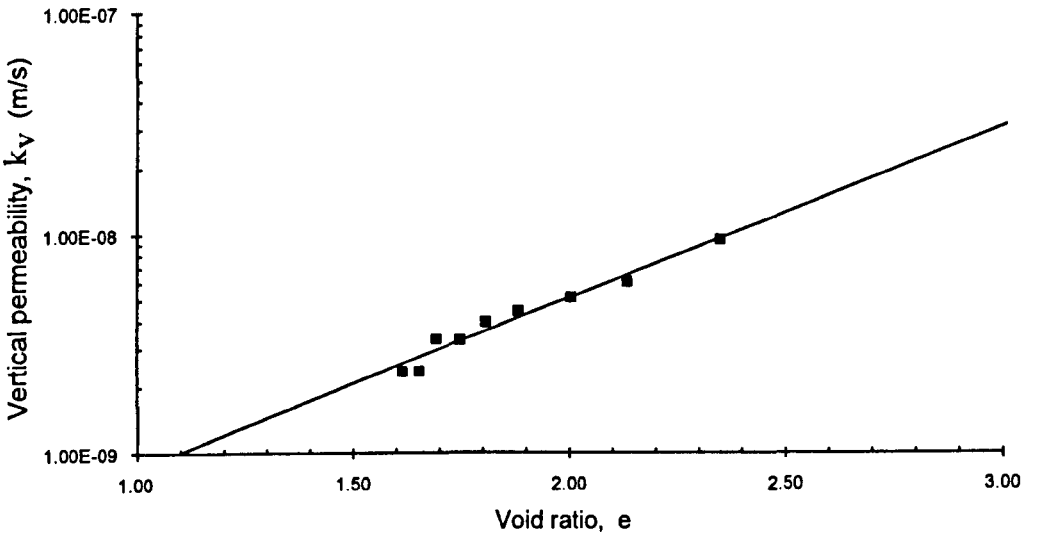

Fig.-5.11 Logarithm of vertical permeability vs void ratio for sample in test Series 1V: Eq.-(5.1) compared with data

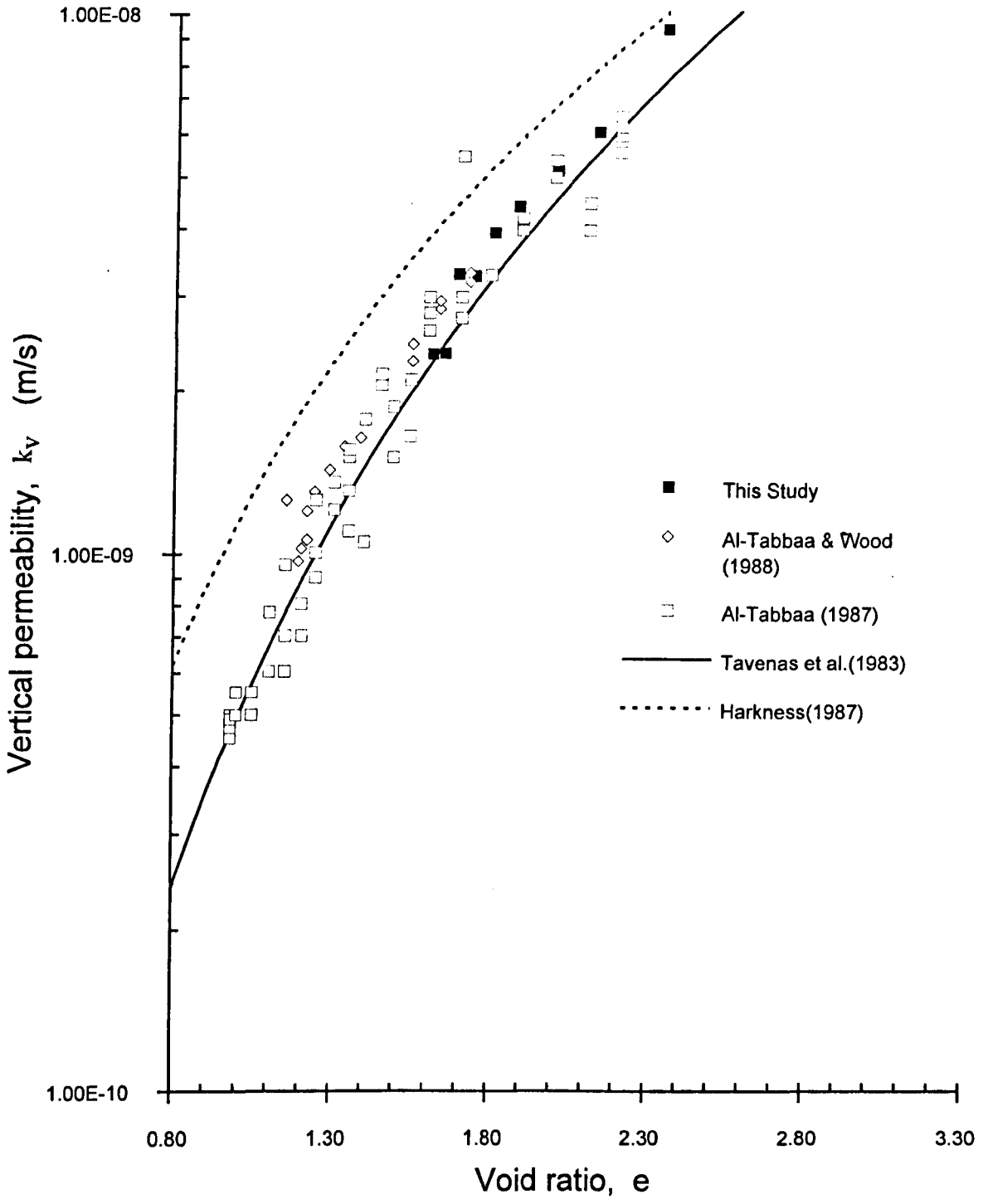

Fig.-5.12 Vertical permeability (k_v) vs void ratio (e) of kaolin by others and in this study

5.4.2 Horizontal permeability and void ratio

The variation of the horizontal permeability with void ratio is shown on a (lg.k_h vs e) plot in *Fig.*-5.13 for the slurry sample (test Series 1H). The results in the figure show that, like the vertical permeability, the logarithm of the horizontal permeability decreases linearly as the void ratio decreases. The lg linear approximation is valid for the void ratio ranging from about 2.70 down to about 1.40 measured in the sample. The exponential law model of the experimental data is described by Eqs.-(5.2) and shown as the solid line in the figure.

$$k_h = 4.48 \times 10^{-10} \times 4.08^{\,e} \quad \text{m/s} \tag{5.2}$$

$$C_{kh} = 1.64 \tag{5.2a}$$

where C_{kh} is a permeability change index associated with Eq.-(5.2).

Horizontal permeability of other kaolin clays reported in the literature are compared with the data obtained in this study in *Fig.*-5.14.

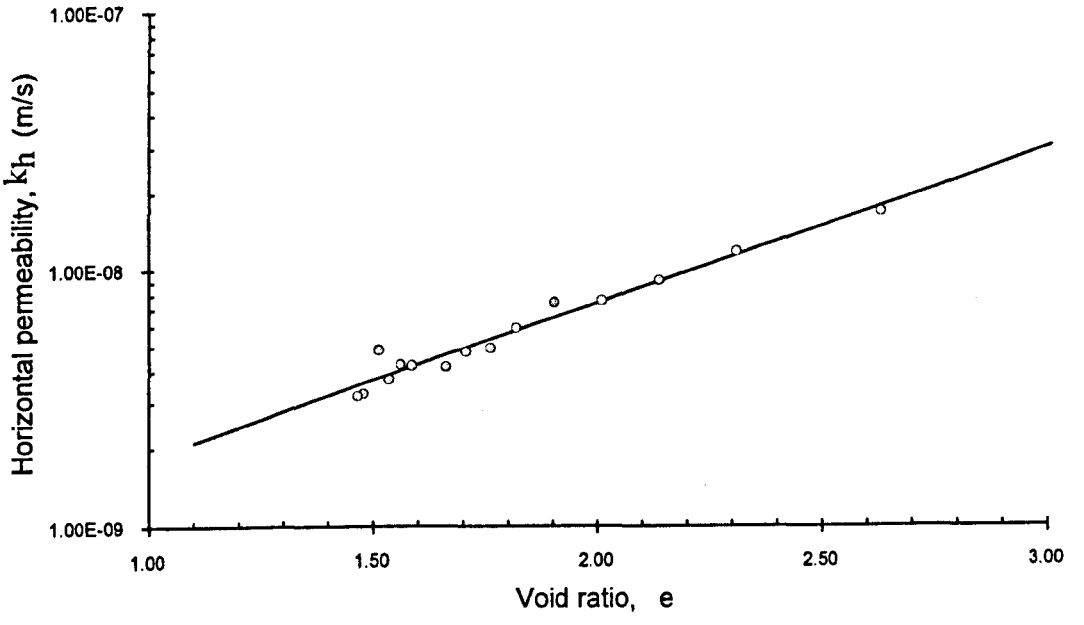

Fig.-5.13 Horizontal permeability (k_h) vs void ratio (e) for sample in test Series 1H: Eq.-(5.2) compared with data

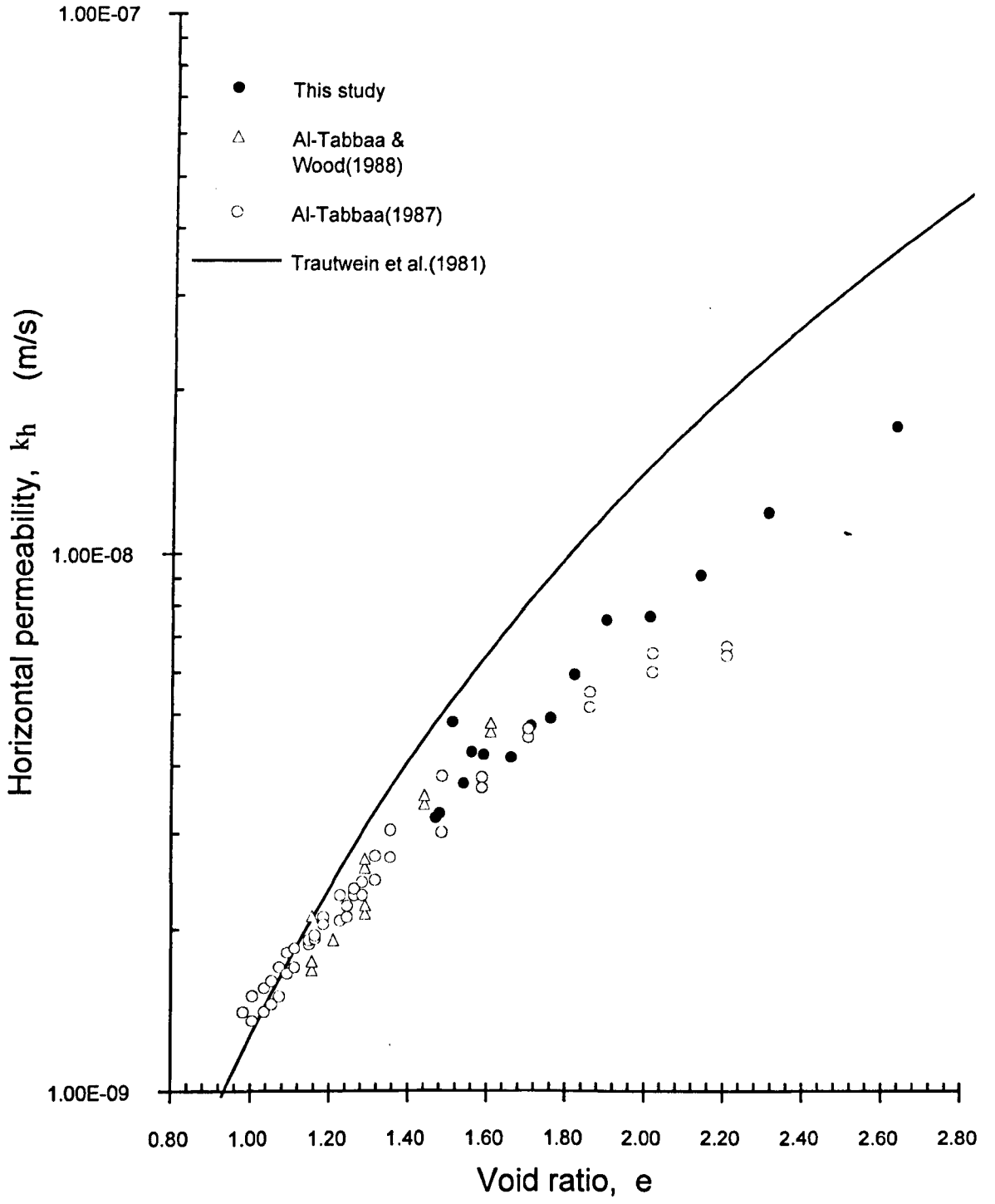

Fig.-5.14 Horizontal permeability (k_h) vs void ratio (e) for kaolin by others compared to data in this study

5.4.3 Effect of overconsolidation on permeability

It is noted that in *Figs.*-5.11 and 5.13 some of the permeability data correspond to the void ratio on the rebound line of the 1-D compression curve. These data fall on the same linear portions of ($lg.k_v$ vs e) and ($lg.k_h$ vs e) lines which indicate that both the vertical and horizontal permeabilities are independent of overconsolidation. Hence for the slurry consolidated clay, permeability is uniquely governed by the magnitude of void ratio irrespective of the stress state in the clay.

The general validity of the linear ($lg.k_v$-e) relation over the overconsolidated and normally consolidated range of the (e-$lg.\sigma'_v$) plot of the clay is demonstrated by more data from results of Series 2 tests. A summary of the results is shown in *Figs.*-5.15(a), 5.15(b), 5.15(c), 5.15(d), 5.15(e) and 5.15(f) for Series 1, Series 2 and Series 3, respectively. Thus with reference to the corresponding rcl and ucl parts of the (e-$lg.\sigma'_v$) plots, although the slope of the (e-$lg.\sigma'_v$) changes from OC to NC loading stages, the linearity of permeability variation with void ratio, (lg.k-e), is unaffected and can still be characterised by the permeability change index, C_{kh} or C_{kv}.

This observation indicates the strong dependence of permeability on geometrical parameter such as the void ratio while it is quite unaffected by the history of the 1-D loading or the OCR. The horizontal and vertical permeabilities of supreme kaolin are primarily dependent on the void ratio in any state of stress and are independent of the OCR as summarized.

5.4.4 Summary of permeability and void ratio relationships

Variations of permeability with void ratio presented in Sections 5.4.1 and 5.4.2 for anisotropically consolidated supreme kaolin clay slurry (Series 1 test), are shown to be adequately represented by the empirical exponential law $k=C.D^e$ as exhibited by the linear (lg.k vs e) plots. The vertical strain ε_v ranged from 0 to about 40% with the corresponding range in void ratio of 3.10 to 1.30 and vertical effective stress of 0 to 580kPa.

Experimental data for Series 2 tests also show linear relations of lg.k with e for the range of void ratio encountered. These results of vertical permeability and horizontal permeability as functions of void ratio are summarised in *Table*-5.3 consisting of the empirical index parameters C, D and C_k for the exponential law model $k=C.D^e$. Corresponding index and exponent parameters C and D for the power law model $k=C.e^D$ are also tabulated. Results of Series 1 test are shown in *Table*-5.3 to be regarded as the reference permeability data.

Since only one type of clay is involved and that material homogeneity is controlled for the slurry (Series 1) and block samples (Series 2), the latter can thus be regarded as

'undisturbed' block samples while the slurry is a 'remoulded' version of the block samples. Thus differences in permeability behaviour between Series 1 and Series 2 tests would therefore reflect to some extent the influence of the samples' stress history assuming that the consolidation cylinder or tank have the same influence in the constitution of the clay's structure.

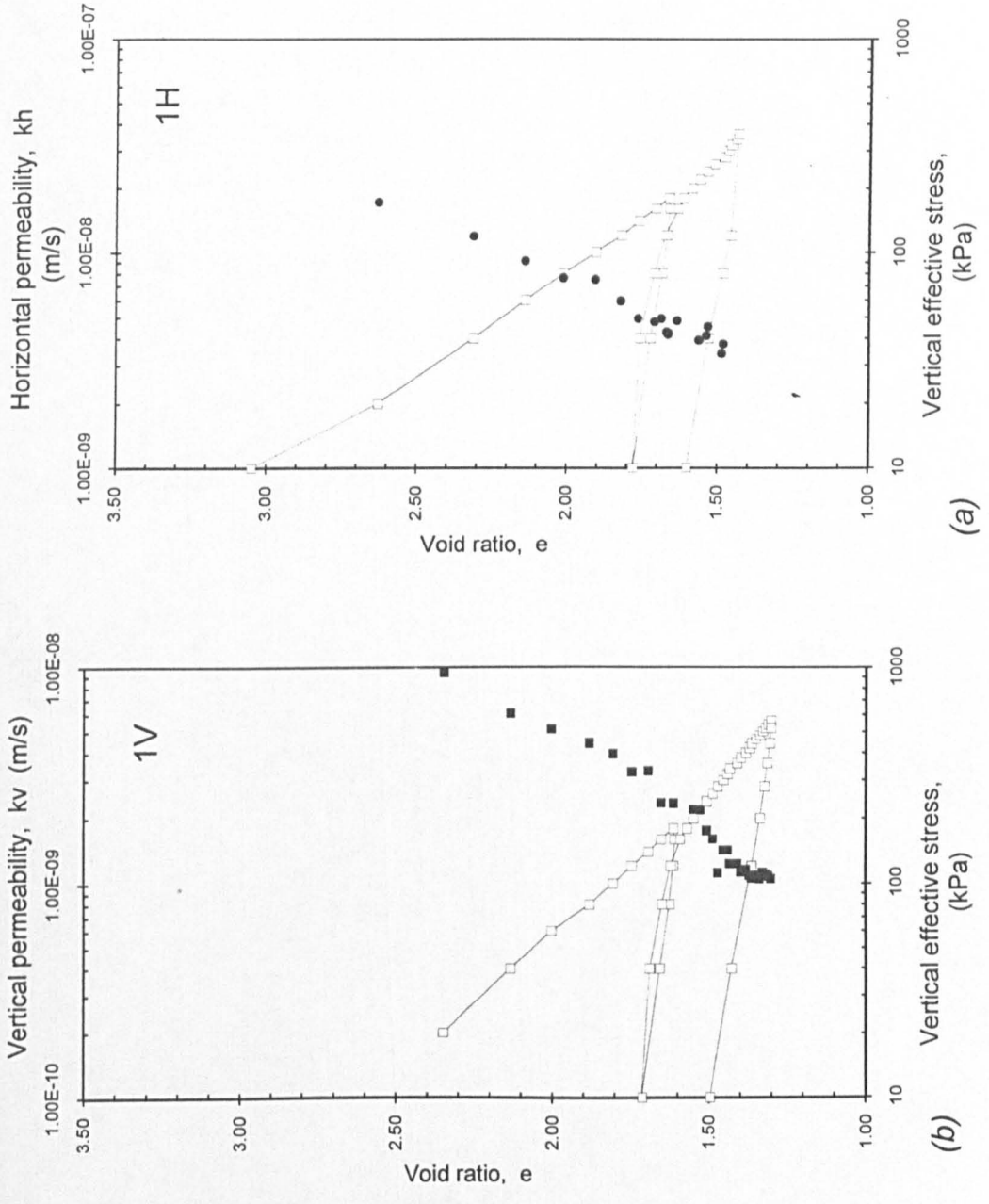

Fig.-5.15 Combine plots of (e-lg.σ'_v) and (lg.k vs e): (a) Series 1H; (b) Series 1V

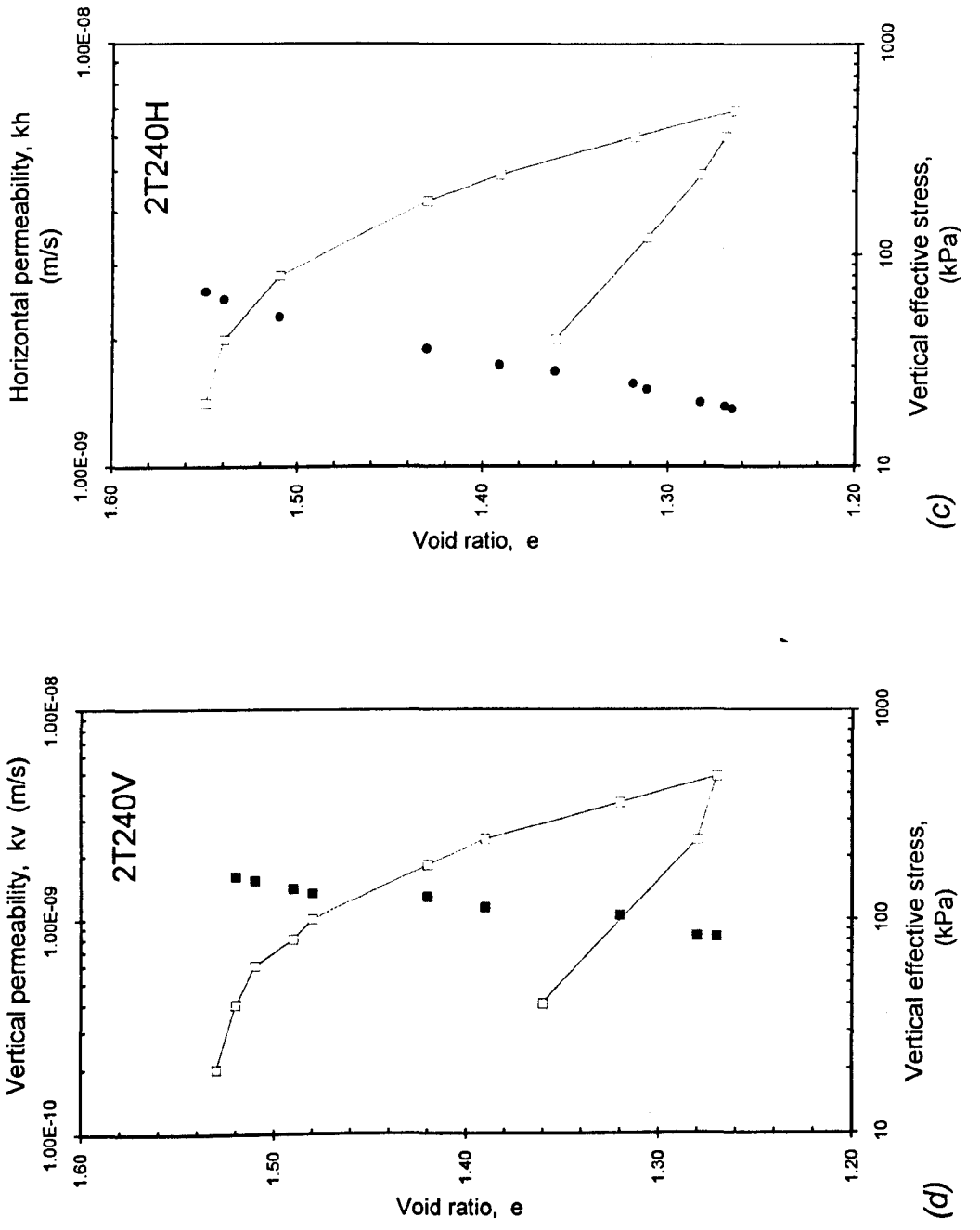

Fig.-5.15 *Cont.* Plots of (e-lg.σ'_v) and (lg.k vs e): (c) Series 2T240H; (d) Series 2T240V

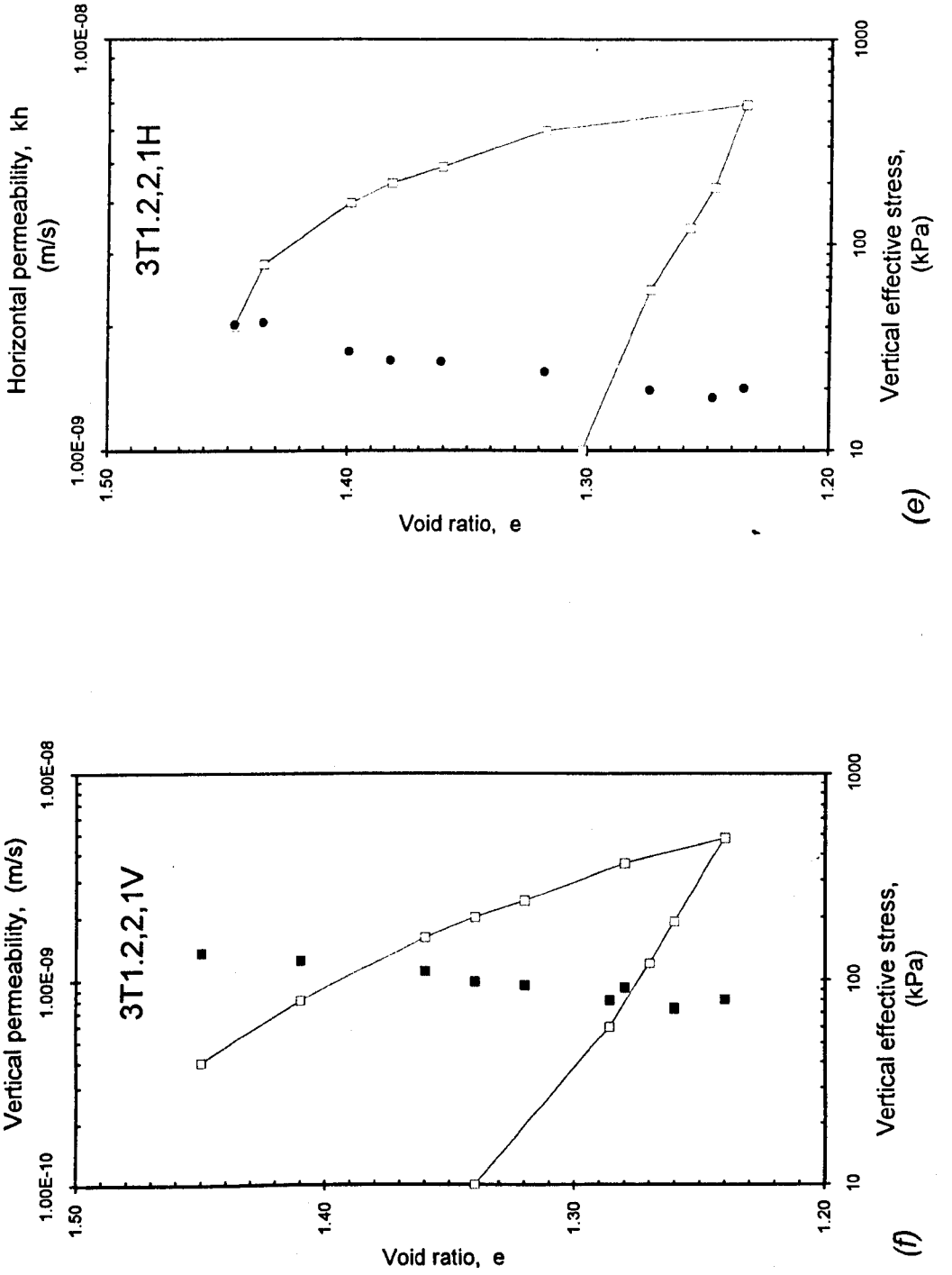

Fig.-5.15 *Cont.* Plots of (e-lg.σ'_v) and (lg.k vs e): (e) Series 3T1.2,2,1H; (f) Series 3T1.2,2,1V

Table-5.3 Values of permeability parameters C, D and C_k in the exponential and power law models for 1-D consolidated samples of supreme kaolin

No.	Test series:	σ'_{vp}(kPa)	σ'_{vc}(kPa)	Exponential law model: $k = C.D^e$, $C_k = 1/\lg D$ C	D	C_k	Power law model: $k = C.e^D$ C	D
	Series 1:							
1	1H from		580	4.48×10^{-10}	4.08	1.64	1.18×10^{-9}	2.72
	1V slurry			1.38×10^{-10}	6.08	1.28	0.456×10^{-9}	3.52
	OEDH(Al-Tabbaa)						1.43×10^{-9}	2.09
	OEDV(Al-Tabbaa)*			4.9×10^{-10}	3.21	1.97	0.5×10^{-9}	3.25
	Series 2:							
2	2C40H	40	60	5.09×10^{-10}	3.19	1.99	1.23×10^{-9}	2.06
	2C40V			8.38×10^{-11}	8.62	1.07	4.45×10^{-10}	3.77
3	2T120H	120	240	2.42×10^{-10}	4.57	1.51	0.989×10^{-9}	2.15
	2T120V			3.27×10^{-11}	11.45	0.94	0.277×10^{-9}	3.75
4	2T240H	240	480	9.76×10^{-11}	8.06	1.10	0.721×10^{-9}	2.73
	2T240V			5.18×10^{-11}	9.26	1.03	0.42×10^{-9}	3.06
5	2C240H	240	360	1.56×10^{-10}	5.89	1.30	0.821×10^{-9}	2.44
	2C240V			9.10×10^{-11}	6.68	1.21	0.536×10^{-9}	2.63
6	2C360H	360	580	9.50×10^{-11}	8.44	1.08	0.756×10^{-9}	2.68
	2C360V			3.54×10^{-11}	10.53	0.98	0.327×10^{-9}	3.20
	Series 2	Av. 2...H		1.29×10^{-10}	6.84	1.20		
		Av. 2...V		1.60×10^{-11}	20.23	0.77		

Notes: σ'_{vp} = Max. vertical effective stress applied to the sample during 1-D consolidation (ie. from slurry, in cylinder, tank and filter press)

σ'_{vc} = Max. vertical effective stress applied to sample during the consolidation/permeability test

e = void ratio

C_k = permeability change index defined by $\Delta e = C_k \Delta \lg.k$

C_k = C_{kv} for vertical flow and $k = k_v$

= C_{kh} for radial flow and $k = k_h$

* = from Al-Tabbaa assuming e_o=2.2 and $k_{vo} = 7 \times 10^{-9}$m/s

5.5 Permeability anisotropy

5.5.1 Development of permeability anisotropy

Fig.-5.16 shows the combined plot of vertical permeability, k_v and horizontal permeability, k_h with void ratio e for the slurry samples of Series 1V and 1H. From this figure the variation of permeability anisotropy, r_k with void ratio is developed as shown in *Fig.*-5.17. At each void ratio, permeability anisotropy is given by the basic definition $r_k=(k_h/k_v)$ and following Eqs.-(5.1) and (5.2),

$$r_k = 3.25 \times 0.671^e \tag{5.9}$$

Eq.-(5.9) is shown in the figure as the continuous solid line together with the individual r_k values evaluated from *Figs.*-5.11 and 5.13, and Eqs.-(5.2) and (5.1), respectively. The open circles indicate results from the horizontal permeability while the solid squares are from the vertical permeability. Each r_k value corresponds to their respective void ratio as in *Fig.*-5.16.

The (r_k vs e) plot in *Fig.*-5.17 gives the following observations: (1) 1-D consolidation of the clay from its low stress slurry state to a low vertical effective stress of about 10 to 15kPa produced a rather isotropic permeability. Thus r_k = 1.0 at e = 2.95 when σ'_{vp} = 10~15kPa. The horizontal and vertical permeability $k_h = k_v = 2.83 \times 10^{-8}$m/s; (2) With increasing 1-D consolidation, permeability anisotropy develops from isotropic to anisotropic condition to r_k= 1.93 at vertical effective stress of 580kPa with e = 1.30; (3) The vertical strain experienced by the clay in the 1-D compression ranged from ε_v = 0% to 40%.

Permeability anisotropy as obtained from Eq.-(5.9) arises from a combination of two processes namely the 1-D slurry consolidation and the different direction of drainage that occurred from the start of compression. Series 1H was under an all time horizontal drainage while Series 1V was under an all time vertical drainage conditions. Further evaluations of permeability anisotropy are considered by adopting the various experimental results for k_v and k_h of Series 1 and Series 2 as given below.

$$r_k = \frac{2C40H}{2C40V}, \frac{2T120H}{2T120V}, \frac{2T240H}{2T240V}, \frac{2C240H}{2C240V} \text{ and } \frac{2C360H}{2C360V} \tag{5.10}$$

$$r_k = \frac{\text{Average } k_h \text{ from Series 2}}{\text{Average } k_v \text{ from Series 2}} = 8.11 \times 0.338^e \tag{5.11}$$

Explanatory notes for data symbols in *Fig.*-5.17

1. $r_k = 3.25 \times 0.671^e$ ....Eq.-(5.9) $\equiv \frac{1H}{1V}$ ie. Curve 1 is represented by the thick solid line
2. Solid squares are values of r_k given by:

$$r_k = \frac{\text{Value of } k_h \text{ from Eq.-(5.2)}}{\text{Experimental value of } k_v}$$ at void ratio corresponding to experimental value of k_v.

3. Hollow circles are values of r_k given by:

$$r_k = \frac{\text{Experimental value of } k_h}{\text{Value of } k_v \text{ from Eq.-(5.1)}}$$ at void ratio corresponding to experimental value of k_h.

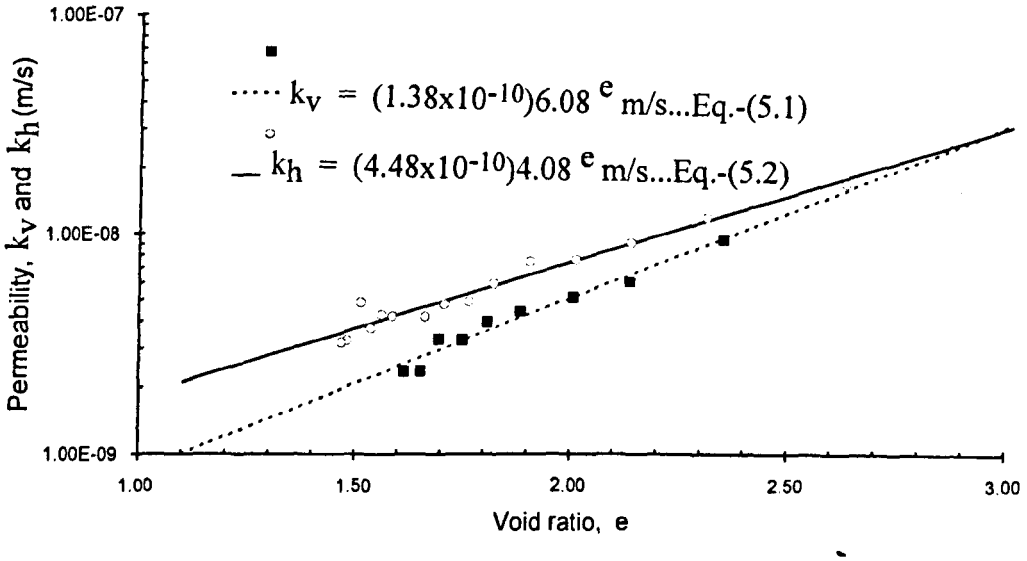

Fig.-5.16 Variation of permeability with void ratio for test series: 1V and 1H

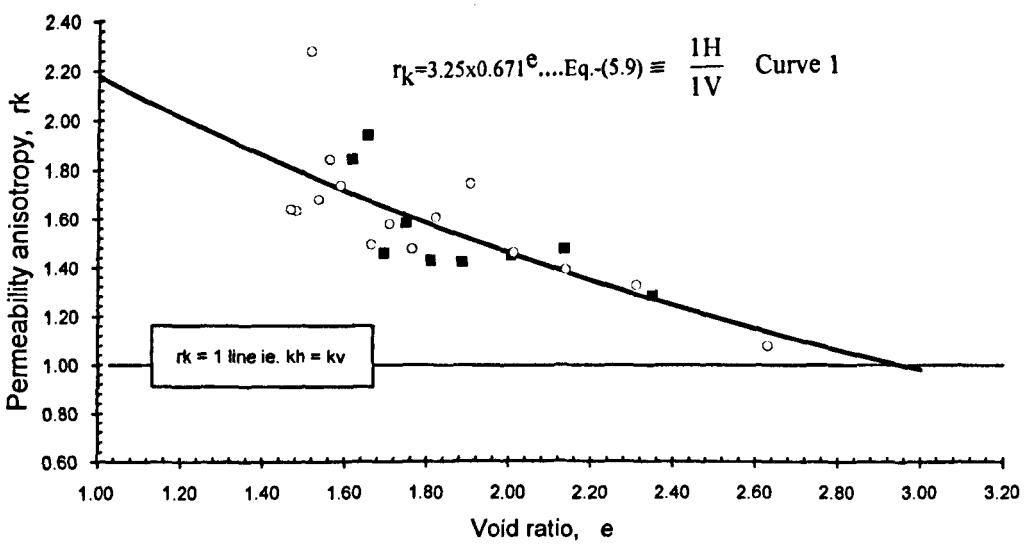

Fig.-5.17 Variation of permeability anisotropy with void ratio for test series 1V and 1H

$$r_k = \frac{\text{Average } k_h \text{ from Series 1 and 2}}{\text{Average } k_v \text{ from Series 1 and 2}} = 4.64 \times 0.52^e \qquad (5.12)$$

Eq.-(5.10) gives r_k values from individual Series 2 results. The early part of these r_k values could be considered to represent permeability anisotropy resulting from truly 1-D compression with vertical drainage where the sample is not quite yet affected from the influence of the horizontal drainage condition. Eq.-(5.11) gives r_k values from the average permeability lines of Series 2 results. Evaluations of permeability anisotropy from this equation assume that results of Series 2 could be approximated by a single line each for the ($\lg.k_h$ vs e) and ($\lg.k_v$ vs e) relations. For the case of Eq.-(5.12), values of r_k produced consider all the results of Series 1 and 2 as one in the same relation each for the vertical permeability and horizontal permeability.

The validity of Eqs.-(5.9) to (5.12) as indicators of permeability anisotropy should be applicable within the range of void ratio likely to be involved in the estimate of the permeability. More likely the range of void ratio would be based on the (e-$\lg.\sigma'_v$) lines for each of the Series.

Variations of permeability anisotropy with void ratio, (r_k vs e) as obtained from Eqs.-(5.9), (5.11) and (5.12) are shown in *Fig.*-5.18 as Curves 1, 2 and 3, respectively. The (r_k vs e) relations from Eq.-(5.10) are for the 5 block samples of Series 2 whose averages are represented by Eq.-(5.11) or Curve 2. Curve 1 is for Series 1, the reference r_k which has been discussed in the early part of this Section.

Fig.-5.18 shows that r_k increases with decreasing e for both Curves 1 and 2, the increase being higher for Curve 2 than Curve 1 in a given decrease of void ratio.

The fact that the two curves intersect indicates the presence of a unique point where the slurry and average of block samples have equal (e,r_k) values.

The (r_k vs e) relations from Eq.-(5.10) are shown in Fig.-5.19

$$\text{——}\quad r_k = 3.25 \times 0.671^{e} \text{.....Eq.-(5.9)} \equiv \frac{1H}{1V}$$

$$\text{- - -}\quad r_k = 8.11 \times 0.338^{e} \text{.....Eq.-(5.11)} \equiv \frac{\text{Average 2...H}}{\text{Average 2...V}}$$

$$\text{— -}\quad r_k = 4.64 \times 0.52^{e} \text{.....Eq.-(5.12)} \equiv \frac{\text{Average 1H \& 2...H}}{\text{Average 1V \& 2...V}}$$

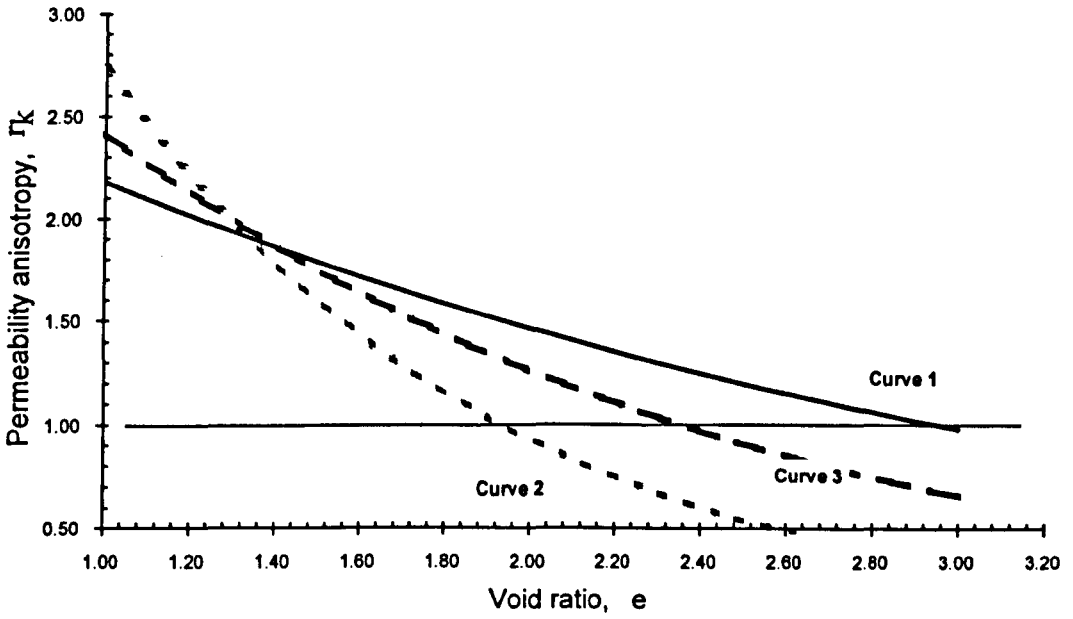

Fig.-5.18 Basic variation of permeability anisotropy with void ratio for slurry (Series 1) and block (Series 2) samples

Series	From Eqs.-(5.10)	
2C40	$r_k = (6.07)0.37^e$	$\equiv \frac{2C40H}{2C40V}$
2T120	$r_k = (7.40)0.40^e$	$\equiv \frac{2T120H}{2T120V}$
2T240	$r_k = (1.88)0.87^e$	$\equiv \frac{2T240H}{2T240V}$
2C240	$r_k = (1.71)0.88^e$	$\equiv \frac{2C240H}{2C240V}$
2C360	$r_k = (2.68)0.80^e$	$\equiv \frac{2C360H}{2C360V}$

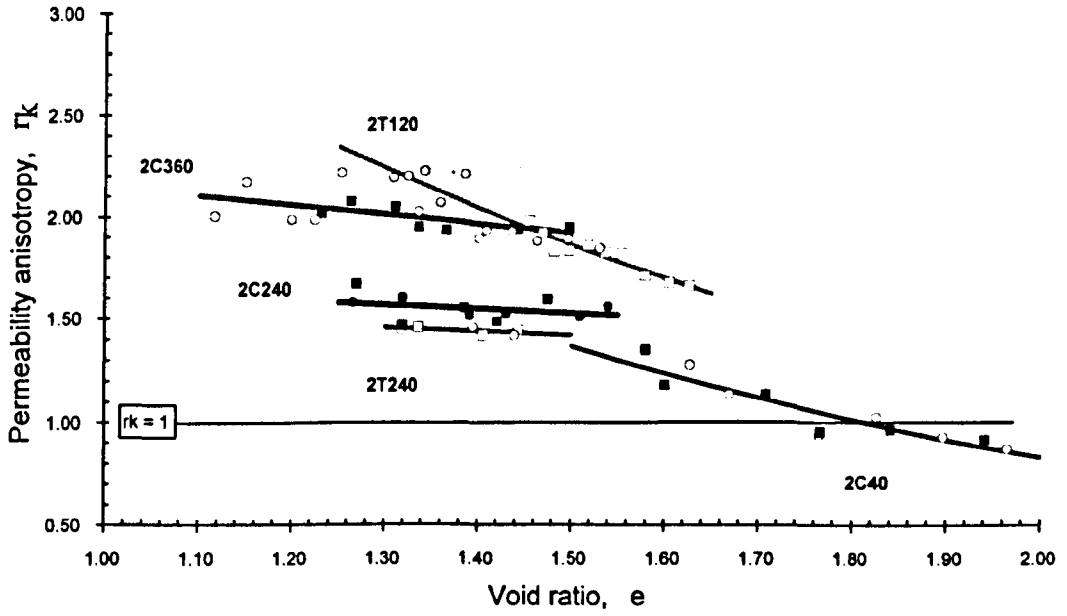

Fig.-5.19 Variation of permeability anisotropy with void ratio for individual Series 2 samples

5.5.2 Effects of stress history on permeability

Comparison between permeability tests results from Series 1 and Series 2 as summarised in *Table*-5.3 will be used to investigate the effects of stress history on changes in permeability behaviour.

In looking at possible changes in trends of permeability behaviour due to factors related to stress history of the samples, two approaches to scrutinise the results have been considered. Firstly, the effects of sample preparation, disturbance, and testing differences are considered insignificant and uniform throughout. In this case, all data from the Series 2 test could be considered to represent one sample and the results consist of *averages* from all data of that series into a single line. The results are examined from both the ($\lg.k_V$-e) and (e-$\lg.\sigma'_v$) relations. The second approach is to consider the above factors to be significant such as to cause substantial changes in permeability trends. In this case data from each of Series 2 test are treated on *individual* basis and they are related to each other in certain order based on the values of σ'_{vp} and drainage directions. Hence, each ($\lg.k_V$-e) and (e-$\lg.\sigma'_v$) relations are considered.

In both approaches the ratios of the same permeability ie. k_h or k_V compared from the different test series, ie. Series 1 and Series 2 are used. The ratios of horizontal and vertical permeabilities are given below for evaluation.

$$r_{hk} = \frac{1H}{\text{Average } k_h \text{ from Series 2}} = 3.47 \times 0.6^{e} \qquad (5.13)$$

$$r_{hk} = \frac{1H}{2C40H}, \frac{1H}{2T120H}, \frac{1H}{2T240H}, \frac{1H}{2C240H} \text{ and } \frac{1H}{2C360H} \qquad (5.14)$$

$$r_{vk} = \frac{1V}{\text{Average } k_V \text{ from Series 2}} = 8.625 \times 0.3^{e} \qquad (5.15)$$

$$r_{vk} = \frac{1V}{2C40V}, \frac{1V}{2T120V}, \frac{1V}{2T240V}, \frac{1V}{2C240V} \text{ and } \frac{1V}{2C360V} \qquad (5.16)$$

Horizontal permeability of the block samples (Series 2C..H & 2T..H) as averages is compared to that of the slurry sample (Series 1H) in *Fig.*-5.20(a). Result of Series 1H, ie. Eqs.-(5.2) is noted by the thick solid line while permeability data for Series 2 tests are shown with the exponential law line drawn through them. It is observed that at void ratio e=2.00, $k_h(1H) = 1.24k_h(2...H)$ and at e=1.00, $k_h(1H) = 2.07k_h(2...H)$.

For the case of vertical permeability, k_V for Series 2C..V & 2T..V and Series 1V are as shown in *Fig.*-5.20(b). The results indicate that at an early void ratio of e=2.00,

$k_V(1V)$ is less than $k_V(2...V)$ given by $k_V(1V)=0.79k_V(2...V)$ but with decreasing void ratio, $k_V(1V)$ is greater than $k_V(2...V)$ with $k_V(1V) = 2.56k_V(2...V)$ at e=1.00.

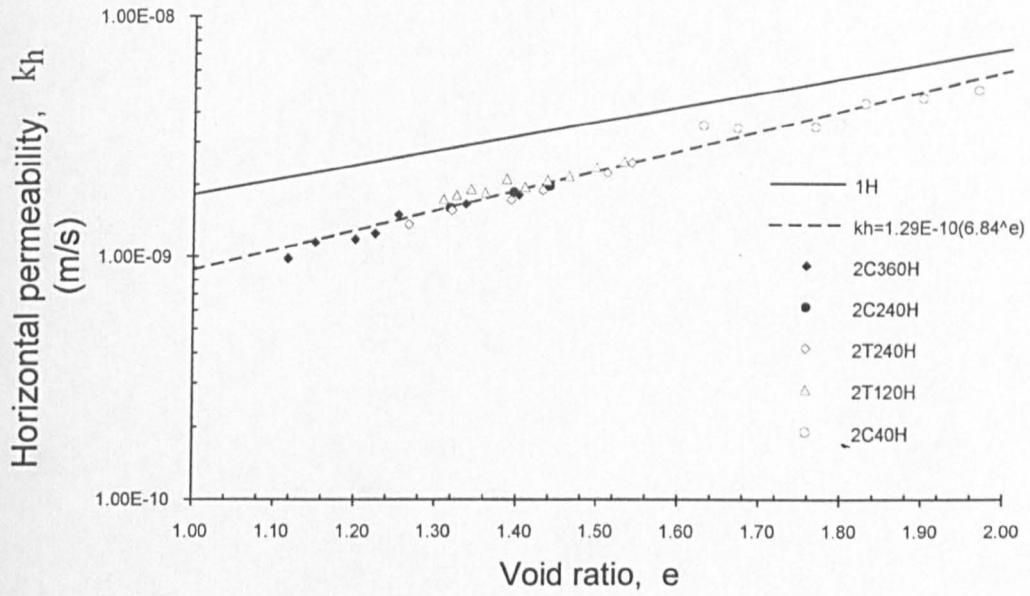

(a)

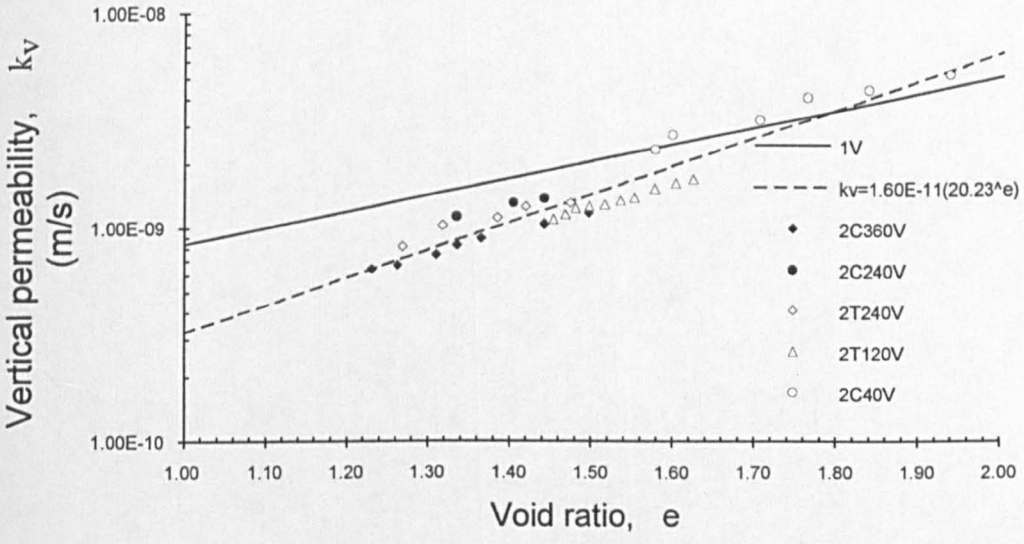

(b)

Figs.-5.20 Permeability vs void ratio (Average data): (a) Series 2C..H and 2T..H compared with Series 1H; (b) Series 2C..V and 2T..V compared with Series 1V

Horizontal permeability of the block samples (Series 2C..H & 2T..H) now as *individual series* is compared to that of the horizontal slurry sample (Series 1H) in *Fig.*-5.21(a) in a similar manner as in *Fig.*-5.20(a). The beginning of data points in the figure is indicated by the arrow heads ↓, which gives permeability values according to the exponential fitting line at the initial void ratio e_o inferred from the ncl of the sample. Although by definition the initial void ratios generally refer to their values when the samples are not yet reconsolidated, the adopted e_o here refer to the void ratio at σ'_v=10kPa. The lengths of the arrow heads give some measure of the permeability drops [except Series 2C40V in *Fig.*-5.21(b)] that occur between Series 1 sample and the individual Series 2 samples. On a similar presentation, the vertical permeability of the block samples (Series 2C..V & 2T..V) as *individual* series is compared to that of the vertical slurry sample (Series 1V) in *Fig.*-5.21(b).

Referring firstly to the horizontal permeability, the following observations are noted from *Figs.*-5.20(a) and 5.21(a). (1) A general tendency of decreasing permeability with void ratio. The C_{kh} values vary between 0.89 to 1.09 about the value of 0.98 for the curve in *Fig.*-5.20(a). Thus for a unit change in void ratio, permeability changes by a factor of 8 to 13. (2) Series 1 sample when compared to individual block sample gives the upper limit of permeability at all void ratio. (3) At the same void ratio within the bounds of their (e-lg.σ'_v) curve, permeability decreases with increasing past consolidation pressure σ'_{vp}. (4) At any given void ratio, differences in permeability with values of σ'_{vp} are only very slight. The tendency is stronger for the permeability to follow a single common (lg.k_h vs e) line independent of σ'_{vp}. The effect of σ'_{vp} is mainly to change the value of e_o of the various samples and this in turn affects permeability values. The void ratio therefore presents the final parameter that determine the value of permeability.

Secondly, the vertical permeability shares the same features as with the horizontal permeability for all of the four descriptions above but in detail differ mainly in magnitudes. The (lg.k_h vs e) lines for individual block samples are closer to the (lg.k_h vs e) reference line (ie. Series 1V).

A summary of the results discussed earlier is shown in *Fig.*-5.22 and *Fig.*-5.23 for samples in Series 1H, 2...H, and Series 1V, 2...V, respectively. The figures relate the permeabilities of the series at selected void ratios with their positions based on σ'_{vp}, and the states of stresses (in nc or oc regions). The thickened solid line cutting through lines of constant void ratios represents the boundary between the overconsolidated and normal consolidated states of the sample. Since the slurry sample does not experienced any maximum past consolidation pressure, its permeability values are all occuring at void ratios in the normally consolidated states. Permeability data are

calculated from the individual expressions for permeability $k=C.D^e$, with values of C and D taken from *Table*-5.3.

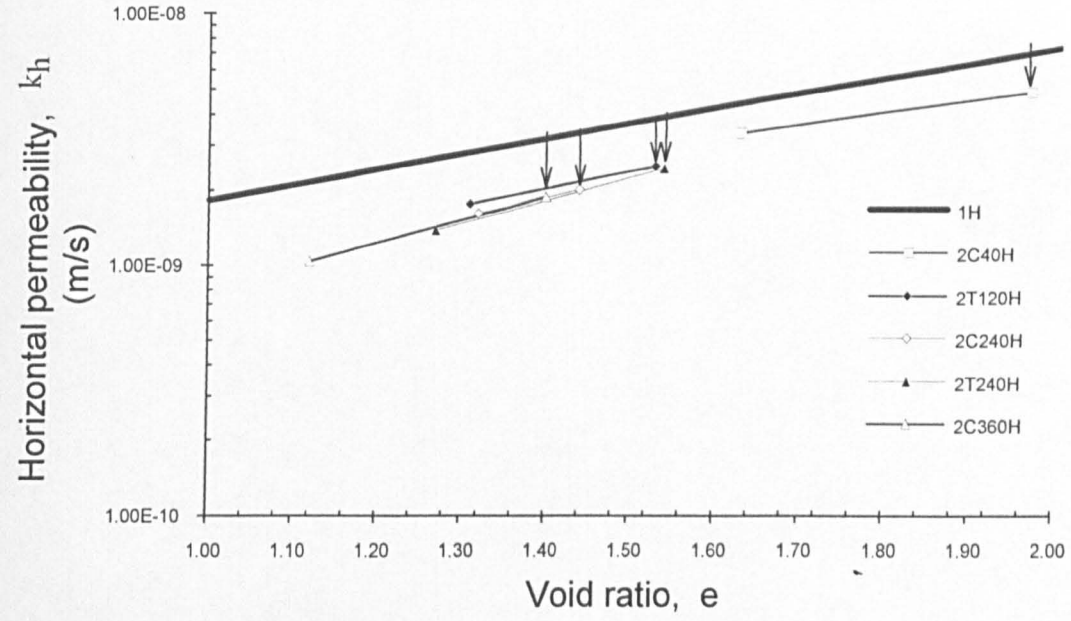

(a)

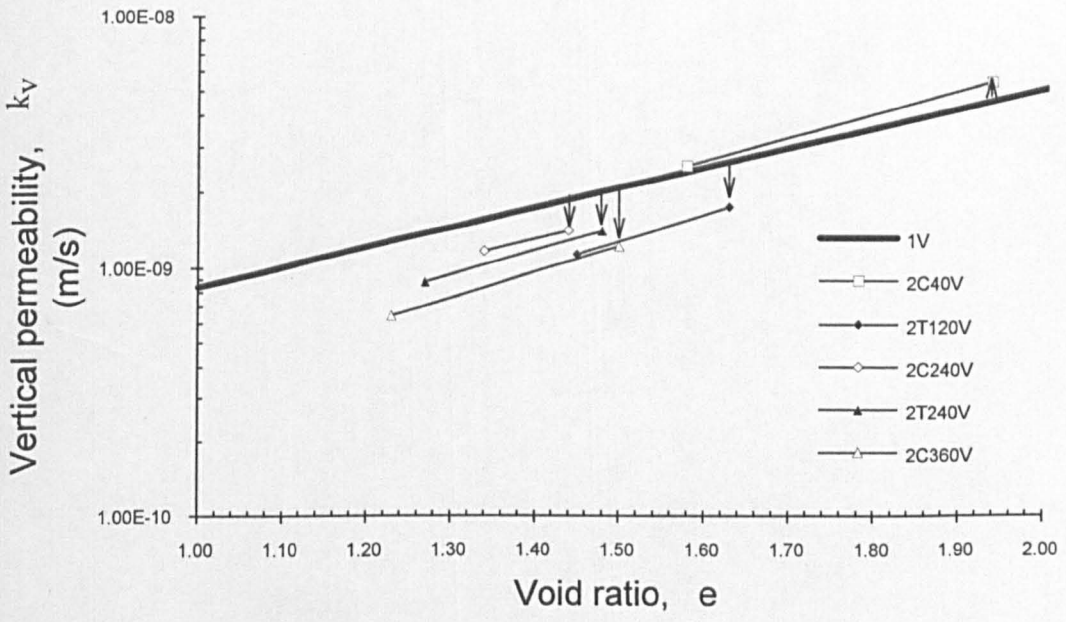

(b)

Fig.-5.21 Permeability vs void ratio (Individual data): (a) Series 2C..H and 2T..H compared with Series 1H; (b) Series 2C..V and 2T..V compared with Series 1V

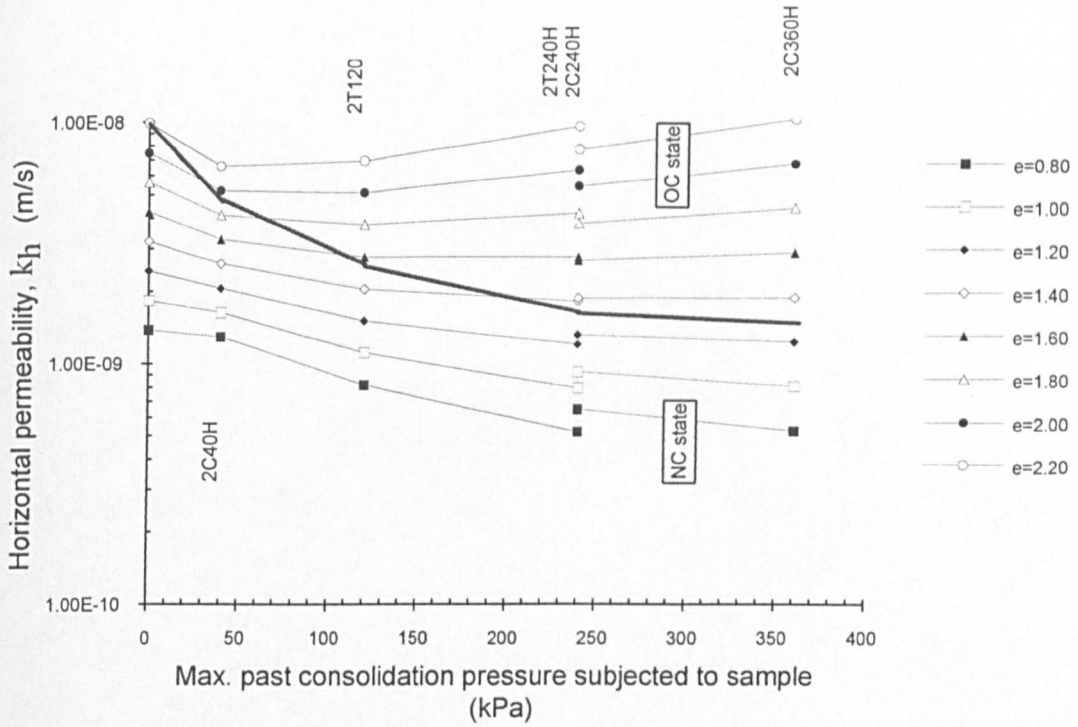

Figs.-5.22 Permeability at constant void ratios for horizontal permeability: Series 1H & 2...H

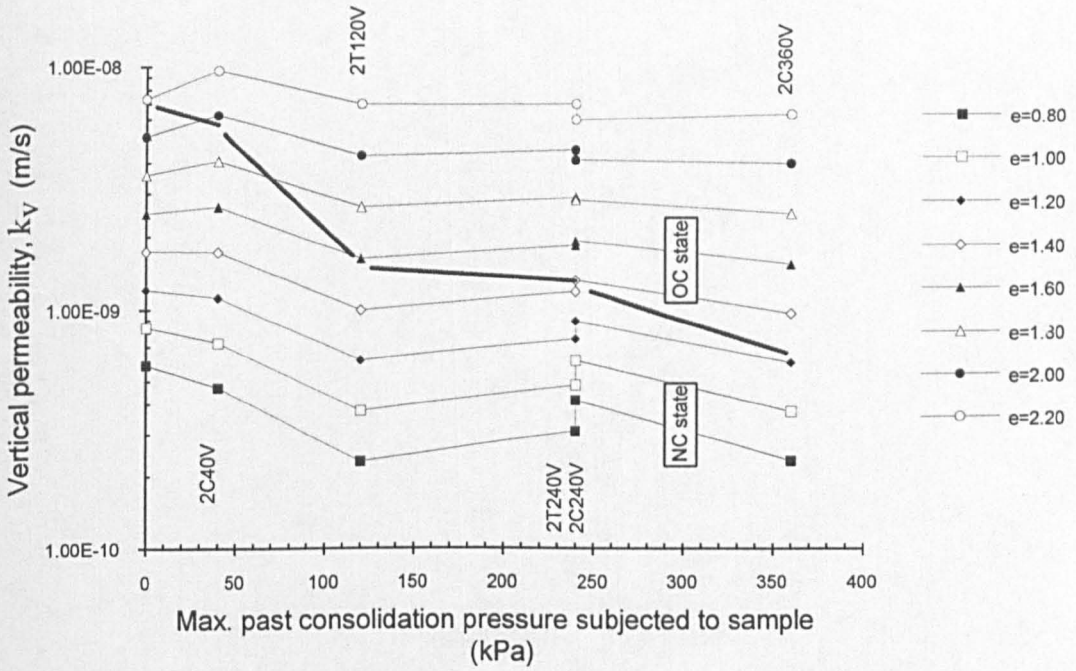

Figs.-5.23 Permeability at constant void ratios for vertical permeability: Series 1V & 2...V

The results in Figs.-5.22 and 5.23 confirm the earlier findings (Section 5.4.1 & 5.4.2) that permeability decrease with decreasing void ratio and in this case summarise succinctly data for other test series. Relatively small permeability change (Δk), is also seen as the sample passes through a history of lower σ'_{vp} to higher σ'_{vp} as compared to the Δk resulting from a history of high e to low e. The trend is more toward maintaining a reasonably constant permeability independent of the value of maximum past consolidation pressure, σ'_{vp} or whether the sample is in nc or oc state.

5.5.3 Influence of drainage direction on permeability

The development of permeability anisotropy for Series 1 samples (ie. 1H & 1V) in *Fig.*-5.16 shows the r_k values in which Series 1H was under an all time horizontal drainage while Series 1V was under an all time vertical drainage. Permeability anisotropy therefore resulted from a combination of two processes namely 1-D compression and the different direction of drainage that occurred from the start of compression. Permeability anisotropy r_k resulting from 1-D compression only could be represented from results of Series 2 tests where drainage in these samples before permeability tests was always constrained vertically.

The ratios of horizontal and vertical permeabilities as defined by Eqs.-(5.13) and (5.15) are shown together with the basic permeability anisotropy [Eqs.-(5.9) and (5.11)] in *Fig.*-5.24. It is seen that the shapes of the curves from the pair of two ratios ie. Eqs.-(5.9) and (5.13), and Eqs.-(5.11) and (5.15) are reasonably identical. This shape appeared to be controlled by the closeness of permeability equations for Series 1V and Series 2...H. Series 1V stands for vertical permeability for sample in fully vertical drainage condition while Series 2...H stands for horizontal permeability also for sample in 'fully vertical drainage condition'.

——— $r_k = 3.25x0.671^e$.....Eq.-(5.9) $\equiv \frac{1H}{1V}$

- - - $r_k = 8.11x0.338^e$.....Eq.-(5.11) $\equiv \frac{\text{Average 2...H}}{\text{Average 2...V}}$

— - - $r_{hk} = 3.47x0.6^e$.....Eq.-(5.13) $\equiv \frac{1H}{\text{Average 2....H}}$

— - $r_{vk} = 8.625x0.3^e$.....Eq.-(5.15) $\equiv \frac{1V}{\text{Average 2....V}}$

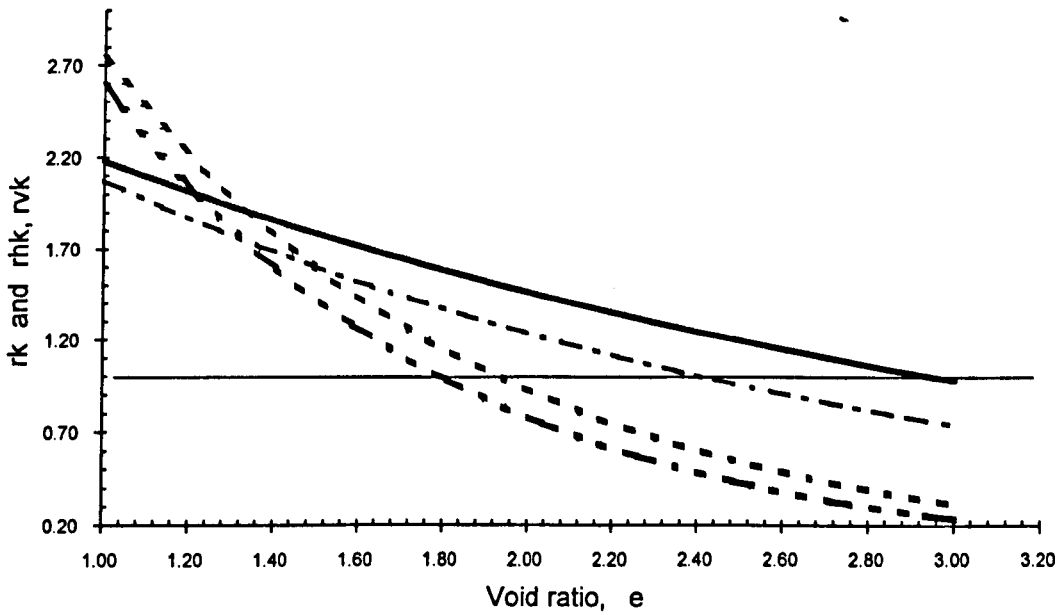

Fig.-5.24 Ratios of horizontal and vertical permeabilities, r_{hk} and r_{vk} compared with permeability anisotropy r_k for Series 1 and 2

5.5.4 Effects of undrained shearing on development of permeability and permeability anisotropy

The effects of undrained shearing on permeability and development of permeability anisotropy of the clay sample are presented and discussed in this Section. Experimental results on tested samples are those as specified in Group I and Group II and outlined in Section 3.2.2. Samples from both groups were prepared from kaolin slurry. Samples in Group I were subjected to one-dimensional consolidation in the low pressure filter press to a maximum consolidation pressure of σ'_{vmax} = 100kPa. They were then extruded, trimmed, set up and reconsolidated isotropically in the triaxial cell to effective stress σ'_3 = 100kPa and followed by undrained compression test (CIU). Samples in Group II were similarly consolidated one-dimensionally, however, consolidation was performed in a stronger consolidation cylinder to a maximum consolidation pressure of σ'_{vmax} = 600kPa. They were then sampled out and reconsolidated isotropically in the triaxial cell to effective stress σ'_3 = 300kPa and followed by the CIU test.

At each CIU test, the sample was sheared to various vertical strains. Within the scope of this experimental programme, 2 strain levels are chosen ranging from a low value to a higher strain but not to the extent of the sample reaching failure.

After the CIU tests the samples were sampled out, set up and subjected to the usual procedures of vertical and radial permeability tests in the hydraulic oedometers (see Section 3.3.2). In the discussion of experimental results that follow, data for both the horizontal and vertical permeabilities are shown to expose an overview of the main effects of one dimensional consolidation and undrained shear on the variation of permeability with void ratio.

The linear trends of all logarithm of permeability vs void ratio established earlier in this thesis (Sections 5.4.1 and 5.4.2) provide a reasonable foundation of using the exponential law model in the discussions of available data that follows. A summary of the vertical permeability and horizontal permeability for the sheared samples is presented in *Table*-5.4 consisting of the empirical index parameters C, D and C_k for the exponential law model $k=C.D^e$. Corresponding index and exponent parameters C and D for the power law model $k=C.e^D$ are also tabulated. Thus the development of permeability anisotropy r_k with void ratio e could be figured out since r_k follows the same form of expression as k_v or k_h ie. $r_k=A.B^e$ where A and B are empirical parameters determined from the test results.

Table-5.4 Values of permeability parameters C, D and C_k in the exponential and power law models for sheared samples

No.	Test series	σ'_{vp}	σ'_{3iso}	σ'_{vc}	Exponential law model $k = C.D^e$ $C_k = 1/\lg D$			Power law model $k = C.e^D$	
		(kPa)	(kPa)	(kPa)	C	D	C_{kh} or C_{kv}	C	D
	Group I								
7	3F1,1,1H	100	100	120	1.23×10^{-11}	25.12	0.71	2.27×10^{-10}	4.78
	3F1,1,1V				5.94×10^{-11}	9.61	1.02	4.53×10^{-10}	3.40
8	3F1,1,2H	100	100	120	7.26×10^{-14}	693.1	0.35	1.90×10^{-11}	10.4
	3F1,1,2V				6.28×10^{-11}	9.62	1.02	4.32×10^{-10}	3.61
9	3F1,1,3H	100	100	120	1.52×10^{-11}	24.68	0.72	2.44×10^{-10}	5.01
	3F1,1,3V				9.15×10^{-11}	7.61	1.13	5.40×10^{-10}	3.13
	Group II								
10	3T1.2,2,1H	120	200	480	1.21 x 10-10	7.03	1.18	7.73×10^{-10}	2.60
	3T1.2,2,1V				3.55×10^{-11}	11.52	0.94	3.60×10^{-10}	3.30
11	3T2.4,2,1H	240	200	360	2.48×10^{-10}	4.44	1.55	1.02×10^{-9}	1.98
	3T2.4,2,1V				2.79×10^{-11}	15.25	0.85	3.66×10^{-9}	3.69
12	3T6,3,1H	600	300	480	8.47×10^{-12}	58.72	0.57	4.59×10^{-10}	4.92
	3T6,3,1V				2.96×10^{-11}	18.05	0.80	5.02×10^{-10}	3.53
13	3T6,3,2H	600	300	480	7.29×10^{-12}	60.88	0.56	4.00×10^{-10}	5.08
	3T6,3,2V				6.43×10^{-11}	7.43	1.15	4.56×10^{-10}	2.46

Notes: σ'_{vp} = Max. vertical effective stress applied to sample during 1-D consolidation

σ'_{vc} = Max. vertical effective stress applied to sample during the consolidation / permeability test

σ'_{3iso} = Isotropic effective stress in the sample before undrained shear

C_{kv}, C_{kh} = Permeability change index for vertical, and horizontal permeability respectively.

As noted earlier, permeability anisotropy r_k and its development with void ratio is described by Eqs.-(5.9) to (5.12) where r_k is the ratio of horizontal permeability to the vertical permeability. The ratios r_{hk} or r_{vk} as described by Eqs.-(5.13) to (5.16), however, are ratios of permeability in the same direction. This Section will discuss on development of r_{hk} and r_{vk}, and followed by r_k.

Going back to basic definitions of the ratios of vertical and horizontal permeabilities, for the case of Series 3, Group I samples,

$$r_{vkF} = \frac{1V}{3F...V} \tag{5.17}$$

$$r_{hkF} = \frac{1H}{3F...H} \tag{5.18}$$

For Series 3, Group II samples,

$$r_{vkT} = \frac{1V}{3T...V}, \frac{1V}{3T1.2,2,1V}, \frac{1V}{3T2.4,2,1V}, \frac{1V}{3T6,3,1V} \text{ and } \frac{1V}{3T6,3,2V} \tag{5.19}$$

$$r_{hkT} = \frac{1H}{3T...H} \tag{5.20}$$

Subscripts F and T are added in the permeability ratios for identification of Group I and II samples. As will be seen later, the vertical permeability for Series 3, Group II samples (ie. Series 3T), exhibit more individual trends rather than a single average so that r_{vkT} will be evaluated from both averages of 3T's and individual 3T's as given by Eqs.-(5.19).

Comparison will also be made to the vertical and horizontal permeability ratios with respect to Series 2 samples defined as,

$$r_{vk} = \frac{1V}{2...V} \tag{5.21}$$

$$r_{hk} = \frac{1H}{2...H} \tag{5.22}$$

Except for the notation, Eq.-(5.21) is essentially similar to Eq.-(5.15) and Eq.-(5.22) to Eq.-(5.13).

Fig.-5.25(a) presents the vertical permeability data for samples from Group I (Test series 3F1,1,1V; 3F1,1,2V; and 3F1,1,3V) which had been sheared undrained to vertical strains of ε_v = 3.9%, 7.9%, and 11.5%, respectively. The ($\lg.k_v$-e) relation for

Series 1V is also shown as the thick solid line for comparison. Permeability variations for the three Series 3F...V are quite close to each other to enable a single line representation.

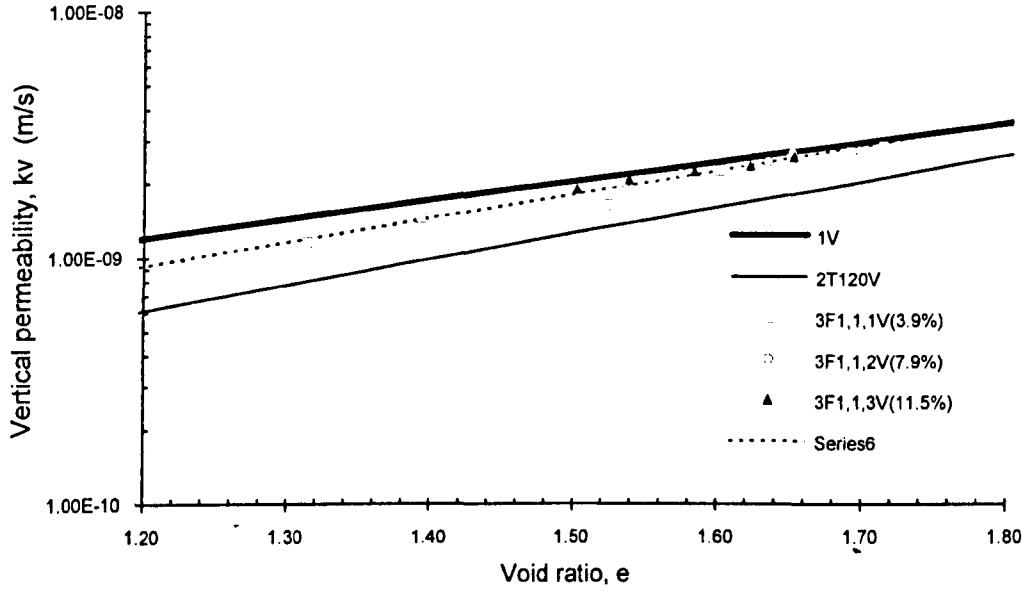

(a)

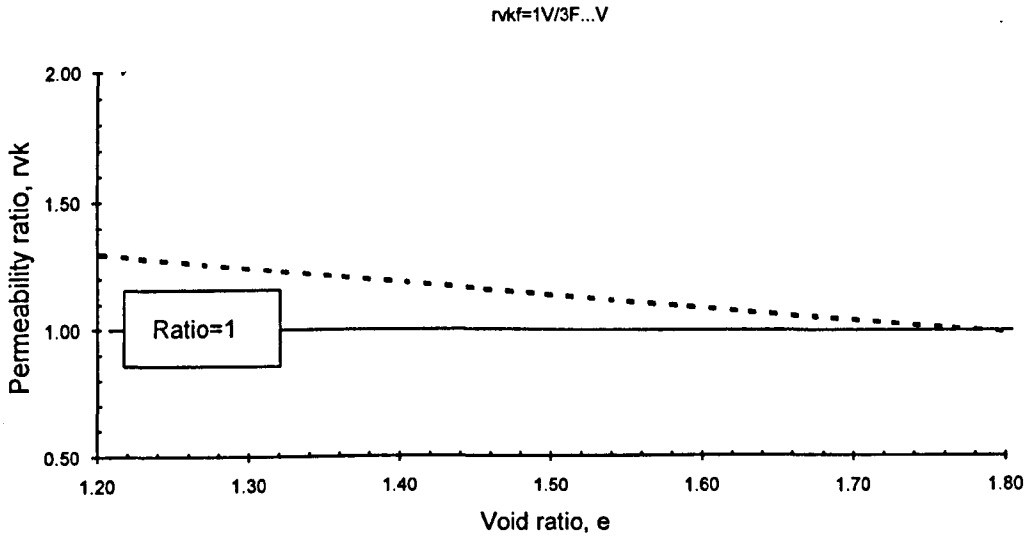

(b)

Fig.-5.25 (a) Permeability vs void ratio, Series 3F...V compared with Series 1V and 2T120V; (b) Permeability ratio r_{vk} = 1V/ 3F...V vs void ratio

This average relation (shown as dotted line) is also close with the reference ($lg.k_V$-e) line of Series 1V especially at the initial void ratios and also at all values of ε_V.

The variation of permeability with void ratio for test series 2T120V (σ'_{vp}=120kPa) is included in *Fig.*-5.25(a) to represent unsheared sample for comparison. The ratio $r_{vkF} = \frac{1V}{3F...V}$, [Eq.-(5.17)] is shown in *Fig.*-5.25(b).

Similar results for the horizontal permeability data for samples from Group I are shown in *Fig.*-5.26(a) compared with the reference ($lg.k_h$-e) lines of Series 1H and 2T120H. The ratio $r_{hkF} = \frac{1H}{3F...H}$, [Eq.-(5.18)] is shown in *Fig.*-5.26(b). As with the vertical permeability, the horizontal permeability data for the three Series 3F...H also show sufficiently small scatter for a single line approximation of ($lg.k_h$-e) variation. Looking at the ratios r_{vkF} and r_{hkF}, the vertical permeability is closer to the reference ($lg.k_V$-e) line with r_{vkF} values ranging from unity at e=1.79 to just about 1.30 at e=1.2. The horizontal permeability, however, decreases more rapidly from its reference ($lg.k_h$-e) line with its r_{hkF} values ranging from close to unity at e=1.80 to just over 4 at e=1.2.

It is noted that the average (lg.k-e) lines for both vertical and horizontal permeabilities meet their respective reference (lg.k-e) lines at about the same void ratio of around e =1.80.

Results for the vertical permeability data for samples from Group II are shown in *Fig.*-5.27(a) compared with the reference ($lg.k_V$-e) lines of Series 1V and 2T120V. Unlike the data in *Fig.*-5.25(a), results in *Fig.*-5.27(a) show that each individual series are more prominent in their own individual ($lg.k_V$-e) lines.

Similar results for the horizontal permeability data for samples from Group II (Series 3T1.2,2,1H; 3T2.4,2,1H; 3T6,3,1H and 3T6,3,2H) are shown in *Fig.*-5.28(a) compared with the reference ($lg.k_h$-e) lines of Series 1H and 2T120H. The ratio $r_{hkT} = \frac{1H}{3T...H}$, [Eq.-(5.20)] is shown in *Fig.*-5.28(b).

Permeability ratios r_{hk}, r_{hkF}, & r_{hkT} and r_{vk}, r_{vkF}, & r_{vkT} are summarized in *Figs.*-5.29(a) and 5.29(b) for the three Series 2, 3F and 3T, respectively. The results show that for the range of void ratio e=1.65 and less the 'reference' permeability ratios r_{hk} and r_{vk} seem to provide lower and upper boundaries for the horizontal and vertical permeability ratios, respectively. It will be noted here that for void ratio greater than 1.65, the r_{hkF} or the r_{vkF} lines would not be applicable for the sheared samples. Perhaps 'sheared samples 3S...H & 3S...V' with σ'_{vp}<100kPa, say σ'_{vp}=60kPa are required to give void ratio greater than 1.65 but still end up with the resulting r_{hkS} line lying above 'reference' r_{hk} line and the r_{vkS} line falling below 'reference' r_{vk} line.

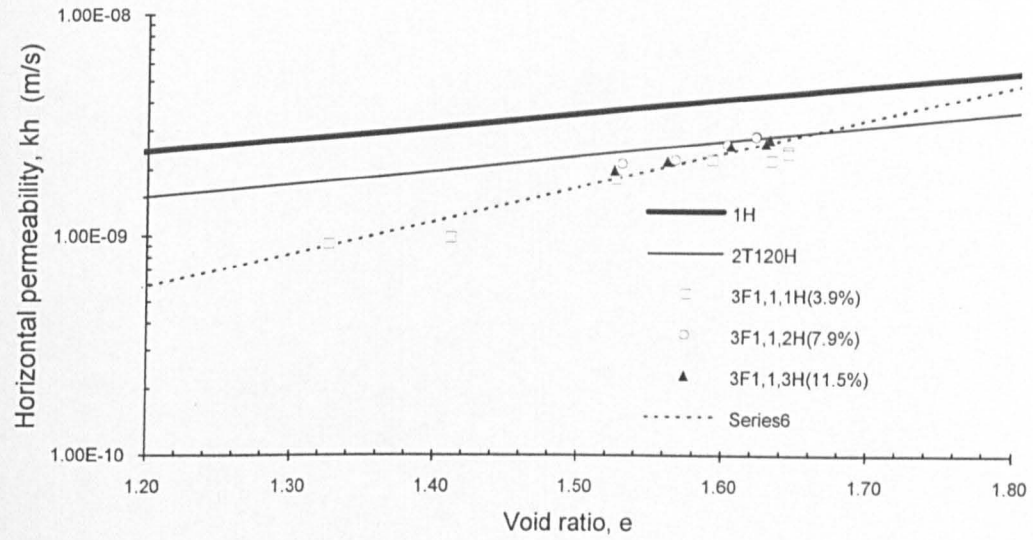

(a)

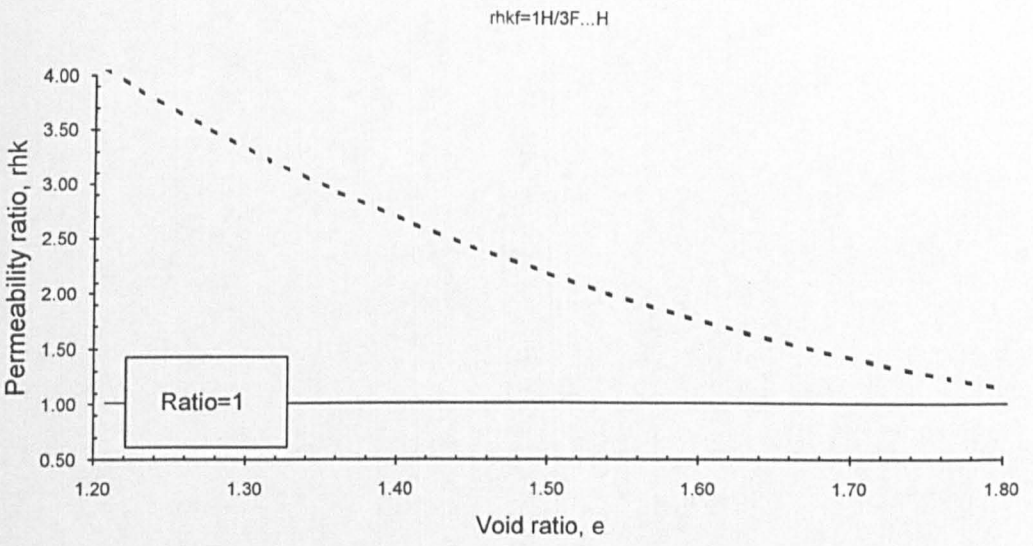

(b)

Fig.-5.26 (a) Permeability vs void ratio, Series 3F...H compared with Series 1H and 2T120H; (b) Permeability ratio r_{hkF} = 1H/ 3F...H vs void ratio

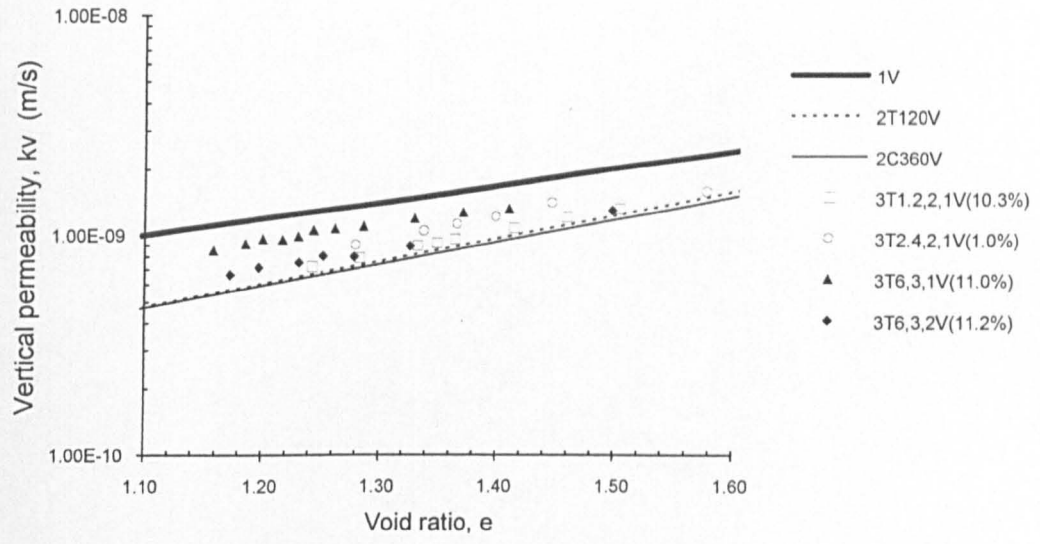

(a)

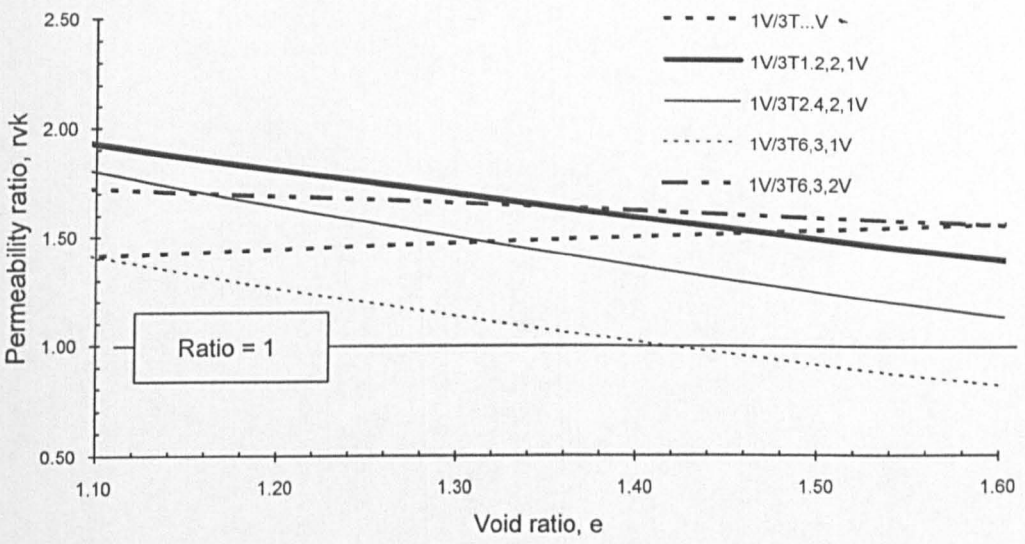

(b)

Fig.-5.27 (a) Permeability vs void ratio, Series 3T...V compared with Series 1V, 2T120V and 2C360V; (b) Permeability ratio r_{vkT} = 1V/ 3T...V vs void ratio

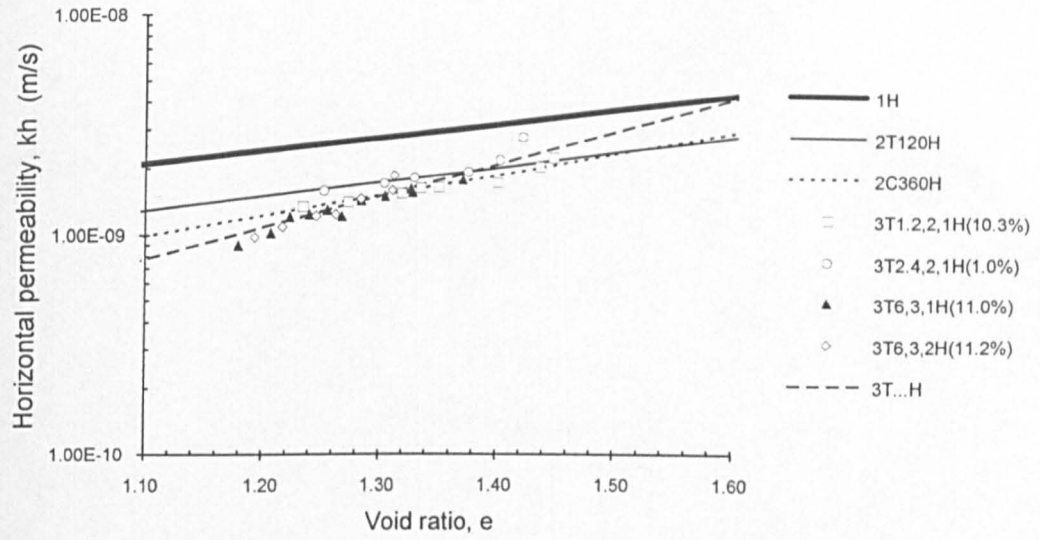

(a)

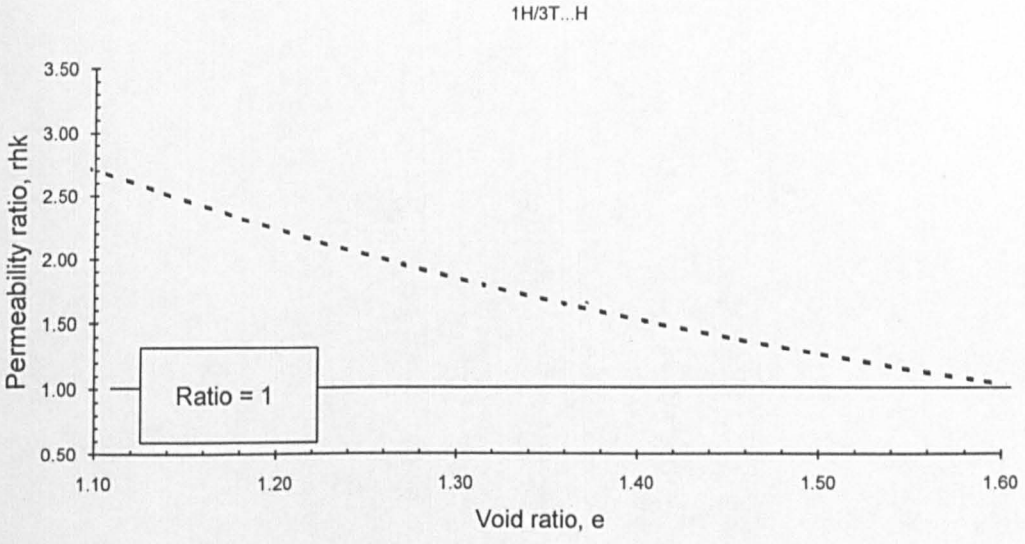

(b)

Fig.-5.28 (a) Permeability vs void ratio, Series 3T...H compared with Series 1H, 2T120H and 2C360H; (b) Permeability ratio r_{hkT} = 1H/ 3T...H vs void ratio

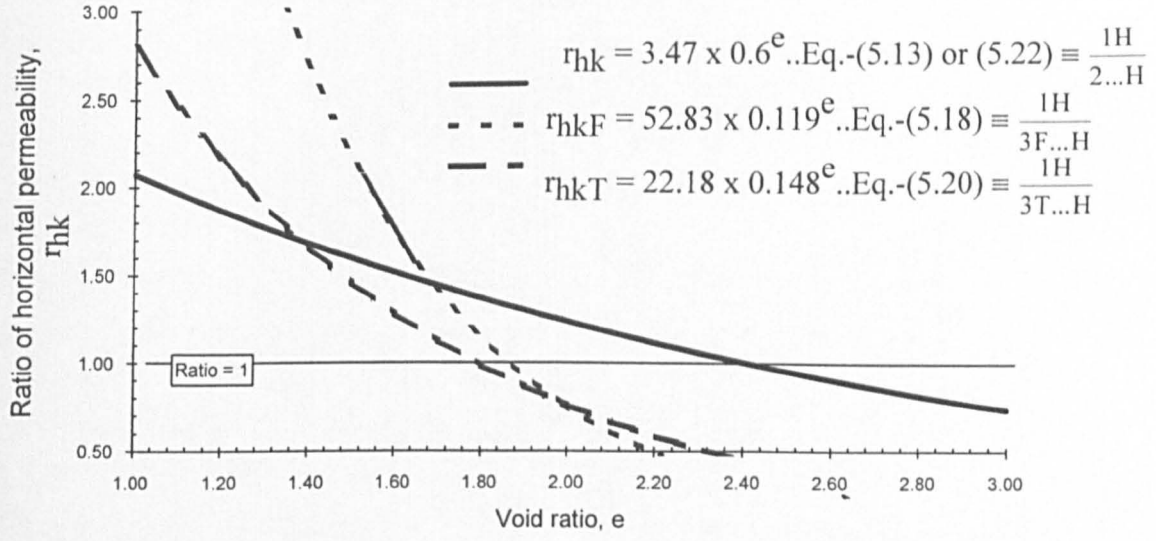

(a)

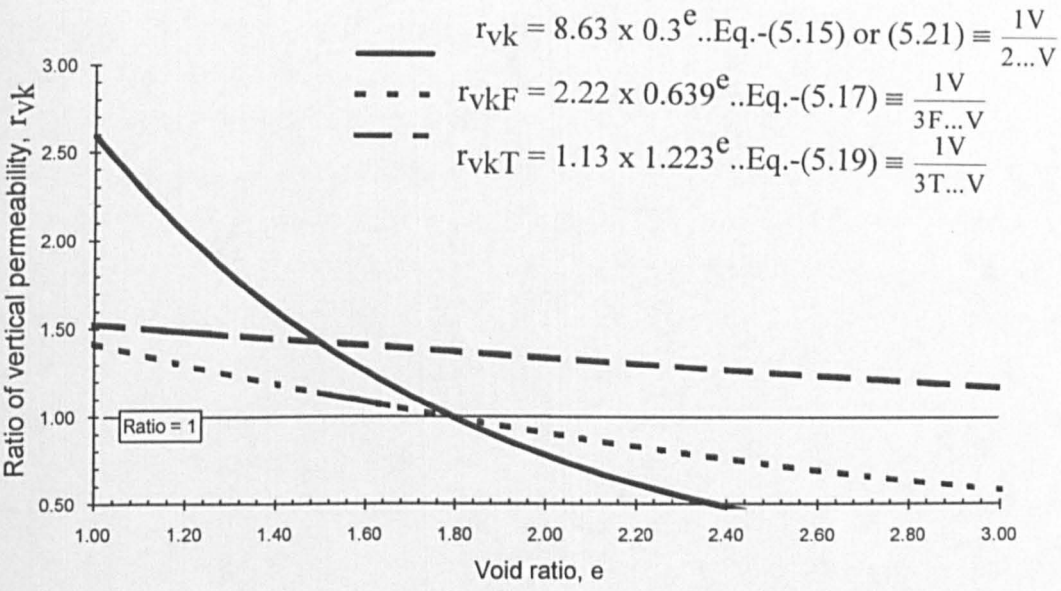

(b)

Fig.-5.29 Permeability ratios vs void ratio (a) Horizontal permeability; (b) Vertical permeability

Fig.-5.29(a) shows that above the basic r_{hk} line and along a given initial void ratio line, values of r_{hkF} and r_{hkT} are greater than r_{hk}. This means that the undrained shear has the effect of decreasing the horizontal permeability of the sample. The figure further shows that the decrease in k_h is slightly smaller for the softer sample compared to the stiffer sample since the difference $\Delta r_{hkF} < \Delta r_{hkT}$. For the case of *Fig.*-5.29(b), below the basic r_{vk} line and along a given initial void ratio line, the values of r_{vkF} and r_{vkT} seem to be less than r_{vk} resulting to increases in values of vertical permeability. The effect of undrained shear therefore leads to increases in vertical permeability. The increase in k_v is lesser for softer sample as compared to stiffer sample since the difference $\Delta r_{vkF} < \Delta r_{vkT}$.

To appreciate further the influence of undrained shear on permeability, relationships between changes in permeability, Δk and initial permeabilities, k_o are considered. *Figs.*-5.30(a) and 5.30(b) present the changes in horizontal permeability, Δk_h vs initial horizontal permeability, k_{ho}. The initial horizontal permeability, k_{ho} in this case refer to Series 2T120H & 2C360H for *Fig.*-5.30(a) and Series 1H for *Fig.*-5.30(b). It is the permeability of the 'reference' sample at void ratio before shearing, of the sheared sample. Ignoring one data at e=1.67, *Figs.*-5.30 indicate that the change in horizontal permeability of sheared samples decreases as the initial horizontal permeability of the 1-D sample increases. Although the signs of changes in permeability can be +ve or -ve as shown in the figures, the change appears to decrease with the increase of both k_{ho} and e. This decreasing change of Δk_h with increasing k_{ho} and e is seen to be quite independent of whether Series 2T120H & 2C360H or Series 1H is being used for the reference k_{ho} as shown in *Figs.*-5.30(a) and 5.30(b).

The above case for vertical permeability is presented in *Figs.*-5.31(a) and 5.31(b). Again ignoring one data at e=1.33, *Figs.*-5.31 indicate that the change in vertical permeability Δk_v of sheared samples increases as the initial vertical permeability of the 1-D sample k_{vo}, increases. The increasing change of Δk_v with increasing k_{vo} and e is also seen to be quite independent of whether Series 2T120V & 2C360V or Series 1V is being used for the reference k_{vo} as shown in *Figs.*-5.31(a) and 5.31(b).

Both *Figs.*-5.30 and 5.31 indicate that consistent with the permeability-void ratio relations, k_{ho} and k_{vo} always increase with increasing e. The results further show that the vertical strain ε_v of the CIU compression shear triaxial test, along constant initial void ratio lines: $e=e_o$, do not show any consistent pattern on the changes in horizontal or vertical permeability.

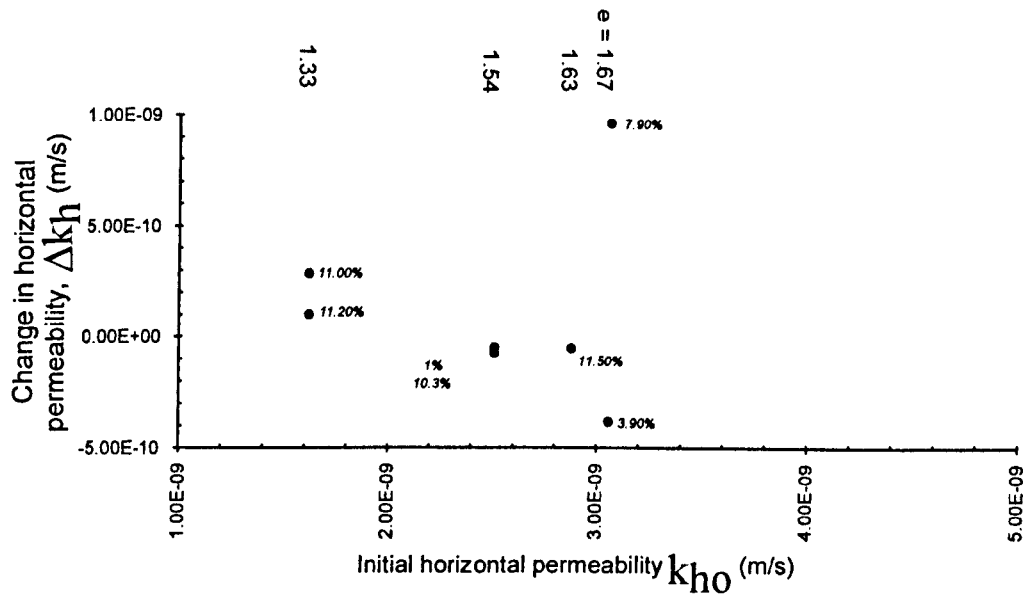

(a)

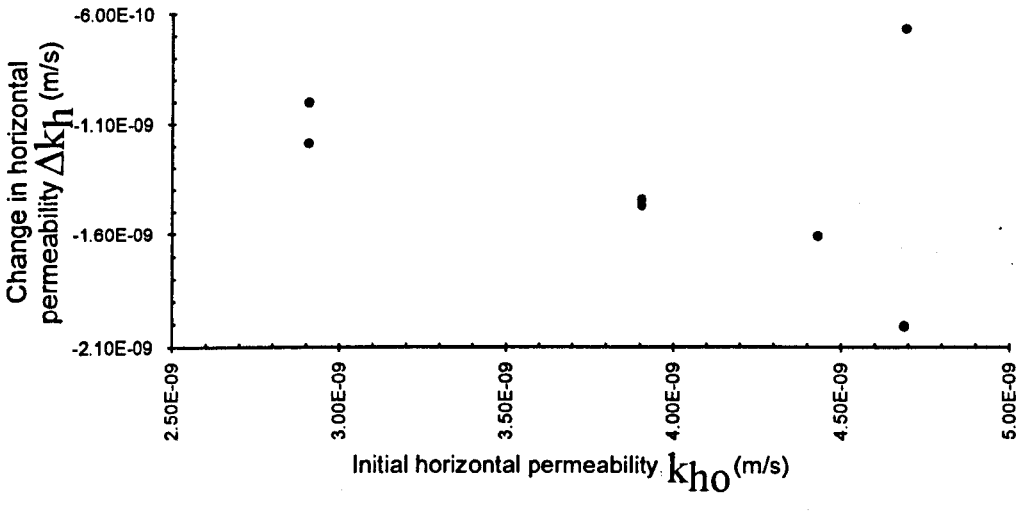

(b)

Figs.-5.30 Change in horizontal permeability Δk_h vs initial horizontal permeability k_{ho} for sheared samples with k_{ho} referenced to: (a) Series 2T120H & 2C360H; (b) Series 1H

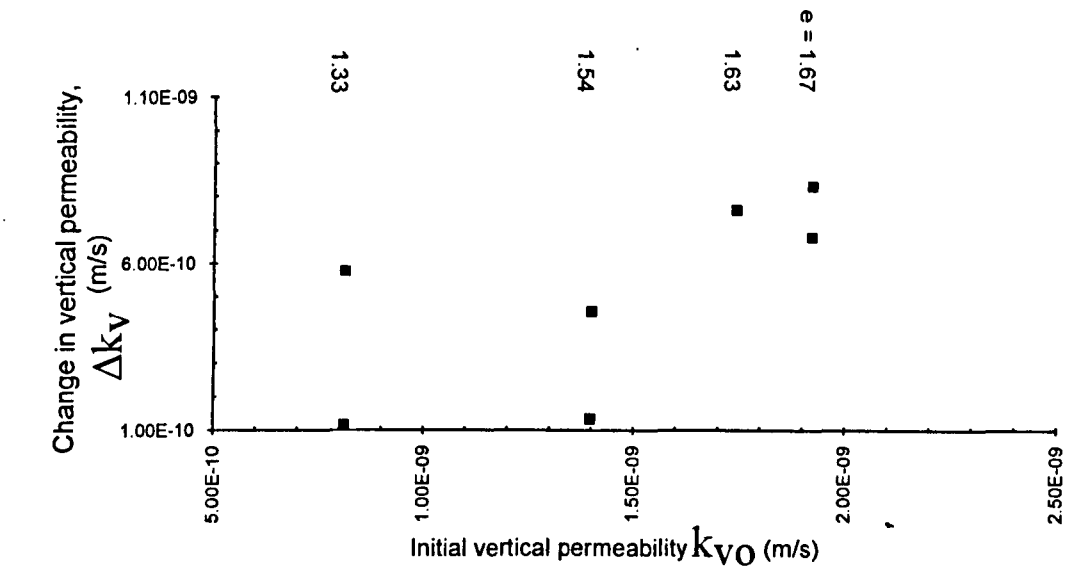

(a)

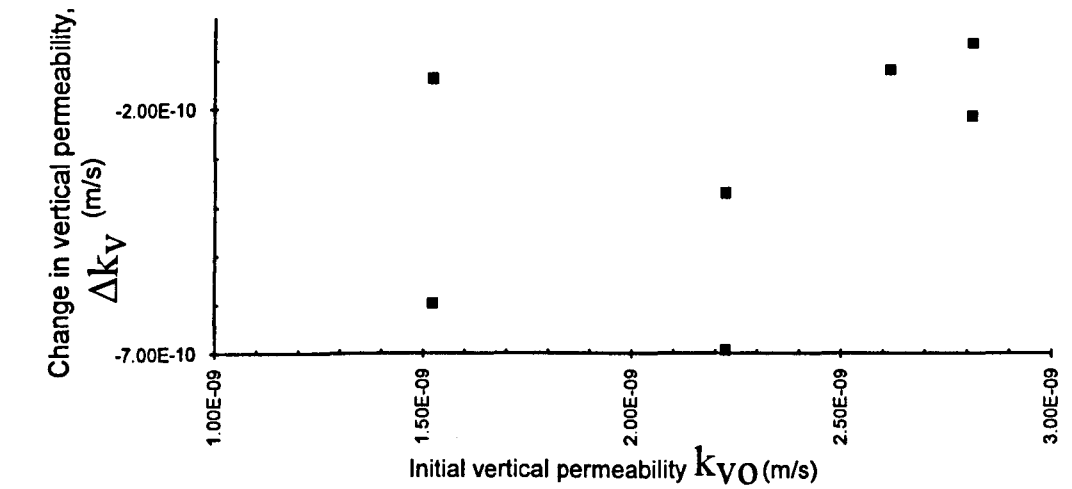

(b)

Figs.-5.31 Change in vertical permeability Δk_V vs initial vertical permeability k_{VO} for sheared samples with k_{VO} referenced to: (a) Series 2T120V & 2C360V; (b) Series 1V

The development of permeability anisotropy when the stress history was changed from one of anisotropic condition to shearing at constant void ratio can be referred to the combination of *Figs.*-5.25(a) and 5.26(a) for samples from Group I, and *Figs.*-5.27(a) and 5.28(a) for samples from Group II respectively. Because of their relatively low states of pre-consolidation stress of 100kPa, the range of void ratio lies between 1.65 to 1.50 for samples in Group I while the void ratio values range between 1.28 to 1.15 for the stiffer Group II samples whose pre-consolidation stress was 600kPa.

The permeability anisotropy r_k for Series 3F ie. Group I, are shown plotted against void ratio e in *Fig.*-5.32(a) together with the 'reference' r_k results of Series 2T120H:2T120V and 1H:1V. The r_k values for Series 3F in the figure are for the three individual series with r_k following the basic definition by Eq.-(5.10): $r_{kF} = \frac{3F1,1,1H}{3F1,1,1V}$, $\frac{3F1,1,2H}{3F1,1,2V}$ and $\frac{3F1,1,3H}{3F1,1,3V}$. At the beginning of the lines these r_{kF} values corresponding to their early void ratios are obtained as: r_{kF} = 1.04, 1.49 and 1.13.

Permeability anisotropy r_k for Series 3F1 based on averages of the individual series is shown plotted against void ratio e in *Fig.*-5.32(b) and in this case r_k follows the definition given by Eq.-(5.11): $r_{kF} = \frac{3F...H}{3F...V} = 0.14x3.60^e$

The exponential law model of the permeability variation with void ratio gives values of C_{k_v} for the three test series (3F1,1,1V; 3F1,1,2V; and 3F1,1,3V), as 0.98, 1.02, and 1.13 respectively. The samples in these series have a past history of σ'_{vp}=100kPa. The influence of shear on permeability anisotropy is examined through the latter's variation with a given void ratio such as suggested by the line AB in *Fig.*-5.32(a). The general effect of shear seems to decrease the permeability anisotropy at any given vertical strain of $\varepsilon_v = 0$ to about 11.5%. Thus for the case of *Fig.*-5.32(b), at an initial sample void ratio of e_o=1.68(approximately), r_{kF} decreases from a value of 1.65 to 1.17 when the clay was compressed to various vertical strains in the CIU test. The value of 1.65 refers to r_k for Series 1 but reference to Series 2 also results in the reduction of r_{kF} upon shear. As the void ratio decreases in the post-anisotropic compression, values of r_k decrease further to values less than 1 [Fig.-5.32(b)]. It is seen that the profound influence of 1-D consolidation/compression in enhancing the permeability anisotropy of slurry and 1-D compressed samples is now no longer effective on sheared samples and this points to the possibility of radical change in the structure of the samples upon shear deformation.

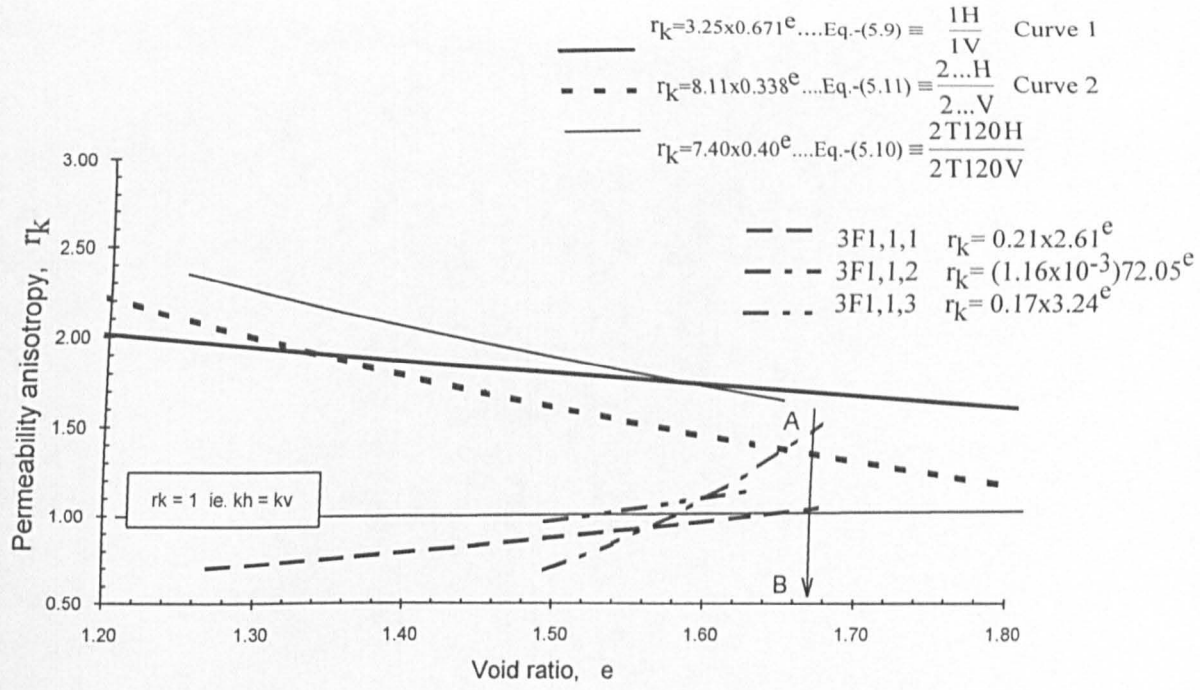

(a)

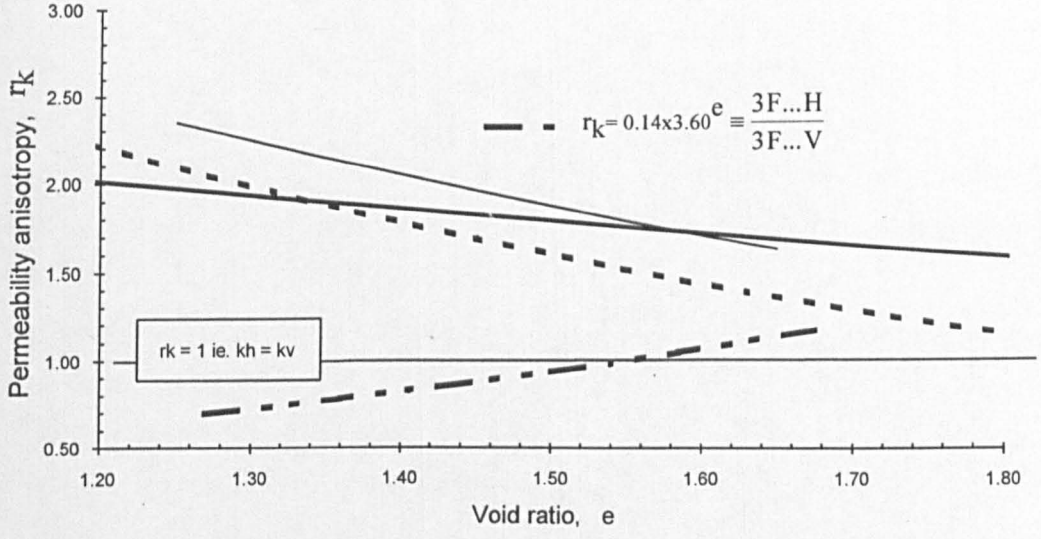

(b)

Fig.-5.32 (a) Permeability anisotropy r_k for sheared samples (Group I) compared with unsheared samples (Series 1 and 2T120); (b) as (a) above but from averages

Again based on Eq.-(5.10), the permeability anisotropy r_k for Group II samples are shown plotted against void ratio in *Fig.*-5.33(a) compared with the 'reference' r_k results of Series 2C360H:2C360V and 1H:1V.

Permeability anisotropy r_k for Series 3T based on averages of the indivdual series is shown plotted against void ratio e in *Fig.*-5.33(b).

Looking back at *Fig.*-5.16, *Fig.*-5.19 and also *Figs.*-5.32 & 5.33, the following observations could be stated as regard the outcome of vertical and horizontal permeability tests on the three types of samples, viz the slurry, (Series 1); anisotropically consolidated block samples, (Series 2); and CIU sheared samples, (Series 3): (1) For the Series 1 sample, anisotropy of permeability at the beginning of the permeability tests (at σ'_v=40kPa) was practically nil to qualify the testing procedure as sufficiently accurate not to influence any early development of permeability anisotropy; (2) Anisotropy of permeability has been detected on Series 2 and Series 3 samples at the beginning of the permeability tests. This could be attributed to the existing anisotropic conditions (fabric anisotropy and stress anisotropy) that have developed in the sample; (3) Permeability anisotropy increases with the applied effective stresses for the slurry sample which has not experienced any consolidation stresses earlier. The continuing vertical effective stresses therefore further enhances development of permeability anisotropy with compression; (4) For the anisotropically consolidated samples the existing developed permeability anisotropy does not increase or decrease but remains relatively unchanged on further compression; (5) For the CIU sheared samples the existing developed permeability anisotropy decreased gradually on further compression. Permeability anisotropy developed at the end of the shearing process was reduced as compared to the anisotropy developed due to anisotropic consolidation.

Furthermore, by selecting r_k values at early parts of the (r_k-e) lines, [ie. as denoted by the arrow heads ↓ at some of the lines in *Figs.*-5.33(a) and 5.33(b)], permeability anisotropy developed as a result of 1-D and CIU compression test could be approximately compared to see any differences. A pattern emerged to indicate that r_k developed after the 1-D compression does not change much on further 1-D compression or after CIU to some strains. This is shown in *Fig.*-5.34 by the solid circles for r_k following the 1-D compression and the hollow squares for r_k following the CIU strains. The average (r_k vs e) line shown is quite closed to the averages of Series 2 [ie. Eq.-(5.11)] of the 1-D block samples.

Another view on the effects of shear on permeability may be visualized from the plots of r_k vs vertical strain ε_v, for various values of void ratios as in *Figs.*-5.35(a) and 5.35(b).

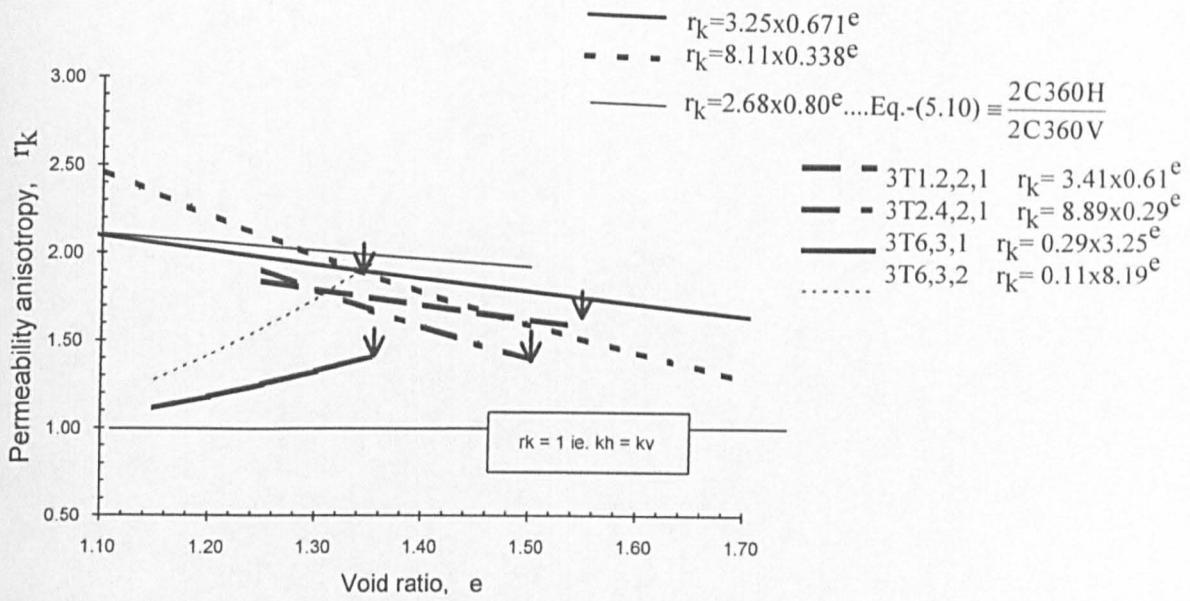

(a)

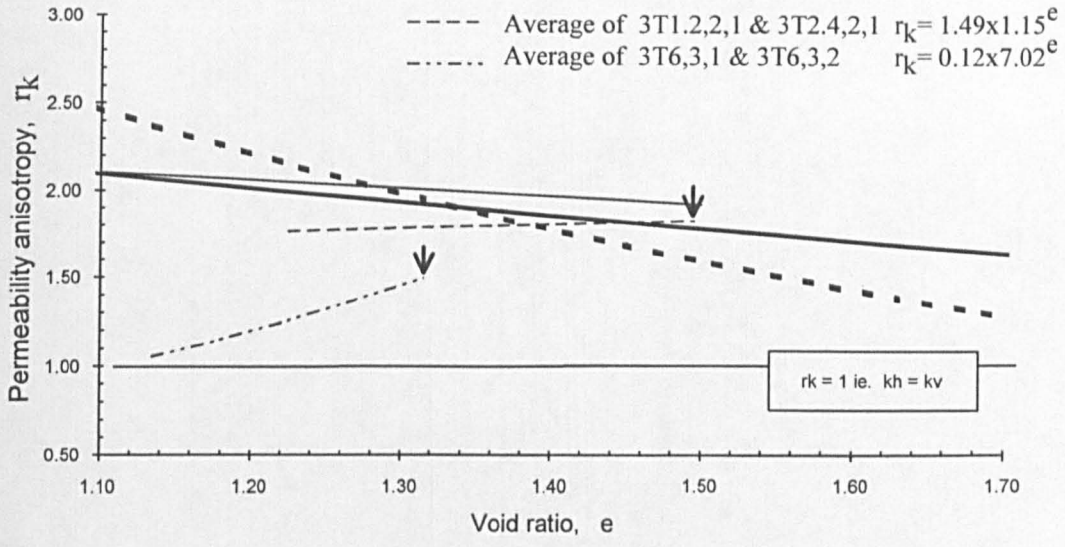

(b)

Fig.-5.33 (a) Permeability anisotropy r_k for sheared samples (Group II) compared with unsheared samples (Series 1 and 2C360); (b) as (a) above but from averages

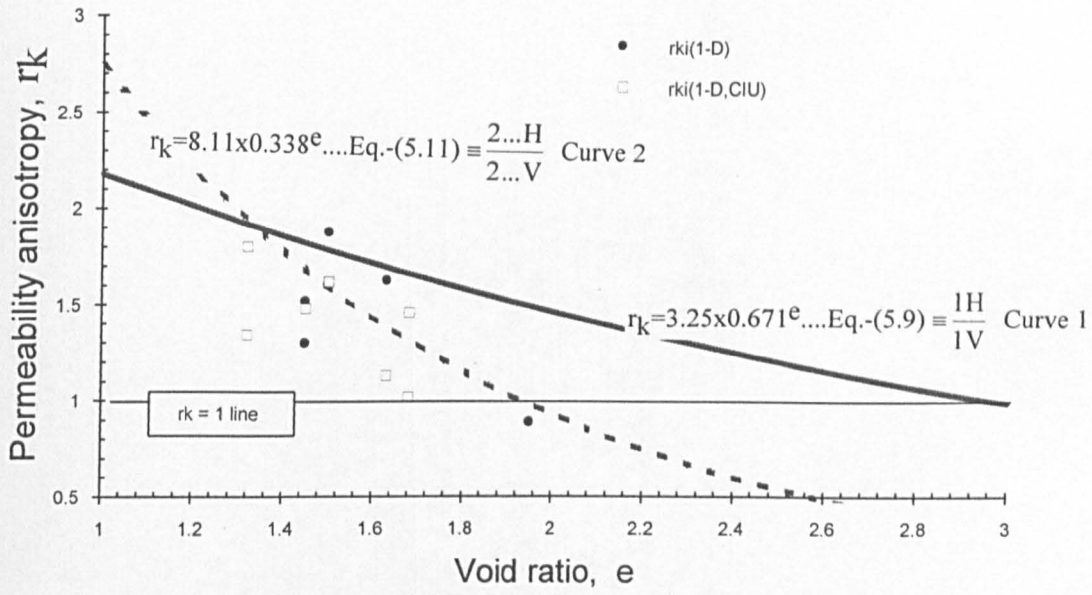

Fig.-5.34 Early values of permeability anisotropy after 1-D compression and CIU shear test

As shown in *Fig.*-5.35(a) for the softer Series 3F samples, the actual range of void ratio of e≈1.70~1.50 is shown by dotted lines. Based on the resulting shapes of these (r_K vs ε_V) lines, the following generalized description on the development of r_K could be suggested according to 3 modes of behaviour. By assigning arbitrary but relative notations for the degree of r_K such as: L-low, M1-moderate and M2-medium, the three modes are:

1. e=1.70 LM1→M1M2→M1
2. e=1.60 LM1→M1→M1
3. e=1.50 LM1→L→M1

Similarly for the case of stiffer Series 3T samples and neglecting anomalous results at ε_V>10.3%, the following generalized descriptions are presented [*Fig.*-5.35(b)]

1. e=1.40 H→M3
2. e=1.20 M3→M3
3. e=1.00 M2→M3

where the arbitrary scales for r_K are denoted by: H-high, M3-medium/high and M2-medium.

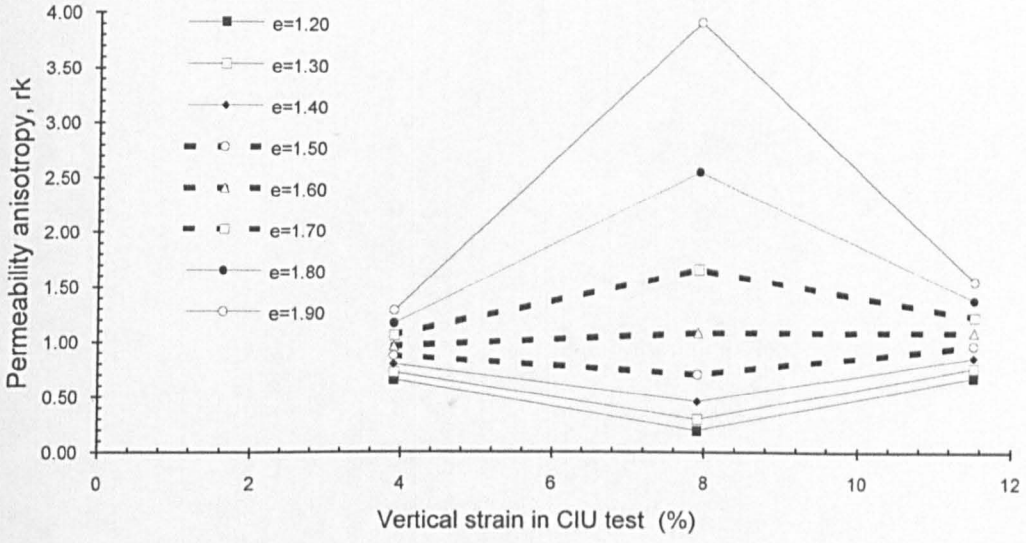

(a)

Figs.-5.35 (a) Permeability anisotropy r_k vs vertical strain ε_v for Series 3F (e = 1.90 - 1.20)

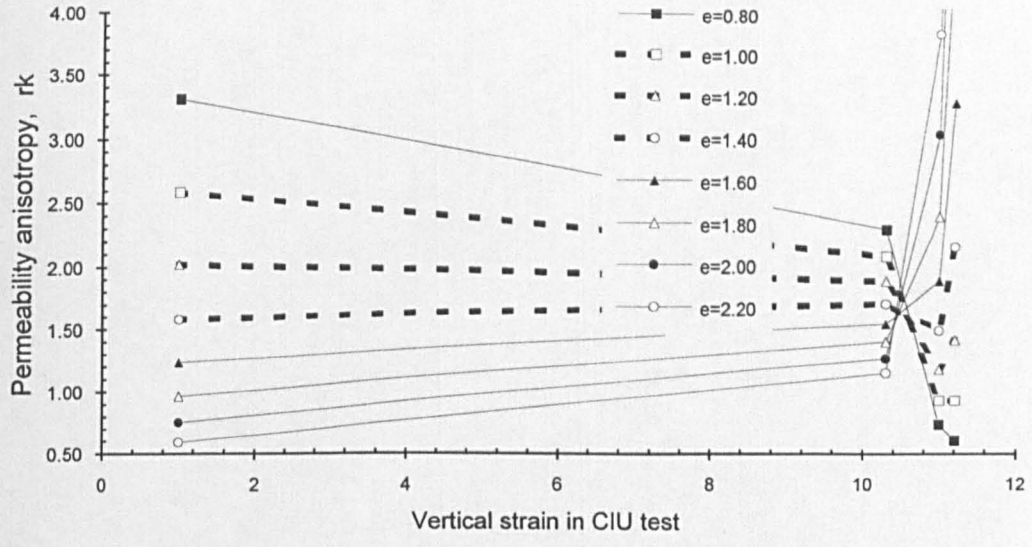

(b)

Figs.-5.35 (b) Permeability anisotropy r_k vs vertical strain ε_v for Series 3T (e = 2.20 - 0.80)

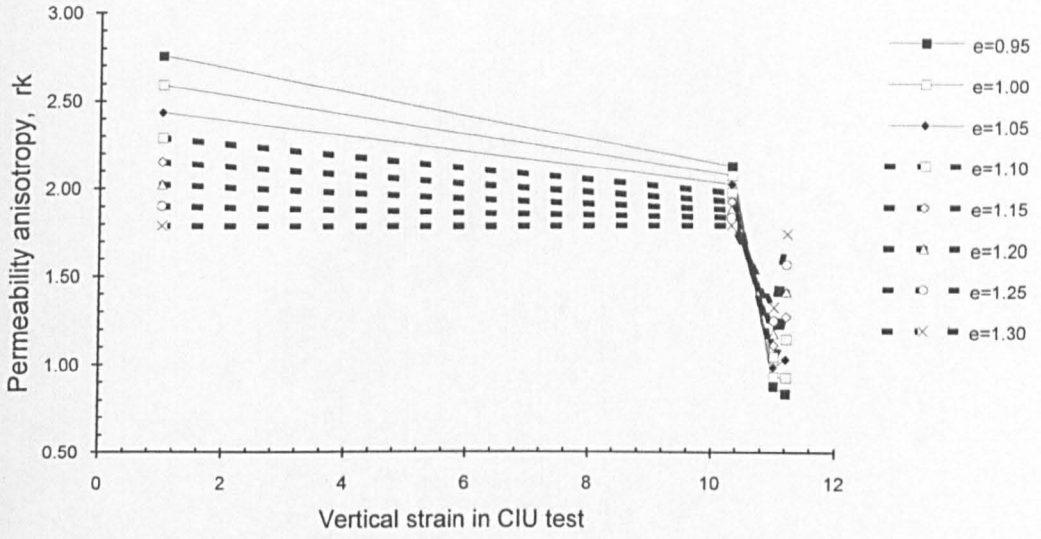

(c)

Figs.-5.35 *cont.* (c) Permeability anisotropy r_k vs vertical strain ε_v for Series 3T (e = 1.30 - 0.95)

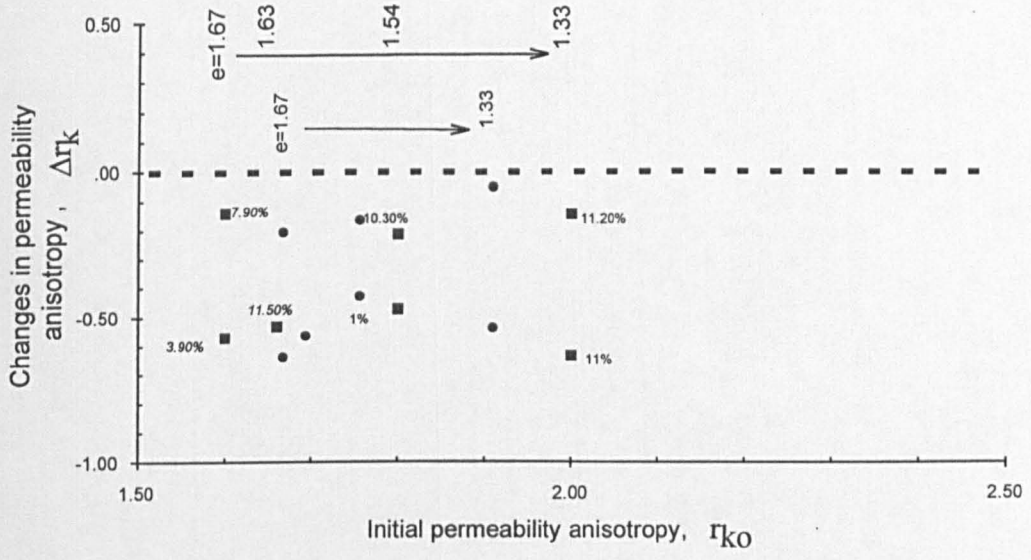

Fig.-5.36 Changes in permeability anisotropy Δr_k vs initial r_k

Just as there exists some relationships between changes in permeability and the initial permeability (*Figs.*-5.30 and 5.31), the influence of CIU shear deformation could lead to possible explanation in terms of changes in permeability anisotropy and the importance of the existing anisotropy in controlling the resulting course of anisotropic behaviour. The results in *Fig.*-5.36 attempt to relate the changes in permeability anisotropy Δr_k, with the initial permeability anisotropy $r_k = r_{ko}$, of the sheared samples. The *italic* nos. beside the data points represent the vertical strain ε_v% for Series 3F while the regular nos. are ε_v% for Series 3T. The square data are evaluated based on reference to unsheared permeability values of Series 2T120 and 2C360 and the round data are referred from Series 1.

The results in *Fig.*-5.36 show that all samples experienced a decrease in permeability anisotropy as indicated by the -ve. changes in permeability anisotropy at all values of the initial permeability anisotropy. Similar to observations in *Figs.*-5.30 and 5.31 the vertical strains ε_v from the shear tests do not show any consistent trends in the results of the changes in permeability anisotropy.

5.6 Permeability data from consolidation tests

The consolidation test provides an indirect means of evaluating the permeability of the clay sample. Darcy's law has been one of the essential assumptions in the consolidation process and this provides a useful deduction to back calculate the permeability of the clay from the observation of the rate of consolidation of the test. Two points must be borne in mind, however, (1) Darcy's law must be applicable in conditions of varying high gradients occurring in the consolidation process, and (2) the transient nature of the consolidation phenomenon affects both the flow of pore water and the dissipation of pore pressure leading to volume changes. Consolidation parameters, c (ie. c_v and c_r or c_h) and m_v are first discussed followed by the calculated permeability.

The results from consolidation tests are shown as graphs of vertical settlement, Δh, plotted against the square root of time, $\sqrt{t}$, and t_{90} is determined using the Taylor's curve-fitting method. Some typical results for consolidation with vertical and radial flows in the slurry samples (test series 1V and 1H) are shown in *Fig.*-5.37 for various vertical effective stress levels. The vertical stress increments applied in each of the consolidation steps are also shown in the figure. For calculations of vertical permeability, values of c_v were calculated using $T_{90} = 0.848$ and $\alpha = 1.15$ (Section 4.3). For calculations of the horizontal permeability, values of c_h from the expressions of both Terzaghi's and Biot's theories of consolidation were used. From Terzaghi's theory the values used were $T_{90} = 0.81$ and $\alpha = 1.21$ and from Biot's theory $T_{90} = 0.892$ and $\alpha = 1.1725$ (*Table*-4.3, Section 4.3).

Vertical and horizontal permeabilities are back calculated from the relationships expressed by Eq.-(4.13) and values of $\sqrt{t_{90}}$ are obtained from results such as those shown in *Fig.*-5.37.

The values of the coefficients of consolidation c_v and c_h for the test Series 1V and 1H are shown in *Fig.*-5.38 plotted against the logarithm of vertical effective stress. This figure shows a tendency for both c_v and c_h to decrease as the vertical effective stress increases. The results also show that value of c_v can be appreciably greater or lesser than that of c_h depending on the magnitude of the vertical effective stress. At relatively low σ'_v=10 to 80kPa, $c_v > c_h$. Average values are c_v=4.2m^2/yr and c_h=3.6m^2/yr in this stress range. From σ'_v=100 to about 300kPa, $c_v < c_h$ and in this stress range both coefficients decrease rapidly to merge into a constant value of about 0.6m^2/yr. Values of c_v and c_h for test Series 2 from the block samples are shown in *Fig.*-5.39 plotted against the logarithm of vertical effective stress which shows a rather random spread in the variation of the c values with σ_v'. As a rough

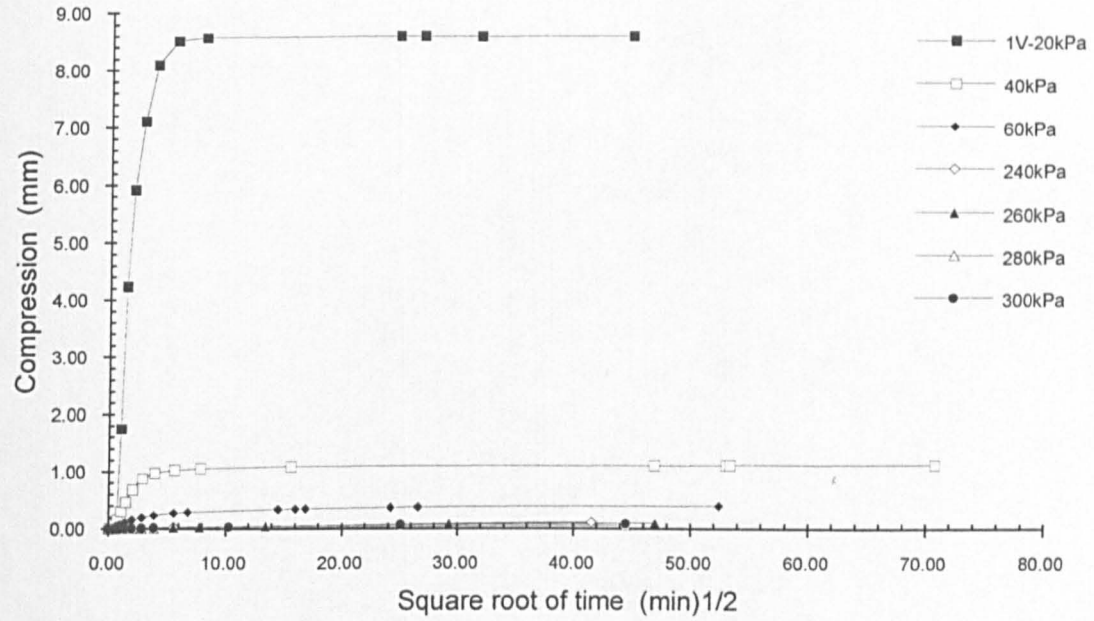

(a)

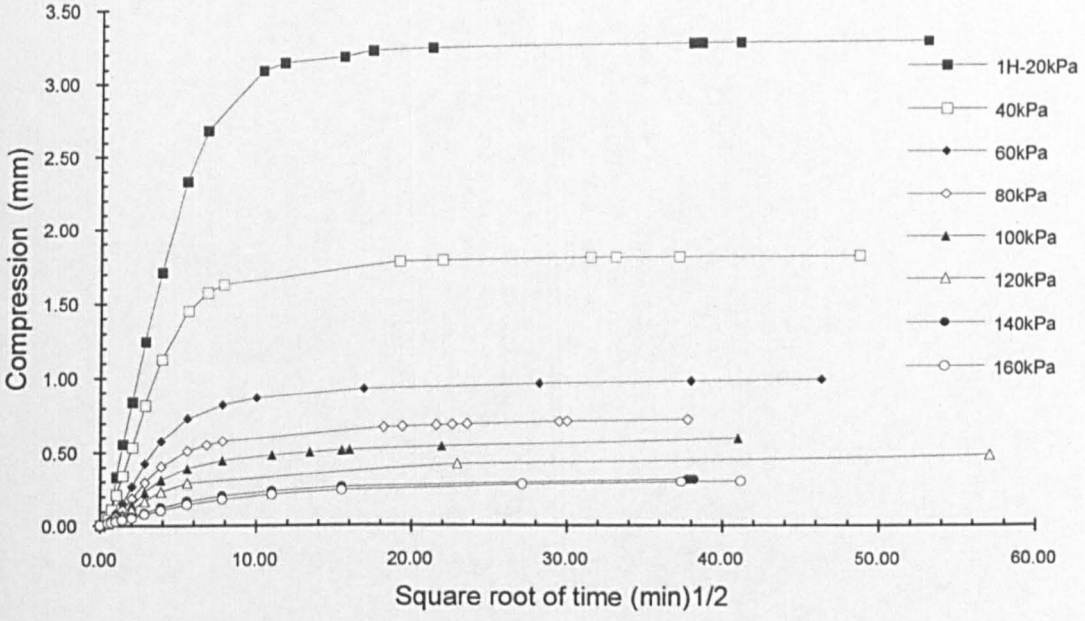

(b)

Fig.-5.37 Time compression curves ie. Compression vs $\sqrt{t}$ for samples in test series 1V and 1H

approximation, however, an average constant value for the coefficient of consolidation common for both the horizontal and vertical flow samples can be assumed to be about $13m^2/yr$. Compared with the slurry sample the coefficient of consolidation c(Series 2)>c(Series1).

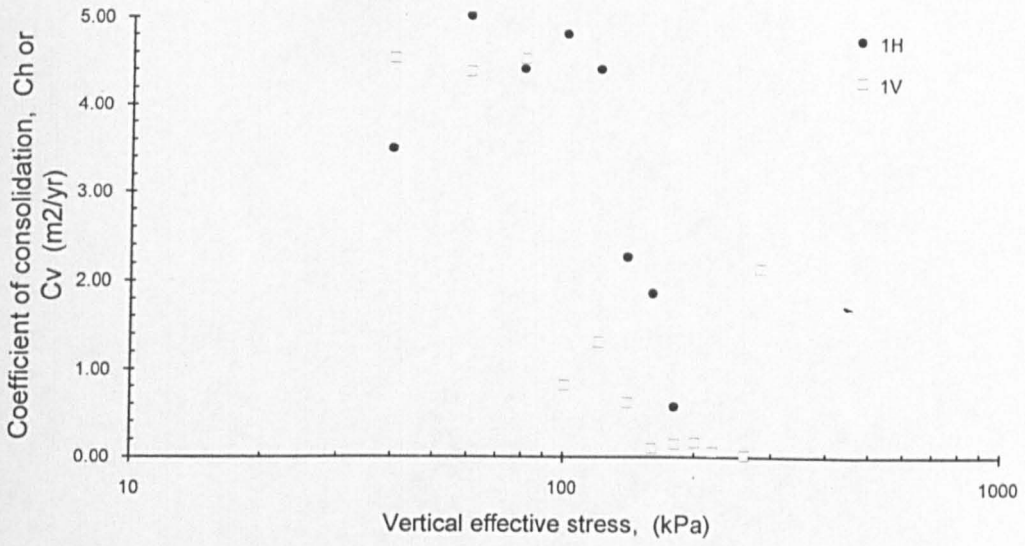

Fig.-5.38 Coefficients of consolidation vs $\lg.\sigma'_v$ for samples in test series 1V and 1H

Values of the coefficient of volume compressibility m_v were obtained from the tabulated results of void ratio against vertical effective stress or more practically from the current height against the latter [see Eq.-(4.26)]. Typical results from the vertical and a horizontal flow consolidation test are presented in *Fig.*-5.40 for the test Series 1V and 1H which show that the shape of the compressibility curves are much the same for both drainage conditions. The values of m_{vh} and m_{vv} are of the same order indicating that the compression behaviour is essentially independent of the direction of flow. The values of m_{vh} approaching 0 for σ'_v>400kPa, however, look unreal for the behaviour of the sample. A possible reason for this observation is that the central drain tip could have reached the oedometer base.

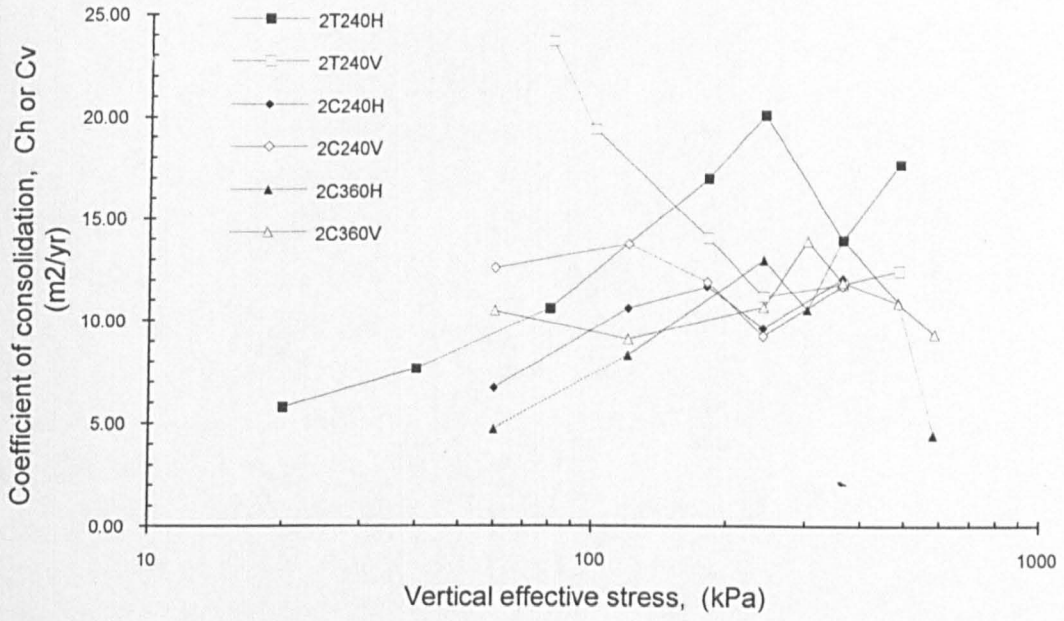

Fig.-5.39 Coefficients of consolidation vs lg.σ'_v for samples in test series 2T120V & 2T120H; 2T240V & 2T240H; 2C240V & 2C240H and 2C360V & 2C360H

For other test series from the block samples which were not sheared, the variation of m_{vh} and m_{vv} with the vertical effective stress shows a general trend of increasing stiffness and the compressibilities merge together irrespective of the flow directions at higher vertical effective stresses (*Fig.*-5.41). This pattern of behaviour is also true for block samples which were sheared.

The results in *Figs.*-5.40 and 5.41 roughly indicate that the slurry sample of Series 1V and 1H will gradually approach similar (m_v-lg.σ'_v) relation with those of the block samples (Series 2C.... & 2T....) at values of σ'_v greater than 200kPa.

The influence of unsheared and sheared sample on compressibility behaviour of the vertical flow sample is examined by plotting the ratio $(m_{vh}/m_{vv})=r_m$ against the vertical effective stress as shown in *Figs.*-5.42, 5.43 and 5.44 for Series 1, 2 and 3 respectively. *Fig.*-5.42 for the slurry sample shows the ratio $r_m=(m_{vh}/m_{vv})$ ranges

from 1 to 1.5 for σ'_v from about 30~300kPa and at higher σ'_v, r_m becomes less than 1. As stated ealier, values of m_{vh} or r_m approaching 0 at higher σ'_v seem to appear unreal in describing the compressibility behaviour. It may be assumed that r_m could decrease to 0.5 and thereafter regain back to 1 as the vertical effective stress increases. Any value <0.5 is logically attributed to the boundary influence of the central drain in the radial flow oedometer. It is further noted in *Figs.*-5.42 and 5.43 for 1-D compression, that a majority of data give values of r_m=1 to about 1.7 indicating a more compressible behaviour when drainage is allowed in horizontal direction.

For 1-D compressed samples followed by shearing in the CIU compression test, the variation of the ratio r_m with σ'_v is shown in *Fig.*-5.44. As suggested earlier, very small values of r_m must be treated with caution as they do not reflect the actual behaviour of the sample but rather could be attributed to the jamming of the central drain at any consolidation stage. It is seen that a majority of data in *Fig.*-5.44 give values of r_m less than 1, indicating a less compressible behaviour for sheared sample when drainage is allowed in horizontal direction.

Knowing the values of c and m_v the permeability values were calculated using Eqs.-(4.38) and (4.43) for vertical and horizontal flows respectively. Values of c (=c_v or c_r) are based on the $\sqrt{t}$-method using the appropriate slope factors, α for the values of t_{90}.

Fig.-5.45 presents the results in the form of calculated permeability k_c plotted against measured permeability k_m for test Series 1V and 1H. Data for Series 1V are shown as solid squares and Series 1H as solid and hollow circles. For Series 1V it is evident that for the same range of void ratio, values of k_c may range by a factor of up to 100 whereas values of k_m range by a factor of 4.5. Similar observations can be said for results of Series 2. Also for Series 2, permeability values deduced from consolidation tests using Terzaghi's theory are slightly lower than those deduced from Biot's theory although both sets of data do not show much agreement when compared to measured values.

Results of other test series from the block samples are shown in *Fig.*-5.46. For a given void ratio, a majority of the data in the figure fall within the range bounded by the lines $k_c=k_m$ and $k_c=(½)k_m$.

The general findings in *Figs.*-5.45 and 5.46 show that calculated permeability k_c as deduced from the theory of consolidation can be equal to but is almost always less than measured permeability k_m for both cases of vertical and horizontal flows.

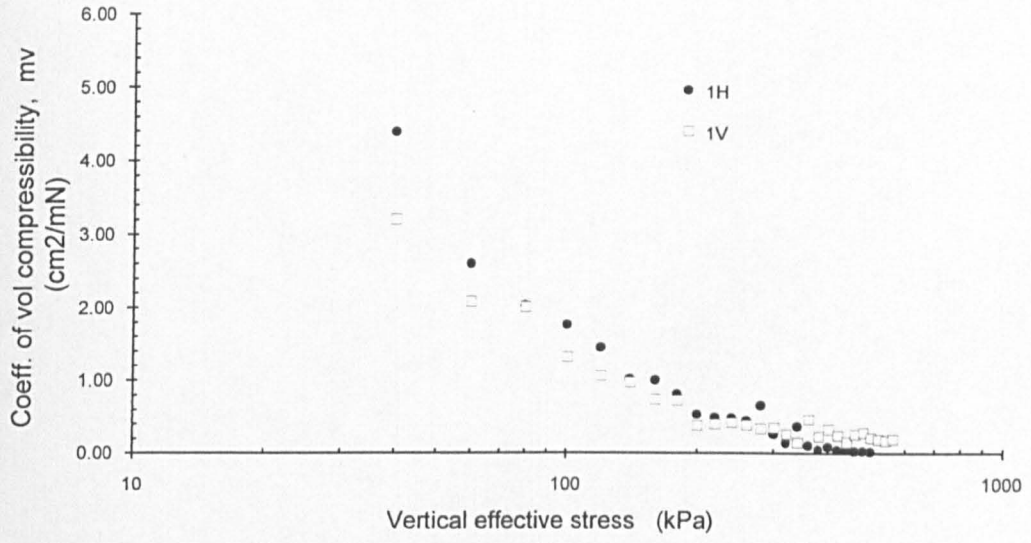

Fig.-5.40 Coefficients of volume compressibility m_V vs $lg.\sigma'_v$ for samples in test Series 1V and 1H

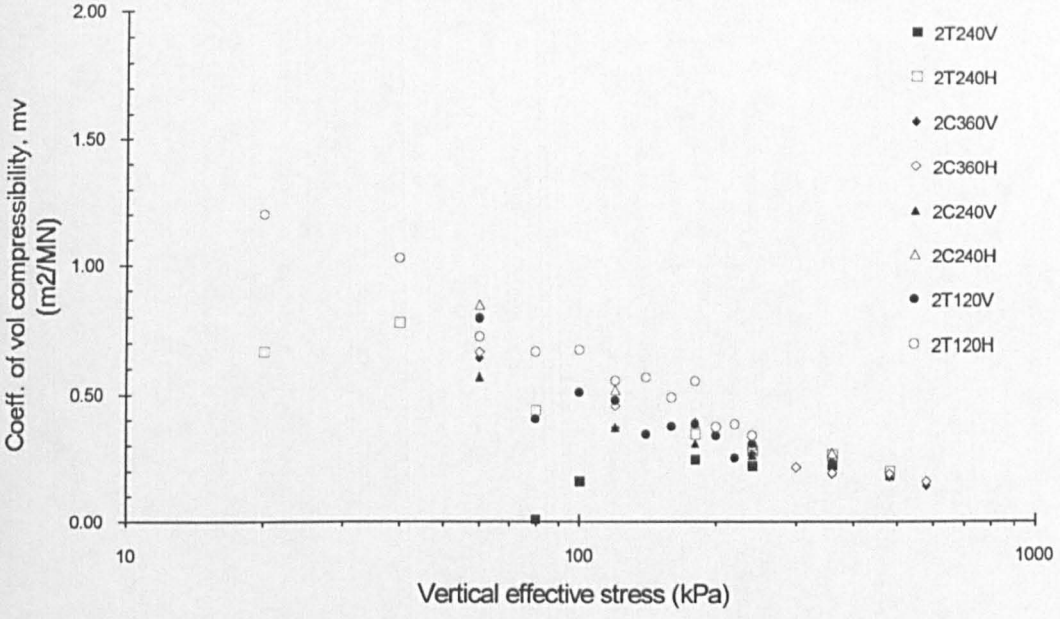

Fig.-5.41 Coefficients of volume compressibility m_V vs $lg.\sigma'_v$ for samples in test series 2T120V & 2T120H; 2T240V & 2T240H; 2C240V & 2C240H and 2C360V & 2C360H

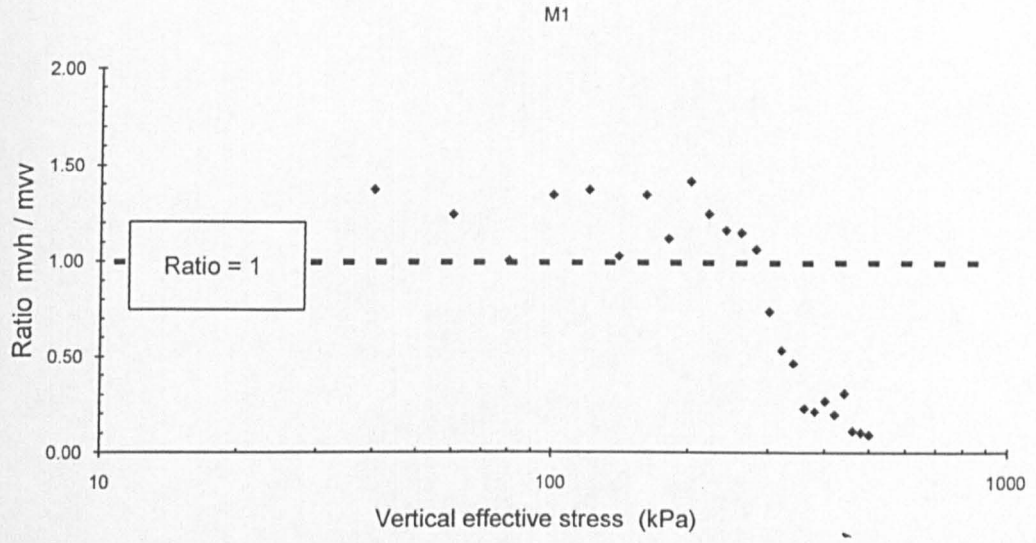

Fig.-5.42 Ratios of coefficients of volume compressibility, m_{vh}/m_{vv} vs $\lg.\sigma'_v$ for samples in test series 1V and 1H

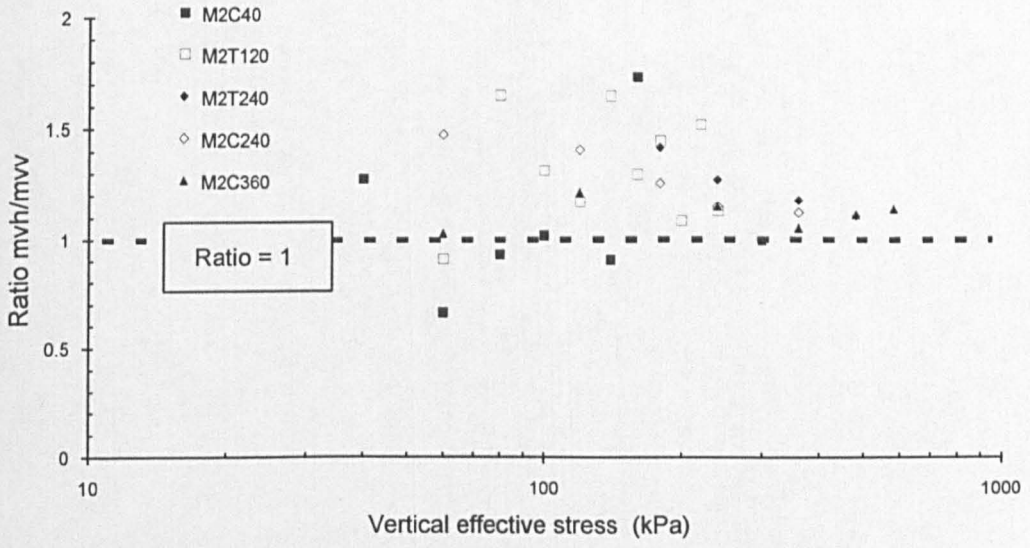

Fig.-5.43 Ratios of coefficients of volume compressibility, m_{vh}/m_{vv} vs $\lg.\sigma'_v$ for samples in test Series 2T120V & 2T120H; 2T240V & 2T240H; 2C240V & 2C240H and 2C360V & 2C360H

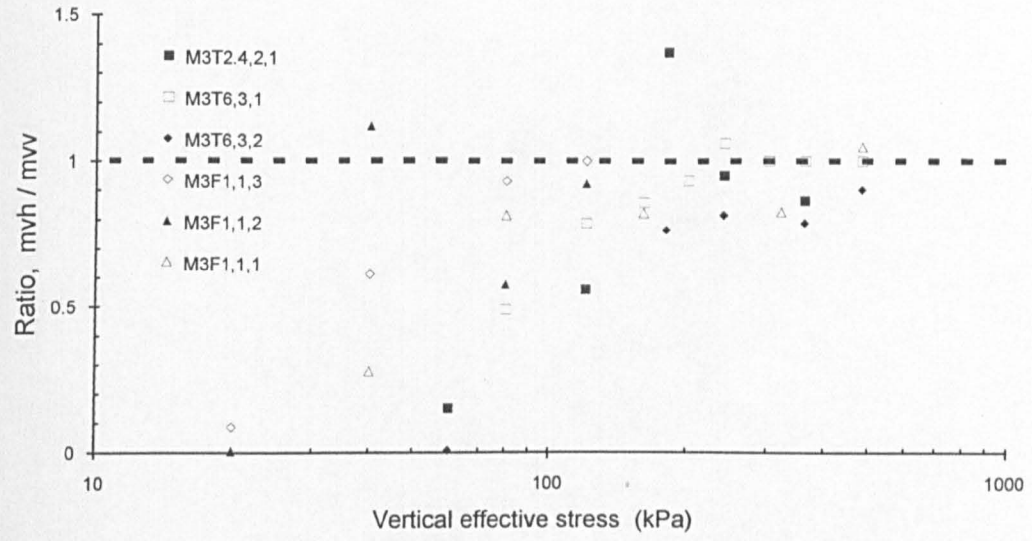

Fig.-5.44 Ratios of coefficients of volume compressibility, m_{vh}/m_{vv} vs $\lg.\sigma'_v$: Series 3T2.4,2,1V & H, 3T6,3,1V & H, 3T6,3,2V & H, 3F1,1,3V & H, 3F1,1,2V & H and 3F1,1,1V & H

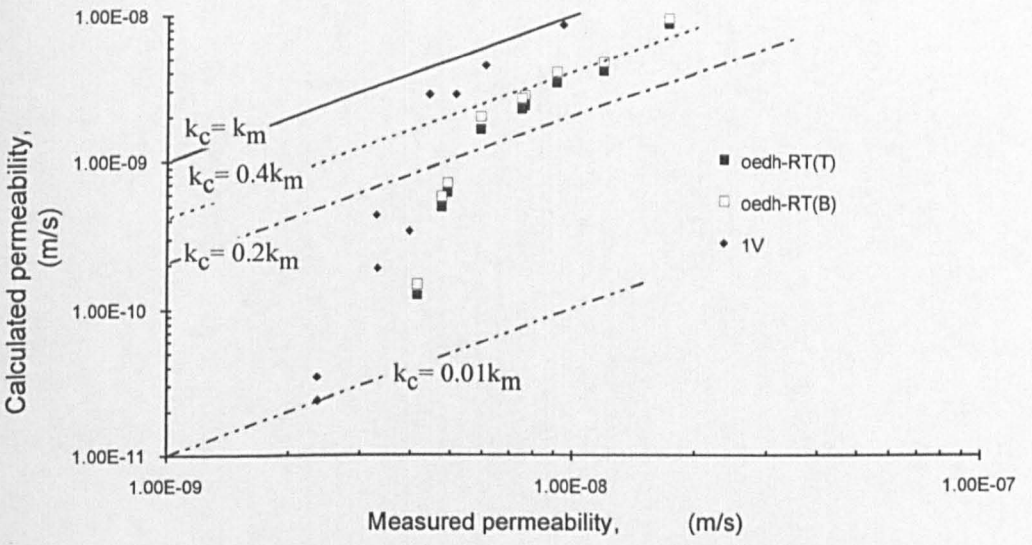

Fig.-5.45 Calculated (k_c) vs Measured (k_m) permeabilty: Series 1V and 1H

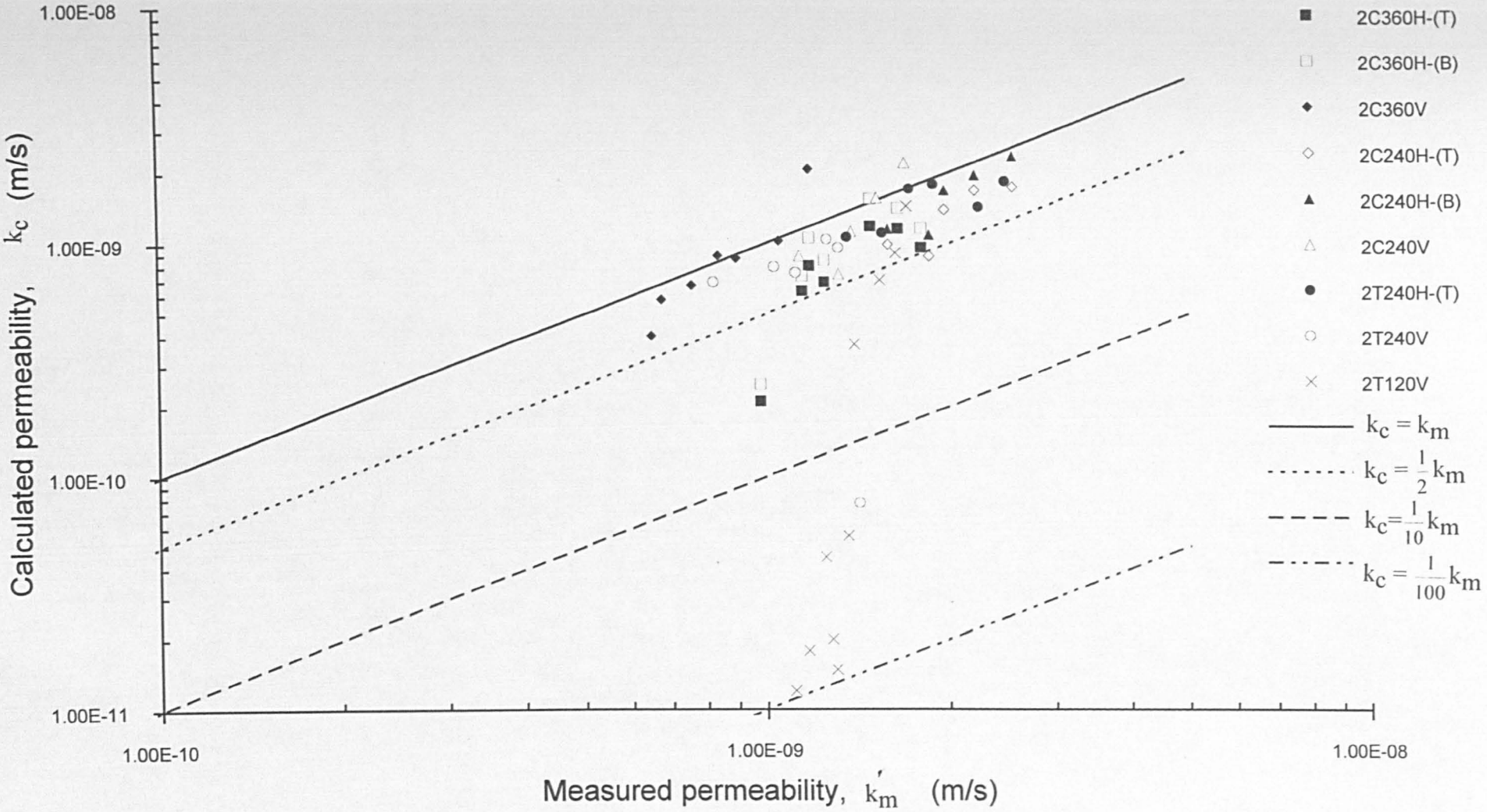

Fig.-5.46 Calculated (k_c) vs Measured (k_m) permeabilty:
Series 2C360V & 2C360H, 2C240V & 2C240H, 2T240V & 2T240H, and 2T120V

5.7 Consolidation characteristics from permeability tests

5.7.1 Transient phase of the constant flow rate permeability test

5.7.1.1 Vertical flow

As described in Chapter 4 (Section 4.2.4), the transient phase of the constant flow rate permeability test provides a direct means of evaluating the consolidation parameters of the clay sample as well as permeability from the early time records of the test data.

The method outlined in Section 4.2.4.1 is applied here. The unique type-curve for model of the forced constant flow rate is reproduced in *Fig.*-5.47. The experimental data points of the induced pressure difference-time graph (or pressure response curve) depicted in *Fig.*-5.6(a) for the sample in test series 2T240V at consolidation stage of σ'_v = 100kPa are plotted on logarithmic scales as shown in *Fig.*-5.48 and these data points are superimposed on the type-curve with the effect as shown in *Fig.*-5.49. Five sets of the experimental data points are shown in *Fig.*-5.48 to account for the 5 constant flow rates imposed in the test series (ie. 3 upward and 2 downward flows). Also depending on whether the flow rate (FR) is preceded by an earlier flow rate or a constant back pressure, (ie. from lower FR to higher FR or from constant back pressure to FR) the corresponding pressure difference may refer to absolute difference or relative difference, respectively. Therefore the pressure differences, $|\Delta p|$ in Fig.-5.48 would not necessarily equal to $|\Delta p|$ in *Fig.*-5.6(a). The two plots need to be projected on log-log graphs that have identical dimensions for both axes of each log cycle; the coordinate axes of the plots also need to be kept parallel. A type-curve printed on a transparent paper (transparency) which can be moved over the experimental plot is used.

When the curve matching is accomplished, a match point is arbitrarily chosen for convenience of reading the scales from both graphs such as match point A in *Fig.*-5.49 which gives the following sets of readings:

$$T_v = 0.9,\ t = 8\text{min}$$

$$U = 0.4,\ \Delta p = 3\text{kPa}.$$

for sample in the test series 2T240V. Thus from $T_v = c_v t / H_s^2$,

$$c_v = T_v H_s^2 / t$$

$$= \left[\frac{365.25 \times 24 \times 60}{4 \times 10^6}\right] \frac{T_v H_s^2}{t} \qquad m^2/yr \qquad (5.40)$$

where t is in min, H_S is height of the sample in mm and T_V is a non dimensional time factor. The factor 4 [=1/(½)²] is introduced in the denominator of Eq.-(5.40) because half sample height is relevant for the computation of c_V.

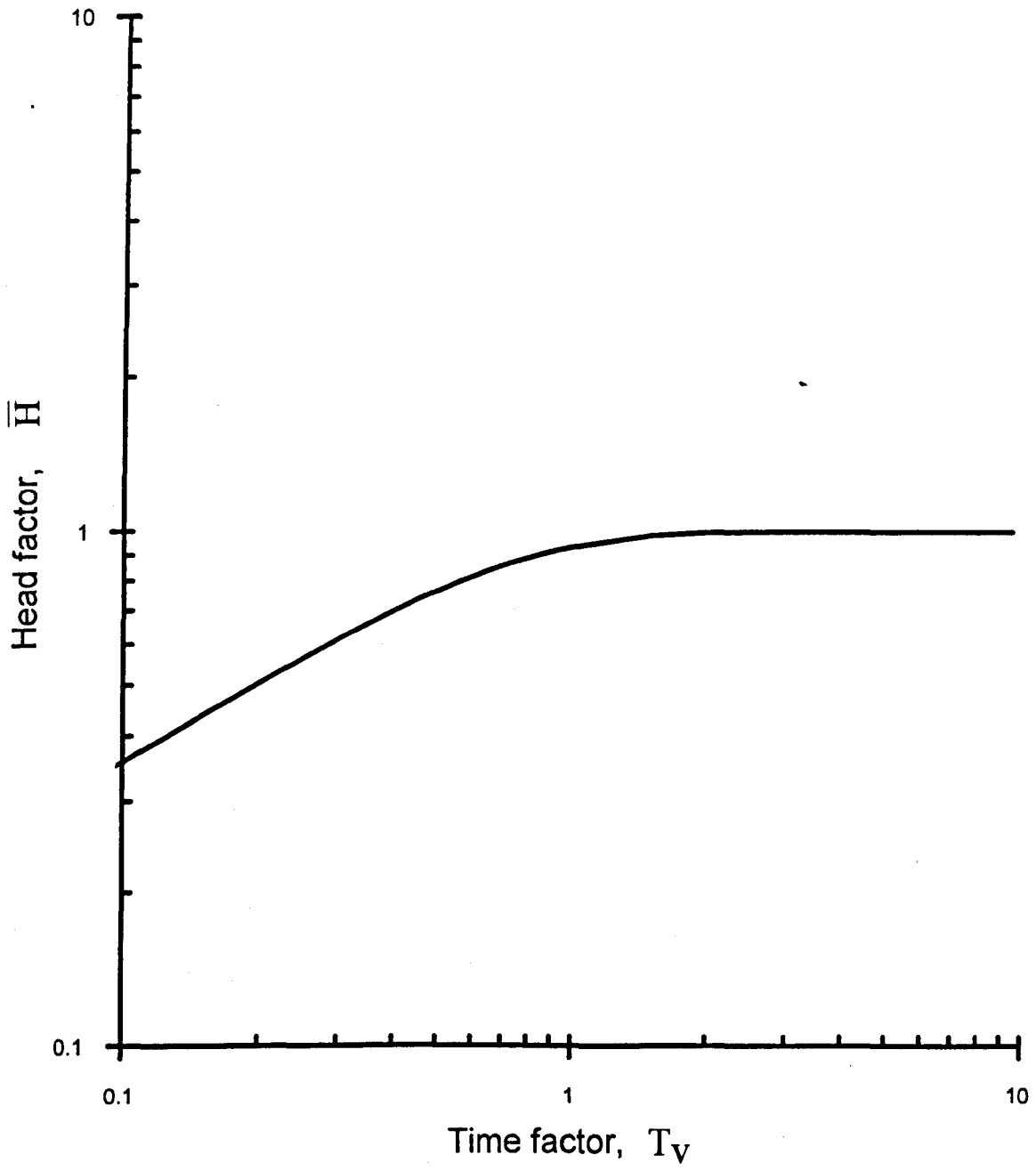

Fig.-5.47 Type curve (Head factor vs Time factor) for vertical constant flow rate permeability test

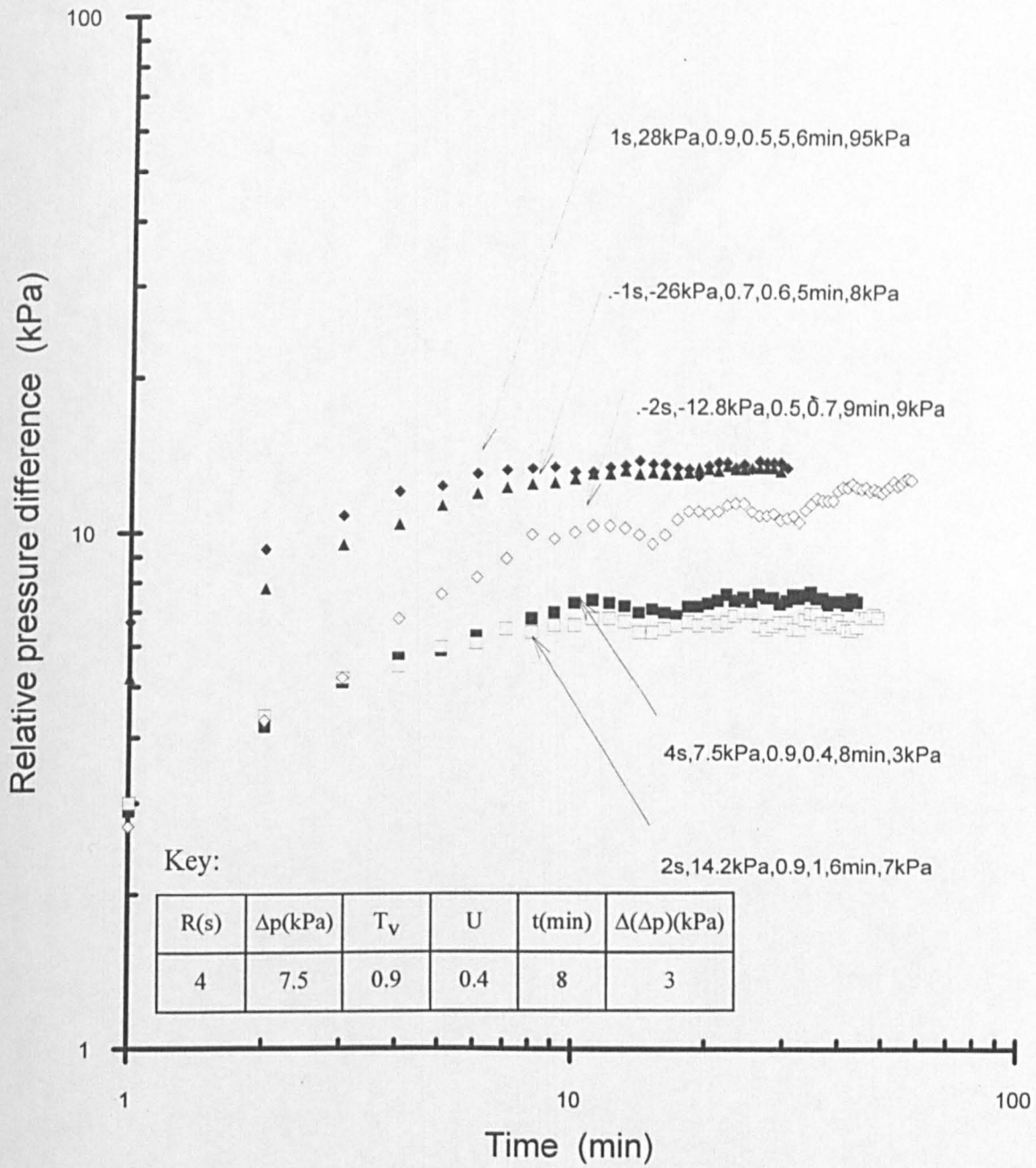

Fig.-5.48 Pressure difference vs time graph for sample in test series 2T240V (σ'_V = 100kPa)

BRITISH LIBRARY

IMAGING SERVICES NORTH

Boston Spa, Wetherby
West Yorkshire, LS23 7BQ
www.bl.uk

VOLUME CONTAINS CLEAR OVERLAY

OVERLAY HAVE BEEN SCANNED SEPERATELY AND THEN AGAIN OVER THE RELEVANT PAGE

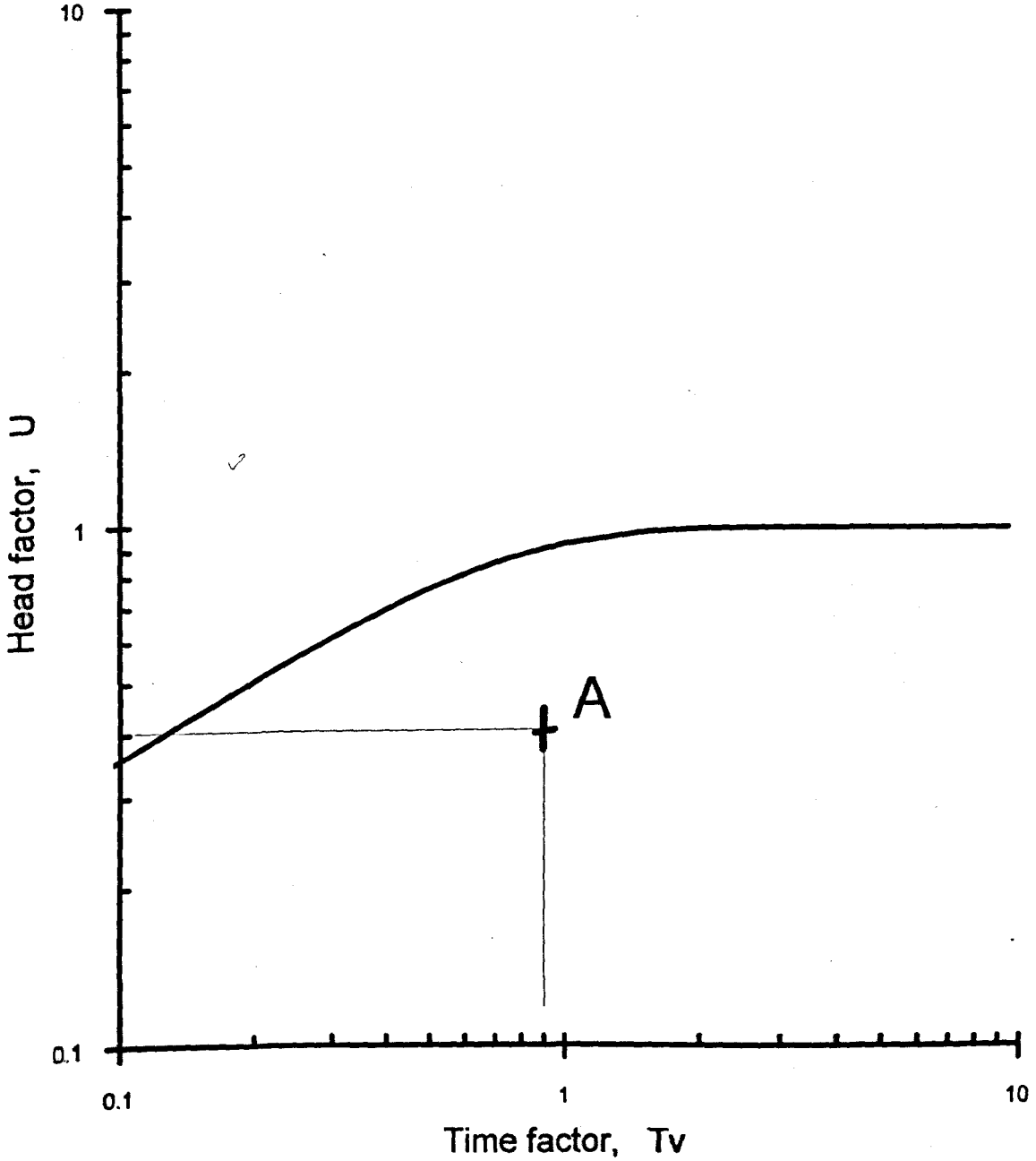
10
1
0.1
Head factor, U
A
0.1
1
10
Time factor, Tv

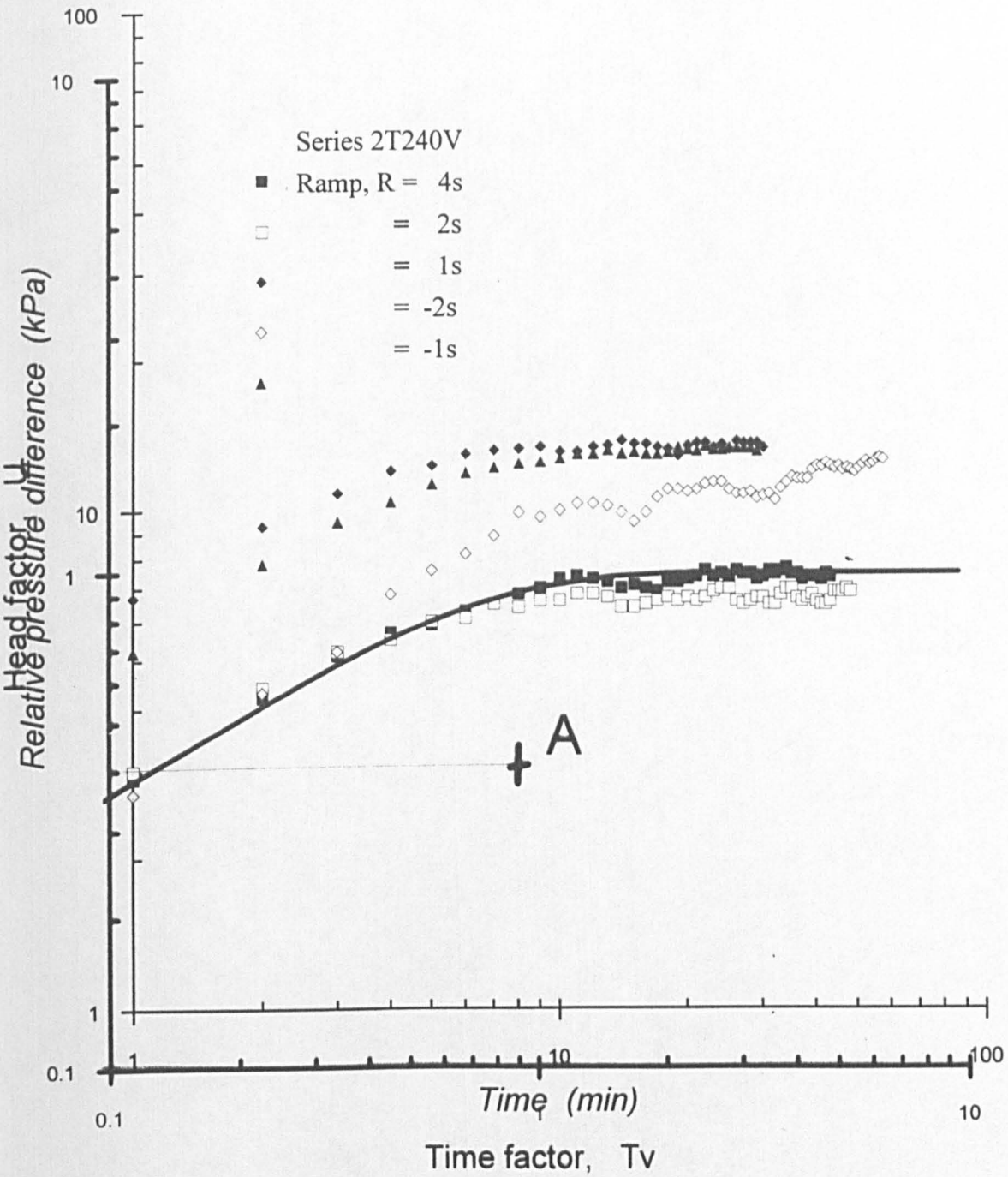

Fig.-5.49 Curve matching of experimental data to theoretical type curve for sample in test series 2T240V (σ'_V = 100kPa) at match point A

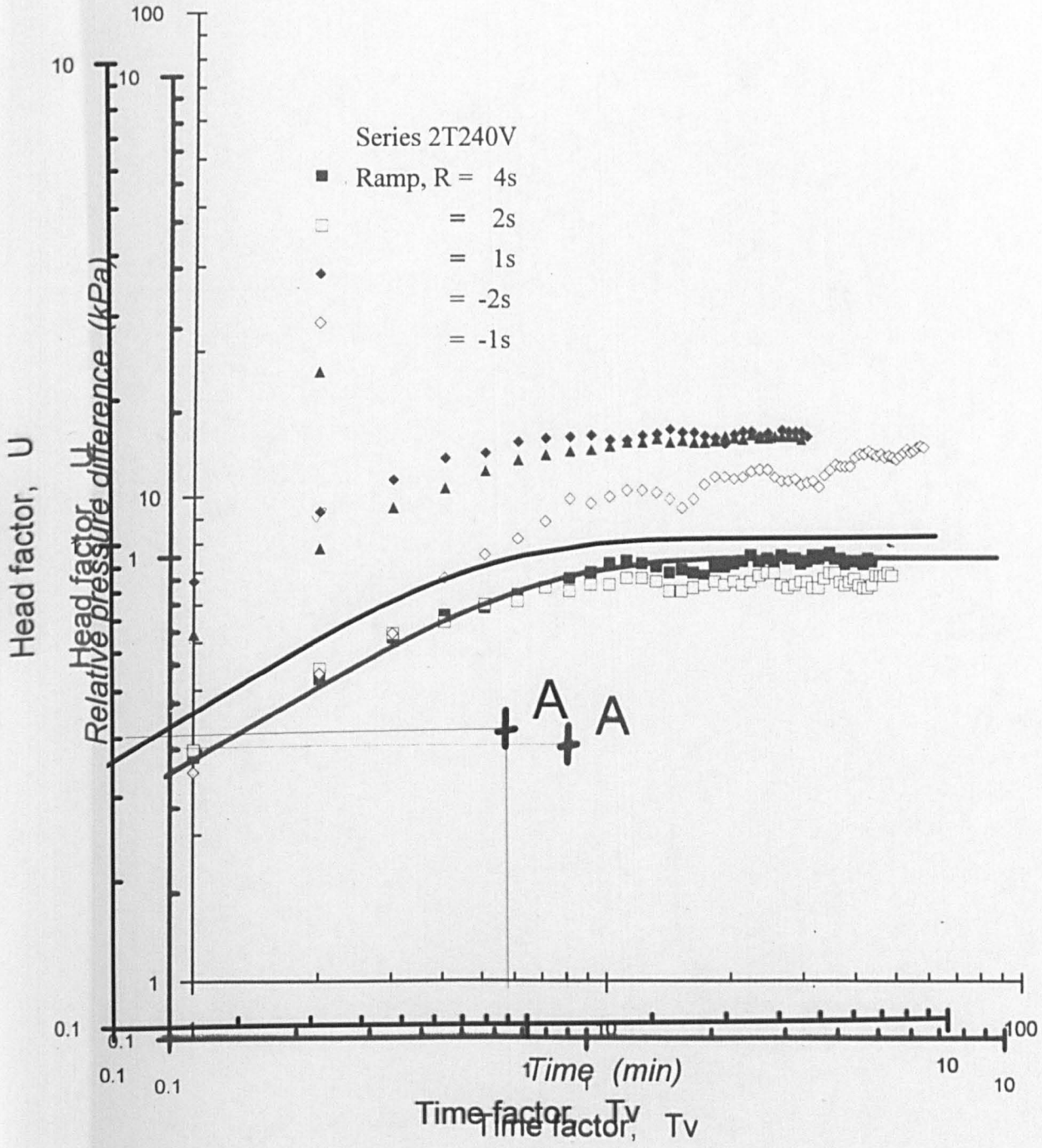

Fig.-5.49 Curve matching of experimental data to theoretical type curve for sample in test series 2T240V (σ'_v = 100kPa) at match point A

Also from $U = kHA / (QH_S)$ and with the relations $Q = 1/(2R)$ and $H = \Delta p / \gamma_W$,

$$k_V = \frac{H_S U \gamma_w}{4 \Delta p A R}$$

$$= \left[\frac{98070}{4}\right] \frac{H_S U}{\Delta p A R} 10^{-10} \quad \text{m/s} \qquad (5.41)$$

where Δp is in unit of kPa and A in mm^2 (ie. $A = 4560mm^2$). U is a dimensionless factor and R is the ramp in second.

The above values of T_V, t, U, Δp, $H_S = 33.34mm$ and ramp $R = 4s$ give a c_V value of $16.44m^2/yr$ and the permeability $k_V = 5.97 \times 10^{-10} m/s$.

Several of the pressure response curves are evaluated by the above curve matching procedure and the results are summarized in *Table*-5.5. Permeability values are shown in cols. [12] and [11] of *Table*-5.5 for the transient and steady state phases of the constant flow rate test, respectively. Average values are shown for the transient phase case. In retrospect, the steady state k_V are also average values taken out from data of the different flow rates imposed in the testing as inferred from the value of the slope S (see for example *Fig.*-5.9). Some differences exist between the two k_V values calculated from the transient phase and the steady phase of the test. Such differences are to be expected considering the various assumptions inherent in each method of permeability evaluation. Permeability values evaluated from the transient phase data involve the diffusion of pressure difference across the drainage boundaries in accordance with the Terzaghi consolidation equation whereas the k_V values evaluated from the steady phase condition utilise a direct calculation using Darcy's law. However, the transient phase data are also relevant for permeability evaluation since the sample is not deforming which is the same preferred condition that is experienced in the normal, steady phase regime of the permeability testing. In contrast, the consolidation process involves a complete deformation with time which makes the back calculated permeability values as the real indirect interpretation of the property.

In most cases permeability between the two phases are within 50% of the steady state permeability values with the transient phase k_V values being consistently lower than the steady state values, but it is not unusual to see permeability values of a clay sample differ by as much as an order of magnitude difference in replicate tests.

Comparisons between the experimental data and theoretical relationship of the head factor and time factor for the test series 2T240V at σ'_V=100, 180 and 480kPa are shown in *Figs.*-5.50(a), 5.50(b) and 5.50(c), respectively. Both experimental data from upward and downward flows are considered as denoted by the sign of the ramp

Table 5.5 - Summary of curve matching results from some data of the vertical test series

Test series	Scale reading from match curve: Cols. [2] to [5]				Sample ht.	Ramp	From transient data		Consolidation	From steady data	Average of transient data		Consolidation	Average[8]
	t(min)	Tv	Delta P(kPa)	U	Hs(mm)	R(s)	cv(m2/yr)	kv(m/s)	mv(m2/MN)	kv(m/s)	kv(m/s) from [9]	(kts-kss)/kss	cv(m2/yr)	cv(m2/yr)
[1]	[2]	[3]	[4]	[5]	[6]	[7]	[8]	[9]	[10]	[11]	[12]	[13]	[14]	[15]
see Eq.5.40	0.13149													
see Eq.5.41	5.3762E-10													
2T120V-180kPa														
4TV10	40	3	5	0.4	30.48	2	9.16	6.55E-10	0.38	1.28E-09	9.42E-10	-26.39%	16.75	11.91
4TV10B	50	6	4	0.3	30.48	1	14.66	1.23E-09						
2T240V-100kPa														
4ATV6*	8	0.9	3	0.4	33.34	4	*19.38*	5.97E-10	0.16	1.33E-09	1.04E-09	-21.67%	19.38	18.45
4ATV6	8	0.9	3	0.4	33.34	4	16.44	5.97E-10						
4ATV6A	6	0.9	7	1	33.34	2	21.92	1.28E-09						
4ATV6B	5	0.9	6.95	0.5	33.34	1	26.31	1.29E-09						
4ATV6C	9	0.5	9	0.7	33.34	-2	8.12	6.97E-10						
4ATV6D	5	0.7	8	0.6	33.34	-1	20.46	1.34E-09						
2T240V-180kPa														
4ATV10*	5	0.9	8	0.6	32.71	2	*14.04*	6.59E-10	0.24	1.27E-09	8.65E-10	-31.92%	14.04	14.95
4ATV10	8	0.9	6	0.4	32.71	2	15.83	5.86E-10						
4ATV10A	5	1	6.9	0.4	32.71	1	28.14	1.02E-09						
4ATV10B	10	0.9	7	0.6	32.71	-2	12.66	7.54E-10						
4ATV10C	10	1	8	0.5	32.71	-1	14.07	1.10E-09						
2T240V-240kPa														
4ATV13	10	0.9	10	0.6	32.27	2	12.33	5.21E-10	0.22	1.13E-09	7.16E-10	-36.66%	11.2	17.12
4ATV13A	5	0.9	10	0.6	32.27	1	24.65	1.04E-09						
4ATV13B	10	1	6	0.5	32.27	-2	13.70	7.23E-10						
4ATV13C	5	0.8	30	1	32.27	-1	21.91	5.78E-10						
2T240V-480kPa														
4ATV25	6	1	9.35	0.9	30.62	4	20.55	3.96E-10	0.18	8.25E-10	5.97E-10	-27.58%	12.45	18.91
4ATV25A	8	0.6	10	0.9	30.62	2	9.25	7.41E-10						
4ATV25B	10	0.8	7	1	30.62	-4	9.86	5.88E-10						
4ATV25D	10	1	8.5	0.4	30.62	2	12.33	3.87E-10						
4ATV25E	6	0.8	9	0.4	30.62	1	16.44	7.32E-10						
	5	0.7	20	0.9	30.62	1	17.26	7.41E-10						
2C240V-240kPa														
4ACV13	9	0.5	20	1	33.61	2	8.25	4.52E-10	0.26	9.01E-10	4.52E-10	-49.86%	10.67	8.25
4ACV13A	9	0.5	20	1	33.61	-2	8.25	4.52E-10						
2C240V-480kPa														
4ACV25	5	0.4	8	0.7	32.16	4	10.88	3.78E-10	0.17	6.76E-10	3.48E-10	-48.53%	10.87	9.52
4ACV25A	10	1	10	0.4	32.16	2	13.60	3.46E-10						
4ACV25B	6	0.5	10	0.8	32.16	-4	11.33	3.46E-10						
4ACV25C	6	1	8	0.3	32.16	-2	22.67	3.24E-10						
4ACV25D	10	0.6	10	0.4	32.16	2	8.16	3.46E-10						

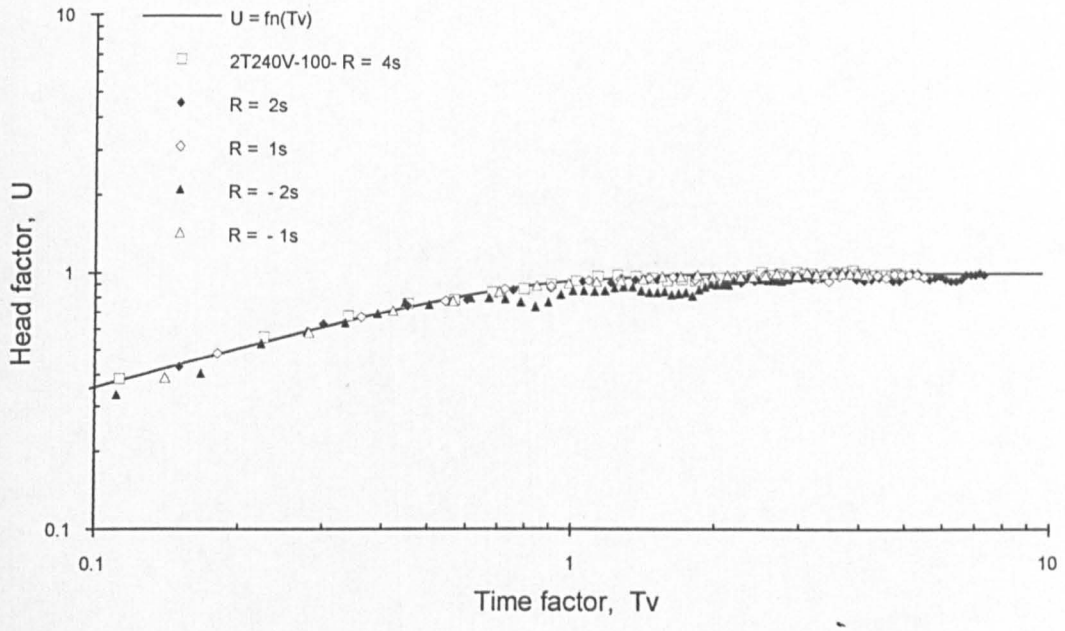

(a)

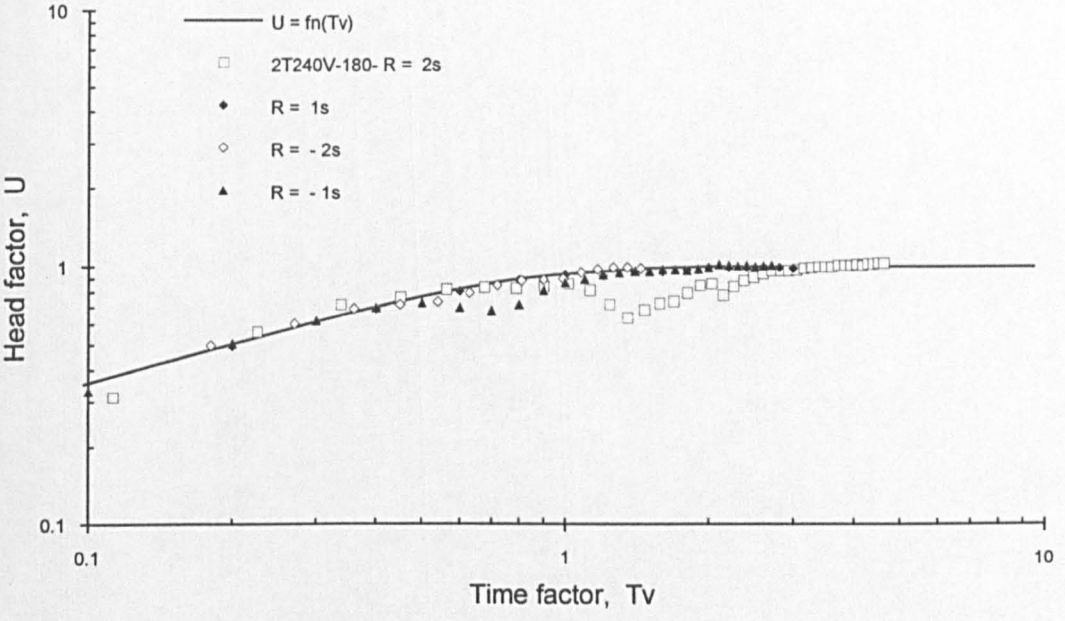

(b)

Fig.-5.50 Comparison between experimental data and theoretical relation of head factor, U and time factor, T_V for Series 2T240V at: (a) σ'_V=100kPa; (b) σ'_V=180kPa;

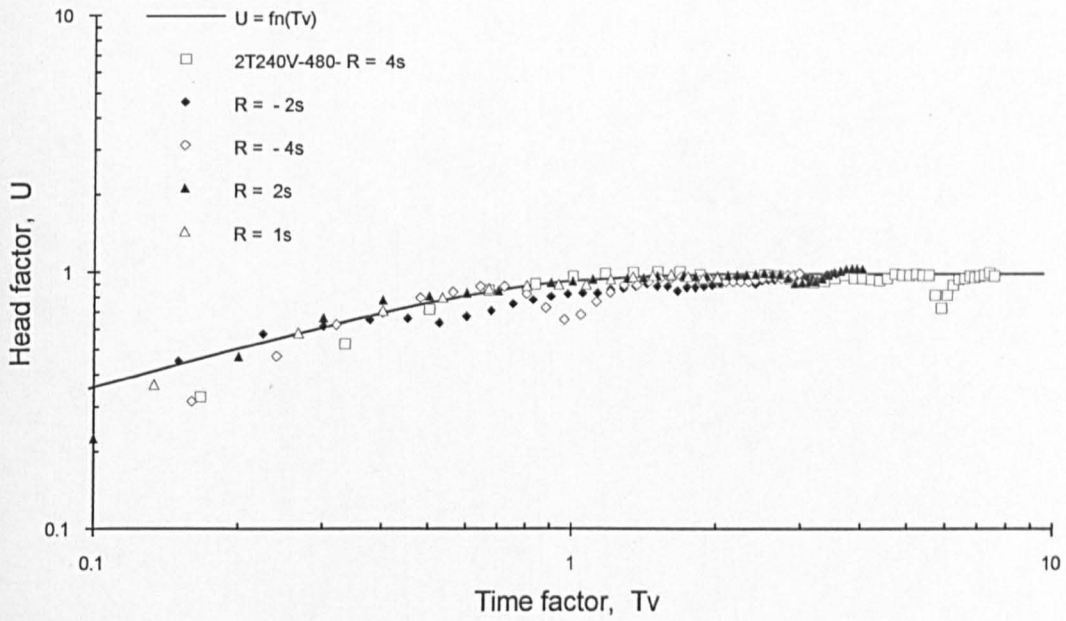

(c)

Fig.-5.50 *cont.* (c) σ'_V=480kPa

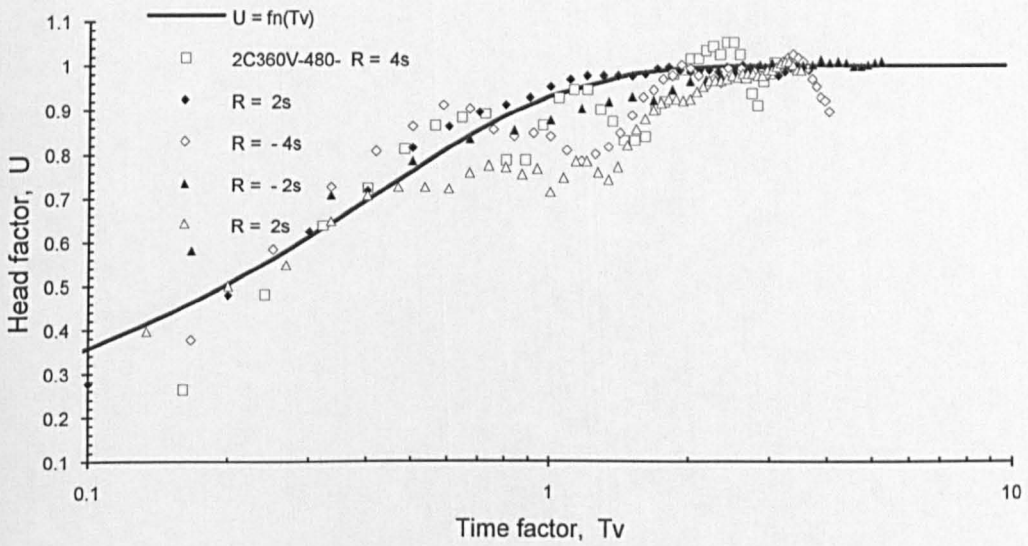

Fig.-5.51 Experimental data and theoretical U vs T_V for Series 2C360V at σ'_V = 480kPa

in the figures.

Similar experimental data and theoretical relationship of the head factor and time factor for Series 2C360V at consolidation stage of σ'_V = 480kPa are shown in the more classic type of plot in *Fig.*-5.51. Results shown in *Figs.*-5.50 and 5.51 indicate the relevance of the Terzaghi's consolidation equation with the appropriate boundary conditions in describing the development of induced pressure difference in the constant flow rate permeability tests. These plots developed from results of the curve matching technique indicate the potential use of this semi graphical approach as a reliable method of interpreting the constant flow rate data. As shown in the figures, experimental data that do not coincide with the theoretical line are more associated with the scatter in experimental results rather than failure of the theory or the curve matching technique. These 'deviated' experimental points are easily identified from parts of test Series 2T240V at the various consolidation pressures, σ'_V and flow rates, R as follows: at σ'_V=100kPa, R=-2s in *Fig.*-5.50(a); at σ'_V=180kPa, R=2s and R=-1s in *Fig.*-5.50(b); and at σ'_V=480kPa at flow rates R=4s, R=2s, and R=-4s in *Fig.*-5.50(c). These observations are consistent with results displayed earlier in *Figs.*-5.6(a) and 5.6(c) ie. at times approximately = 16min, and 13, 36min, respectively, in those figures.

Vertical permeability values evaluated by the two methods, ie. steady state k_V and transient state k_V in the CFR test, and from the consolidation tests, $k_{VC_{VT}}$ are summarized in *Figs.*-5.52. Permeability given by the steady state k_V values are considered reference values because these are the most common method of evaluation which uses Darcy's law directly. As shown in *Figs.*-5.52, permeabilities obtained from the transient records are generally within a factor of 2 of the steady state values whereas the consolidation results give values in variation by 1 or 2 orders of magnitude. Besides the simplifying assumptions in the conventional consolidation theory being surmounted by the experimental constraints, an important aspect of the testing procedure could well contribute to the large variation in the permeability results. Permeability according to the consolidation theory is considered a constant value for a range of pressure increment during the test. Thus although the primary phase of the consolidation took only a few minutes (ie. generally less than 10minutes), the range of void ratio during that pressure increment is considered too large to warrant a constant k. Contrary to the consolidation test, the permeability phase of the testing does not at all involve the sample deformation such that the transient or the steady records of testing are occurring at a pressure increment that has brought about stabilised conditions ie. as near as possible at a constant void ratio. Effects of these nature could be seen when the (Δh-$\sqrt{t}$) or (Δh-lg.t) experimental curves do not conform to their expected theoretically fitted type curves especially at the very early

and later stages of consolidation. The large variation in permeability values occur mainly at later stages of consolidation when the void ratio gets smaller at larger values of σ'_v. Poorly defined (Δh-$\sqrt{t}$) experimental curves were obtained where the majority of the compression is controlled by secondary compression. The primary consolidation was mainly completed in less than a minute.

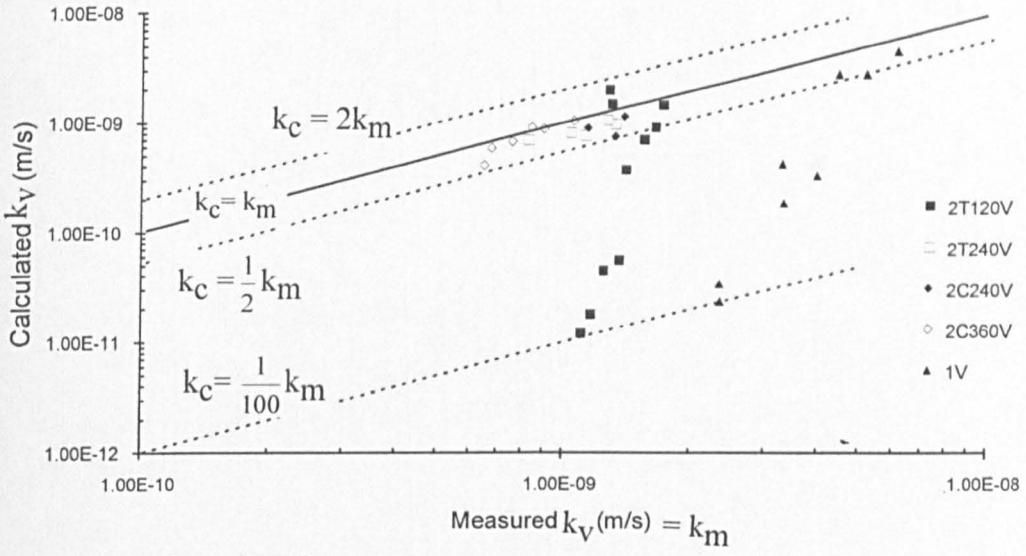

(a)

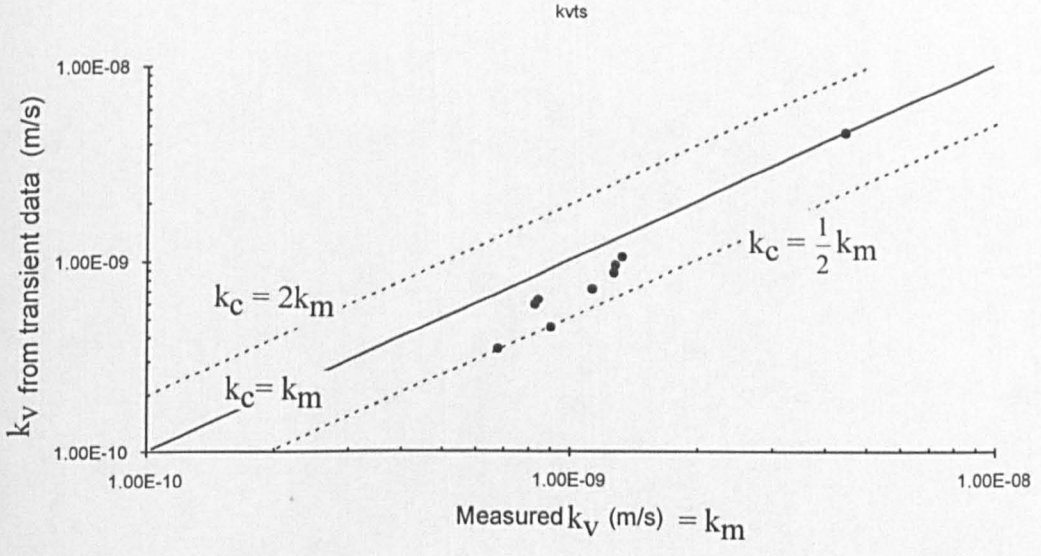

(b)

Fig.-5.52 Comparison of vertical permeability: (a) From consolidation test data; (b) From transient data of CFR permeability test

5.7.1.2 Radial flow

Consideration of Section 4.2.4.1 for the radial constant flow rate permeability test indicates the close similarity of the radial flow in Rowe cell and the well pumping analyses for a confined aquifer when subjected to certain important assumptions. The measurement of interest in the radial CFR permeability test is the development of induced pressure difference, Δp with time at the central drain while in the pumping test analyses, we are concerned with the drawdown, s with time at the well or other specified point from the well.

Following the notation of *Fig.*-4.4(a) the linear-logarithmic relation between drawdown, s and time, t is shown as plots of Δp against t in *Figs.*-5.53(a), 5.53(b) and 5.53(c) for records of the CFR test Series 2T240H at consolidation stages of σ'_v=180, 240 and 480kPa, respectively. The linearity of the (Δp vs lg.t) relations at very early times is observed to occur between 0.2 to about 4mins. This confirms the applicability of the Cooper-Jacob drawdown equation, Eq.-(4.13) where the combination of t and r is sufficiently small to give good approximation to the Theis nonequilibrium equation. From these linear portions of the plots, the necessary properties of the sample are evaluated from the following parameters:

The transmissivity T and storage coefficient or storativity S_S given by

$$T = 2.3\gamma_w Q/(4\pi m) \tag{5.40}$$

$$S_S = 2.25TC/r^2 \tag{5.41}$$

where m = 1/lg.D, is the slope of the experimental (Δp vs lg.t) plot and C = 10^{t_o} where t_o is the intercept on the time axis of the plot. The unit weight of water γ_w appear in Eq.-(5.40) because Δp is a pressure head while the drawdown s is originally defined in terms of head of water. As with the case of permeability-void ratio laws, the relation between Δp and t is one of linear-lg type given by

$$t = C.D^{\Delta p/\gamma_w} \tag{5.42}$$

Permeability k_h and the coefficient of consolidation c_v are now easily calculated from the relations

$$k_h = T/H_S \tag{5.43}$$

$$c_v = k_h/S_S \tag{5.44}$$

where H_S is height of the sample. Consistent with groundwater flows, transmissivity of the sample is the product of permeability and the sample thickness.

Appropriate with the units used in this study where Δp is in kPa, t is in min, then the units for Q and γ_w in Eq.-(5.40) must be in m^3/min and kN/m^3, respectively, so

that the unit for T is m/min-m. The unit for H_S in Eq.-(5.43) must therefore be in m giving the unit for permeability k_h as m/min. Similarly, the unit for radius of the central drain must be in m. With this convention of units, Eqs.-(5.40) to (5.44) without confusing factors attached to them, are easily applied using values of C and D giving k_h and c_v in m/min and m^2/min, respectively.

Values of the transmissivity T and storativity S_S of the sample are evaluated from the transient records of the CFR tests from the experimental parameters D and C, respectively [see Eqs.-(5.40) and (5.41)]. From Eq.-(4.40) in Section 4.4.4, the coefficient of volume compressibility m_{vh} is given by,

$$m_{vh} = k_h/(c_r \gamma_w)$$

$$= S_S/(\gamma_w) \qquad (5.45)$$

Subsequent values of k_h and c_v follow from Eqs.-(5.43) and (5.44), respectively with the results summarized in *Table*-5.6. Permeability values are shown in cols. [13] and [12] of *Table*-5.6 for the transient and steady state phases of the constant flow rate test, respectively. Average values are shown for the transient phase case. Values of k_h and c_v are finally converted to m/s and m^2/yr as appropriate. Values of m_{vh} determined from Eq.-(5.45) are also shown in the table.

Results exhibited by *Figs.*-5.53(a), 5.53(b) and 5.53(c) for records of the CFR test Series 2T240H at consolidation stages of σ'_v=180, 240 and 480kPa, respectively, are typical of other test series in the radial CFR permeability tests. Two portions of the plot are apparent - the linear initial records which represent the transient phase and the records that stabilised to a constant value once the steady state condition predominates in the flow. This kind of Δp vs lg.t plot in which the data markedly depart from an inclined linearity to the horizontal clearly demarcate the steady phase from the transient phase. Fluctuations of the records in the stabilised period also occurred which may be attributed with the experimental problems rather than the sample behaviour.

Results shown in *Figs.*-5.53(a), 5.53(b) and 5.53(c) are cast back into the actual pressure response record as shown in Figs.-5.54(a), 5.54(b) and 5.54(c). The departure of the experimental data from the non-equilibrium line indicates the finite nature of the transient period from starting the test up to about 10min duration.

The heat flow analogy is known to be equally valid for both a sink and source as also is the well flow analyses for pumping and recharge. The results shown in *Figs.*-5.53 in which the plots take the same form irrespective of whether the flow is forward or reverse and that both boundaries are subject to infusion/withdrawal or

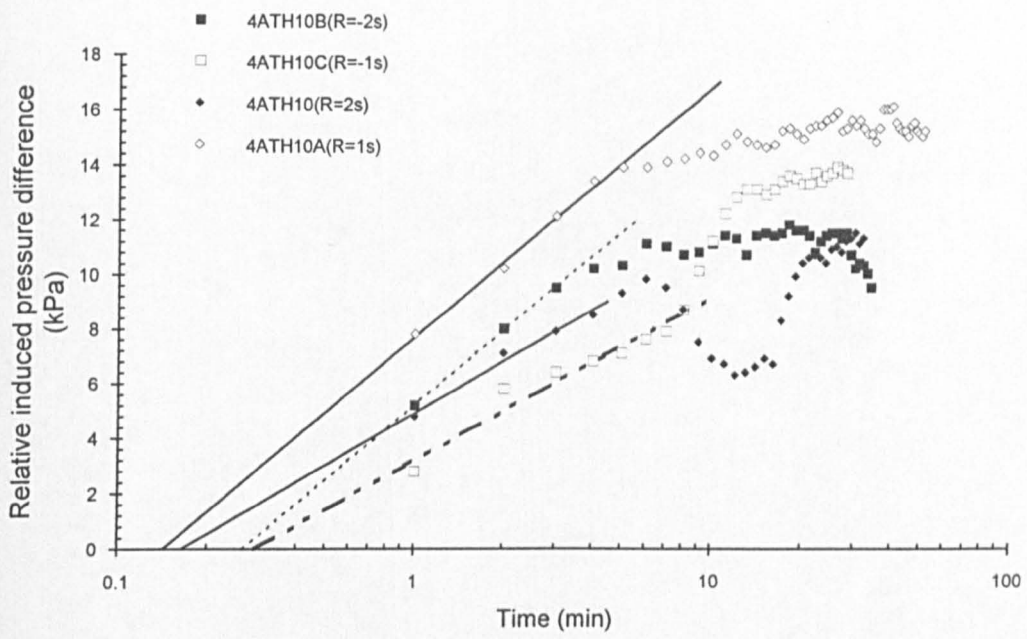

(a)

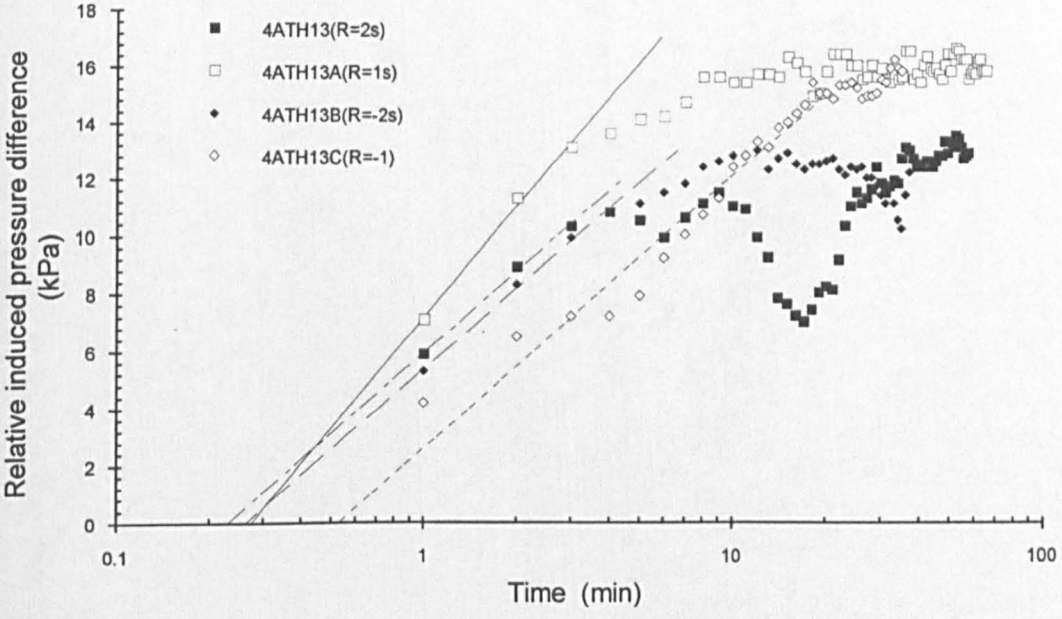

(b)

Fig.-5.53 Relative induced pressure difference, Δp against time for records of the radial CFR permeability test for Series 2T240H at:
(a) $\sigma'_V = 180kPa$; (b) $\sigma'_V = 240kPa$

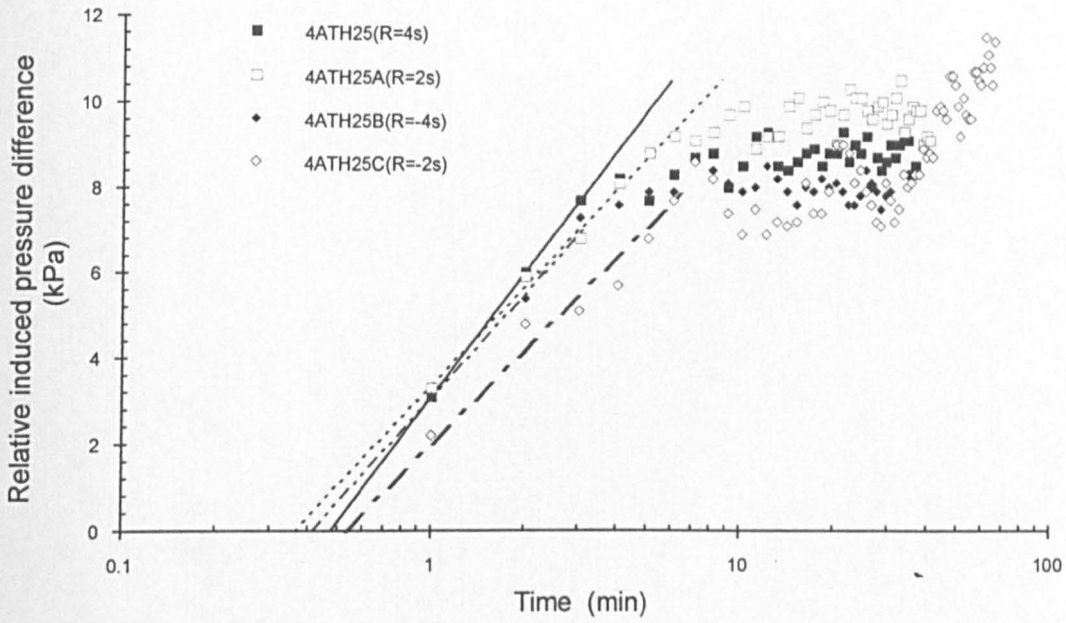

(c)

Fig.-5.53 *cont.* (c) $\sigma'_V = 480\text{kPa}$

Table 5.6 - Summary of Cooper Jacob method applied to some data from radial test series

Test series	C	D	Ck	T (m2/min)	S	Sample ht. Hs(mm)	Ramp R(s)	From ransient data cv(m2/yr)	kh(m/s)	Consolidation mv(m2/MN)	From steady data kh(m/s)	Average of transientdata kh(m/s) from [10]	(kts-kss)/kss	Consolidation cv(m2/yr)
[1]	[2]	[3]	[4]	[5]	[6]	[7]	[8]	[9]	[10]	[11]	[12]	[13]	[14]	[15]
4*pi/gamma=	1.28													
r2=(m2)	3.25E-05													
2T240H-40kPa														
4ATH3	0.21	1.47	5.97	4.51E-09	6.64E-05	32.69	2	18.19	2.30E-09	0.78	2.49E-09	3.14E-09	25.94%	7.63
4ATH3A	0.11	1.49	5.81	9.27E-09	6.79E-05	32.69	1	36.60	4.73E-09					
4ATH3B	0.19	1.49	5.76	4.67E-09	6.18E-05	32.69	-2	20.28	2.38E-09					
4ATH3C	1.05	1.30	8.75	6.15E-09	4.46E-04	32.69	-1	3.70	3.14E-09					
2T240H-80kPa														
4ATH5A	0.17	1.35	7.65	7.04E-09	8.11E-05	32.12	1	23.67	3.65E-09	0.44	2.26E-09	2.97E-09	31.60%	10.58
4ATH5B	0.19	1.46	6.08	4.43E-09	5.89E-05	32.12	-2	20.50	2.30E-09					
2T240H-180kPa														
4ATH10	0.17	1.44	6.28	4.29E-09	4.90E-05	31.02	2	24.72	2.30E-09	0.34	1.90E-09	2.99E-09	57.12%	16.94
4ATH10A	0.14	1.29	9.10	5.91E-09	5.85E-05	31.02	1	28.57	3.18E-09					
4ATH10B	0.26	1.29	9.05	2.98E-09	5.46E-05	31.02	-2	15.40	1.60E-09					
4ATH10C	0.29	1.47	5.95	9.04E-09	1.82E-04	31.02	-1	14.03	4.86E-09					
2T240H-240kPa														
4ATH13	1.47	1.18	14.09	1.91E-09	1.94E-04	32.69	2	2.64	9.74E-10	0.28	1.74E-09	1.87E-09	7.60%	20.09
4ATH13A	0.27	1.20	12.80	4.21E-09	8.01E-05	32.69	1	14.09	2.14E-09					
4ATH13B	0.26	1.28	9.27	2.91E-09	5.29E-05	32.69	-2	14.73	1.48E-09					
4ATH13C	0.53	1.27	9.50	5.67E-09	2.09E-04	32.69	-1	7.27	2.89E-09					
2T240H-360kPa														
4ATH19	0.38	1.42	6.55	2.06E-09	5.47E-05	29.56	4	11.14	1.16E-09	2.60E-01	1.57E-09	1.47E-09	-6.54%	13.95
4ATH19A	2.71	1.22	11.72	2.30E-09	4.31E-04	29.56	2	1.58	1.30E-09					
4ATH19B	0.15	1.60	4.91	2.74E-09	2.86E-05	29.56	-4	28.38	1.54E-09					
4ATH19C	2.15	1.33	8.12	3.32E-09	4.94E-04	29.56	-2	1.99	1.87E-09					
2T240H-480kPa														
4ATH25	0.48	1.27	9.64	1.40E-09	4.61E-05	28.87	4	9.19	8.06E-10	0.2	1.37E-09	1.48E-09	8.25%	17.66
4ATH25A	0.36	1.35	7.67	3.51E-09	8.86E-05	28.87	2	12.03	2.03E-09					
4ATH25B	0.41	1.33	8.03	1.68E-09	4.80E-05	28.87	-4	10.60	9.68E-10					
4ATH25C	0.53	1.37	7.29	3.69E-09	1.37E-04	28.87	-2	8.21	2.13E-09					
2C360H-60kPa														
4ACH4	0.27	1.35	7.64	3.52E-09	6.51E-05	29.59	2	16.03	1.99E-09	0.66	1.82E-09	2.40E-09	31.76%	4.70
4ACH4A	0.27	1.26	9.99	5.39E-09	1.02E-04	29.59	1	15.70	3.03E-09					
4ACH44B	0.34	1.31	8.50	3.17E-09	7.43E-05	29.59	-2	12.63	1.78E-09					
4ACH4C	1.37	1.24	10.88	4.95E-09	4.69E-04	29.59	-1	3.12	2.79E-09					

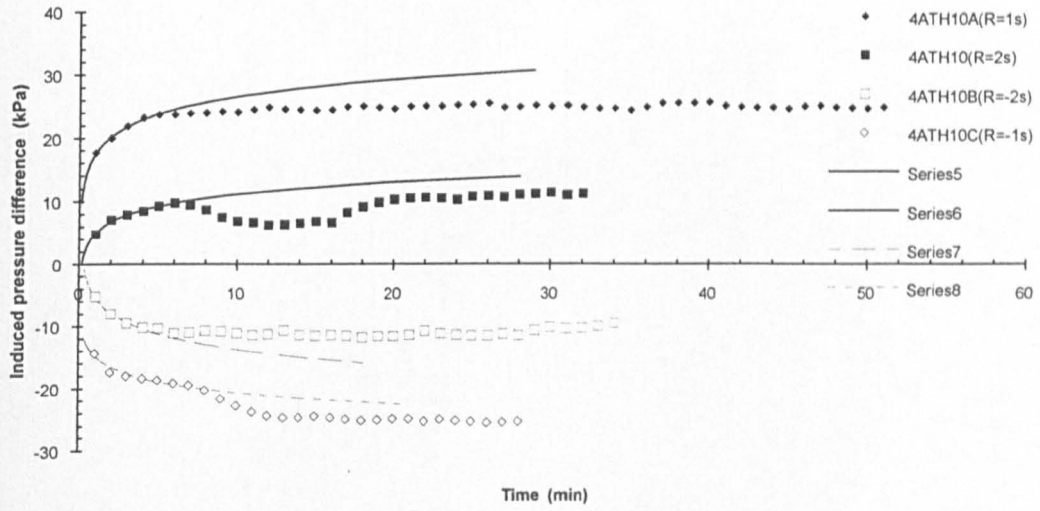

(a)

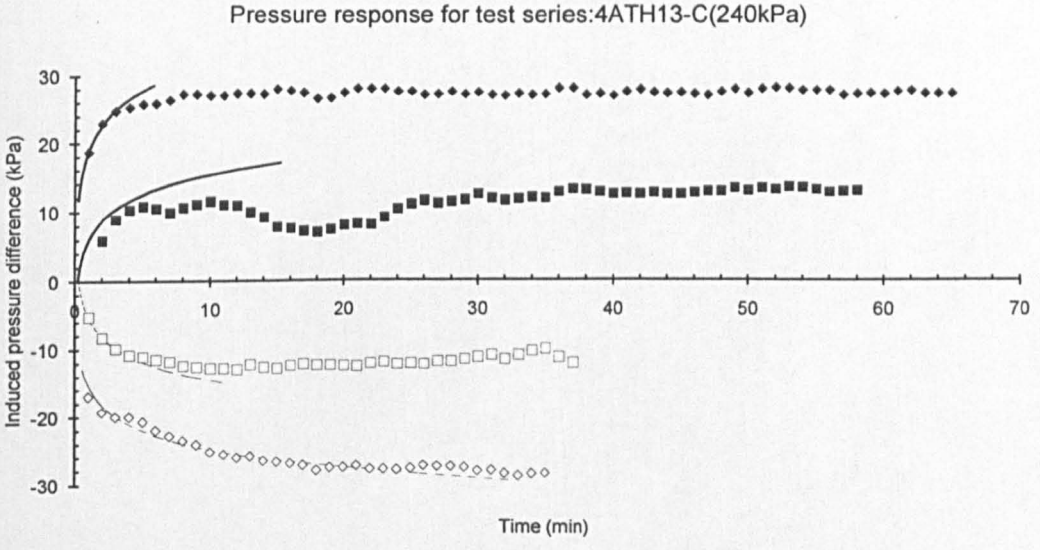

(b)

Fig.-5.54 Theoretical pressure response compared with data from results of *Figs.*-5.8 for Series 2T240H at: (a) σ_V'=180kPa; (b) σ_V'=240kPa;

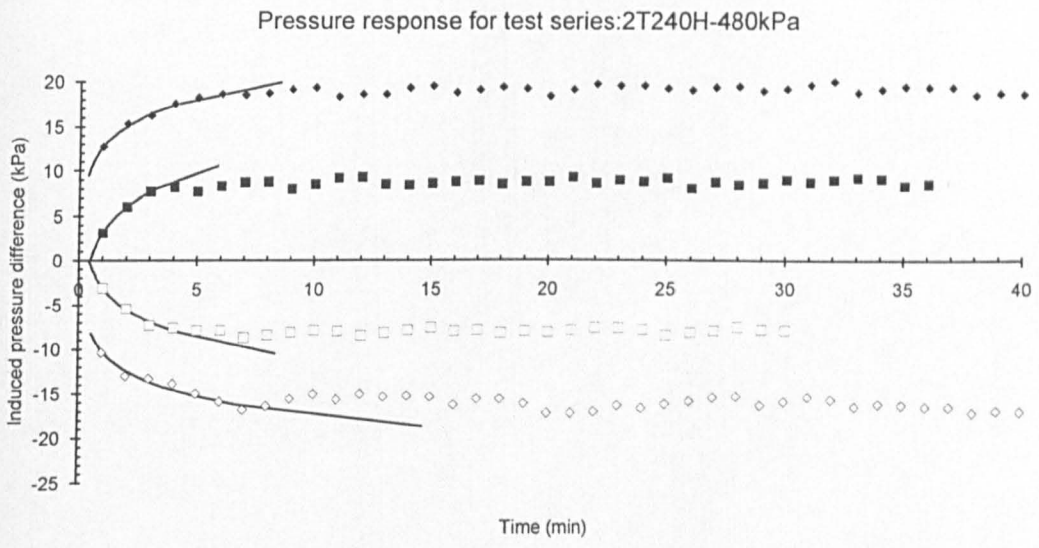

(c)

Fig.-5.54 *cont.* (c) $\sigma_V' = 480$kPa

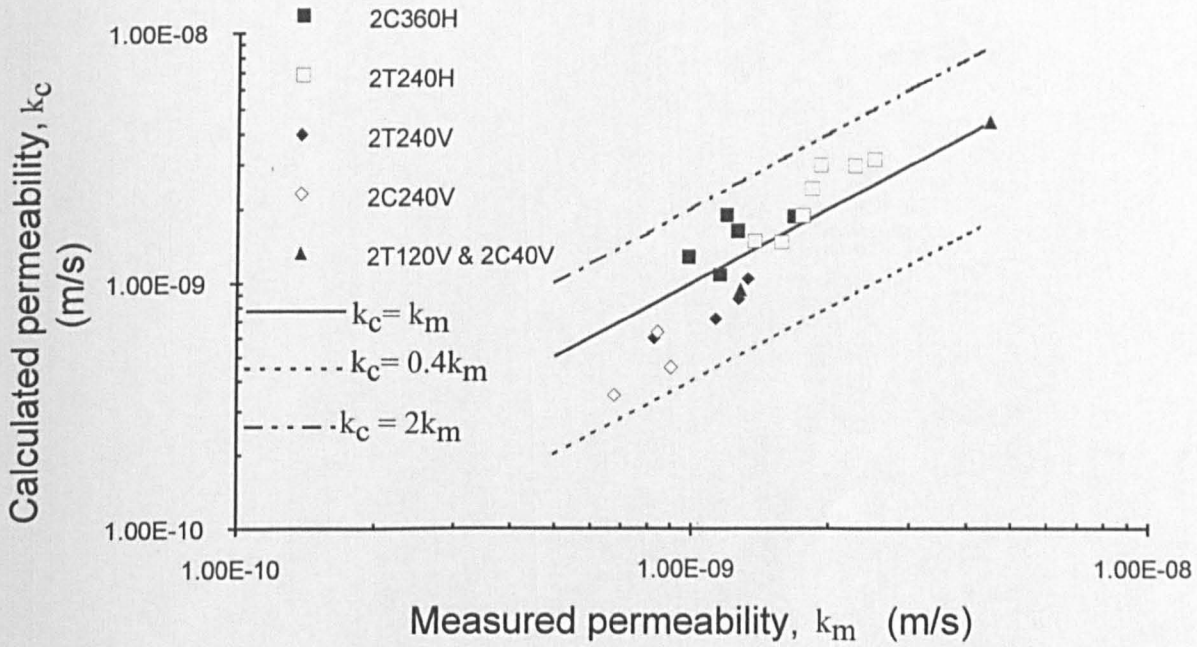

Fig.-5.55 Calculated (k_c) vs Measured (k_m) permeability: Comparison of results from transient data to steady state data of the CFR permeability test

vice-versa, confirm the suitability of the above analogy for data of CFR permeability test in the radial flow Rowe cell. This is further confirmed by the plots in *Figs.*-5.54 where the experimental data and theoretical lines having equal magnitude of flow rates tend to be symmetrical about the time axis.

Horizontal permeability values evaluated by the two methods, ie. steady state k_h and transient state k_h in the CFR test are summarized in *Fig.*-5.55. The solid and open square data points are for the horizontal Series 2C360H and 2T240H. The solid and open rhombus data points and the solid triangles are for vertical series. The figure shows that permeabilities obtained from the transient records are generally within a factor ranging from 2 to 0.4 of the steady state values whereas the consolidation results [as shown in Figs.-5.45, 5.46 or 5.52(a)] may give values of deduced permeability in variation by up to 2 orders of magnitude of the measured value.

CHAPTER 6

6. CONCLUSION

This Chapter presents the conclusions that have been obtained in this study. The conclusions presented in Sections 6.1, 6.2 and 6.3 are more specific and definite while the conclusions presented in Section 6.4 are rather general because of the preliminary and exploratory nature of the results that have been obtained. Nevertheless the programme of experimental testing that has been described in this thesis should open up opportunities in research concerning the development of permeability anisotropy resulting from shear deformation of soft clays.

The samples of the supreme kaolin tested consists of three Series: Series 1- Slurry, Series 2- 1-D consolidated block samples, and Series 3- 1-D consolidated block samples followed by CIU isotropic recompression and undrained shear.

The conclusions drawn from the permeability measurements made with both the one-dimensionally compressed block samples and the CIU samples might be divided into two parts: (1)-The initial measurements conducted at the beginning of the permeability tests; and (2)-The subsequent permeability measurements made after further one-dimensional compression. The first simply shows the immediate effect of the particular history on the values of permeability and anisotropy; the second shows the effect of the history on subsequent *changes* in permeability and anisotropy.

As a matter of record, it seems that measurements of vertical and horizontal permeability of clays from samples that have experienced CIU undrained shearing have not been previously attempted. Thus little is known about the development of permeability anisotropy for clay samples that have experienced shear deformation. This is in contrast with information on fabric anisotropy data for soils with a range of stress histories which are available from optical or electron microscopic studies which have been accumulated for two or three decades.

6.1 Laboratory permeability testing methods

Based on the observed test data on supreme kaolin, the constant head and constant flow rate permeability tests gave practically equal permeability values for the range of consolidation pressures considered. Permeability decreased by about two orders of magnitude from 1.00×10^{-9} m/s to 1.00×10^{-11} m/s when the slurry specimen was compressed to a vertical strain of 42%, corresponding to a range of consolidation pressures from 60kPa to 580kPa. Shorter testing times of 0.5 to 2 h were possible when the permeability value was on the higher side, however, the time required for

attainment of steady state conditions increased considerably to more than 24 h when permeability reached 1.00 x 10^{-10} m/s or lower. In both cases the pressure difference was kept within a narrow range of less than 15% of the current consolidation pressure in order to reduce the effects of effective stress changes within the sample. It appeared that the response time could, however, be shortened for the low permeability clays to 2 to 8 h by increasing the pressure difference or the flow rate. Sample volume changes which could have been detected in the form of vertical compression of the sample were negligible for the magnitudes of pressure difference adopted in the tests. It is found that the requirement of $\Delta u < 10\%$ of σ'_v could be restrictive at the low consolidation pressures of up to 150kPa. Above this value, Δu may be raised up to $0.3\sigma'_v$ and still not produce significant sample volume changes since the sample is rather stiff. With sample volume changes negligible, the changes in permeability that could accompany changes in effective stress will also be negligible and interpretation of the observations in terms of a uniform sample permeability will still be acceptable.

A back pressure of 50kPa was used to ensure that even when the largest pressure differences were used positive water pressures would be maintained within the apparatus. Positive pressure is desirable to minimise any possibility of reverse leakage of air into the system. A pressure of 25kPa was used in initial tests, resulting in negative pressures in the outflow part of the sample during the permeability stages.

The constant flow rate (CFR), permeability test is strongly recommended as part of any permeability testing in the soil mechanics laboratory. The transient and steady phases of the experimental data can be interpreted to provide information on the consolidation characteristics of the clay in addition to estimation of values of permeability. The CFR test can usually be completed in much shorter time than the constant head test because the attainment of steady state conditions can be detected from observation of current pressure difference, whereas flow rate is harder to measure accurately at any given instant. By plotting the pressure difference Δp against lg(time), the transient and steady phases of the test can be defined accurately.

The available constant flow rate permeability test data for radial flow, although limited, allow the relevant use of the Theis nonequilibrium equation in the determination of permeability and consolidation characteristics of clay samples from the transient stage of the flow process.

Although the Rowe cell hydraulic oedometer has advantages over conventional oedometers for the study of permeability characteristics of soils, because of the closed pore water system, the experimental study described here has shown that there are possible errors of interpretation that can arise from the water that is trapped around the bellows system that applies the load to the clay. These will lead to differences in

volume changes calculated from the water received in the flow pumps and from the change in sample height recorded with a dial gauge. There can similarly be uncertainties in the actual vertical effective stress experienced by the sample because of the slightly unknown area of contact between bellows and loading plate. Small zero errors, which may relate to the hydraulic resistance of the connecting pipework, have shown that it is important to measure pressure differences for a number of controlled flow rates through the sample in order to obtain satisfactory estimates of permeability. Single observations may not be reliable.

6.2 Forms of permeability-void ratio relationship

The present study on the permeability characteristics of supreme kaolin clay shows that the relationships for vertical permeability and horizontal permeability with void ratio obey the exponential form of variation given by:

$$k = C.D^e \qquad (6.1)$$

where C and D are empirical factors. The fitted Eq.-(6.1) is valid for both vertical and horizontal permeability values obtained for both normally consolidated and over-consolidated one-dimensionally compressed clay. Other conditions established in the research regarding the validity of permeability Eq.-(6.1) may be stated as follows:

(1) Uniqueness : Experimental data are adequately described by a single permeability equation.

(a) Series 1: One-dimensional compression from slurry in Rowe cells - H & V. The data fall consistently on single relationships between permeability and void ratio.

(b) Series 2: One-dimensional compression from slurry in consolidation tank, followed by sampling and placement in Rowe cell for continued testing. Reasonably consistent data have been obtained, but the average relationships between permeability and void ratio are somewhat different from those obtained from the Series 1 tests.

(c) Series 3: One-dimensional compression from slurry in consolidation tank, followed by sampling and placement in triaxial apparatus for recompression and undrained shearing. Reasonably consistent data have been obtained. Before shearing the data fall within the range set by Series 1 and Series 2 tests. After shearing, monotonic relationships between permeability and void ratio have been obtained, but in many of the tests the degree of anisotropy decreased with further one-dimensional compression (see section 6.4).

(2) Void ratio- From the various results obtained, such as those presented in *Figs.*-5.15 and 5.21 the void ratio e has been found to be the principal parameter responsible for controlling permeability of the clay. An increase or decrease in the value of e would simply raise or reduce the value of k in accordance with Eq.-(6.1)

for each sample: values of D are always greater than unity (D>1, log D >0). The actual values of permeability are, however, influenced by the history of the sample, and this controls the values of C and D in Eq.-(6.1).

6.3 Influence of anisotropic compression on permeability anisotropy

The programmes of experimental testing that have been conducted have attempted to determine permeability changes of consolidated kaolin clay samples after they have been subjected to anisotropic one-dimensional compression in a consolidation tank to vertical effective stresses of σ'_{vmax} = 40, 120, 240 and 360kPa. The clay was then unloaded and sampled and set up in the Rowe cells for measurement of permeability and measurement of development of permeability with further compression. These were the tests of Series 2. For convenience the samples will be described as 'soft' for $\sigma'_{v\,max} \leq 120$ kPa and 'stiff' for $\sigma'_{v\,max} > 120$ kPa.

Altogether a total of six samples (1 slurry, 2 softer and 3 stiffer) were tested. For the block samples, 5 pairs were trimmed and set up to determine their vertical and horizontal permeability. Developments of permeability with void ratio were obtained for each sample. Comparisons were made of the changes of vertical and horizontal permeability and development of permeability anisotropy with continued one-dimensional compression and decreasing void ratio.

All the samples that had experienced anisotropic compression indicated a certain degree of initial permeability anisotropy, r_{ko} at their initial void ratio e_o. Further anisotropic compression either further enhances or just stabilises the existing permeability anisotropy of the samples as the void ratio decreases further, depending on whether the samples were 'stiff' or 'soft'. There were some differences between the degrees of anisotropy of these block samples and of the samples which were compressed only from slurry in the Rowe cells. Some of the differences in vertical permeability must be attributed to experimental variability, but the differences in anisotropy are probably the result of the different drainage conditions that exist in the soil before it is sampled (only vertical drainage) by comparison with those in the Rowe cell, where the sample being used to measure horizontal permeability is subjected to vertical deformation with radial drainage.

The slurry sample by virtue of its initial stress free condition, shows no sign of permeability anisotropy in the early part of loading but soon r_k develops from a value of 1.0 at e = 3.1, to 2.1 at e = 1.30, given by the approximate empirical relation $r_k = 3.25 \times 0.671^e$. For the block samples, each has its own initial

permeability anisotropy the value of which depends on the maximum vertical effective stress applied to the sample during the earlier one-dimensional compression.

Setting up of very soft block samples can easily destroy the existing low r_k to $r_k < 1$ but on further anisotropic compression, r_k rises significantly.

For other block samples, further anisotropic compression leads to increase in permeability anisotropy r_k with decreasing void ratio, which can be approximately described by the relation $r_k = C.D^e$ where each sample has its own values for the parameters C and D. The difference in behaviour between samples which are relatively 'softer' and 'stiffer' is that anisotropic compression renders the permeability of the softer sample more anisotropic. The permeability anisotropy of the stiffer samples does not increase much with further compression but remains more or less unchanged (*Fig.*-5.19).

6.4 Influence of undrained shear on permeability anisotropy

Examination of observations of development of arrangements of clay plates and domains of particles during pre-peak shear deformation made using optical and electron microscopy suggests that deformation increases the anisotropy of initially isotropic clays and decreases the anisotropy of initially strongly anisotropic clays: in other words, that the anisotropy may be converging on some critical anisotropic state just as there is a critical void ratio. The findings of the rather limited study that has been reported here indicate that the effects of undrained shear deformation can reduce the permeability anisotropy significantly.

The techniques and programmes of experimental testing conducted in the present study have attempted to determine permeability changes of consolidated kaolin samples after they have undergone CIU isotropic recompression followed by undrained shearing to various axial strains in the triaxial apparatus. These results were obtained from the Series 3 samples which experience sampling-out and setting-up operations on two occasions: firstly for the triaxial testing, and secondly, after the triaxial testing, for the permeability testing. The samples that were tested can be divided roughly into two groups: Group I ('soft') where σ'_{vmax}=100kPa and σ'_3=100kPa (the effective radial stress used for the triaxial tests); and Group II ('stiff') where the sets of stresses used were σ'_{vmax}=120kPa and σ'_3=200kPa; σ'_{vmax}=240kPa and σ'_3=200kPa; and $\sigma'_{v\,max}$ = 600 kPa and σ'_3=300kPa.

Altogether a total of seven samples (3 softer, 4 stiffer) were sheared and from these, 7 pairs were trimmed and set up to determine their vertical and horizontal permeabilities. Developments of permeability with void ratio were obtained for each

sample. Comparisons were made of the changes of vertical and horizontal permeabilities for the sheared samples and for the earlier similar batch of one-dimensionally compressed samples.

As mentioned earlier, there are two aspects to the anisotropy of permeability seen in these CIU tested samples: (1)-the initial permeability anisotropy measured at the beginning of the permeability tests; and (2)-the subsequent change of permeability anisotropy measured during the subsequent continued one-dimensional compression.

During the subsequent compression, the variation of permeability with void ratio follows the same form of expression as that seen for the one-dimensionally compressed samples, namely $k=C.D^e$ which is indicated by the linear (lg.k vs e) plots.

The application of undrained shear does not appear to alter much of the initial permeability anisotropy of the clay sample. This could be due to the strong anisotropic structure developed through the initial one-dimensional compression, and, to a lesser extent, during the isotropic reconsolidation prior to undrained shear (*Fig.*-5.34). However, whereas this initial anisotropy of permeability did not appear to have been much affected by the undrained shear, the behaviour during the subsequent one-dimensional compression was quite different from that observed in samples which did not experience undrained shearing. A decrease in permeability anisotropy r_k with decreasing void ratio was observed in 5 out of the seven samples tested, and in three of these samples the anisotropy ratio fell to less than one, implying that the horizontal permeability was ultimately lower than the vertical permeability [*Figs.*-5.32(a) and 5.33(a)].

6.5 Suggestions for future research on stress-strain and permeability anisotropy of clays

The experimental study of permeability and development of permeability anisotropy of clays is not easy. The tests require long periods of time in order that the samples can be consolidated completely and uniformly. Although this study has demonstrated that the actual measurement of permeability at any stage can be substantially achieved in a couple of hours, by employing the constant flow rate method, the main time consuming part of the experimental study lies in the process of consolidation and re-consolidation of samples. It has also been noted that it is desirable to use several different flow rates, and to allow flow equilibrium to be achieved for each flow rate, in order to obtain a satisfactory application of Darcy's law to the determination of permeability. It is for these reasons that the programme of tests reported here was not more extensive, but it is clear that there are areas where additional testing is desirable.

The existing equipment, consisting of some 3 tanks, 1 cylinder and three filter presses, all designed for producing high quality uniform block samples, provides a sufficient quantity and range of of sample preparation apparatus. However, the aparatus presently available for permeability testing (vertical & horizontal) - consisting of the pairs of Rowe cells each with a pair of GDS flow pumps - could be expanded with advantage. It was often necessary to wait for long periods in order to complete a particular stage of permeability testing while more samples completed the consolidation and shear phase of the experiments. Consequently an additional set of oedometers and flow pumps would be useful if this type of research is to continue and expand.

One of the consequences of the limited programme of tests is that there has not been as much attention paid to repetition of tests as would have been desirable. Repetitive tests on replicate samples under a single set of controlled water content and past stress conditions would be the best approach to assess the reproducibility of the test results. There are certainly disturbance effects associated with the sampling-out, trimming and setting-up operations when samples are prepared for the Rowe cells (and when they are prepared for the triaxial apparatus). Different sampling procedures could be used, with repeated tests, in order to discover whether these have as much effect on permeability values as it is kown that they have on stress-strain response.

Placing slurry into the Rowe cells (for measurement of vertical or radial permeability and compression characteristics) is less difficult than inserting block samples. While the setting up of vertical block specimens in the Rowe cell is reasonably straightforward, the setting up of specimens for measurement of horizontal flow characteristics is less easy because of the need to place the rigid internal porous drain. Because of the intricacy of the necessary procedure, it is possible that the setting up of the horizontal flow samples may itself introduce some distorting factor into the observed permeability and permeability anisotropy values, by comparison with the vertical flow characteristics which are nominally measured on identical samples.

Setting up of specimen into the Rowe cell under water has proved to be too difficult and not practical, especially for the horizontal flow specimens. Thus the method was abandoned after a few trials during the early part of this study. A procedure was adopted instead involving the application of vacuum. Once the specimen is already inside the oedometer, the whole apparatus is immersed in water in an airtight chamber (such as a desiccator) and all valves opened. The chamber is then evacuated for about 30min to remove any air bubbles and also ensure a deaired permeant. It may be desirable to investigate other sample preparation strategies.

The study of the effect of undrained shearing on the permeability of the kaolin is clearly rather inconclusive. Time has not permitted a more extensive study, but the preliminary results that have been obtained have revealed aspects of response which should certainly be investigated further. With these tests it will be particularly important to perform many replicate experiments in order to be confident that the effects that are observed are indeed real, and are not artefacts of the experimental procedure. The observation of decreasing anisotropy with further compression after undrained shearing is perhaps curious, and should be combined with further microscopy of these same samples in order to discover whether there is evidence that the fabric anisotropy is clearly changing in the same way.

Finally, all the testing that has been reported here has been performed on an artificial laboratory clay, kaolin. While this is a convenient clay to use for such a laboratory study, it is hardly representative of most natural clays. With the testing procedures having reached a level of reasonable confidence, it may be possible to extract undisturbed samples from various soft (or stiff) clay sites in order to measure the permeabilities and permeability anisotropy for comparison with values obtained from in situ measurements. Anisotropy is important in its influence on the mechanical behaviour of clays, and a desirable long term research aim would be to relate the mechanical anisotropy, which can require quite elaborate testing for its evaluation, to the permeability anisotropy, which, as has been demonstrated here, can be determined rather quickly with a pair of samples allowed to reach flow equilibrium. It would be desirable to combine these tests on field samples with optical and electron microscope studies of the in situ fabric of the clays that are being tested in order to provide a three-way attack on the problem of the quantitative description of anisotropy of natural soils.

7. REFERENCES

Aas, G. (1967). Vane tests for investigation of anisotropy of undrained shear strength of clays. *Proc. Geotech. Conf. on shear strength properties of natural soils and rocks*, Oslo **1**, 3-8.

Aiban, S.A. and Znidarcic, D. (1989). Evaluation of the flow pump and constant head techniques for permeability measurements. *Geotechnique* **39**, No.4, 655-666.

Al-Dhahir, Z.A. and Tan, S.B. (1968). A note on one-dimensional constant-head permeability tests. *Geotechnique* **18**, 499-505.

Al-Tabbaa, A. (1987). *Permeability and stress-strain response of speswhite kaolin,* Ph.D. thesis, Cambridge University.

Al-Tabbaa, A. and Wood, D.M. (1987). Some measurements of the permeability of kaolin. *Geotechnique* **37**, No.4, 499-503.

Al-Tabbaa, A. and Wood, D.M. (1988). Some measurements of the permeability of kaolin - Discussion by Znidarcic, D. & Aiban, S.A. *Geotechnique* **38**, No.3, 453-454.

Allison, L.E. (1947). Effect of microorganisms on permeability of soil under prolonged submergence. *Soil Science.* **63**, 439-450.

ASTM STP 874, A.I. Johnson, R.K. Frobel, N.J. Cavalli and C.B. Pettersson, Eds.,American Society for Testing and Materials, Philadelphia, 1985.

Atkinson, J.H. and Bransby, P.L. (1978). *The mechanics of soil. An introduction to critical state soil mechanics.* Maidenhead. McGraw-Hill.

Atkinson, J.H., Evans, J.S. and Ho, E.W.L. (1985). Non-uniformity of triaxial samples due to consolidation with radial drainage. *Geotechnique.* **35**, No.3, 353-355.

Bai, X. and Smart, P. (1994). Study of microstructure of undrained clay.-*to appear in* Int. Symposium on pre-failure deformation characteristics of geomaterials, Hokkaido University, Sapporo, Japan & JSSMFE, 12-14 Sept.1994.

Balasubramaniam, A.S. and Brenner, R.P. (1981). *Chapter 7*- Consolidation and Settlement of Soft Clay. *Soft clay Engineering - Developments in Geotechnical Engineering 20*, E.W.Brand & R.P.Brenner, Eds., Elsevier, pp.477-566.

Bear, J.(1972). Dynamics of fluids in porous media. Elsevier, New York.

Bernaix, J. (1967). *Etude Geotechnique de la Roche de Malpasset*, Dunod, Paris.

Biot, M.A. (1941). General theory of three-dimensional consolidation. *J. Appl. Phys.* **12**, 155-164.

_____(1955). Theory of elasticity and consolidation for a porous anisotropic solids. *J. Appl. Phys.* **26**, 182-185.

Bishop, A.W. & Green, G.E. (1965). The influence of end restraint on the compression strength of a cohesionless soil. *Geotechnique.* **15**, No.3, 243-266.

Bishop, A.W. and Henkel, D.J. (1973). Saturating laboratory samples by back pressure. *Journal of the Soil Mechanics and Foundation Engineering Division,Proceeding ASCE, SM1.* 75-93.

Bishop, A.W. and Henkel, D.J. (1962). *The Measurement of Soil Properties in the Triaxial Test.* Ed. 2. London. Edward Arnold Ltd.

Bjerrum, L. and Huder, J. (1957). Measurement of the permeability of compacted clay. *Proceedings, 4th. ICSMFE.* **1**, *London, England,* 6-10.

Bjerrum, L. and Simons, N.E. (1960). Comparison of shear strength characteristics of normally consolidated clays. *Proc.Research Conf. on Shear Strength of Cohesive Soils, Boulder, Colorado (New York: ASCE)* 711-726.

Blight, G.E. (1963). The Effect of Nonuniform Pore Pressures on Laboratory Measurements of the Shear Strength of Soils. *Laboratory Shear Testing of Soils. ASTM* STP No.361, 173-184.

Boynton, S.S. & Daniel, D.E. (1985). Hydraulic conductivity tests on compacted clay. *J. Geotechnical Engineering, ASCE* **111**, No.4, 465-478.

British Standards Institution. (1975). *Methods of Test for Soils for Civil Engineering Purposes, BS1377: 1975,* London:British Standard Institution.

Burghignoli, A., Cavalera, L., Chieppa,V., Jamiolkowski, M., Mancuso, C., Marchetti, S., Pane, V., Paoliani, P., Silvestri, F., Vinale, F & Vittori, E.(1991). Geotechnical characterization of Fucino clay. *Proc. 10th. European Conf. on Soil Mech. & Foundation Engineering.* Vol. 1, pp. 27-40.

Butterfield, R. (1979). A natural compression law for soils. *Geotechnique.* **29**, 469-480,

Carman, P.C. (1956). *Flow in gases through porous media,* New York Academic Press.

Carslaw, H.S. and Jaeger, J.C. (1959). *Conduction of heat in solids.* Ed. 2 Oxford. Clarendon Press.

Casagrande, A. and Carillo, N. (1944). Shear failure of anisotropic materials. *Proc.Boston Soc.of Civ.Engrs.* 31:74-87.

Chakrabarti, S. & Horvath, R.G. (1985). Slopes of Consolidation lines. *Can. Geotech. J.* **22**, 254-258.

Chan, H.R. and Kenney, T.C. (1973). Laboratory investigation of permeability ratio of New Liskeard Varved Soil. *Can. Geotech. J.* **10**, 453-472.

Chandler, R.J., Leroueil, S. and Trenter, N.A. (1990). Measurements of the permeability of London clay using a self-boring permeameter. *Geotechnique* **40** No. 1, 113-124.

Chapuis, R.P., Gill, D.E.,& Bass, K. (1989) Laboratory permeability tests on sands: Influence of the compaction method on anisotropy. *Can. Geotech. J.* **26**, 614-622.

Christian, J.T., Boehmer, J.W.,& Martin, P.T. (1972). Consolidation of a Layer under a Strip Load, *J. Soil Mech. Found. Div. ASCE*, **98**, No. SM7, 693-707.

Collins, K. and McGown, A. (1974). The form and function of microfabric features in a variety of natural soils. *Geotechnique* **24**, No.2, 223-254

Cooper, H.H. and Jacob, C.E. (1946). A generalized graphical method for evaluating formation constants and summarizing well-field history. *Trans. Amer. Geophysical Union.* **27**, 526-534.

Day, S.R. and Daniel, D.E.(1985). Field permeability test for clay liners. *Hydraulic Barriers in Soil and Rock, ASTM STP 874*, A.I. Johnson, R.K. Frobel, N.J. Cavalli and C.B. Pettersson, Eds.,American Society for Testing and Materials, Philadelphia, pp. 276-288.

DeWiest, R.J.M. (1965). *Geohydrology*, John Wiley & Sons, New York, 366 pp.

Di Biagio, E. and Aas, G. (1967). The in situ undrained shear strength measured on a horizontal failure plane by large scale direct shear tests in quick clay. *Proc. Geotech. Conf. Oslo.* 1:19-26.

Domenico, P.A. (1972). *Concepts and Models in Groundwater Hydrology.* McGraw-Hill, Inc.

Donaghe, R.T., Chaney, R.C. and Silver, M.L. (1988). *Advanced triaxial testing of soil and rock. ASTM* STP977, Philadelphia:American Society for Testing Materials.

Ducasse, P., Mieussens, C., Moreau, M. and Soyez, B.(1986). Oedometric Testing in the Laboratoires des Ponts et Chaussees, France. *Consolidation of Soils: Testing and Evaluation, ASTM STP 892*, R.N.Yong and F.C.Townsend, Eds., American Society for Testing and Materials, Philadelphia, pp.282-298.

Dunn, R.J. and Mitchel, J.K. (1984). Fluid conductivity testing of fine-grained soils. *J. Geotech. Engng Div. ASCE*, **110**, 1648-1665.

Edil, T.B. & Erickson, A.E. (1985). Procedure and Equipment Factors Affecting Permeability Testing of a Bentonite-Sand Liner Material. *Hydraulic Barriers in Soil and Rock, ASTM STP 874*, A.I. Johnson, R.K. Frobel, N.J. Cavalli and C.B. Pettersson, Eds.,American Society for Testing and Materials, Philadelphia, pp. 155-170.

Fernandez, F. and Quigley, R.M. (1985). Hydraulic conductivity of natural clays permeated with simple liquid hydrocarbons. *Can. Geotech. J.* **22**, 205-214.

Fernandez, F. and Quigley, R.M. (1991). Controlling the destructive effects of clay-organic liquid interactions by application of effective stresses. *Can. Geotech. J.* **28**, 388-398.

Foster, R.H. & De, P.K. (1971). Optical and electron microscopic investigation of shear induced structures in lightly consolidated (soft) and heavily consolidated (hard) kaolinite. *Clays and Clay Minerals* **19**, 31- 47.

Gazetas, G. (1982). Stresses and Displacements in Cross-Anisotropic Soils. *Journal of The Geotechnical Engineering Division, ASCE.* **108**, GT4, 532-553.

Gerrard, C.M. (1977). Background to Mathematical Modelling in Geomechanics: The Roles of Fabric and Stress-History. *Finite Elements in Geomechanics*, G. Gudehus, Ed., John Wiley & Sons, Inc., New York, N.Y., pp. 33-120.

Gibson, R.E. (1963). An analysis of system flexibility of its effect on the time-lag in pore water pressure measurements. *Geotechnique* **13**,1-11.

Graham, J., Crooks, J.H.A. and Bell, A.L. (1985). Time effects on the stress-strain behaviour of natural soft clays. *Geotechnique.* **33**, No.3, 327-340.

Graham, J. and Houlsby, G.T. (1983). Elastic anisotropy of a natural clay. *Geotechnique.* **33**, No.2, 165-180,

Hansbo, S. (1960). *Consolidation of Clay, with Special Reference to Influence of Vertical Sand Drains*, Stockholm:Swed.Geotech.Inst.Proc.18.

Hardcastle, J.H. and Mitchell, J.K. (1974). Electrolyte concentration-permeability relationship in sodium illite-silt mixtures. *Clays and Clay Minerals.* **22**:143-154.

Harkness, R.M.(1987). "Personal Communication".

Harr, M.E. *Foundations of theoretical soil mechanics.* (1966). New York:McGraw-Hill.

Head, K.H. (1982). *Manual of Soil Laboratory Testing-Vol. 2: Permeability, Shear Strength and Compressibility Tests*, New York:John Wiley and Sons.

Henkel, D.J. & Sowa, V. (1963). The Influence of Stress History on Stress Paths in Undrained Triaxial Tests on Clay. *Laboratory Shear Testing of Soils, ASTM STP 361*, Ottawa, Canada, 280-294.

Herbert, R. (1972) *Correspondence. Geotechnique* **26**, No. 1, 173-184

Jamiolkowski, M., Ladd, C.C., Germaine, J.T. and Lancellotta, R. (1985). New developments in field and laboratory testing of soils. Proceedings, 11th. International Conference on Soil Mechanics and Foundation Engineering, San Francisco, Vol. 1, pp. 57-153.

Januskevicius, C.E. & Vey, E. (1965). Stresses and strains in Triaxial specimens. *Instruments and Apparatus for Soil and Rock Mechanics, ASTM STP 392*, Am. Soc. Testing Materials, pp.37-54.

Juarez-Badillo, E. (1984). The permeability of natural soft clays- Part II: Permeability characteristics: Discussion. *Can. Geotech. J.* **21**, 730-731.

_____ (1986). General Theory of Consolidation for Clays. *Consolidation of Soils: Testing and Evaluation, ASTM STP 892,* R.N.Yong and F.C. Townsend, Eds., American Society for Testing and Materials, Philadelphia, 1986, pp.137-153.

_____(1991). Laboratory permeability tests on sand: influence of the compaction method on anisotropy: Discussion. *Can. Geotech. J.* **28**, 171-172.

Kozeny, J. (1927). Uber Kapillare Leitung des Wassers im Boden. Wien, Akad, Wiss., **136**, Pt. 2a, pp.271.

Lacerda, W.A., Costa Filho, L.M., Coutinho, R.Q. & Duarte, A.E.R. (1977). Consolidation Characteristics of Rio De Janeiro Soft Clay. *Geotechnical Aspects of Soft Clays, Proc. Int. Symposium on Soft Clay*, Bangkok. Eds. Brenner, R.P. & Brand, E.W., 231-243.

Ladd,C.C.(1973). Settlement analysis for cohesive soils. *Res. Rep.* R71-2, *Soils Publ.*272, *Dept. of Civil Engineering, Mass. Inst. of Technology.* Cambridge, Mass., 115 pp. (revised 1973).

Ladd,C.C.(1973). *Proc. 8th. Int. Conf. Soil Mech. Found. Eng.*, Moscow, Vol.4.2:108-115.

Ladd,C.C., Foott,R., Ishihara, K., Schlosser, F. and Poulos,H.G. (1977). Stress-deformation and strength characteristics. *Proc. 9th. Int. Conf. Soil Mech. Found. Eng.*, Tokyo, 2:421-494.

Lambe, T.W. (1954). The permeability of fine grained soils. *ASTM Special Publication* 163:56-57.

Lambe, T.W. and Whitman, R.V. (1969). *Soil Mechanics*, New York: John Wiley and Sons.

Landva, A. (1964) Equipment for cutting and mounting undisturbed specimens of clay in testing devices, Publication No. 56, pp.1-5, Norwegian Geotechnical Institute, Oslo.

Lapierre, C., Leroueil, S. & Locat, J. (1990). Mercury intrusion and permeability of Louiseville clay. *Can. Geotech. J.* **27**, 761-773.

Lee, K.L. and Morrison, R.A. (1970). Strength of anisotropically consolidated compacted clay. *JSMFD, ASCE,Proc.Paper No. 7703* x,(No.SM6),:2025-2043.

Lee, K.L., Morrison, R.A. and Haley, S.C. (1969). A note on the pore pressure parameter B. *Proc.7th. Int.Conf.on Soil Mech. and Found. Engr.,Mexico City.* 1:231-238.

Lefebvre,G., Langlois, P., Lupien, C. & Lavallee, J.-G. (1984). Laboratory testing and *in-situ* behaviour of peat as embankment foundation. *Can. Geotech. J.* **21**, 322-337.

Leonards, G.A. (1962). *Foundation Engineering*, McGraw-Hill, New York.

Leroueil, S. (1988). Tenth Canadian Geotechnical Colloquium: Recent developments in consolidation of natural clays. *Can. Geotech. J.* **25**, 85-107.

Leroueil, S., Diene, M., Tavenas, F., Kabbaj, M. and La Rochelle, P.(1988). Direct determination of permeability of clay under embankment. *Journal of Geotechnical Engineering* **114**, No.6, 645-657.

Leroueil, S., Bouclin, G., Tavenas, F., Bergeron, L. & La Rochelle, P. (1990). Permeability anisotropy of natural clays as a function of strain. *Can. Geotech. J.* **27**, 568-579.

Leroueil, S., Magnan, J-P and Tavenas, F.(1990). Embankments on Soft Clays. Ellis Horwood, England.

Little, J.A., Muirwood, D., Paul, M.A. and Bouazza, A. (1992). Some laboratory measurements of permeability of Bothkennar clay in relation to soil fabric. *Geotechnique* **42**, No.2, 355-361.

Lo, K.Y. (1965). Stability of slopes in anisotropic soils. *Proc.Soil Mech.Found.Div.Am.Soc.Civ.Engrs.* **91** (SM4), 85-106.

Loudon, A.G.(1952). The computation of permeability from simple soil tests. *Geotechnique* **3**, 165-183.

Louis, C., Dessenne, J.-L. & Feuga, B. (1977). Interaction between Water Flow Phenomena and the Mechanical Behaviour of Soil or Rock Masses. *Finite Elements in Geomechanics*, G. Gudehus, Ed., John Wiley & Sons, Inc., New York, N.Y., pp. 479-511.

Lowe, J. and Johnson, T.C. (1960). Use of backpressure to increase degree of saturation of triaxial test specimens. *Research Conference on Shear Strength of Cohesive Soils, ASCE, Boulder, CO.* pp. 819-836.

Matyas, E.L. (1966). Air and water permeability of compacted soils: Permeability and Capillarity of soils. *ASTM, SPT 417.*

Mayne, P.W. and Kulhawy, F.H. (1982). Ko-OCR relationships in soil. *Journal of The Geotechnical Engineering Division, ASCE.* **108**,GT6, 851-872.

McConnachie, I. (1974). Fabric changes in consolidated kaolin, *Geotechnique* **24**, No.2, 207-222.

Mc Kinlay, D.G. (1961). A laboratory study of rates of consolidation in clays with particular reference to conditions of radial porewater drainage. *Proc. 5th. Int.Conf.on Soil Mech. and Found. Eng.* Vol.1, pp.225-228.

Menzies, B.K. & Mailey, L.K.(1976). Some measurements of strength anisotropy in soft clays using diamond-shaped shear vanes, *Geotechnique*, **26**, No.3, 535-538.

Menzies, B.K. & Simons,N.E. (1978). Stability of Embankments on Soft Ground. *Developments in soil mechanics-1.* C.R. Scott, Ed., Applied Science Publishers Ltd., London, England, pp.393-435.

Mesri, G. & Choi, Y.K. (1985). Settlement Analysis of Embankments on Soft Clays, *J. Geotech. Eng. ASCE*, **111**, No.4, 441-465.

Mesri, G. and Olson, R.E. (1971). Mechanisms controlling the permeability of clays. *Clays and Clay Minerals*, **19**, 151-158.

Michaels, A.S. and Lin, C.S. (1954). The permeability of Kaolinite. *Industrial and Engineering Chemistry.* **46**, 1239-1246.

Mitchell, J.K. (1956). *The fabric of natural clays and its relation to engineering properties.* Proceedings of the Highway Research Board **35**, 693-713.

Mitchell, J.K. (1976). *Fundamentals of Soil Behaviour*, John Wiley and Sons, Inc. New York.

Mitchell, J.K., Hooper, D.R. & Campanella, R.G. (1965). Permeability of compacted clay. *JSMFD, ASCE,* **91**, No.SM4, 41-65.

Mitchell, J.K. and Younger, J.S. (1967). Abnormalities in hydraulic flow through fine-grained soils. *ASTM,* STP 417, 106-141.

Monte, J.L. & Krizek, R.J. (1976). One-dimensional mathematical model for large-strain consolidation. *Geotechnique* **26**, No.3, 495-510.

Morgenstern, N.R. & Tchalenko, J.S. (1967). Microscopic changes in kaolin subjected to direct shear, *Geotechnique* **17**, No., 207-222.

Morin, R.H., and Olsen, H.W. (1987). Theoretical Analysis of the Transient Pressure Response from a Constant Flow Rate Hydraulic Conductivity Test. *Water Resources Research* **23**, No.8, 1461-1470.

Morin, R.H., Olsen, H.W., Nelson, K.R. and Gill, J.D. (1989). Graphical Method for Determining the Coefficient of Consolidation c_v from a Flow-Pump Permeability Test, *Geotechnical Testing J.* GTJODJ, **12**, No.4, 302-307.

Moser, M.A. (1977). The Effectiveness of Sand Drains in Soft Soils. *Geotechnical Aspects of Soft Clays, Proc. Int. Symposium on Soft Clay*, Bangkok. Eds. Brenner, R.P. & Brand, E.W., 261-270.

Murray, R.T. (1978). Developments in two and three-dimensional consolidation theory. *Developments in soil mechanics-1.* C.R. Scott, Ed., Applied Science Publishers Ltd., London, England, pp.103-147.

Ohtsubo, M., Egashira, K.,& Takayama, M. (1985). Properties of a low-swelling smectitic marine clay of interest in soil engineering.*Can. Geotech. J.* **22**, 241-245.

Olsen, H.W. (1962). Hydraulic flow through saturated clays. *Proceedings of the 9th. National Conference on Clays and Clay Minerals, Clays and Clay Minerals.* **9**, 131-161.

_____(1965). Deviations from Darcy's law in saturated clays, *Soil Sci. Soc. Am. Proc.*, **29**(2), 135-140.

_____(1969). Simultaneous fluxes of liquid and charge through saturated kaolinite. *Soil Sci. Soc. Am. Proc.*, **33**(3), 338-344.

_____(1966). Darcy's Law in saturated kaolinite. *Water Resources Research* **2**(6), 287-295.

_____(1985). Osmosis: a cause of apparent deviations from Darcy's law. *Can. Geotech. J.* **22**, 238-241

Olsen, H.W., Nichols, R.W. and Rice, T.L. (1985). Low gradient permeability measurements in a triaxial system. *Geotechnique* **35**, No.2, 145-157.

Olson, R.E.(1960) Discussion: The Migration of Pore fluid During Shear in Consolidated-Undrained (R) Triaxial Tests in Session 3- *Shear Strength of Saturated, Remolded Clays*, ASCE Research Conf. on Shear Strength of Cohesive Soils.

_____(1986). State-of-the-art: Consolidation Testing. *Consolidation of Soils: Testing and Evaluation, ASTM STP 892*, R.N.Yong and F.C.Townsend, Eds., American Society for Testing and Materials, Philadelphia, pp.7-70.

Olson, R.E. & Daniel, D.E. (1981). Measurement of the hydraulic conductivity of fine-grained soils. *ASTM Symp. on Permeability and groundwater contaminant transport*, STP 746, 18-64.

Pane, V., Croce, P., Znidarcic, D., Ko, H.Y., Olsen, H.W. and Schiffman, R.L. (1983). Effects of consolidation on permeability measurements for soft clay. *Geotechnique* **33**, No.1, 67-72.

Parry, R.H.G. & Nadarajah, V. (1973). Observations of Laboratory Prepared Lightly Overconsolidated Specimens of Kaolin. *Geotechnique* **24**, No.3, 345-358.

Parry, R.H.G. & Wroth, C.P.(1981). *Chapter 4* - Shear stress-strain properties of soft clay. *Soft clay Engineering - Developments in Geotechnical Engineering 20*, E.W.Brand & R.P.Brenner, Eds., Elsevier, pp.311-362.

Poulos, S.J.(1981). Discussion of Soil Testing Practices, *Laboratory Shear Strength of Soil, ASTM STP 740*, R.N.Yong and F.C.Townsend, Eds.,American Society for Testing and Materials, pp. 659-666.

Rendulic, L. (1938). Eine Betrachtung zur Frage der plastischen Grenzzustande (A consideration of the problem of the limiting conditions of plasticity). Der Bauingenieur, Vol. 19, pp. 159-164.

Robertson, P.K. and Campanella, R.G. (1983). Interpretation of cone penetration tests. Part II: Clay. *Can. Geotech. J.* **20**, 734-745.

Roscoe, K.H., Schofield, A.N. and Thurairajah, A. (1963). An Evaluation of Test Data for Selecting a Yield Criterion for Soils. *Laboratory Shear Testing of Soils, ASTM STP No. 361*, pp.111-128.

Rowe, P.W. (1972). The relevance of soil fabric to site investigation practice. *Geotechnique* **22**, No.2, 195-300.

Rowe, P.W. and Barden, L. (1964). Importance of free ends in the triaxial testing. *Journal of the Soil Mechanics and Foundation Engineering Division, ASCE.* 90 (SM1):1-27.

Samarasinghe, A.M., Huang, Y.H. and Drnevich, V.P. (1982). Permeability and consolidation of normally consolidated soils. *Journal of The Geotechnical Engineering Division, ASCE.* 108 (GT6):835-850.

Sandbaekken, G., Berre, T. and Lacasse, S. (1986). Oedometer Testing at the Norwegian Geotechnical Institute. *Consolidation of Soils: Testing and Evaluation, ASTM STP 892*, R.N.Yong and F.C.Townsend, Eds., American Society for Testing and Materials, Philadelphia, pp.329-353.

Sangrey,D.A.(1972). Naturally cemented sensitive soils. *Geotechnique* **22**, No.1, 139-152.

Sangrey,D.A. and Townsend,D.L. (1969). Characteristics of three sensitive Canadian clays. Research Report No.63, Department of Civil Engineering, Queen's University at Kingston, Ontario.

Scott, R.F. (1963). *Principles of Soil Mechanics*, Reading, MA.:Addison-Wesley Publ.Co.

Seed, H.B. and Chan, C.K. (1959) Structure and strength characteristics of compacted clays. *JSMFD. ASCE.* **85** (No.SM5):87-128.

Scheidegger, A.E.(1954). Statistical hydrodynamics in porous media. *Journal of Applied Physics,* **25**: 994-1001.

_____(1974). The physics of flow through porous media. 3rd. Ed. Chap.6, University of Toronto Press, Toronto.

Shields, D.H.(1976). Consolidation test. *Geotechnique.* **26**, No.1, 209-212.

Shields, D.H. and Rowe, P.W.(1965). A radial drainage oedometer for laminated clays. *Journal of the Soil Mechanics and Foundation Engineering Division, Proc. ASCE.* 91 (SM1):15-23.

Skempton, A.W. (1954). The pore pressure coefficient A and B. *Geotechnique.* **4** No.1, 143-147.

Smart, P. (1966a). Optical microscopy and soil structure. *Nature* 210, 1400.

Smart, P. (1985). Measurement of Anisotropy by Polarising Microphotometry. *in Optical microscopy in geotechnical engineering.* Presented at 7th. Int. working meeting on soil micromorphology, Paris.

Smart, P. (1993).Microstructure, manipulation. *Encyclopedia of Soil Science*, Part 1, 2nd. Edition. Dowden, Hutchinson and Ross, Stroudsburg, Pennsylvania.

Stephenson, D. (1978). Drawdowns in embankments. *Geotechnique.* **28**, No.3, 273-280.

Swartzendruber, D. (1968). The applicability of Darcy's Law. *Soil Sci. Soc. Amer. Proc.* **32**:11-18.

Tavenas, F.(1981). Some Aspects of Clay Behaviour and Their Consequences on Modeling Techniques. *Laboratory Shear Strength of Soil, ASTM STP 740*, R.N.Yong and F.C.Townsend, Eds.,American Society for Testing and Materials, pp. 667-677.

Tavenas, F., Jean, P., Leblond, P. & Leroueil, S. (1983a). The permeability of natural clays- Part II: Permeability characteristics. *Can. Geotech. J.* **20**, No.4, 645-660.

Tavenas, F., Leblond, P., Jean, P. & Leroueil, S. (1983b). The permeability of natural soft clays- Part 1: Methods of laboratory measurement. *Can. Geotech. J.* **20**, No. 4, 629-644.

Taylor, D.W. (1948). *Fundamentals of Soil Mechanics*, New York: John Wiley & Sons, Inc., p.228.

Terzaghi, K. (1925). Determination of the permeability of clay: *Engineering News Record* **95**, 832-836.

Todd, D.K. (1980). *Groundwater Hydrology*, 2nd. Ed. John Wiley & Sons, Inc.

Trautwein, S.J., Olson. R.E. and Thomas, R.L.(1981). Radial flow consolidation testing. *Proc. 10th. Int. Conf. Soil Mech. and Found. Eng.* Stockholm, Vol. 1, pp.811-814

Ward, W.H., Marsland, A. and Samuel, S.G. (1965). Properties of the London clay at the Ashford Common Shaft: in situ and undrained strength tests. *Geotechnique* **15**, No.4, 321-344.

Wesley, L.D. (1988). Compression Index: Misleading Parameter? *J. Geotech. Eng. ASCE*, **114**, No.6, 718-723.

Yanful, E.K., Haug, M.D., and Wong, L.C. (1990). The impact of synthetic leachate on the hydraulic conductivity of a smectitic till underlying a landfill near Saskatoon, Saskatchewan. *Can. Geotech. J.* **27**, 507-519.

Zimmie, T.F. (1981). Geotechnical Testing Considerations in the Determination of Laboratory Permeability for Hazardous Waste Disposal Sitting, *Hazardous Solid Waste Testing: First Conference, ASTM STP 760*, R.A.Conway & B.C.Malloys, Eds., American Society for Testing and Materials, Philadelphia, pp. 293-320.

Zimmie, T.F., Doynow, J.S. and Wardell, J.T. (1981). Permeability testing of soils for hazardous waste disposal sites. *Proc.10th.Int.Conf.Soil Mech. and Found.Eng., Stockholm*, Balkema Publishers, Rotterdam., Vol.2, pp.403-406.

8. APPENDIX

Details of the test set up, sample preparation and experimental procedure are described in Sections A, B and C respectively. Contents of these sections are listed below for convenience. Some of the main data are presented in Section D.

Some notes on the data are as follows: Value of permeability is in (m/s); Consolidation pressure or vertical effective stress is in (kPa). (L) and (UL) denote loading and unloading, respectively. Present test series corresponds with previous designations as follows:
2C40V-V; 2T120V-TV; 2T240V-ATV; 2C240V-CV; 2C360V-ACV; 3F1,1,1V-K2V; 3F1,1,2V-K1V; 3F1,1,3V-K100SV; 3T1.2,2,1V-ASTV; 3T2.4,2,1V-STV; 3T6,3,1V-TSV; 3T6,3,2V-TS1V; 1V-OEDV. Same system applies for horizontal case.

A. TEST SET UP

A1. Equipment for consolidation and permeability test

The type of hydraulic oedometer or consolidation cell used in this research is generally known as the Rowe cell. The design of the cell allowed the test sample to be loaded hydraulically by water pressure acting on a flexible diaphragm, instead of a mechanical lever system. Important features are the ability to control drainage (ie. volumetric measurement of expelled water) and to measure pore water pressure during the course of consolidation tests. Vertical or radial drainage conditions are possible and back pressure could be applied to the sample in a closed circuit pressure system. Deformation is strictly constrained in the vertical direction. In a typical test run when the consolidation stage of the test is completed, permeability test is started in the form of constant head or constant flow rate methods.

A1.1 Hydraulic oedometers

Vertical flow cell

A 75-mm vertical flow Rowe cell is shown in *Fig.*-A1(a). The specimen is enclosed in rigid smooth brass ring C of internal diameter 76.2mm. The jack pressure chamber is separated from the specimen by the rubber jack (or diaphragm) and 2.9mm thick circular brass plate. Vyon porous plastic sheets (1.6mm thick each) placed at the top and bottom of the specimen provide the necessary top and bottom drainage boundaries. The cell base, ring and cover are all clamped tightly by three tie-bolts. The height of the ring is 55.6mm. The recommended specimen height before application of load is 30mm.

A hollow settlement drainage rod serves a dual purpose of providing top drainage and following the specimen deformation. Movement of the top of this rod is monitored by a Mercer dial gauge (range 13mm, resolution of 0.002mm). With the rigid brass plate inplaced, the specimen is loaded under 'equal strain' condition with two way drainage in the vertical direction.

Radial flow cell

A section of the 75-mm radial flow Rowe cell is shown in *Fig.*-A1(b). All features of this cell are similar with the vertical flow cell with the exception of the drainage details to allow radial drainage condition while keeping the compression constrained in the vertical direction. Radial drainage is achieved by placing a rigid central drain assembly as shown in *Fig.*-A1(b) and the cell ring is lined with a vyon porous plastic sheet, making the diameter of the specimen smaller from 76.2mm to 72.8mm. The central drain is also lined up with a pre-formed vyon porous tube giving a fixed diameter of 11.0mm. To allow free movement of the central drain in the axial direction while consolidation takes place, a hole is formed in the cell base of sufficient depth (20mm). Therefore for an initial specimen thickness of 32.8mm (typical dimension), compression of about 59% could be achieved before the drain tip touch the cell base.

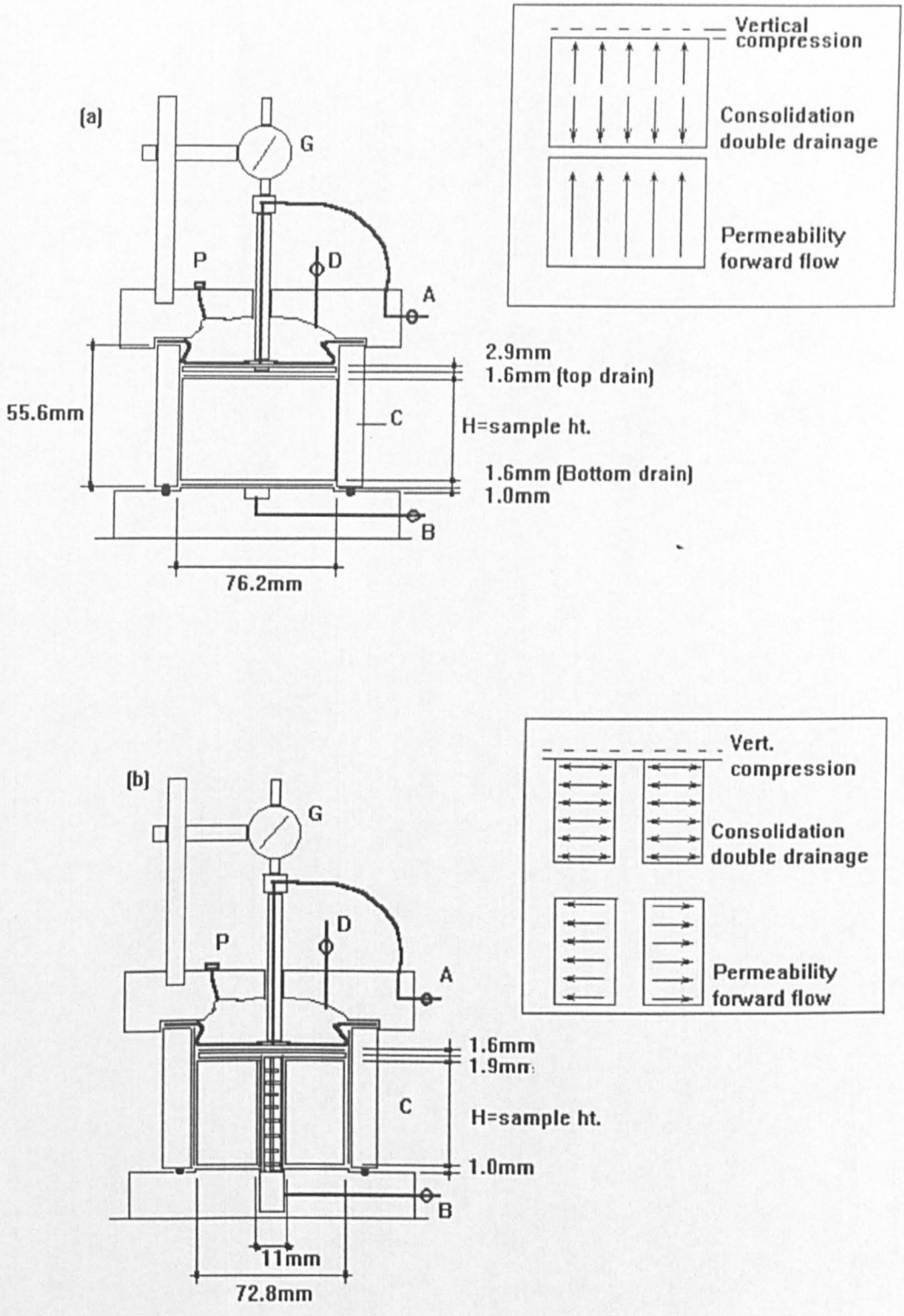

Fig.-A1 Vertical section of 75-mm Rowe cells:

(a) Vertical flow; (b) Radial flow

A1.2 The digital controllers

The digital controller shown in the photograph in *Fig.*-A2 is a microprocessor controlled hydraulic actuator used for precise regulation and measurement of liquid pressure and liquid volume change. For the oedometric testing of test specimen the volumetric capacity of this model is 200cm^3 and the pressure range is 0 to 2000kPa. Pressure measurement is resolved to 0.2kPa, and pressure is controlled to 0.5kPa. The principles of operation are shown in the schematic diagram in *Fig.*-A3 and are fully explained by Menzies (1987).

In stand-alone mode the device is a general purpose constant pressure source, a volume change gauge, a pore pressure measuring system, a flow pump and a digital pipette. It can be programmed through its own control panel to ramp and cycle pressure and volume change linearly with respect to time. For the purpose of providing the necessary control and data logging during consolidation or permeability tests, two digital controllers are linked to a microcomputer (OPUS PC III) with printer.

A1.3 Plumbing system

A schematic of the plumbing layout is shown in *Fig.*-A4. Each oedometer has three plumbing connections (at A, B and D in *Fig.*-A4). Water pressure (controlled from the mains supply through the air/bladder/water interface in a pressure cell) provides the jack pressure through D which drives the consolidation process. Drainage from ports A and B of the oedometer are connected to the two digital controllers (GDS1 and GDS2) which measure both the pressure and the flow of water on each drainage line. To equalise pressure and set an initial reference reading at the start of consolidation test a by pass line is introduced through valve C which when opened will ensure a common pressure to exist between GDS1 and GDS2 and the drainage lines of the oedometer.

A2. Equipment for triaxial test

A2.1 The compression machine

The equipment used for triaxial tests was similar to that described by Bishop and Henkel (1962). The triaxial machines used in all strength tests in this research was a constant rate of deformation machine manufactured by Wykeham Farrance. The capacity of the load frame and the compression/tension machine is 50kN. The samples tested were 102mm high and 101.7mm diameter. The axial deformation is applied by a mechanical jack operated by a motorized gearbox. The motor applies continuous rates of deformation the magnitude depending upon the gear setting. There are 5 change positions selected by a gear lever, also a set of 5 gear wheels, giving 25 rates of deformation ranging from 0.015 to 0.000048 in/min.

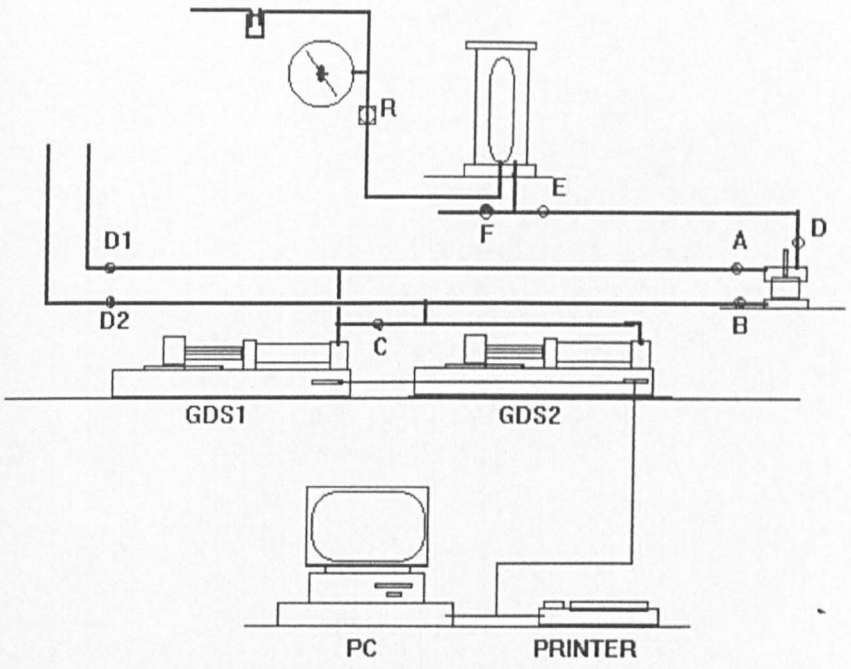

Fig.-A2 Digital pressure controller (GDS)

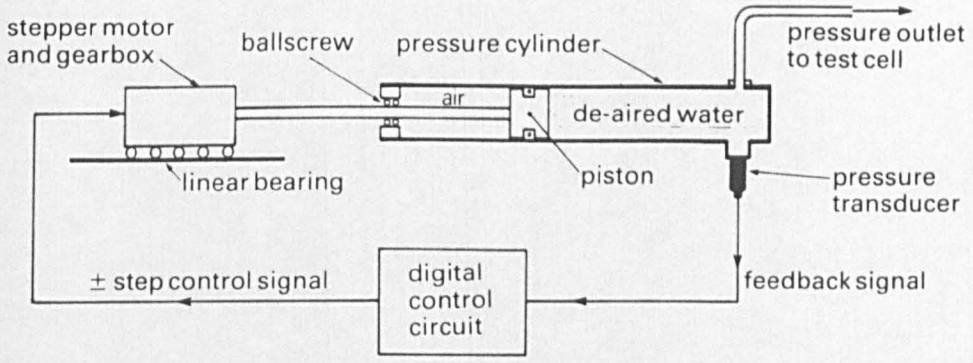

Fig.-A3 Principle of operation of digital hydraulic pressure controller,GDS
(after Menzies & Sutton, 1980; from Head, 1986)

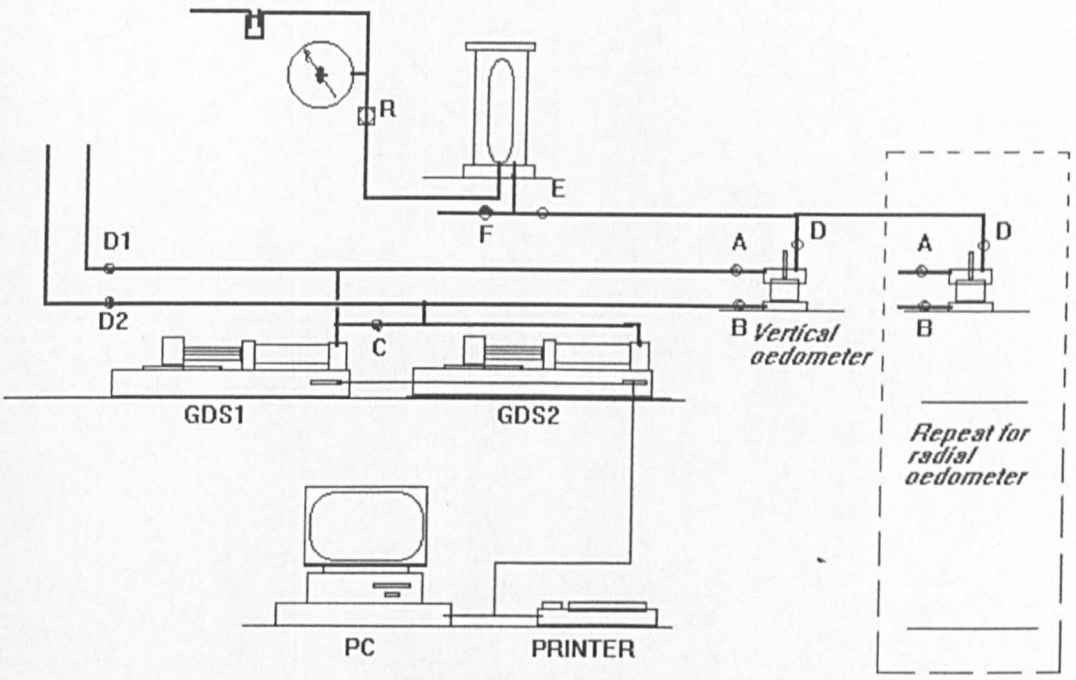

Fig.-A4 Plumbing layout for the consolidation / permeability test set up

A2.2 Triaxial cell

Standard triaxial cell (Wykeham-Farrance Co.Ltd.) is used. Details of the cell are shown schematically in *Fig.*-A5 which consists of : 1. cell base, 2. cell body and cover/top, 3. loading piston or plunger, and 4. loading caps (base pedestal and top cap). Full description of these components are given in a manual by Head (Vol.2 &3,1985) and the manufacturer's instruction manual. Details of the loading caps are described here since they replace the existing caps to allow for 'free-ends' testing of specimens having height/dia. ratio of 1 . The end caps take the form of smooth perspex surface with enlarged diameter of 118mm to allow for radial strain exceeding 10%. Drainage surfaces (12mm dia.) are provided at the centre of the caps and connected to drainage ports through 1-mm diameter drilled holes. Negligible friction is obtained between the specimen ends and the loading caps by lubricating the latter and placing a layer of rubber membranes (dia.=102mm, thk.=0.2mm). To allow for drainage and pore pressure measurement, a central hole 10mm dia. is made on the membranes to coincide with drainage areas at the top and base pedestals. Also, four radial cuts, 17mm long are made at right angles on the menbranes to minimise circumferential stress arising as a result of radial expansion at the ends of the

specimen during shearing. A screw connection at the top cap ensure that specimen surface remains horizontal and tilting is avoided.

A2.3 Strain dials, proving ring and pressure system

The axial deformations were measured by means of Mercer dial gauge. This gauge is sensitive to 0.001" (25.4m) movement and has a travelling range of 2.0" (50mm). The gauge was fitted to rigid attachments at the bottom of the proving ring and tested on adjustable arm clamped to pillars screwed on the top cover of the triaxial cell.

The axial load was measured by means of high tensile steel proving ring (Type No. 800, Serial No.1070) having a capacity of 10kN and a constant of 1.6N/div. of the load dial gauge. The proving ring was placed between the top of the triaxial cell plunger and the crossbar of the load frame. It was calibrated before the testing program and recalibrated twice thereafter by means of a dead load system.

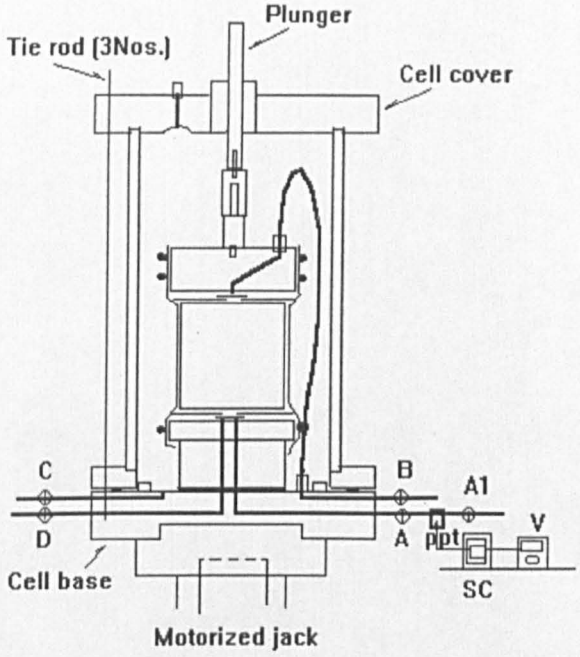

(a)

Fig.-A5(a) Triaxial cell for 100-mm dia. sample

Pressure required for the triaxial cell and backpressure line was continuously supplied from the laboratory main compressed air supply. This pressure mains was regulated by a number of pressure regulators (Regulator type: Norgren, range 0-4bar, and 0-10bar) and fluid pressure to the cell and back pressure lines were effected through the air/bladder/water interface in pressure cells. A full description of this pressure system is given in Vol. 2, Section 8.2.4 of Head (1986). The air/water interfaced by

bladder ensured complete protection of the pressure regulators from water attack while at same time provide a closed circuit pressure system so that problems associated with diffusion of air could be minimised.

The maximum available stable pressure from the mains was 600kPa and constant pressure was readily achieved in a single-stage pressure regulation. Measurement of cell and back pressures was by standard test gauges, 250mm diameter, reading 0-12bar in 0.1bar div.(0-170psi. in 1psi divisions). The accuracy and repeatability of these gauges are within 1% of the indicated reading within the range 10-90% of full-scale reading.

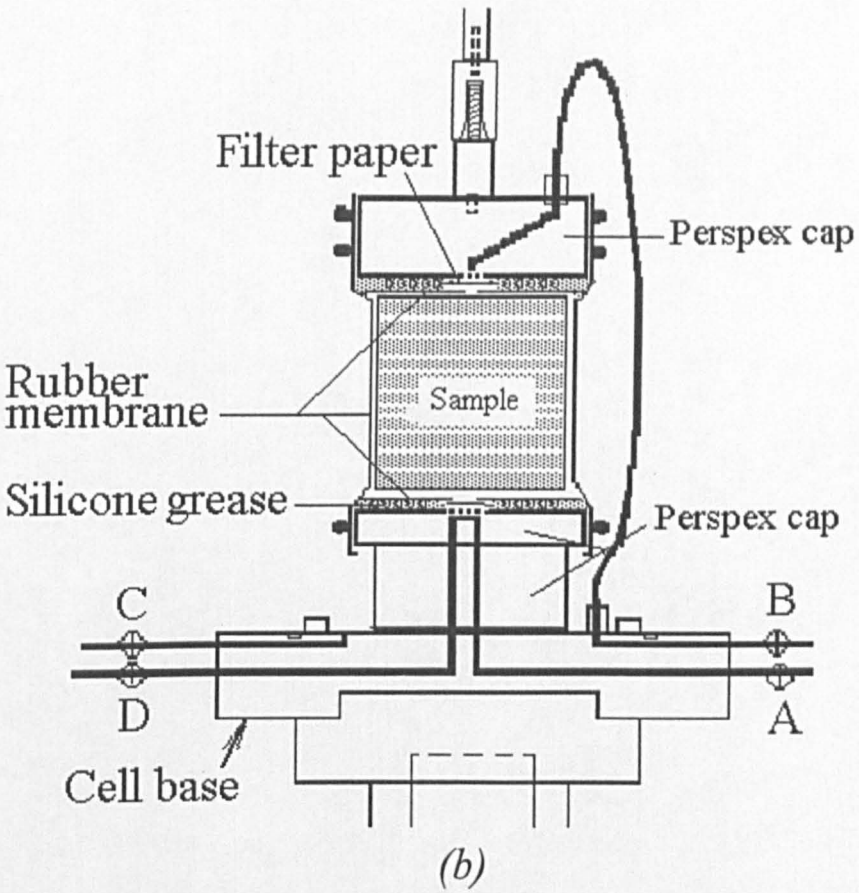

cont.- Fig.-A5(b) Details of loading caps for 100-mm dia. sample

A3. Cylindrical vessel for consolidation of slurry

A3.1 Large consolidation tank

A large consolidation tank was used to consolidate the kaolin slurry from which block samples of known stress history and consolidation characteristics were later derived and trimmed into identical specimens for further consolidation and permeability tests. The consolidation tank has been used earlier by Ponniah(1984) in the study of model plate anchors in kaolin.

A schematic layout of the tank is shown in *Fig.*-A6. The tank essentially consists of three parts: a cylindrical body, a removable cover and the base. The body is split with a central flange with bolt holes for securing the upper and lower halves together. The internal diameter of 298mm provides cylindrical block sample of sufficient diameter to produce practically four identical specimens of diameters ranging from 72.8mm to 101.7mm for the oedometers and triaxial specimens respectively. The base is fitted with a loading jack of rubber bellow, the bottom edge of which provides a seal between the base and the body. The bellow, when fully filled with water and pressurised, provides a convenient means of transmitting a uniform pressure to the sample above, bounded by rigid circular steel plate and perforated perspex disc over the bellow and the removable steel cover at the top of the tank. Effectivve seal is established at the cover, body and base by means of rubber gaskets, grease and bolting.

Water pressure to the bellow was provided through valve C by an air/water pressure cylinder with the pressure regulation occuring on the air line. A translucent tubing connected to the top and bottom of the cylinder acts as an indicator tube such that the water level could be easily monitored. Essential valve connections are also shown in *Fig.*-A6. This plumbing arrangement provides an uninterrupted consolidation of the kaolin slurry while the pressure cylinder is refilled with water to maintain the water-pressurised bellow which travels upward. The consolidation tank, in fact resembles a giant hydraulic oedometer in an inverted position.

As the slurry is consolidated, the expelled water is collected and measured directly from the top and also through the spiral tube at the base through valves D and A respectively. This double drainage was permitted at the top and bottom through two layers of filter papers each, and then through valves A and D.

By pressure regulation, a small vacuum would depress the bellow to 200mm and a pressure of approximately 5kPa would stretch it upward to 550mm giving a vertical travel range of 350mm within the tank which represent a vertical strain of about 90%. During calibration of the tank for vertical movement of the plate a small tilt was observed (angular distortion, $\delta/D = 0.05$) and this deviation from horizontal plane remained practically unchanged as the plate moved upward or downward. It should be noted that during calibration, the plate was held level by placing four 5 pounds weights on it. In the actual process of consolidating the slurry, the cover at the top would have been fastened in position, and the bottom plate under uniform pressure would be in a better condition to remain horizontal as movement was constrained in the vertical direction. A movement of 10mm of the water level in the indicator tube of the pressure cylinder corresponds to a vertical travel of 1.4mm of the plate in the tank and this provides the basis of measurement of vertical compression of the slurry. All connections and valves were ensured to be free of leakage since a slight leakage would result in a serious underestimate of the actual compression of the slurry. Vertical movement of the plate might also be inferred from the volume of water collected from valves A and D. However, this calibration was not carried out although attempts would be made to measure the volume of water expelled during the slurry consolidation.

Increments of consolidation pressure were provided by the cell pressure and controlled by a pressure

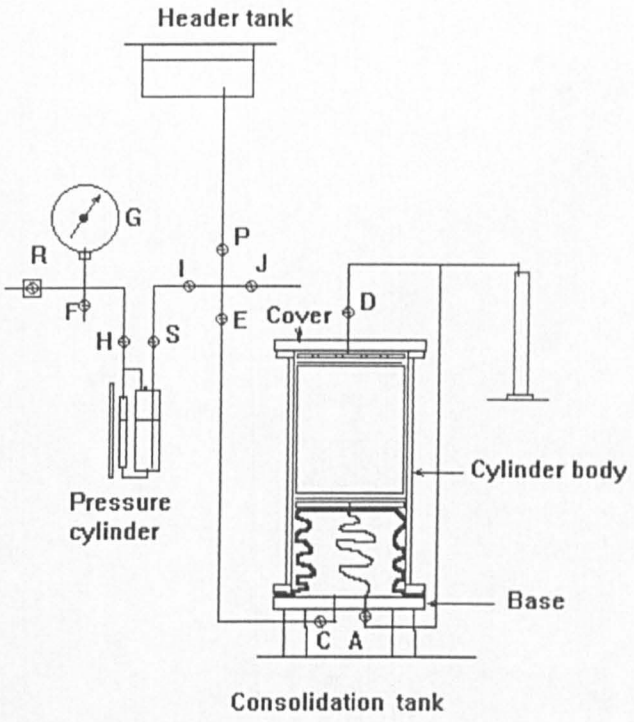

Fig.-A6 Schematic of the large consolidation tank and its plumbing layout

regulator through the air/bladder/water interface. Volumetric changes occuring in the sample could be monitored by measuring the volume of water expelled from the drainage lines and as well as from movement of the top cap as monitored at top of the plunger. With the arrangement shown in*Fig.*-A8, the set up would perform the function of hydraulic oedometer and the falling head permeameter. After one cycle of consolidation and permeability tests, the triaxial cell and cylinder could be removed without much disturbance on the sample.

A3.2 Consolidation cylinder

A vertical section of the consolidation cylinder is shown in*Fig.*-A7. It consists of a piece of thick-walled aluminium cylinder of internal diameter 101.7mm, wall thickness of 12mm and 250mm in height. This cylinder was precision machined to fit exactly around the bottom pedestal and top cap of a triaxial cell for the 100-mm specimen. A plumbing arrangement of the cylinder as enclosed in the triaxial cell is shown schematically in *Fig.*-A7(b). Kaolin slurry inside the cylinder bounded by the bottom pedestal and the movable top cap of the triaxial cell, was compressed vertically, the consolidation pressure being applied to the top cap using the cell pressure. Pairs of O-ring seals were used in the grooves around the bottom pedestal and top cap to avoid any leakage between the cell chamber and the inside of the cylinder. A socket connection between the top cap and the loading piston enabled easy withdrawal of the latter when required after rhe desired consolidation of the slurry was

achieved. When connected, a tolerance of ±1mm in vertical and horizontal directions was allowed at the socket connection to avoid any chances of jamming between the loading piston and the top cap during consolidation process.

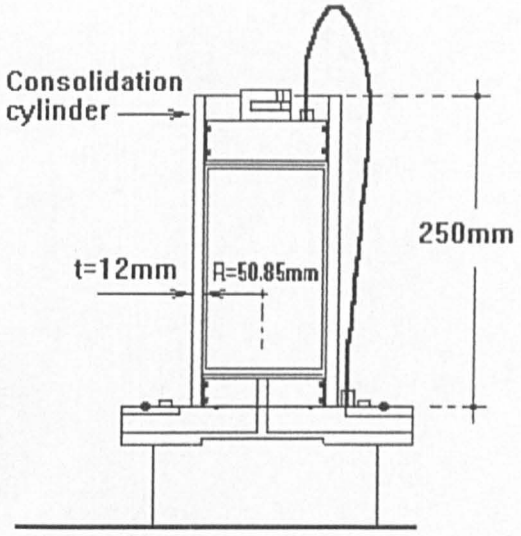

(a)

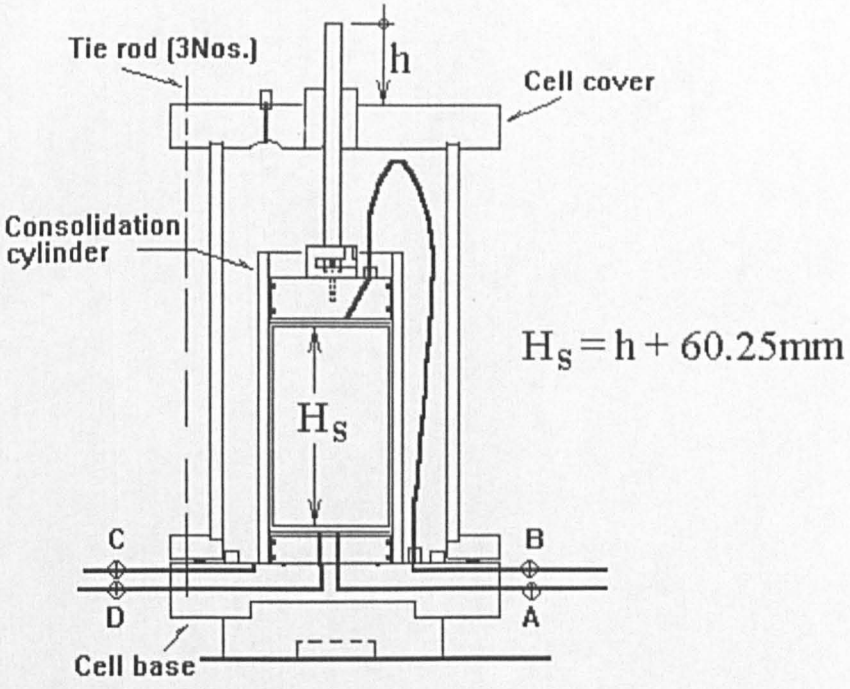

(b)

Fig.-A7 (a) Vertical section of consolidation cylinder
(b) Consolidation cylinder as located inside triaxial cell

B. SAMPLE PREPARATION

B1. Slurry and block sample

Specimens for testing were obtained from kaolin slurry and also from consolidated kaolin block samples. Two groups of clay blocks were prepared to produce specimens of known stress history and with specified drainage pattern for testing.

One group of the blocks was prepared from kaolin slurry consolidated in the large tank and another group was produced from the same batch of slurry and consolidated in a similar manner as the first group in the smaller consolidation cylinder.

B1.1 Making of slurry and consolidation to form block sample

Slurry sample

Kaolin slurry was prepared by mixing kaolin powder and water in an electrically driven drum mixer. Approximately 23.25kg of kaolin powder was mixed with 27,900cm3 of water to produce sufficient slurry for consolidation in the large tank and the smaller cylinder. To meet the capacity of the drum mixer, the kaolin powder and water were divided into 3 equal portions ie. 7.750kg and 9,30Qcm3 respectively.

Slurry was formed by adding small amount of kaolin powder at a time in the volume of deaired water and letting it settled before pouring in the next addition. This procedure ensured full saturation and avoided formation of trapped air bubbles. It was found that 9,300cm3 of water readily accepted kaolin powder to disperse and settle down until the mass of the latter reached about 5.706kg giving a water content of 163%. The remainder 2.0044kg of the powder was similarly added and the mix was mechanically stirred to produce a uniform, homogeneous mass of slurry. Mixing took about 5min after each addition of kaolin and the final slurry was further stirred for about 30min. This procedure was followed for the next two portions of kaolin and water and the whole slurry mass was stored in a large plastic bucket to further hydrate for a minimum period of 48h.

The water content of the slurry was found to be 114%, as determined from representative portions of the stored slurry mass.

Block sample

Block sample was derived from kaolin slurry that has been previously consolidated in the large consolidation tank. Prior to placement of slurry and its subsequent consolidation, it was essential to properly saturate the pressure bellow, the space between the bellow and tank wall, and all connecting drainage lines. This was achieved by applying a vacuum via valve J (*Fig.*-A6), and manipulation of the various valves to let water in from the header tank into the bellow. When the bellow had stretched to about mid-height within the tank valve C was closed. (Valve J was kept closed once the vacuum was stopped and the line fully saturated).

The pressure cylinder was filled with water simply by opening valves P, I, S and the bleed port B located at the cylinder top. Water was allowed to overflow for a few minutes before P and B were closed. A pressure of 10kPa was set up in the cylinder by adjusting regulator R. The tank chamber itself was then saturated from bottom up through the spiralling drainage tube through valve A and letting the water rise to approximately 10mm above the bellow top.

The perforated perspex disc and wet filter paper (2 layers) were then placed over the bellow to serve the dual purpose of providing bottom drainage and minimising the flow of slurry into the sides of the bellow and tank. Any air bubbles found were rubbed off and let to float.

The depth of the bellow top below the rim was noted to establish the initial thickness of the slurry. The kaolin slurry was then poured in small amount with careful and thorough mixing carried out in order not to trap any air pockets. Typical pour consisted of a layer 50 to 100mm thick with the top surface being always submerged under about 50mm depth of water. In this manner development of air pockets during stirring was avoided and a fairly homogeneous mass of slurry was obtained.

When the slurry had reached the top of the tank (approximately 5mm from the rim) the surface was levelled using a straight edge taking care to keep it always underwater. Wet filter paper (2 layers) and a perforated perspex disc were then placed on top of the slurry. Rubber gasket was then placed flat above the the greased rim. Small amount but continous flow of water was let through the top steel cover (through valve D) when covering the top of the tank slowly in order to flush out any trapped air layers. The top of the tank was completely flooded during this operation. The tank was finally sealed off by tightening the bolts (12 nos. altogether) which held firmly the cover and tank. Pairs of diametrically opposite bolts were tightened in sequence.

The completed set up ready for stressing is shown in *Fig.*-B1. The pressure existing in the bellow was increased to consolidate the slurry in the following manner:

1. A small pressure of 10kPa was applied basically to provide a uniform top and bottom seat on the slurry and initiate flow and consolidation. This pressure was maintained until compression of the slurry was less than about 5mm per day;
2. The pressure was gradually increased in stages of 20, 40, 60, 80kPa, insteps of 20kPa until 560kPa. These pressures would also be adopted to those experienced by the slurry in oedometer cells (ie. as in *Table*-3.2, Chapter 3). Each pressure was maintained until the compression rate recorded was less than about 5mm per day;
3. At 9 consolidation stages starting from 60kPa, the pressure on the slurry was released in decrements of 40kPa until 0kPa for the purpose of making block samples. A cylindrical bock sample of thickness 120mm was obtained and it was neatly cut and divided into two (initially) and waxed. During the various phases of this work extreme care was exercised to ensure that the sample was fully supported and subjected to as minimum physical disturbance as possible.

A summary of the stress history for the block sample and taking it out for specimen trimming is illustrated in *Fig.*-B2.

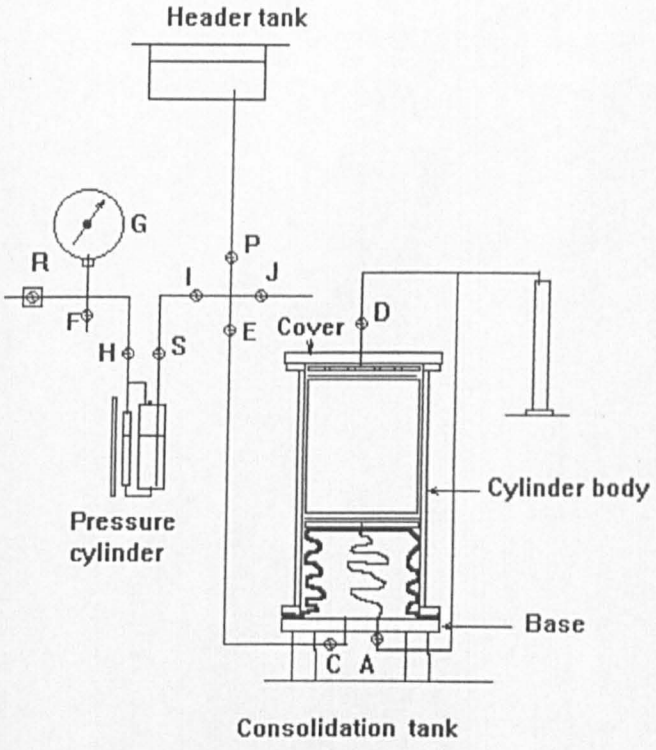

Procedure of applying stress to slurry

1. Valves: A, C, D, E, H, I - OPEN
   B, F, J, P, S - CLOSE
2. Fully saturate lines from D and A and connect to bottom of 50cm3 burette
3. Adjust pressure regulator R until gauge G reads 10kPa
4. Record water level in graduated tube of pressure cylinder
5. Start test by opening valve S. Record water level in (4) and vol. expelled (2) at elapsed times of 0, 15, 30s, 1, 2, 4, 8, 15, 30min etc.

Fig.-B1 Stressing of slurry in consolidation tank

B1.2 Sampling out and waxing

After the desired consolidation pressures had been reached (ie. at consolidation stages of 120kPa and 600kPa), the pressure was released in decrements until 0kPa for the purpose of cutting out for block samples. Unloading was made under fully drained conditions with valves A and D opened and tips of tubing always under water [*Fig.*-B1 for tank sample or valves A, A2 and B, B2 in *Fig.*-A7(b) for cylinder sample].

Tank sample

Close valve C. Ensure that tips of tubings at D_{out} and A_{out} are under water. Open valves A and D. ie. the stress in the sample is now released.

Loosen up and remove all screws on the cover. Ensure that the pressure cylinder is fully filled up. Set the bellow pressure to about 100kPa. Remove the top cover. Open valve C and S so that the pressurised bellow will push up the sample. When the sample had projected to 120mm close valve S.

Remove the top filter papers. A cylindrical block sample of thickness 120mm and diameter 300mm could now be obtained by cutting it horizontally along the rim of the tank using a wire saw. After two or three cuttings the whole block should be easily pushed and slid across on to a ready held flat plate to fully support the sample.

The block sample was further cut into two pieces to the shape shown in *Fig.*-B3 in a special shape perspex box. The samples were completely waxed and stored in a humid chamber pending further cutting and testing.

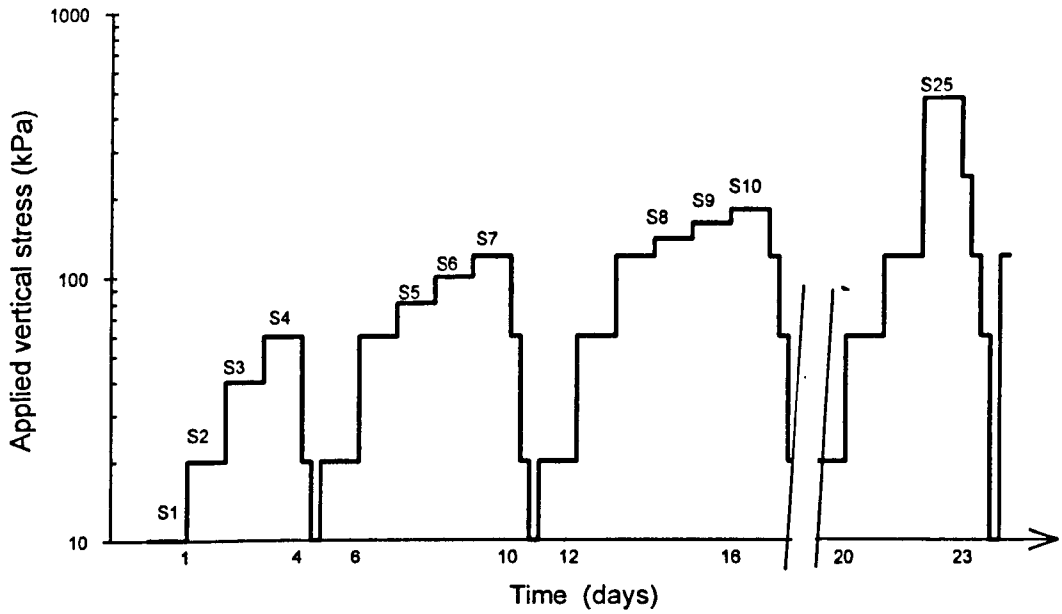

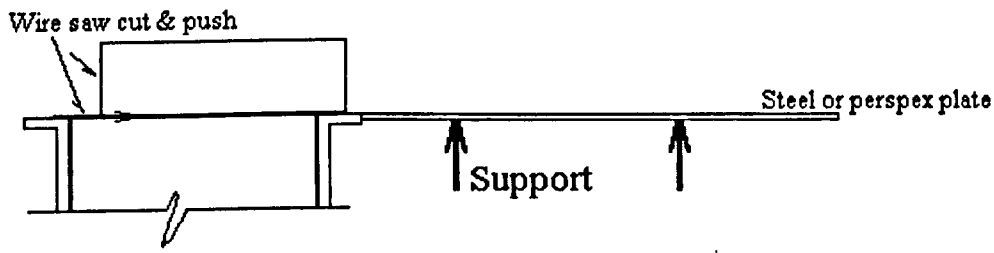

Fig.-B2 Summary of stress history for block sample and removing sample from tank

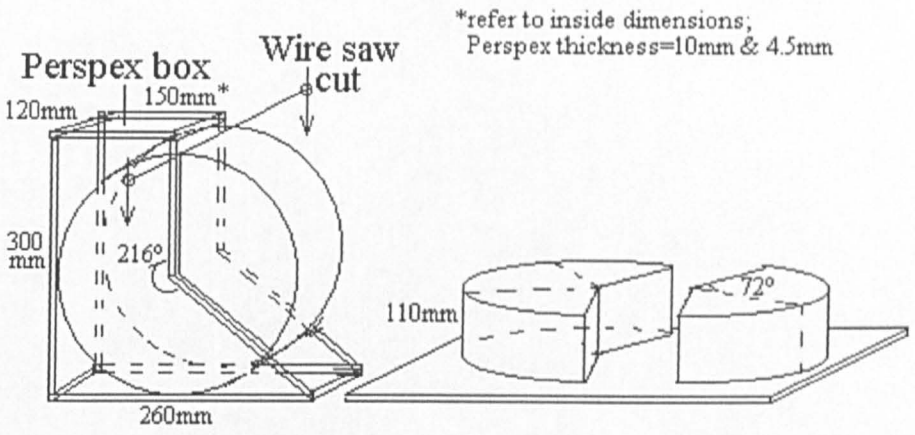

Fig.-B3 Cutting block sample for waxing & storage

Cylinder sample

1. Record the final gauge reading and the corresponding height of the plunger top to the cell cover. Drain off the cell water. Close valves A and D.

2. Disengage plunger from the top cap and extend it to the maximum upward travel.

3. Loosen and remove the tie rod screws (3 nos.). The cell body could now be removed. The cell base was clamped to the compression machine if necessary.

4. To pull out the top cap, a threaded rod guided loosely through a rigid bar was used. The pin at the end of the rod is connected to the socket of the top cap, and by turning the nut clockwise the cap was gradually pulled up [see *Fig.*-B4(a)].

5. Next the cylinder was pulled up using the same technique as in (4) above but a longer threaded rod and a fixed perspex piston were used. The assembly shown in *Fig.*-B4(b) consists of a nut (integrated with collar) threaded along the rod and passing loosely through lifting disc. A fixed perspex piston was attached at the bottom of the rod. When the rod and piston had been lowered down to just touch the top surface of the sample, its top end was fixed at the upper part of the compression machine. The lifting disc was fastened to the cylinder top. With the triaxial base clamped against uplift, the cylinder was steadily pulled up by turning the nut counter clockwise. It is now evident that as the cylinder is pulled up, out of the base pedestal, the perspex piston remained stationary keeping the sample in position over the base.

6. Once the cylinder was just becoming detached from the base (no more than a mm), the top end of the rod was loosened from the upper part of the compression machine. The cylinder and sample inside were carefully slid to rest on to a flat perspex plate (similar operation as in Fig.-B2). Because of the greased cylinder wall the sample would normally remain behind when the cylinder was lifted up slowly.

B1.3 Trimming & cutting and setting up of specimen for testing

Oedometer specimen from slurry

Supreme kaolin slurry at an initial water content of 114% was set up in the oedometer as shown in *Figs.*-B5. Descriptions given below apply to setting up slurry sample in either the vertical flow or the radial flow oedometer. However, in the radial flow case, the perforated brass disc and filter paper were replaced by a filter paper and a central drain brass piece [see *Fig.*-B5(b)(ii)]. The inner wall of the cell formed the peripheral drain and therefore it must not be greased as was the case for the vertical flow cell.

Sample set up was carried out under water in a trough to ensure proper saturation. Porous metal disc and plastic sheet (1.5mm thick Vyon) were saturated by boiling them for an hour and keeping them immersed in the boiled water at all time. Drainage lines through the base and cover of the oedometer were fully saturated by thorough flushing with deionised and deaired water and their ends were then fully closed or placed under water. In *Figs.*-B5(a) to B5(c) the oedometer cell is in an inverted position. The position of the spacer shown therefore occupy the top part of the specimen.

The order of setting up is as follows: (refer *Fig.*-B5)

1. A circular perspex plate with a spacer were placed in the water-filled trough as shown in *Fig.*-B5(a). An oedometer ring was then positioned around the spacer. Any air bubbles found sticking on the cell wall or spacer were removed. Similar removal of air bubbles was applied to later operations where required. Saturated perforated brass disc and the porous plastic (Vyon) were placed over the spacer. The slurry was then spooned evenly throughout the area in the cell using a pair of spatula.

2. When the cell was completely filled up the surface of the sample was levelled using a spatula. To allow for the small projected depth of the oedometer base (=1.5mm), a pre-formed thin perspex piece was used to level the slurry surface [*Figs.*-B5(b)(i) and B5(b)(ii)].

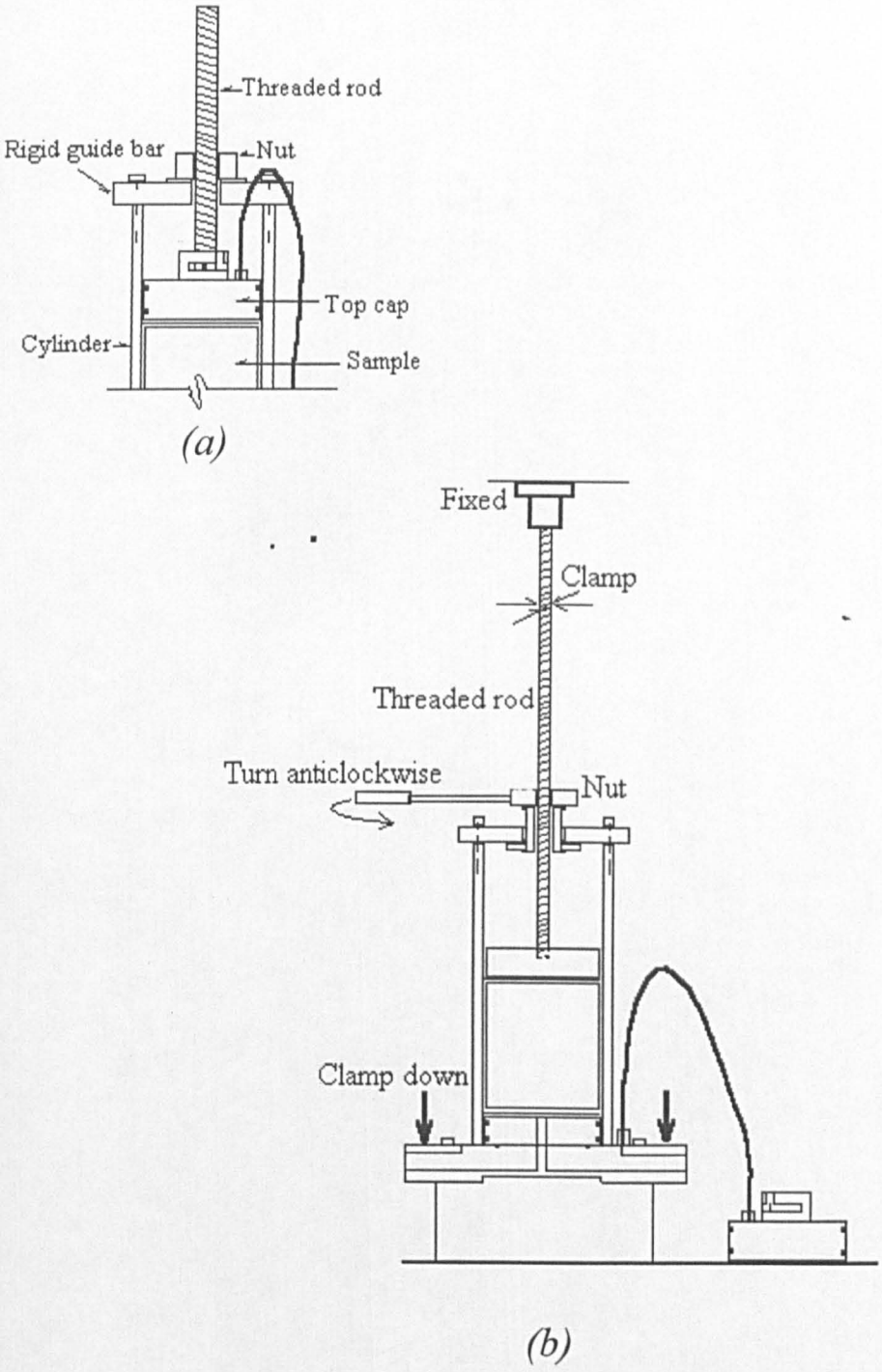

Fig.-B4 Removing consolidated sample from the consolidation cylinder

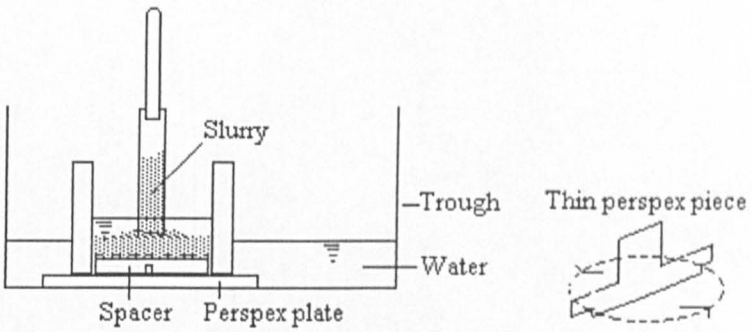

(a)

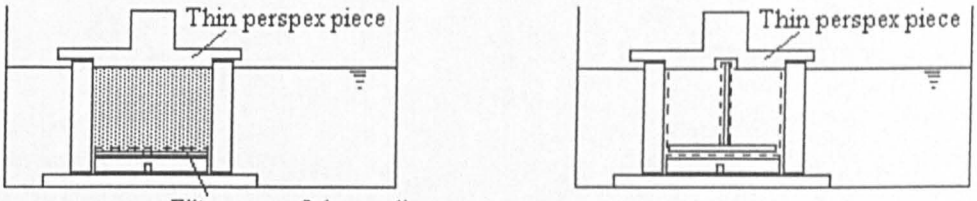

(b)(i) (b)(ii)

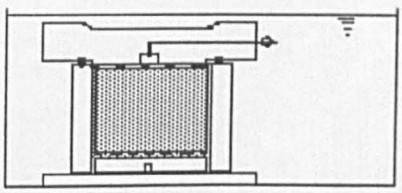

(c)

Initial ht. of sample:

$H_h = 55.6-(a+b+t+1.5)$ mm

$H_v = 55.6-(a+b+2t+1.5)$ mm

a=ht. of spacer block
b=thk. of brass disc
t=thk. of porous plastic

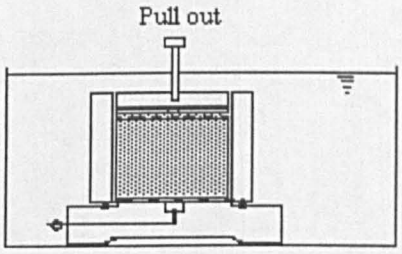

(d)

Fig.-B5 Setting up of slurry sample into oedometer

3. A saturated filter paper was then placed on top and the surface was topped up with deaired water. Meanwhile, the ring bottom was evenly greased and the base was then placed over the ring, taking care not to drop the O-ring seal inside its groove [*Fig.*-B5(c)].

4. The inverted oedometer (base and ring held firmly) was then turned quickly to its upright position and the spacer was slowly pulled out [*Fig.*-B5(d)]. The saturated diaphragm (or convoluted rubber jack) and oedometer cover was fitted and tightened taking care that the greased contact between cover, diaphragm and ring was fully flat and even. To tighten the cover, all three nuts were tightened at once in equal turns to ensure uniform seals at the top and bottom of the ring.

The completed sample set up is similar to *Fig.*-A2 and the complete assembly of the consolidation/permeability apparatus is shown schematically in Fig.-A4. All connecting drainage lines (in Fig.-A4) were saturated by thorough flushing with deaired water supplied from the header tank.

Oedometer specimen from block sample

Trimming and cutting of block samples is carried out under conditions of full support. A procedure and device similar to that described by Landva(1969) is adopted. Further techniques for trimming and mounting procedures whereby the clay sample is directly extruded into the oedometer ring has been described by Sandbaekken et al.(1986).

1. A hand operated hydraulic jack sample extruder [*Fig.*-B6(a)] is used to push and cut specimen directly into oedometer ring through an adapted cutter ring [*Fig.*-B6(b)]. Steps (i) to (iv) are shown in [*Fig.*-B6(b)]. The plate (A) is clamped to two vertical rods which are fixed to the base plate attached to the top of the hydraulic jack [step (i)]. The cutter ring (B) appropriate to the diameter of sample that is required, and the corresponding oedometer ring (C) (with external radial drain in position for a horizontal flow sample) are located on plate (A) [step (ii)]. The oedometer ring is held down by brackets (D) to prevent it from lifting as the sample moves through it. The cutting ring, and the oedometer ring (when there is no radial drain) are lightly oiled to reduce friction with the sample.

2. A block of clay (cut from the waxed sample *Fig.*-B3) is placed on the piston of the extrusion ram and jacked up slowly against the cutter ring (B) [step (iii)]. Excess clay is trimmed off as the block of soil is raised steadily until a sufficient height of clay has been enclosed in the cutter ring and oedometer ring.

2(a). For the radial flow sample, the brackets (D) were removed to allow for locating the drill guide so that a hole 11.4mm dia. could be formed in the sample for insertion of the central drain later on [*Fig.*-B6(b)(i)]. For this purpose a central drainage hole was formed using the a standard drill bit (of diameter 11.0mm for the 75mm diameter samples) guided by a perspex block which located on top of the oedometer ring.

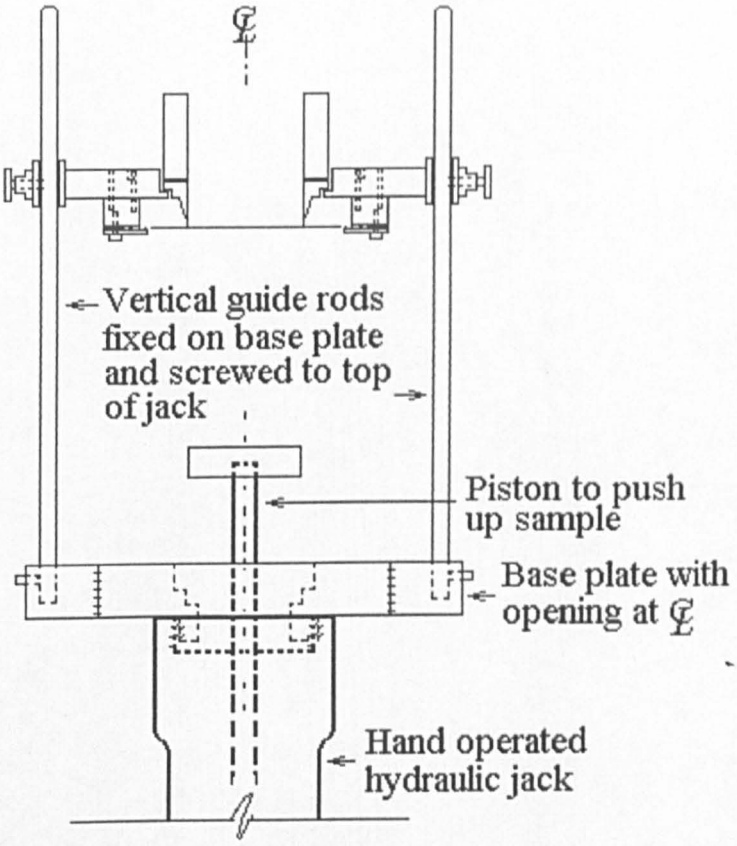

(a)

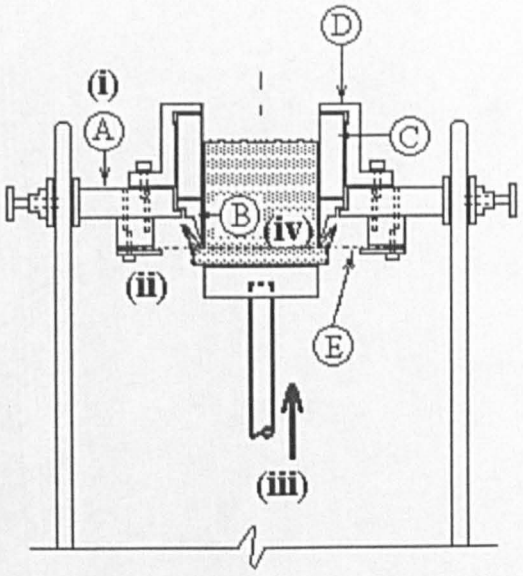

(A) Support plate attached to sample extruder
(B) Cutter ring
(C) Oedometer ring
(D) Bracket holding down oedometer and cutter ring
(E) Cutting line of wire saw through sample.

(b)

Fig.-B6 (a) Sample extruder and adaptation for setting up block sample; (b) Jacking up sample into oedometer ring

3. A clean lower face to the clay sample is now formed by first cutting through the clay against the cutter ring using a wire saw and then sliding a knife-edge plate(E) through the sample at this same level [*Fig.*-B7 (a)]. This plate slides in grooves on brackets attached to the plate (A).

4. With the sample now supported on plate(E), the piston is lowered and the remaining clay on it is removed and replaced by a perspex spacer block of the correct height and of diameter just to fit inside the cutting ring (B). For vertical flow sample the top drainage and the rigid brass disc were placed on the spacer block to provide the top drainage boundary.

For horizontal flow sample the porous plastic disc and the central drain were placed on the spacer block to form the central and peripheral drainage boundaries.

It is noted that actually the use of the knife-edge plate (E) could be avoided because it interferred too much with the 'adhesive' surface of the sample causing smearing for vertical sample and surface distortion for vertical and horizontal samples. Therefore with experience and skill, after the wire cut, the piston was lowered, the remaining clay on it quickly removed and replaced by the spacer block and drains/platen and proceed to 5 below without the plate (E).

5. The ram is now raised again until the perspex block is in contact with plate(E) which is now removed. The ram is further raised, until the perspex block has just entirely entered the cutting ring(B) and the plate(E) reinserted [*Fig.*-B7 (b)]. This ensures that once the surplus clay now protruding from the top of the oedometer ring has been trimmed off with a wire saw and pallet knife, the sample height could be precisely determined [*Fig.*-B7(c)].

6. The clamps are released so that the whole assembly can be removed from the hydraulic jack and placed on a table top [*Fig.*-B7(d)]. For the vertical flow sample a saturated porous plastic was placed over the sample followed by putting the oedometer base. An O-ring provides a seal between the oedometer ring and the base.

For the horizontal flow sample, the oedometer base (surface lightly greased) was positioned over the sample and ring without any porous disc. The cutting ring and perspex block are removed with Plate(A), leaving the sample in its ring on the base.

7. With a firm hold on the oedometer base, ring and Plate(A), the whole assembly was quickly turned upside down to the upright position. Holding down the oedometer ring & base, the holder could now be removed followed by the cutter ring and spacer block.

With this position the sample was secured in oedometer ring and base with the bottom drain fully saturated. Valve B always shut.

8. A layer of water was placed at the top surface of the sample and the oedometer cover, with the shaped jack membrane, was attached carefully, avoiding the trapping of any air between the membrane and the clay with its drainage boundaries.

The cover was tightened taking care that the greased contact between cover, diaphragm and ring was fully flat and even. To tighten the cover, all three nuts (3 nos.) were tightened one after the other in equal turns to ensure uniform seals throughout the top and bottom surface of the ring.

9. Clay that had been trimmed during this sample preparation process was used for determination of natural water content and the liquid and plastic limits. The liquid limit was determined using the fall-cone technique [Test 2(A) in BS1377, 1990] and the plastic limit determined by rolling out a clay thread (Test 3 in BS1377, 1990).

10. A completed sample in the vertical and radial flow oedometer is shown in *Figs.*-A1(a) and A1(b) respectively. Final deairing and saturating is performed by drowning the whole oedometer in water and opening all valves (A, B, D and plug P) and apply vacuum for about 15-30 minutes (The dial gauge G and post was not fixed yet).

Triaxial specimen

1. Consolidated sample from the cylinder (dia.=101.7mm), after extrusion was cut using a fine wire saw to a length of 102mm as shown in *Fig.*-B8(a). Block sample from the tank (after stripping off the wax) was trimmed to dimension 101.7mm in diameter and 102mm in length using the standard soil-specimen trimming frame as shown in *Fig.*-B8(b). A wire saw was used to cut the sample vertically as guided by vertical sides of the frame. The sample rested on circular base such that after each cut it could rotate freely for the next vertical cut. The cutting and rotating process was repeated many times until a smooth-sided right circular sample is obtained. This trimming procedure is similar to that practised in the Norwegian Geotechnical Institute as described by Simon and Bjerrum(1960). After completing the trimming process, the triaxial specimen was placed into a humid dessicator and the clay trimmings were quickly weighed to minimise moisture loss.

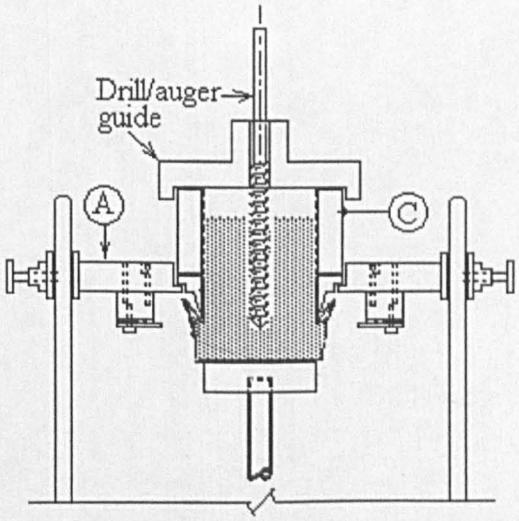

Fig.-B6 *cont.* (c) Jacking up and forming central hole for radial flow sample into oedometer ring

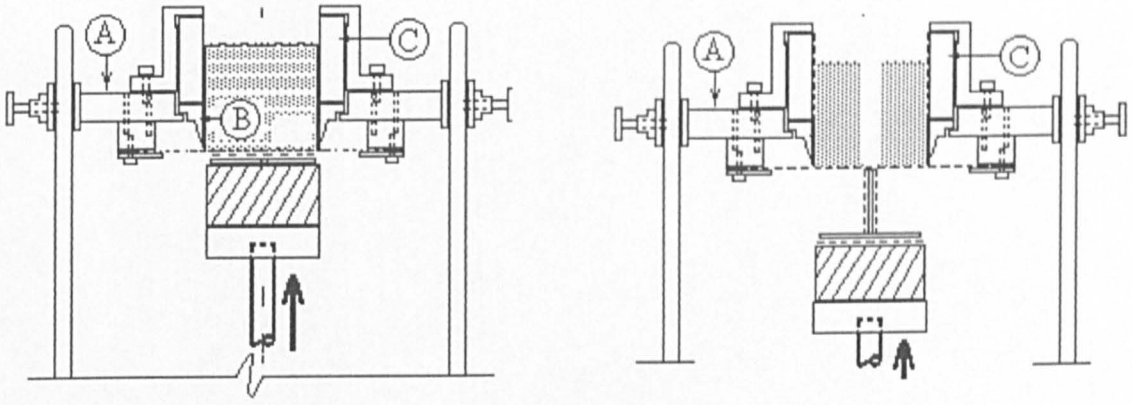

(a)

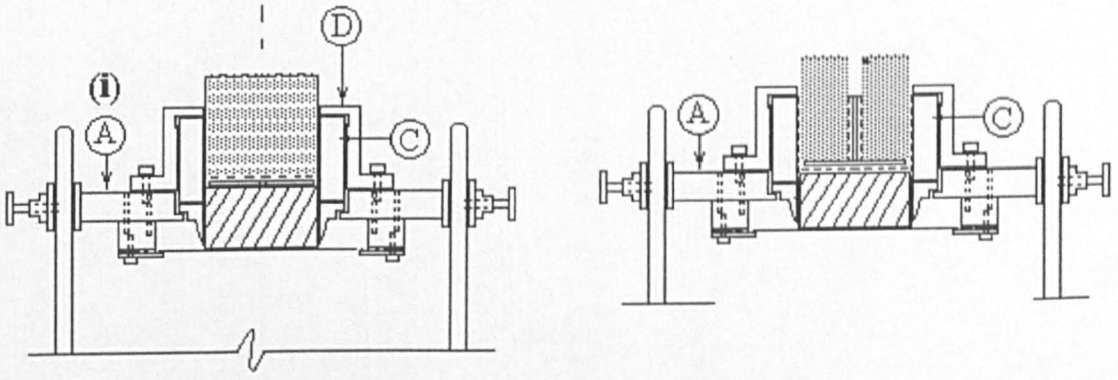

(b)

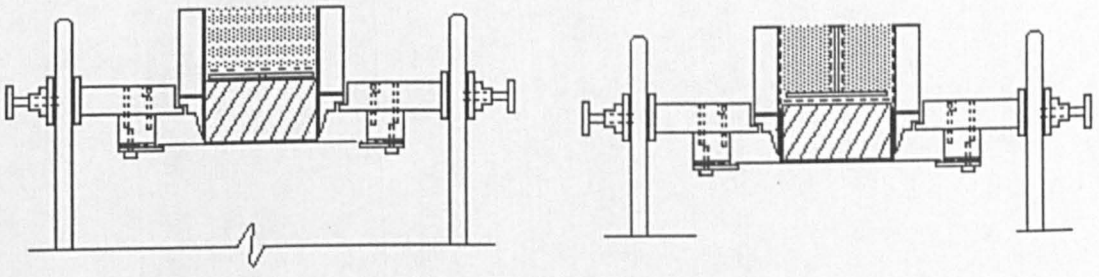

(c)

Fig.-B7 Stages of setting up block sample

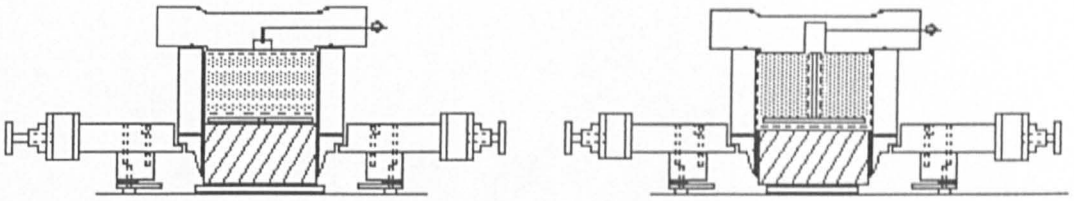

(d)

Fig.-B7 *cont.* Stages of setting up block sample

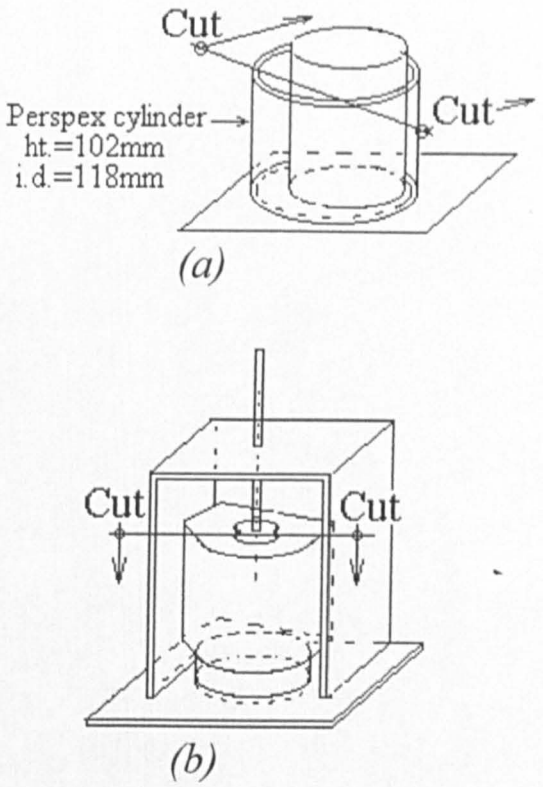

Fig.-B8 Cutting or trimming of sample for triaxial testing (a) Cylinder sample; (b) Tank sample

B2. Setting up of apparatus & specimen

B2.1 Consolidation and permeability test

Initial preparation

1. Saturate the drainage lines with deaired water from header tank by manipulating the opening and closing of various valves in a systematic order. After meeting the full saturation condition, all valves should have been closed.

2. Next step is to initialise and equalise the zero readings of GDS1 and GDS2. This is usually performed at regular intervals (weekly) as follows: Close A, B and open C, D1. Target pressures in the two GDS to zero (ie. zero reading). Close C and open A, B. For the weekly routine, before the*last statement*, close D1 and target pressure to 50kPa.

3. Drainage lines could now be pressurised to maximum back pressure, BP of 50kPa. This is done simultaneously on the sample as well. The details are covered in C1.2 - *Back pressure stage*.

Initial measurement

4. Normally the initial conditions of the apparatus and sample were as follows:

Valves:

A, A1, B, B1, D, E - open

C, C1, D1, D2, F - close;

GDS1 & GDS2: Target pressure set to 50kPa and data logging on;

Cell pressure regulator, R: Pressure set to 60kPa;

Dial gauge, G: Readings monitored regularly until completion of consolidation was evident.

This initial stage had been previously set and left for over 24h to let the specimen stabilise with a pore pressure of 50kPa and vertical effective stress of 10kPa. The dial gauge reading was noted and the data logging was switched on at 1-min interval.

B2.2 Triaxial testing

Initial preparation

1. Saturate the pore pressure line with deaired water. Plug the base pedestal, apply maximum working pressure and leave under pressure for several hours. A substantial volume change indicates a leak, which must be rectified.

2. Close valve A, remove plug and open valve A slowly to let more water coming out to form a small pool. Place a small filter paper..

3. Connect valve D to another source of deaired water and flush up to the base pedestal. Close valve D.

4. Smear the base pedestal with silicone grease and position the rubber membrane. [See *Fig.*-B9(a)]. Similarly apply an even smear of silicone grease on the smooth surface of the top pedestal and position the rubber membrane. The central area of about 10mm dia. on the pedestals must not be greased but placed with wet filter papers (10mmx10mm sq.) instead for the pore pressure and drainage lines.

5. Saturate the backpressure line up to B1. Close valve B. The line from the top pedestal to tip of the tubing (to be connected to B1 later on after setting up specimen) is also saturated by temporary connection to a rubber tubing and filling the whole length with water. End of rubber tubing is clipped to stop water escape. Grease evenly sides of base and top pedestals. Get a new rubber membrane to enclose the specimen. Used the membrane stretcher, apply vacuum (-5 to -10psi) and get ready to cover the specimen.

6. Let some water to pool on the rubber membrane on the base pedestal.

Setting up

7. Carefully position the specimen on the pedestal. Any surplus water pool on the membrane will be pressed out under the specimen. Next pool some water on top surface of the specimen and similarly place the top pedestal carefully on the top surface of the specimen.

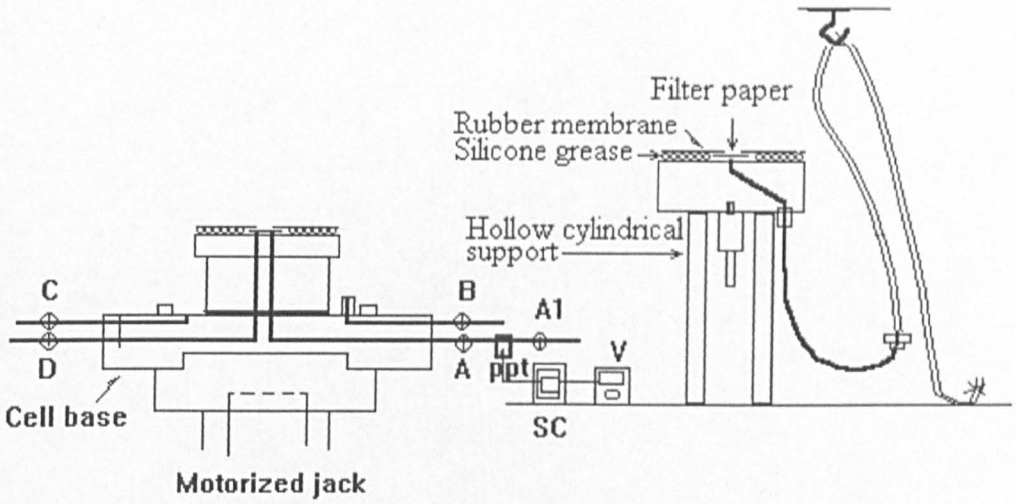

Fig.-B9(a) Saturation of drainage & pore pressure lines and preparation of smooth base and top pedestals

8. Place a small plastic tubing around the top and bottom pedestals as shown in*Fig.*-B9(b). The purpose of the plastic tubing is to release any trapped air when the membrane grip the specimen in step 9 below. Previous experience indicated that without this means of opening, the air trapped would cause the top pedestal to be raised and got hung up over the specimen since the air could not escape and the membrane cover the pedestal earlier rather than the specimen side.

9. The specimen as positioned is now ready to be enclosed by the laterally stretched rubber membrane. Pass the membrane carefully all the way through top drainage line until it enclose completely the top and bottom pedestals. Now slowly release the vacuum so that the membrane could snugly cover the specimen side and pedestals. Adjust the membrane lightly so that it follows truly vertical and horizontal surfaces of the pedestals as well as the specimen sides. The small plastic tubes can now be removed.

10. A pair of O-ring seals could be snapped carefully around the bottom and top pedestals. Extreme care is required to avoid accidental release of O-rings to the sample.

11. It is now left to connect the drainage line to B1. Before this, raised the tip of the tubing slightly higher than the top pedestal and slowly open the clip so as to force some more water into any space within the specimen and membrane under a small head. Tighten up the clip again and now carefully remove the rubber tubing from the drainage line under water. Quickly fasten the tip to B1 and tighten the screw connection. *This step conclude setting up of the triaxial specimen.* The next step is to place the triaxial cell on its base, connect plunger to the pedestal top, fill up cell chamber with water and commence the saturation and reconsolidation process.

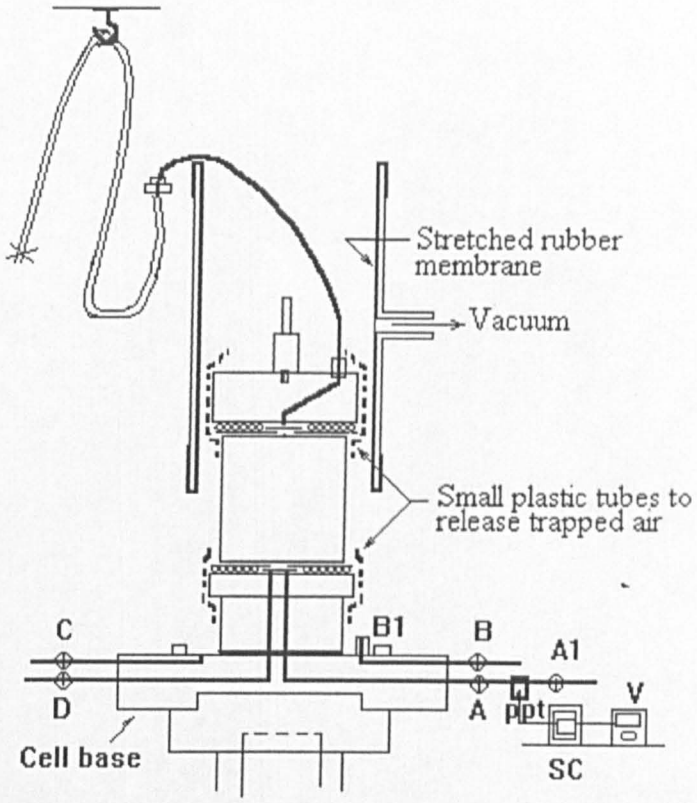

Fig.-B9(b) Enclosing the rubber membrane

12. Before placing the triaxial cell, ensure that the plunger is raised up, the outside and inside portion of its length is generously applied with silicone grease (to minimise friction and leakage), and the O-ring on the cell base is greased. Carefully and avoid touching the specimen and pedestal, lower the cell into position. During this operation the back pressure line should be guided to loosely wind its way around the specimen. When the cell is correctly positioned on its base, the three tie-rod screws could be easily engaged and tightened.

13. Allow the plunger to fall slowly into contact with the top pedestal connection. The conical entrance would ensure easy attachment if the specimen is slightly misaligned. The threaded connection was completed by turning the plunger clockwise until some resistance was felt.

14. Fill the cell with water (deaired) through valve C with the air bleed E open. Close valve C when water begins to emerge from E. Keep the bleed E open until the cell is about to be pressurised, to maintain the cell at atmospheric pressure. The specimen is now ready for starting the saturation stage of the test.

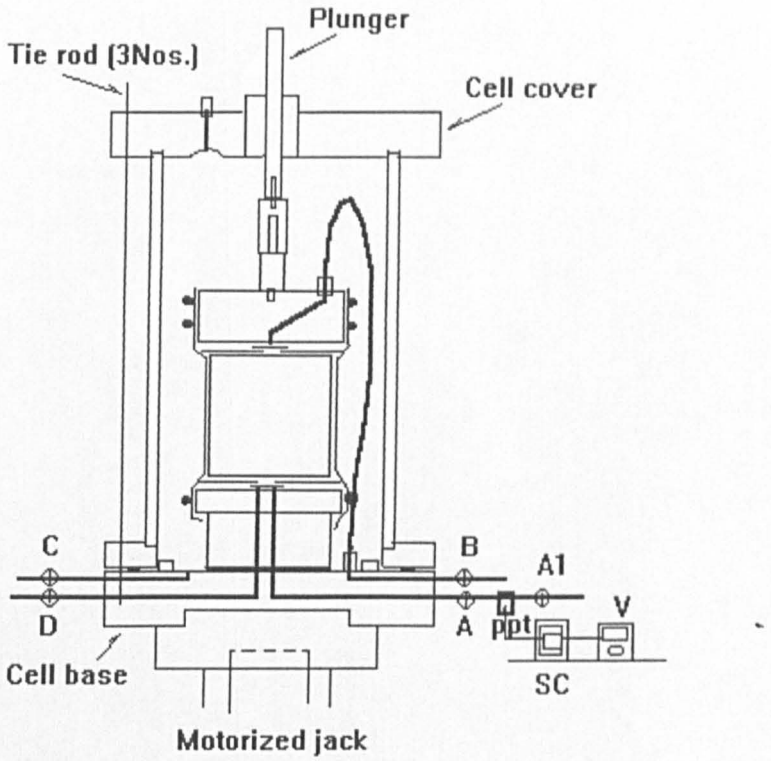

Fig.-B9 Apparatus preparation & setting up of triaxial sample

C. EXPERIMENTAL PROCEDURE

C1. Consolidation and permeability test

C1.1 Calibration of equipment readings

Data readout adjustment

Due to equipment characteristics, each GDS was observed to register slightly different pressure readings for the same pressure ie. even though they are interconnected and the valve between them (valve C in *Fig.*-A4) was opened. In performing consolidation tests later on, it is much easier to have the two GDS set to target for the same pressure giving the same readings (ie. back pressure of 50kPa). Similarly, in the constant head permeability test, pressure in one GDS was increased while pressure in the other GDS was decreased by equal amount without much confusion if the two GDS have been referred to the same zero reading value. For this reason it was desirable to equalise the pressure readings of GDS1 and GDS2.

Pressure readings in the two GDS were equalised by closing A, B and opening C, D1, and setting target pressures to zero. D1 was then closed, target pressures set to 50kPa, C closed and A, B opened. The zero readings of the GDS here refer to atmospheric datum.

Fixing dial gauge position

Dial gauge G - The gauge stem was adjusted until it reached the near top end of its travel, but not fully compressed. This gave ample downward movement required, of approximately 14mm, as the sample is compressed later on.

Calibration of jack and GDS pressures

Readings of the pressure gauge J were calibrated against the GDS pressure so that the correct consolidation pressure could be inferred later on. This calibration was performed after completing the GDS data readout adjustment above. Close A, B and D. Disconnect the tube at D and connect it to D2. Open D1, D2 and E and flush the line with water by raising pressure regulator R slightly. Reduce R so that J reads zero. Close D1 and log the GDS to record readings at 1-min interval. The jack pressure was raised every minute in increments of 10kPa for the first 100kPa and thereafter in 20kPa until the pressure reached 650kPa. Reduce the jack pressure in similar manner but at larger decrements (say 50kPa).

C1.2 Saturation

Back pressure stage

The two GDS were fixed to their target volume mode according to their respective volumes displayed to achieve the undrained condition in the sample. The jack pressure, ie. the vertical total stress σ_v was raised in steps of 10kPa every 2 min until 60kPa for both slurry and block samples. If the sample is fully saturated and there is no leakage in the system, the pore pressure increase will equal the jack pressure increment (ie. 10kPa) in a short time. When the jack pressure has reached 60kPa the two GDS should display pressures of 50kPa. The back pressure in the sample was finally brought to 50kPa by setting the GDS to target pressure mode of 50kPa.

With this procedure, the initial consolidation pressure was brought to 10kPa in both the slurry sample and block sample.

C1.3 Consolidation test

Testing procedure for consolidation test has been described briefly in Section 3.4.1 of the Thesis. Further details are as follows:

1. Record dial gauge reading.
2. Log GDS at 1-min interval (open into file V2)
3. To start consolidation, adjust R to 70kPa immediately after one of those 1-min interval and record G at elapsed times of 10, 15, 30s, 1, 2, 4, 8, 15, 30min, 1, 2, 4, 8, and 24h.
4. After the first 15min log the GDS at 15min interval (open into file V2A).
5. For the next consolidation stage repeat 1 and 2 but now open into file V3 and follow the same steps 3 to 4 above with R adjusted to 90kPa in Step 3. Data file opened will be V3, V3A.

C1.4 Permeability test

As for the consolidation test, testing procedure for permeability test is described in Section 3.4.2 of the Thesis. The following notes apply:

1. Pressure head across the drains is limited to 30% of the consolidation pressure.
2. At beginning and end of test always record dial gauge reading.
3. When setting target pressures or ramp in the GDS always reply 'NO'. Reply 'YES' at logging stage only. This ensures that the two GDS will be acti· :ed together at the same instant.

Constant head test

Consider end of stage V2 ie. Jack pressure = 70kPa, σ'_v=20kPa (Vertical flow).

1. Log GDS at 1min interval (open file 3V2)
2. Target pressures in GDS1 to 49kPa and GDS2 to 51kPa. Log GDS at 1min interval (open file 3V2A).
3. After the first 15min, log GDS at 15min interval (open file 3V2B).

Constant flow rate test

1. Set positive ramp of 3s in GDS1 and negative ramp of 3s in GDS2. Log GDS at 1min interval (open file 4V3).
2. After the first 15min, log GDS at 15min interval (open file 4V3A).

C1.5 Dismantling after test

At the end of unloading stage, usually the jack pressure had been decremented toσ_v=60kPa, and the back pressure was still u=50kPa. The final dial gauge reading was recorded. Under this condition, valves D, A and B were closed and the GDS were switched to stand by mode. Pressure leads leading to A, B and D were detached. Loosen the three tie-bolts and the oedometer top cover was prised open. The sample height was recorded. Sample from the vertical oedometer was cut into 4 equal quadrants, and that from the radial oedometer cut into two for determination of final water contents.

C2. Triaxial test

C2.1 Saturation

General

1. The specimen is saturated by back pressure applied in 3 increments. The back pressure is applied to the specimen following every undrained increment of cell pressure. The first two cell pressure increments are 50kPa and the third is 100kPa. A differential of 10kPa (ie. cell pressure - back pressure = 10kPa) is maintained after each back pressure increment. The final back pressure is 200kPa ie. when the cell pressure is 210kPa.

2. Initially valves B and C are closed. Valves A1 and D are always closed and A always open to enable the pressure transducer to measure pore pressure. Record pore water pressure as u_0, $\sigma_3 = 0$, and BP = 0. Typical data entry for triaxial saturation is shown in the table below. For triaxial cell details and drainage/pressure lines layout refer *Figs.*-A5 & 3.5(a).

Saturation procedure

3. Increase pressure in cell pressure line to 50kPa. Wait about 5min to allow for any expansion of pressure lines.

4. Open valve C to admit the pressure into the cell. The cell pressure increase will cause an increase of pore water pressure in the specimen.

5. When the pore pressure is steady, record it as u_1.

6. Calculate the initial value of the pore pressure coefficient B from the equation $B = \Delta u/\Delta\sigma_3$ $= (u_1-u_0)/\Delta\sigma_3$

7. Up to this step valve C is opened while valve B is closed.

8. Increase the pressure in the back pressure line to 10kPa below the cell pressure ie. to 40kPa for the first step. Wait for the back pressure volume burette reading to reach a steady value, then record it in the 'before' column as V1.

9. Open valve B to admit the back pressure into the sample. Observe the increase of pore pressure on the voltmeter. Also keep under observation the flow of water into the specimen through the back pressure volume gauge. Allow the pore pressure to build up.

10. When the pore pressure is virtually equal to the back pressure, or when the pore pressure or volume changes have ceased, record the pore pressure u_2, the back pressure volume gauge as V2(under 'after') . Close valves B and C.

11. Increase the pressure in the cell line, as in step 3 by 50kPa to give 100kPa.

12. Repeat operations described in steps 4 to 10. The pore pressure increases from u_2 to u_3 in response to the cell pressure increase from 50 to 100, giving the B value derived on Row 4. The back pressure is increased to 90kPa at step 8 (Row 5 and P4) and the pore pressure increases to U_4 at step 9.

13. Read all subsequent pore pressures on the pressure gauge.

14. Increase the cell pressure by 100kPa but otherwise proceed as in step 3. Repeat steps 4 to 10 again, giving pore pressure values represented by U_5, U_6 (R_6C_4 and R_7C_4). The back pressure is increased to 10kPa below the cell pressure at step 8.

15. Repeat step 14 as many times as necessary until the B value calculated at step 6 reaches 0.97 or greater.

16. When the coefficient B reaches 0.97, saturation is terminated by closing valves C and A and omitting steps 7 onwards. The specimen is then ready for consolidation stage.

σ_3(kPa)	BP=u(mV)	u=	Δu(mV)	B-value	Before	After	
0		u_0					
50	-	u_1	(u_1-u_0)	$(u_1-u_0)/50$			Step 5 & 6
50	40	u_2			V1	V2	Step 10
100	-	u_3	(u_3-u_2)	$(u_3-u_2)/50$			Step 11
100	90	u_4			V3	V4	Step 12
200	-	u_5	(u_5-u_4)	$(u_5-u_4)/50$			
200	190	u_6			V5	V6	
210	-	u_7	(u_7-u_6)	$(u_7-u_6)/50$			

C2.2 Consolidation

General

1. The consolidation stage follows immediately after the saturation stage. Consolidation of the specimen is isotropic although drainage condition is one way (ie. toward the back pressure line at the top pedestal). The object of the consolidation stage is to bring the specimen to the state of effective stress required for carrying out the compression test. Data obtained from the consolidation stage are used to:

* estimate a suitable rate of strain to be applied during compression
* determine when consolidation is complete, and
* compute the dimensions of the specimen at the start of the compression stage.

2. The effective stress in the specimen is increased to the desired value by raising the cell pressure and dissipating the resulting excess pore pressure to an appropriate back pressure. The specimen is consolidated in one single stress increment.

Procedure

3. After completion of the saturation stage, the back pressure and cell pressure valves are closed and the final pore pressure and volume change indicator readings are recorded.

4. Close valves A_1, B and C. (D always remain closed). Increase the pressure in the cell pressure line and adjust the back pressure if necessary, to give a difference equal to the required effective consolidation pressure (σ_3') such that $\sigma'_3 = \sigma_3 - u$

eg. for σ_3 = 500kPa, u = 200kPa, then $\sigma_{3iso'} = \sigma_{3iso} - u$ = 300kPa.

5. Open valve C to admit the cell pressure and observe the consequent rise of pore pressure. Record pore pressure and volume gauge readings when they are steady. Calculate the new B value from changes of pore pressure and cell pressure. The difference between the final steady pore pressure and the back pressure (as yet isolated from the specimen because valve B is still closed, is the excess pore pressure to be dissipated during consolidation.

6. Set the clock to zero and record pore pressure and volume gauge readings on the consolidation test sheet as zero values.

7. Start the consolidation by opening the drainage line (ie. valve B of the back pressure line) at instant of starting the clock.

8. Record readings of dissipation of pore pressure and back pressure volume change burette at time intervals similar to those used in the oedometer consolidation test.

9. Plot graphs of sample volume change against log time. The consolidation stage is deemed complete when at least 95% dissipation is reached.

10. Terminate the consolidation stage by closing valve B. Leave valve C open. The end of stage pore pressure measured at the sample base is denoted by u_1 so that

$$\sigma_3' = \sigma_3 - u'$$

where u' = mean pore pressure within the sample. Pore pressure at the top is equal to the back pressure u_b. Assuming a parabolic pore pressure distribution,

$$u' = (2/3)\, u_1 + (1/3)\, u_b$$

However, if the measured pore pressure u_1 is within a few kPa of the back pressure, u' can be assumed equal to the arithmetical mean pressure $(1/2)(u_1 + u_b)$.

11. The consolidated specimen is then ready for the undrained compression test.

C2.3 Compression

General

1. This test is designated as CIU test with pore pressure measurement. It is an isotropically consolidated undrained test. In the test during the compression stage the cell pressure is maintained constant while the specimen is sheared at a constant rate of axial deformation (ie. strain-controlled compression) until a certain axial strain is reached or failure occurs as the case may be. No drainage is permitted and therefore the moisture content remains constant during compression. The resulting changes in pore pressure are measured at the base of the specimen, and the rate of axial deformation is applied slowly enough to ensure adequate equalization of excess pore pressures.

Test procedure

Adjustments for shearing

2. Referring to *Fig.*-A5 valve B must be kept closed. Valve C remains open to the cell pressure line and valve A is open to enable the pore pressure readings to be observed.

3. Set the gearbox or speed controller on the compression machine to give the required rate of deformation. The switch must be set correctly for upward movement of the machine platen, in accordance with the manufacturer's instructions.

4. At this stage the piston has been adjusted earlier such that its top part is in contact with the anvil of the proving ring. Wind down the platen (by turning the manual handle of the compression machine anti-clockwise) to leave a small gap between the piston top and the proving ring anvil. Now wind up the platen by hand until the piston makes contact with the proving ring. Make sure that the conical taper seats correctly on the ball. A small seating load will be indicated on the load dial gauge.

5. Secure the srain dial gauge vertically in position, and adjust the bracket on which the stem rests to set the dial to zero, or to a convenient initial reading. Ensure that the dial gauge has enough travel, and that clearances are large enough to permit strain movement of at least 25% of the sample length. (ie. deformation of 0.25 x 102mm = 25.5mm).

6. Re-engage the machine speed setting required for the test. Check that contact is maintained between piston top and proving ring anvil, if necessary make small adjustment by switching on the motor momentarily. Set the timer to zero.

7. Observe the following and record them as the initial reading for the compression stage:

(a) clock time and date

(b) Displacement dial gauge

(c) Load dial gauge

(d) Pore water pressure

(e) Cell pressure (check)

Loading stage

8. Switch on the motor to start the test, and at the same instant start the clock.

9. Take readings [consisting of 7(b), 7(c) and 7(d)] at regular intervals of axial deformation, usually corresponding to strain intervals of 0.2% up to 1% strain and 0.5% strain thereafter. When there is sign of abrupt changes (eg. peak deviator stress, or maximum pore pressure) occuring, readings should be observed more frequently.

10. As compression continues, calculate each line of data to enable the plot of deviator stress versus strain be made as the test proceeds.

11. When the peak deviator stress is being approached, reading intervals should be reduced from 0.5% strain to 0.2% strain.

12. Allow the test to continue to specified strain levels.

Completion of test

13. When the displacement reaches the intended limit, and the final readings have been taken, switch off the motor, close valve A and unload the specimen by winding down the machine platen manually until a small gap appears between the plunger top and proving ring anvil.

14. Reduce the cell pressure to zero.

15. Open the bleed plug E and drain off the cell water through valve C.

16. The connection between the plunger and top pedestal is detached by slowly turning the plunger anti-clockwise. Avoid pulling up or pressing down the specimen when turning the plunger by applying just sufficient upward pull to loosen and detach the connection. When the plunger is completely detached from the top pedestal, it is raised up well clear of the latter.

17. When the cell is empty, loosen the tie screws and carefully ease the cell body off the base. Avoid knocking or touching the specimen and drainage lead.

C2.4 Dismantling after test

1. Roll the O-rings upward off the top pedestal and roll down the membrane to expose the specimen.

2. Carefully remove the specimen off the base pedestal, peel out the lubricated rubber disc and quickly start the procedure for trimming and setting up of specimens into the vertical and radial flow oedometers.

Vert. Effective stress	Values of void ratio corresponding to consolidation pressure											
	Lowest	Highest	Series 1	2C40(L)	2C40(UL)	2T120(L)	2T120(UL)	2T240(L)	2T240(UL)	2C240(L)	2C240(UL)	2C360(L)	2C360(UL)
0.00						1.82							
10.00	2.95	3.22	3.05				1.54				1.45		1.32
20.00	2.48	2.81	2.62	2.08	1.66	1.75		1.58		1.60		1.46	
30.00			2.43										
40.00	2.21	2.34	2.28	1.95		1.70	1.49	1.56	1.36		1.39	1.45	
60.00	2.04	2.16	2.10	1.87		1.66				1.55		1.42	1.24
80.00	1.92	2.04	1.95	1.80		1.63		1.51					
100.00	1.84	1.97	1.87	1.74		1.60							
120.00	1.76	1.90	1.79			1.57	1.45		1.31	1.48	1.35	1.36	1.21
140.00	1.71	1.76	1.74	1.63		1.54							
160.00	1.65	1.78	1.68	1.60		1.52							
180.00	1.61	1.71	1.64			1.49		1.43		1.43			
200.00	1.55	1.65	1.57			1.48							
220.00	1.53	1.62	1.55			1.46							
240.00	1.51	1.54	1.53			1.44		1.39	1.28	1.39		1.28	1.18
260.00	1.49	1.51	1.50										
280.00	1.47	1.48	1.48										
300.00	1.45	1.47	1.46									1.25	
320.00			1.44										
340.00			1.43										
360.00			1.41					1.32	1.27	1.31		1.23	
380.00			1.40										
400.00			1.38										
420.00			1.37										
440.00			1.37										
460.00			1.35										
480.00			1.34					1.27				1.18	1.15
500.00			1.33										
520.00			1.32										
540.00			1.31										
560.00			1.30										
580.00												1.15	

Vert. effective stress	Values of void ratio & permeability corresponding to consolidation pressure													
	1V	1V	1V	1V	1H	1H	1H	1H	2C40V	2C40V	2T240V	2T240V	2C360V	2C360V
0														
10	2.95			3.75E-08	3.22			5.81E-08						
20	2.48	2.35	9.48E-09	1.64E-08	2.63	2.63	1.72E-08	2.72E-08						
40	2.21	2.13	6.10E-09	6.10E-09	2.31	2.31	1.19E-08	1.19E-08	1.94	5.26E-09				
60	2.04	2.00	5.16E-09	5.16E-09	2.14	2.14	9.13E-09	9.13E-09	1.84	4.45E-09			1.50	1.19E-09
80	1.92	1.88	4.44E-09	4.44E-09	2.01	2.01	7.61E-09	7.61E-09	1.77	4.12E-09				
100	1.84	1.81	3.97E-09	3.97E-09	1.90	1.90	7.49E-09	7.49E-09	1.71	3.24E-09	1.48	1.33E-09		
120	1.76	1.75	3.29E-09	3.29E-09	1.82	1.82	5.93E-09	5.93E-09					1.44	1.06E-10
140	1.71	1.69	3.32E-09	3.32E-09	1.76	1.76	4.91E-09	4.31E-09	1.60	2.75E-09				
160	1.65	1.65	2.36E-09	2.36E-09	1.71	1.71	4.75E-09	4.75E-09	1.58	2.35E-09				
180	1.61	1.61	2.35E-09	2.35E-09	1.66	1.66	4.15E-09	4.15E-09			1.42	1.27E-09		
200	1.55			2.20E-09	1.59	1.59	4.20E-09	4.20E-09						
220	1.53			2.18E-09	1.56	1.56	4.25E-09	4.25E-09						
240	1.51			1.76E-09	1.54	1.54	3.71E-09	3.71E-09			1.39	1.13E-09	1.37	9.01E-10
260	1.49			1.61E-09	1.51	1.51	4.84E-09	3.14E-09						
280	1.47			1.12E-09	1.48	1.48	3.26E-09	3.26E-09						
300	1.45			1.43E-09	1.47	1.47	3.20E-09	3.20E-09					1.34	8.40E-10
320	1.44			1.43E-09				5.16E-09						
340	1.43			1.23E-09				4.44E-09						
360	1.41			1.23E-09				4.44E-09			1.32	1.04E-09	1.31	7.58E-10
380	1.4			1.13E-09				4.08E-09						
400	1.38			1.16E-09				4.42E-09						
420	1.37			1.09E-09				4.15E-09						
440	1.37			1.06E-09				4.04E-09						
460	1.35			1.09E-09				4.15E-09						
480	1.34			1.05E-09				4.00E-09			1.27	8.25E-10	1.26	6.76E-10
500	1.33			1.12E-09				4.27E-09						
520	1.32			1.10E-09				4.19E-09						
540	1.31			1.08E-09				4.11E-09						
560	1.3			1.05E-09				4.00E-09						
580	1.3			8.60E-10				3.28E-09					1.23	6.49E-10

Vert. effective stress	Values of void ratio & permeability corresponding to consolidation pressure													
	2C240V	2C240V	2T120V	2T120V	2C40H	2C40H	2T240H	2T240H	2C360H	2C360H	2C240H	2C240H	2T120H	2T120H
0														
10														
20														
40					1.97	5.05E-09	1.54	2.49E-09						
60			1.63	1.72E-09	1.90	4.65E-09			1.40	1.82E-09			1.53	2.52E-09
80			1.60	1.65E-09	1.83	4.39E-09	1.51	2.26E-09					1.50	2.38E-09
100			1.58	1.55E-09	1.77	3.53E-09							1.46	2.18E-09
120			1.55	1.41E-09					1.34	1.67E-09			1.44	2.09E-09
140			1.54	1.37E-09	1.67	3.48E-09							1.41	1.96E-09
160			1.52	1.30E-09	1.63	3.57E-09							1.39	2.12E-09
180	1.44	1.40E-09	1.50	1.28E-09			1.43	1.90E-09			1.44	1.98E-09	1.36	1.86E-09
200			1.48	1.25E-09									1.34	1.92E-09
220			1.47	1.17E-09									1.32	1.82E-09
240	1.41	1.33E-09	1.45	1.11E-09			1.39	1.74E-09	1.25	1.50E-09	1.40	1.87E-09	1.31	1.74E-09
260														
280														
300									1.22	1.26E-09				
320														
340														
360	1.34	1.14E-09					1.32	1.57E-09	1.20	1.19E-09	1.32	1.60E-09		
380														
400														
420														
440														
460														
480							1.27	1.37E-09	1.15	1.15E-09				
500														
520														
540														
560														
580									1.12	9.83E-10				